



HIGH GRADE METAMORPHIC AND STRUCTURAL RELATIONSHIPS
NEAR AMATA, MUSGRAVE RANGES, CENTRAL AUSTRALIA

Volume 1

by

Kenneth David Collerson, B.Sc.(Hons) (New England)

Department of Geology and Mineralogy
University of Adelaide

August, 1972

CONTENTS

VOLUME 1

	Page
SUMMARY	(i)
STATEMENT OF ORIGINALITY	(iii)
ACKNOWLEDGEMENTS	(iv)
CHAPTER 1 - INTRODUCTION	1
1.1 - Aim of Thesis	2
1.2 - Geographical Setting	2
1.2.1 - Location and Access	2
1.2.2 - Geomorphology	3
1.2.3 - Vegetation	3
1.2.4 - Local Inhabitants	3
1.3 - Historical and Previous Work	4
1.4 - Regional Geological Setting	7
1.5 - The Term 'Granulite'	8
1.6 - Method of Study	8
CHAPTER 2 -- STRUCTURAL RELATIONSHIPS	10
2.1 - Introduction	11
2.1.1 - General	11
2.1.2 - Terminology and Nomenclature	11
2.1.3 - Structural Maps	12
2.1.4 - Structural Sub-Areas	13
2.2 - Structural Features of the Granulite Facies Rocks	13
2.2.1 - Structural Style	13
2.2.2 - Orientation of Structural Elements	16
2.3 - Structural Features of the Transitional Terrain	17
2.3.1 - Structural Style	17
2.3.2 - Orientation of Structural Elements	21
2.4 - Structural Features of the Amphibolite Facies Rocks	21
2.4.1 - Structural Style	21
2.4.2 - Orientation of Structural Elements	22
2.5 - Major Fault Zones	23
2.5.1 - Davenport Shear	23
2.5.2 - The Woodroffe Thrust Zone	24
2.6 - Concluding Discussion	25
CHAPTER 3 - METAMORPHIC PETROLOGY - PETROGRAPHY	29
3.1 - Introduction	30
3.2 - Metamorphic Microstructures	30
3.2.1 - Proposed New Terminology	32
3.2.2 - Discussion	33
3.2.2.1 - Predominantly Granoblastic Rocks	33
3.2.2.2 - Rocks with Anastomosing Layering	35
3.2.2.3 - Summary	35

	Page
3.3 - Petrography of the Granulite Facies Lithologies	36
3.3.1 - Mafic Lithologies	36
3.3.1.1 - General Description	36
3.3.1.2 - Mineral Assemblages	36
3.3.1.3 - Microstructures	38
3.3.1.4 - Descriptive Mineralogy	39
3.3.2 - Ultramafic Lithologies	47
3.3.2.1 - General Description	47
3.3.2.2 - Mineral Assemblages	48
3.3.2.3 - Microstructures	49
3.3.2.4 - Descriptive Mineralogy	49
3.3.3 - Quartzo-feldspathic Lithologies	54
3.3.3.2 - Mineral Assemblages	55
3.3.3.3 - Microstructures	56
3.3.3.4 - Descriptive Mineralogy	57
3.3.3.5 - Pegmatites	61
3.3.3.5.1 - General Description	61
3.3.3.5.2 - Mineral Assemblages	61
3.3.3.5.3 - Microstructure	61
3.3.3.5.4 - Descriptive Mineralogy	62
3.3.4 - Quartzitic Lithologies	63
3.3.4.1 - General Description	63
3.3.4.2 - Mineral Assemblages	63
3.3.4.3 - Microstructure and Descriptive Mineralogy	63
3.3.5 - Manganiferous Lithologies	65
3.3.5.1 - General Description	65
3.3.5.2 - Mineral Assemblages	65
3.3.5.3 - Microstructures	65
3.3.5.4 - Descriptive Mineralogy	66
3.3.6 - Calc Silicate Lithologies	67
3.3.6.1 - General Description	67
3.3.6.2 - Mineral Assemblages	67
3.3.6.3 - Microstructures	68
3.3.6.4 - Descriptive Mineralogy	68
3.4 - Petrography of the Transitional Terrain Lithologies	71
3.4.1 - Mafic Lithologies	71
3.4.1.1 - General Description	71
3.4.1.2 - Mineral Assemblages	72
3.4.1.3 - Microstructure	73
3.4.1.4 - Descriptive Mineralogy	75
3.4.2 - Ultramafic Rocks	81
3.4.2.1 - General Description	81
3.4.2.2 - Mineral Assemblages	81
3.4.2.3 - Microstructures	82
3.4.2.4 - Descriptive Mineralogy	82
3.4.3 - Intermediate Lithologies	85
3.4.3.1 - General Description	85
3.4.3.2 - Mineral Assemblages	85
3.4.3.3 - Microstructure	86
3.4.3.4 - Descriptive Mineralogy	87

	Page
3.4.4 - Quartzo-feldspathic Lithologies	90
3.4.4.1 - General Description	90
3.4.4.2 - Mineral Assemblages	91
3.4.4.3 - Microstructures	93
3.4.4.4 - Descriptive Mineralogy	94
3.4.5 - Calc Silicate Lithologies	97
3.5 - Petrography of the Amphibolite Facies Lithologies	98
3.5.1 - Mafic Lithologies	98
3.5.1.1 - General Description	98
3.5.1.2 - Mineral Assemblages	98
3.5.1.3 - Microstructures	98
3.5.1.4 - Descriptive Mineralogy	99
3.5.2 - Quartzo-feldspathic Lithologies	101
3.5.2.1 - General Description	101
3.5.2.2 - Mineral Assemblages	101
3.5.2.3 - Microstructures	102
3.5.2.4 - Descriptive Mineralogy	102
3.5.3 - Pelitic Lithologies	105
3.5.3.1 - General Description	105
3.5.3.2 - Mineral Assemblages	105
3.5.3.3 - Microstructure	105
3.5.3.4 - Descriptive Mineralogy	105
 CHAPTER 4 - METAMORPHIC PETROLOGY - CHEMICAL	 107
4.1 - Introduction	108
4.1.1 - Previous Work	108
4.1.2 - Nature of the Analysed Specimens	108
4.1.3 - Petrographic Descriptions	109
4.1.4 - Modal Analyses	109
4.1.5 - Sample Preparation	109
4.1.6 - Methods of Chemical Analysis	109
4.2 - Rock Chemistry	110
4.2.1 - Compositional Classes of Rocks	110
4.2.1.1 - Compositional Abundances	110
4.2.2 - Modal Composition	111
4.2.2.1 - Granulite Facies Lithologies	111
4.2.2.2 - Transitional Lithologies	120
4.2.2.3 - Amphibolite Facies Lithologies	121
4.2.2.4 - Modal Plots	121
4.2.3 - Major Element Chemistry	122
4.2.3.1 - Quartzo-feldspathic Lithologies	122
4.2.3.1.1 - Granulite Facies	122
4.2.3.1.2 - Transitional Rocks	141
4.2.3.1.3 - Amphibolite Facies	141
4.2.3.2 - Mafic Lithologies	145
4.2.3.2.1 - Granulite Facies	145
4.2.3.2.2 - Transitional Rocks	145
4.2.3.2.3 - Amphibolite Facies	147
4.2.3.3 - Ultramafic Lithologies	148

	Page
4.2.3.4 - Calc Silicate Lithologies	148
4.2.3.5 - Manganiferous Granulite	148
4.2.3.6 - Oxidation Ratios	149
4.2.3.6.1 - General	149
4.2.3.6.2 - Relationship between Oxidation Ratio and Rock Composition	150
4.2.3.6.3 - Mobility of Oxygen	151
4.2.3.6.4 - Variation of Oxidation with Metamorphic Grade	152
4.2.3.7 - A.C.F. and A.K.F. Diagrams	153
4.2.3.7.1 - General	153
4.2.3.7.2 - Comparison with 'Average' Rocks	153
4.2.4 - Trace Element Chemistry	156
4.2.4.2 - Rubidium and K/Rb Ratio	156
4.2.4.2.1 - Introduction	156
4.2.4.2.2 - Presentation of Results	159
4.2.4.2.3 - Mineralogical Control of the K/Rb Ratios	165
4.2.4.2.4 - Evidence for Crustal Fractionation	168
4.2.4.3 - Strontium and Rb/Sr Ratio	169
4.2.4.4 - Zirconium	173
4.2.4.5 - Cerium and Lanthanum	175
4.2.4.5.1 - Presentation of Data	175
4.2.4.5.2 - Correlation between Cerium, Lanthanum and Major Elements	176
4.2.4.5.3 - Influence of Mineralogy on Cerium and Lanthanum Distribution	176
4.2.4.5.4 - Fractionation of the REE	177
4.2.4.6 - Thorium and Uranium	179
4.3 - Mineral Chemistry	184
4.3.1 - General	184
4.3.2 - Relationship of Mineral Chemistry to Whole Rock Chemical Ratios	192
4.3.2.1 - Oxidation Ratio	192
4.3.2.2 - Mg/Mg + Fe ²⁺ Ratio	196
4.3.2.3 - Mn/Mn + Mg + Fe ²⁺ Ratio	197
4.3.3 - Systematic Mineral Chemistry	197
4.3.3.1 - Orthopyroxenes	197
4.3.3.1.1 - Nomenclature	197
4.3.3.1.2 - Chemistry	198
4.3.3.2 - Clinopyroxenes	203
4.3.3.2.1 - Nomenclature	203
4.3.3.2.2 - Chemistry	203
4.3.3.3 - Hornblendes	206
4.3.3.3.1 - Nomenclature	206
4.3.3.3.2 - Chemistry	207
4.3.3.4 - Garnets	211
4.3.3.4.1 - Nomenclature	211
4.3.3.4.2 - Cell Dimensions	213
4.3.3.4.3 - Chemistry	213
4.3.3.5 - Micas	215
4.3.3.5.1 - Nomenclature	215

	Page
4.3.3.5.2 - Chemistry	216
4.3.3.6 - Opaque Oxides	217
4.3.3.6.1 - General	217
4.3.3.6.2 - Chemistry	218
4.3.3.6.3 - Application of Experimental Systems	219
4.3.3.7 - Scapolite	221
4.3.3.7.1 - General	221
4.3.3.7.2 - Chemistry	222
4.3.3.8 - Alkali Feldspars	222
4.3.3.8.1 - Chemistry	222
4.3.3.8.2 - Structural State	224
4.3.4 - Element Distribution among Co-existing Minerals	231
4.3.4.1 - General	231
4.3.4.2 - Theoretical Aspects	231
4.3.4.3 - Distribution of Fe ²⁺ and Mg ²⁺	233
4.3.4.3.1 - Orthopyroxene-Clinopyroxene Pairs	233
4.3.4.3.2 - Orthopyroxene-Hornblende and Clinopyroxene-Hornblende Pairs	241
 CHAPTER 5 - CONDITIONS OF METAMORPHISM AND THE ORIGIN OF THE MAFIC AND ULTRAMAFIC ROCKS	 244
5.1 - Partial Pressures	245
5.2 - Physico-Chemical Conditions as Indicated from Bulk Rock and Mineral Chemistry	248
5.3 - Inferred Temperature and Pressure Conditions of Metamorphism from Experimental Studies	251
5.4 - Origin of the Mafic and Ultramafic Rocks	260
5.4.1 - General	260
5.4.2 - Previous Work on the Origin of Metamorphosed Mafic Rocks	260
5.4.3 - Origin of the Amata Mafic Rocks	262
5.4.3.1 - Major Element Data	262
5.4.3.2 - Trace Element Data	263
5.4.3.3 - Field Evidence	264
5.4.3.4 - Discussion	267
5.4.3.5 - Nature of the Igneous Parent	267
 CHAPTER 6 - CONCLUDING DISCUSSION	 271
 APPENDIX 1 - PETROGRAPHIC DETAILS OF ANALYSED ROCKS	 1.1
APPENDIX 2 - TECHNIQUES	2.1
APPENDIX 3 - CALCULATION OF THE MESONORM AND CATANORM	3.1
APPENDIX 4 - CALCULATION OF MASS ABSORPTION COEFFICIENTS	4.1
APPENDIX 5 - SUMMARY OF DATA FOR LINEAR REGRESSION ANALYSIS AND CALCULATION OF REDUCED MAJOR AXES	5.1
APPENDIX 6 - PETROLOGY OF THE MAFIC ROCKS ('PLAGIOCLASE ECLOGITES'(?)) FROM THE DAVENPORT SHEAR	6.1

APPENDIX 7 - MOLE FRACTIONS OF ELEMENTS USED IN THE
CALCULATION OF DISTRIBUTION COEFFICIENTS 7.1

REFERENCES i

SUMMARY

Three groups of metamorphic rocks are recognised in the vicinity of Amata in the western Musgrave Ranges, central Australia, viz. granulite facies, amphibolite facies and lithologies transitional between the two (in the thesis termed transitional lithologies). The granulite facies terrain forms the core of the Ranges and is bounded on the north by the amphibolite facies terrain and on the south by the transitional terrain. Two major east-west trending faults, the Woodroffe Thrust and the Davenport Shear, separate the three groups of rocks.

The granulite facies lithologies are structurally relatively simple and are characterised by the presence of a strong south-westerly plunging mineral streaking lineation. Folds representative of the several phases of deformation in the area are rarely observed. They are tight to isoclinal and commonly rootless. In marked contrast, the transitional rocks show more complexity of folding on a macroscopic scale. They also have a well developed mineral lineation, plunging, however, to the south east. These two lineation orientations are believed to be directions of maximum elongation in the two terrains. The amphibolite facies rocks are also structurally complex, and at least two lineations related to different phases of deformation have been recognised.

Quartzo-feldspathic rock types are dominant in the three metamorphic terrains. Mafic lithologies in the granulite facies terrain have predominantly high alumina basalt composition, and were apparently intruded after trace element fractionation trends had been established in the quartzo-feldspathic granulites. Mafic lithologies in the transitional and amphibolite facies terrains were, however, apparently present during the establishment of trace element trends.

The granulite facies terrain is interpreted to have formed as a result of a single orogenic episode by the metamorphism of a sequence of cover rocks. The transitional terrain probably represents a sequence of reworked basement lithologies. The amphibolite facies terrain is believed to represent a pre-existing basement over which the granulite facies and transitional rocks were thrust.

Granulite facies metamorphic conditions were essentially anhydrous with $P_{H_2O} < P_{load}$, whereas the transitional terrain was more variable with respect to P_{H_2O} and in the amphibolite facies terrain P_{H_2O} was probably equal to P_{load} .

Comparison of the mineral paragenesis with relevant experimental work suggests that:

- (i) the granulite facies terrain was metamorphosed under pressure-temperature conditions of approximately 8 to 9 kilobars and 950-1000°C;
- (ii) the amphibolite facies terrain was metamorphosed under conditions of approximately 4 kilobars and 650°C;
- (iii) the transitional terrain pressure-temperature conditions are more difficult to estimate; they are thought to have been slightly less than those prevailing in the granulite facies terrain.

This thesis contains no material which has been accepted for the award of any other degree or diploma in any University, nor to the best of my knowledge and belief, does it contain any material previously published or written by another person, except where due reference and acknowledgement is made in the text.

A handwritten signature in cursive script, appearing to be 'P. H. ...', followed by a period.

ACKNOWLEDGEMENTS

The project was suggested and supervised by Dr. R.L. Oliver and Professor R.W.R. Rutland. Dr. R.L. Oliver critically assessed the final draft of the thesis.

Other members of the Department of Geology and Mineralogy who have been of considerable assistance, both in the laboratory research stages of the thesis production and in the preparation of the final draft include Drs. M.A. Etheridge, J.B. Jones, A.W. Kleeman and R.W. Nesbitt, Miss E.M. McBriar and Messrs. C.D.A. Coin and H. Mastins. People outside the University have also given freely of their experience and knowledge, viz. Messrs. R.B. Major, B.P. Thomson and A.R. Milnes, Drs. M. Coward, P.D. Fleming, D. Forman, T.P. Hopwood, A.D.T. Goode and A.C. Moore.

My wife Jane, who has been a continuing source of encouragement, excellently drafted many of the text figures and performed countless other tasks associated with the thesis production.

Mrs. K. Round very efficiently and accurately typed the drafts and final copy of the thesis. Miss M. Swan kindly drafted some of the geological maps.

The staff of 'Amata' and the Pitjantjara men, particularly Mr. Douglas Tjurki, were extremely helpful during field work.

The study was carried out during the tenure of a Commonwealth Post Graduate Award. Financial support for field work and microprobe analyses was obtained from the A.R.G.C. through grants to Professor R.W.R. Rutland and Dr. R.L. Oliver.



CHAPTER 1

INTRODUCTION

1.1 AIM OF THESIS

The thesis is principally concerned with an examination of granulite facies, amphibolite facies and transitional granulite to amphibolite facies lithologies in the Amata area of the Musgrave Orogenic Belt (Collerson *et al.*, 1972) in central Australia. As such the thesis embraces a study of the structural, petrological and geochemical relationships between the different metamorphic groups.

1.2 GEOGRAPHICAL SETTING

1.2.1 Location and Access

The area investigated in this thesis is situated in the Musgrave Ranges near 'Amata' (formerly 'Musgrave Park'), in the arid north-western corner of South Australia (Figure 1.1). It lies between latitudes $26^{\circ}08'$ S to $26^{\circ}17'$ S and longitudes $131^{\circ}09'$ to $131^{\circ}15'$, covering an area of roughly 130 sq.km. The total area of outcrop is approximately 70 sq.km.

Permits are required from the South Australian Department of Social Welfare and Aboriginal Affairs in Adelaide to enter the area as it lies within the North West Aboriginal Reserve, entry to which is restricted.

The area is reached from the Stuart Highway (the main Adelaide to Alice Springs road), via the 'Mt. Cavenagh' to Ayers Rock road and the 'Gunbarrel Highway' (a track from 'Mulga Park' to the Giles Meteorological Station in Western Australia), a distance of roughly 200 km.; or by way of the 'Everard Park' - 'Kenmore Park' - 'Ernabella' - 'Amata' track which runs along the southern front of the ranges (Figure 1.1).

1.2.2 Geomorphology

The Musgrave Ranges comprise an elongate chain of isolated, often steeply dissected ridges, low inselbergs and whale-backs, separated by gently sloping rock strewn pediments, rocky and sandy alluvial fans and sandy outwash plains. Sharp breaks of slope occur

where the plains impinge against the ranges.

The plains average approximately 670 metres above sea level and the local relief is as much as 550 metres in the Amata area where Mt. Morris reaches 1249 metres. The highest point along the chain is Mt. Woodroffe (1432 metres).

The drainage pattern is dendritic and the creeks are non-perennial. In the ranges they are extremely youthful and their beds are commonly cobble or boulder strewn. On the plains they commonly form incised meandering patterns.

To the south the outwash plains give way to the monotonous parallel sand ridges of the Great Victoria Desert.

1.2.3 Vegetation

The vegetation is characteristic of arid and semi-arid regions. Clumps of mulga (Acacia sp.), isolated stands of corkwood (Hakea sp.) and desert oak (Casuarina sp.) together with areas of soft small grasses occur on the plains away from the main water courses. Taller eucalypts are found along the major water courses. Trees are relatively uncommon in the granulite facies terrain where spinifex (Trioda sp.) predominates. Stunted eucalypts and native pines together with soft grasses occur in the transitional and amphibolite facies terrains.

1.2.4 Local Inhabitants

The indigenous inhabitants of the Musgrave Ranges belong to the Pitjantjatjara tribe. They have permanent settlements at 'Amata' and 'Ernabella', although small groups still practise a migratory subsistence culture.

1.3 HISTORICAL AND PREVIOUS WORK

The first Europeans to explore and name geographical features in this part of central Australia were Gosse and Giles in 1873 (Gosse, 1874; Giles, 1874 and 1889).

The first to provide geological accounts of the area and make geological collections were Brown (1890), Streich (1893), Basedow (1905),

Jack (1915), and Talbot and Clarke (1917 and 1918). Petrographic descriptions of rocks collected during these expeditions were made by Stelzner (in Streich, 1893), Basedow, Thomson (1911), Farquharson (in Talbot and Clark, 1917), and Robinson (1949). Stelzner commented on the similarity between the Saxon granulites and rocks from the Barrow Range in W.A. Farquharson also noted that rocks from Western Australia were similar to charnockite from India, Africa and Saxony.

The first detailed geological study of the Musgrave Ranges was made by A.F. Wilson in the Ernabella area (Wilson, 1947). His continued interest in the region is manifest in the following publications: Wilson (1948, 1950, 1952a,b, 1953, 1954a,b, 1958, 1959, 1960, 1969a,b); Wilson, Compston, Jeffery and Riley (1960); Wilson and Hudson (1967); Hudson, Wilson and Threadgold (1967) and Wilson, Green and Davidson (1970).

A brief account of the geology and tectonics of the 'Musgrave Mountain Belt' was given by Sprigg and Wilson (1958).

Regional geological mapping at 1:250,000 scale has been carried out by the South Australian Department of Mines (Major et al., 1967).

More detailed studies of specific aspects of the geology of the Musgrave Ranges have been made recently by Virgo (1966, 1968); Lambert and Heier (1968); Arriens and Lambert (1969); Major (1970); Coin (1970); and Collerson et al. (1972).

1.4 REGIONAL GEOLOGICAL SETTING

The Musgrave Ranges form the eastern most extension of the Musgrave Block (Hossfeld, 1954), which covers an area of approximately 140,000 sq.km. in central Australia. The block, which consists of crystalline basement lithologies, extends from the Warburton Ranges in Western Australia eastward to the Kulgera Hills and Ayers Ranges in the Northern Territory, a distance of approximately 700 km. (Figure 1.1). Upper Proterozoic cover rocks of the Orlia Chain and Petermann Ranges extend north west from the Musgrave Ranges into the Northern Territory. They differ from the Musgrave Block metamorphics both in structural geometry and metamorphic grade. To the south of the Musgrave Block

basement rocks are overlain by Precambrian to Ordovician sediments of the Officer Basin¹, and in the north by Precambrian to Permian sediments of the Amadeus Basin. To the west the Canning Basin contains Palaeozoic formations and to the east the Great Artesian Basin contains Mesozoic sediments.

The Musgrave Ranges (Figure 1.1) extend for a distance of 178 km. from east to west and are 51 km. wide at their broadest point.

The central and highest part of the ranges consists of a zone of granulite facies rocks. This is bounded on the north by rocks of amphibolite facies grade, exposed in isolated low whale-backs and deeply dissected inselbergs, and on the south by rocks transitional between granulite and amphibolite facies².

With a few exceptions the lower grade rocks are separated from the granulites by two prominent east-west trending faults, viz. the Woodroffe Thrust³ and the Davenport Shear⁴ (Figures 1.1, 1.2 and 1.3). The Mann Fault occurs to the south of the Davenport Shear and possibly separates the transitional lithologies from another sequence of granulite facies lithologies.

The Woodroffe Thrust forms an extensive zone of shearing traceable for about 100 kilometres. At some localities (e.g. near 'Amata') it swings sharply and runs almost north-south. In the field, the thrust crops out as a prominent scarp and the thrust zone varies in thickness from less than 10 metres to greater than 100 metres. The zone is composed of protomylonites, mylonites, ultramylonites and pseudotachylite. The pseudotachylite occurs predominantly in the upper part of the thrust zone and in the adjacent granulites.

-
1. Sediments ranging up to Tertiary are also possibly present (Major, pers. comm.)
 2. Hereafter these metamorphic divisions will simply be termed the granulite facies- or granulite terrain, the amphibolite facies- or amphibolite terrain and the transitional terrain.
 3. Named after Mt. Woodroffe by Wilson (1960) fig.7, although the shear zone was first noted by Wilson (1959) fig.1. See also Major (1970).
 4. Named by Major et al. (1967).

The Davenport Shear forms an extensive zone dipping steeply to the south. It ranges in width from 10 metres to 100 metres and has been mapped for about 100 km. Although its composition is variable, the main lithologies encountered are recrystallized ultramylonite, quartzo-feldspathic mylonite and altered dolerite. At the western end of the Musgrave Ranges, the Davenport Shear is displaced by a series of strike slip faults, and here the relationships between the rocks transitional between granulite and amphibolite facies and the granulite facies rocks become less clear. Nevertheless, recent work by Coin (1970) has suggested that the Davenport Shear still separates these different groups of rocks.

Except in the Mann Ranges (Figure 1.1), the Mann Fault has a rather discontinuous outcrop pattern (cf. the Woodroffe Thrust and Davenport Shear) (Thomson *et al.*, 1962; Major *et al.*, 1967). The fault zone also strikes approximately east-west and it dips generally to the south.

As well as separating areas of different metamorphic grade, the Davenport Shear and the Woodroffe Thrust also separate areas of differing structural geometry (see Chapter 2). One main phase of deformation (gD_1) has been recognised in the granulite facies rocks of the Amata area and limited although significant evidence exists for the recognition of three later periods of folding deformation (gD_2 , gD_3 and gD_5). Two main periods of folding deformation (tD_1 and tD_2) followed by a third weaker phase (tD_3) have been recognised in the transitional terrain. The amphibolite facies terrain north of the Woodroffe Thrust bears the imprint of three phases of folding deformation (aD_1 , aD_2 and aD_3). A period of thrusting (D_4) has had widespread effects throughout the entire area. The prefixes g, t and a have been used since the geometry sometimes differs between the different areas.

Bodies of mafic rocks which have intruded the granulites are found immediately south of the Woodroffe Thrust. These intrusions presumably form part of the Giles Complex (Nesbitt and Kleeman, 1964; Nesbitt and Talbot, 1966; Nesbitt *et al.*, 1970). The largest of these intrusions, the Woodroffe Basic Intrusion (Wilson, 1947; Major *et al.*, 1967) shows distinct igneous layering. In many places the mafic and

ultramafic bodies have been mylonitized. They were probably intruded along a pre-existing zone of weakness, on which further upthrusting of the granulites occurred after intrusion. A small body of norite has also been mapped in the transitional terrain (Figure 1.3) immediately to the west of a major north-south fault zone. However, whether or not it is related to the Giles intrusive has not been established.

Associated with the amphibolite facies rocks and the transitional rocks are intrusions of massive and gneissic granite which frequently contain xenoliths of quartzo-feldspathic or mafic lithologies.

Several phases of intrusions of dolerite dykes are recognised throughout the area. They have been broadly divided into schistose and non-schistose varieties. In the area mapped in detail, field and petrographic data suggests that the schistosity and lineation in the schistose dolerites was formed during the fourth phase of deformation, which was a phase of major thrust faulting. The last phase of movement on the Woodroffe Thrust and Davenport Shear evidently post-dated the last period of dolerite intrusion as no dolerite dykes have been observed crossing these discordances.

1.5 THE TERM 'GRANULITE'

There has recently been considerable discussion in the literature of the status of the term 'granulite' (Behr *et al.*, 1971; Mehnert, in press). In this thesis the usage of the term is as follows:

'A granulite is a regional metamorphic rock (tectonite) with a predominantly equigranular to inequigranular granoblastic texture (in sections normal to the lineation). Elongate lenses of quartz or prismatic clusters of pyroxene and/or a compositional heterogeneity may give rise to a schistosity or lineation. The rock consists of two or more of the following minerals: plagioclase, alkali feldspar, orthopyroxene, clinopyroxene and garnet. Quartz, iron (or iron-titanium) oxides, amphiboles and mica may or may not be present. If amphiboles and/or mica are present they must not exceed approximately

20% of the total mafic content of the rock.'

(see also Collerson and Etheridge, 1972).

1.6 METHOD OF STUDY

The project involved the detailed mapping of a north-south transect of the Musgrave Ranges in the vicinity of 'Amata', an area which had previously only been mapped on a reconnaissance scale (Major et al., 1967). The field area was chosen for its geological suitability but also because of logistical considerations; these involved communications, availability of water, safety and access to outcrop.

A total of 26 weeks was spent in the field from the middle of April to the end of June in 1968, 1969 and 1970. Mapping was carried out on four times enlargements of 1:70,000 South Australian Department of Lands aerial photographs, runs: Woodward Survey 721 (0056-0058) and Oolperkinta Survey 722 (0023-0026). Field information was transferred to base maps constructed from the enlarged aerial photographs.

In the course of field mapping it became clear that three groups of metamorphic rocks were present and that each group exhibited different structural geometries (see Chapter 2). It also became apparent that the lithological variability of the outcrop patterns was largely structurally controlled (by transposition). The units were found to be discontinuous and pure traverse mapping was impossible. The scale of the photographic enlargements did not permit detailed mapping, unit for unit.

The geology of the Amata area is portrayed in Figures 1.2 and 1.3. In Figure 1.3 it can be seen that some of the mafic units especially in the granulite terrain have outcrop patterns due to topography, which may at first sight be confused with structural configurations¹.

1. Unfortunately a topographic map was not available for use as a base map. The author attempted to construct a contoured base map with the aid of a stereotape plotter, but mechanical difficulties with the equipment rendered this impossible.

In the text, rock specimen and thin section numbers are prefixed by A325/-. The specimens and sections are housed in the Department of Geology and Mineralogy, University of Adelaide.

Details of sample preparation and analytical techniques are described in Appendix 2.

CHAPTER 2

STRUCTURAL RELATIONSHIPS

2.1 INTRODUCTION

2.1.1 General

To understand in more detail the relationships between different groups of metamorphic rocks, especially when the rocks are interpreted to have been formed in differing physico-chemical (and structural) regimes (Holland and Lambert, 1969), it is essential not only to investigate their petrography and geochemistry, but also to examine their structural characteristics.

The structural characteristics of the three metamorphic terrains in the Amata area, and their differences and similarities are therefore described and discussed.

2.1.2 Terminology and Nomenclature

A number of terms, as well as a descriptive notation have been utilized in this thesis to describe and delineate the observed geological structures. The most commonly used terms and the nomenclature followed in their description are given below:

Structural Surfaces: The general term used to signify penetrative planar (including curvi-planar) structures (Turner and Weiss, 1963).

Schistosity: This term is used in the sense of Ramsay (1967, p.177) to describe the penetrative planar fabric developed throughout all the rock material. It is used in the same sense as foliation is by Turner and Weiss (1963, p.97) and denotes all types of mesoscopically recognisable S-surface of metamorphic origin. The schistosities are defined by the sub-parallel alignment of elongate or platy mineral grains or ellipsoidal clusters of mineral grains whose orientation is controlled by closely spaced anastomosing layers.

Compositional layering, banding or lamination: An S-surface produced by variations of composition and/or grain size. The schistosity is developed either parallel or at small to large dihedral angles to this feature. The terms embrace 'layerings' produced by transposition (Turner and Weiss, 1963, p.99) and by

metamorphic differentiation (Talbot and Hobbs, 1968).

Lineation: A linear structure penetrative in hand specimens or in limited outcrop exposures (Turner and Weiss, 1963, p.101). Lineations may be caused in a number of features, some of which are: the intersection of S-surfaces, the presence of parallel ellipsoidal aggregates of mineral grains or the linear preferred orientation of the interfaces of prismatic or tabular crystals.

Folds: Aspects of the descriptive schemes of Turner and Weiss (1963), Fleuty (1964) and Ramsay (1967) are used in the description of the folds recognised throughout the area.

Geological Scale: (Turner and Weiss, 1963, p.15-16).

Microscopic Scale: Covers bodies that can be examined in their entirety with a microscope.

Mesosopic Scale: Covers bodies, ranging from hand specimens to large continuous outcrops, that can be studied in three dimensions by direct observation.

Macroscopic Scale: Covers bodies too extensive or too poorly exposed to be examined in their entirety.

In common with general practice, to represent the various schistositities, lineations and groups of folds recognised throughout the area, the symbols S_n , L_n and F_n have been utilized, subscript n representing any integer less than 5. The notation D_n refers to the deformation producing each group of fold.

The different groups of metamorphic rocks exhibit widely differing structural patterns which may or may not be related to the same phase of deformation. To avoid confusion the symbols used in the above notation are prefixed by the letters g , t and a to differentiate between the structures occurring in the granulite, transitional and amphibolite facies terrains respectively, e.g. gS_1 , aS_2 , gF_3 , tD_2 .

2.1.3 Structural Maps

The planar and linear structural features measured throughout

the area are plotted in Figures 2.1 and 2.2.

2.1.4 Structural Sub-Areas

The area in Figures 1.2, 1.3, 2.1 and 2.2 has been subdivided into nine structurally homogeneous sub-areas (Figure 2.3) on the basis of the orientation of certain linear structural geometrical features, e.g. gL_1 (and gL_2), tL_2 , aL_3 and the streaking lineation in the Woodroffe Thrust (L_4), as follows:

- (1) granulite facies, four sub-areas (numbered 4, 5, 6 and 7);
- (2) transitional rocks, three sub-areas (numbered 1, 2 and 3);
- (3) amphibolite facies, one sub-area (number 8);
- (4) Woodroffe Thrust, one sub-area (number 9).

These sub-areas were defined to enable a better portrayal of the contrasts in orientation of the geometry of the structural features within (and between) the different metamorphic terrains, and therefore aid their interpretation.

2.2 STRUCTURAL FEATURES OF THE GRANULITE FACIES ROCKS

2.2.1 Structural Style

The rocks of the granulite facies are characterised by both layering (gS_0) and schistosity (gS_1). The main penetrative schistosity contains a strong lineation (gL_1) and both features are related to a strong period of folding deformation (gD_1) which resulted in the formation of intra-folial folds (gF_1), in the granulites. There is some evidence of earlier folding and also of three later periods of folding.

The layering, which is statistically parallel to the schistosity, is produced by compositional differences between the various types of quartzo-feldspathic, mafic and ultramafic granulites together with rarer calc silicate, manganiferous and quartzite units (Figure 2.4a). It has been observed on all scales and boundaries between layers have been found to be either sharp or gradational. The mafic units showing gradational relations to more quartzo-feldspathic units are probably

part of the original stratigraphic succession while the discrete mafic units are probably later intrusions. Individual mafic units are up to 60 metres thick and 2.5 kilometres long and no isoclinal folding on this scale has been recognized. The concentration of mafic units in the granulites into two belts north of the Davenport Shear (see Figure 1.3) may correspond to an original stratigraphic sub-division on the largest scale.

Macroscopic isoclinal folds may occur within each of the main lithological units, but have not been recognized. Nevertheless, isoclinal mesoscopic folds of intra-folial character are quite common (Figure 2.5). The fold hinges vary in shape from open to tight and have gently to moderately inclined axial planes. They commonly have a rootless appearance resulting from the separation of fold limbs from their hinge zones (Figures 2.5b,c,e,f and 2.6a). They plunge to the south-west (Figure 2.7a). The main schistosity, which is due to the parallel preferred orientation of platy minerals and groups of minerals in the granulites, is parallel to the axial planes of these folds. The gS_1 schistosity is commonly more strongly developed in the quartzo-feldspathic granulites than in the mafic lithologies, due to the greater isotropy of the latter group (Figure 2.4b). In some of the quartzo-feldspathic granulites, thin lenticles of quartz form small hook-shaped folds (Figure 2.5b) which define the schistosity. The schistosity is often subordinate to the strong gL_1 lineation which has been formed by the preferred orientation of roughly parallel ellipsoidal groups or clusters of prismatic mineral grains. In the acid garnet-free granulites the lineation is expressed as a quartzo-feldspathic streaking, whereas in the garnetiferous acid granulites the lineation is more in the form of a rodding produced by the alignment of irregular groups of garnets (Figure 2.8b). In the intermediate mafic and ultramafic granulites the lineation is often more difficult to observe, but it tends to be produced by the alignment of parallel clusters of prismatic mineral grains, notably orthopyroxene (Figure 2.8a). This lineation is parallel to the axes of the gF_1 intra-folial folds. It is believed that its attitude probably represents the direction of maximum elongation in the rocks during the gD_1 period of

deformation. In one small area several mesoscopic folds were noted in which the lineation was not parallel to the hinges. The folds at this locality were found to vary in shape from open to tight and they have steeply inclined axial planes. If the parallelism of gL_1 and gF_1 is regarded as an essential characteristic of the gD_1 structural geometry, then these folds may represent an earlier generation. However, if the gL_1 lineation is a direction maximum elongation, the parallelism of gL_1 and gF_1 is not essential and these folds could possibly also be of the gF_1 generation. Because as pointed out by Ramsay (1967), during progressive deformation, the geometry of folding requires that the strain axes are commonly obliquely inclined to their earlier positions although the orientation of the governing stress field may not have changed. Therefore differing orientations of fold axes and lineations do not of necessity dictate separate stress environments. Nevertheless, the possibility of deformations earlier than gD_1 cannot be negated; one small refolded rootless isoclinal structure has been observed at station 927 (Figure 2.5A). Schistosity of an earlier deformation may have been transposed into parallelism with gS_1 . Park (1969, p.334) has pointed out that 'co-planarity of successive foliations' is a very significant problem in areas of high grade gneisses, as penetrative planar fabrics are often not obliterated by successive deformations but only (p.333) 'modified and re-modified by repeated transpositions'. Similar problems concern the recognition of the identity of co-linear lineations and folds that are intrafolial to a schistosity (Watterson, 1968, p.68-71; Park, 1969, p.334-335). Khoury (1968) interpreted banding in Lewisian granulites to be due to the accentuation of a pre-existing layering (sedimentary layering(?)) by strong movements along parallel fold limbs. The presence of converging layers and intrafolial folds in the granulites under study favours such an interpretation for much of the banding in the Amata area.

Although the gD_1 fabric is dominant in the granulite area, it has been locally modified by later periods of deformation. At several localities, gS_1 has been found to be folded with the development of a new schistosity gS_2 and a new lineation gL_2 , which are both very weak in comparison with the gD_1 fabric. The gF_2 folds are found on smaller

and larger mesoscopic scales. They vary from open to tight (Figures 2.5G,H,I and 2.6b) and the larger ones, which are always dextral, have one limb faulted out on syn-metamorphic slides to give a 'hockey-stick' appearance. They are approximately co-axial with gF_1 folds and the measured angle between gL_1 and gL_2 at any one locality does not exceed 10° . For this reason, gL_2 and gS_2 can be distinguished from gL_1 and gS_1 only in the hinge zones of the gF_2 folds.

At one locality in sub-area 4, a large mesoscopic closure of gS_1 has been found (Figure 2.9a). It is similar in form to the large mesoscopic gF_2 folds, i.e. it has a 'hockey-stick' appearance resulting from shearing along the axial plane. However, it differs from the gF_2 group of folds in that there is no apparent axial plane schistosity or lineation. As a consequence the re-folding of gL_1 can be observed (Figure 2.9.b). This folding therefore represents a different style and possibly a later stage than gD_2 . The folds have therefore been termed gF_3 and allocated to deformation gD_3 .

A phase of faulting represented by discordant faults and a suite of dykes with a schistose fabric was the next phase of deformation gD_4 . The faults and dykes are grouped together on the basis of a common mineral streaking direction different from that of the preceding fold episodes (Figure 2.10a). The dolerites exhibit an anastomosing schistosity similar to the microstructures developed in the faults, and it may be concluded that the fabric post-dates the main granulite facies metamorphism.

Broad macroscopic folds (gF_5) of the layering and schistosity have also been recognized (Figure 2.7a). These folds are open structures, they have long east-west limbs and short north-south limbs and they have horizontal or shallowly plunging axes.

2.2.2 Orientation of Structural Elements

The orientation of the principal structural elements in the granulites are given in Figures 2.1, 2.2, 2.3 and 2.7. In each sub-area, gS_1 (and therefore gS_0) is essentially planar as indicated by the statistical maxima of gS_1 poles in Figure 2.3. This shows that within the sub-areas there has been little subsequent deformation of gS_1 . The

variation in dip of gS_1 between sub-areas, from 50° southerly in sub-area 4, to 25° south-westerly in sub-area 7, is ascribed to the broad warping of gD_5 . The great circle through the gS_1 maxima would indicate a westerly axis for this deformation.

The point maxima of gS_1 poles are in marked contrast to the spread shown by the gL_1 lineations, a spread which is roughly the same for all sub-areas. It follows, therefore, that the distribution of gL_1 cannot be due to deformation later than gS_1 except in the special case of shear within the gS_1 plane. In fact, the range of the observed variation may occur within single outcrops and it has been noted that variations often occur with changes of lithology. It is therefore believed that the gL_1 variation was produced during gD_1 . It is attributed to inhomogeneity of strain such that the direction of maximum elongation was different in different layers.

Because most mesoscopic structures are exposed on two-dimensional faces it was generally not possible to measure gF_1 fold axes independently of the lineation but where observations were made, with the exception of one locality noted above (p. 15), gF_1 and gL_1 were parallel. The measured fold axes are concentrated in the south-westerly direction roughly central to the spread of the lineations.

The gF_2 folds also fall within the spread of the gL_1 lineations. It is likely that the attitude of gF_2 folds were controlled by the pre-existing anisotropy of the gL_1 lineation.

Figure 2.10a shows that lineations in the dolerites and the discordant faults have a common south-south-westerly orientation in southerly dipping schistosity. They are therefore distinctly different in orientation from the main lineation in the granulites.

2.3 STRUCTURAL FEATURES OF THE TRANSITIONAL TERRAIN

2.3.1 Structural Style

In the transitional terrain the layering and main schistosity are again parallel but they are folded on a macroscopic and mesoscopic scale about south-easterly axes, in marked contrast to the granulite facies terrain.

The rocks have a strong compositional layering (tS_0) which is produced by the intercalation of quartzo-feldspathic, mafic and ultra-mafic lithologies together with rare calc silicate units (Figure 2.11b) (see Chapter 3.4).

A strong schistosity tS_1 is locally parallel to tS_0 except in the hinges of the tF_1 intra-folial folds. This schistosity is the main schistosity recognized in the area and it is defined by the alignment of thin lenticles or slightly elongate xenoblasts of quartz, feldspar, hornblende and/or orthopyroxene in the quartzo-feldspathic gneisses, or by trains of aggregates of rounded to sub-idioblastic garnets in the garnetiferous gneisses. In the mafic lithologies it is defined by the preferred orientation of ellipsoidal or lenticular aggregates of xenoblastic hornblende, orthopyroxene, clinopyroxene and/or plagioclase and by platy phlogopite or biotite in the micaceous varieties.

A weak lineation tL_1 (possibly an elongation type) is present within the tS_1 schistosity. It is defined by the preferred orientation of prismatic clusters of grains of orthopyroxene, hornblende, clinopyroxene and feldspar in rocks of mafic composition and by quartz, feldspar and garnet in rocks of quartzo-feldspathic composition.

The earliest recognizable folds (tF_1) are intra-folial to the tS_0 layering and frequently occur as rootless hooks (Figure 2.12a, 2.13A,B,C). They are isoclinal, have gently to moderately inclined axial planes and well-developed axial plane schistosity tS_1 . The lensoidal nature of the layering reflects this phase of deformation.

The tF_1 fold axes have an irregular distribution and their axial planes dip at moderate to steep angles to the south or south-east (Figure 2.7b). In contrast to the granulite facies area the tF_1 folds are not generally parallel to the tL_1 lineations (Figure 2.14b). It is possible therefore that at least some of the folds and lineations which are termed tF_1 and tL_1 respectively could be the result of an earlier phase or earlier phases of folding deformation. Their haphazard distribution could signify redistribution by both the tD_1 and tD_2 deformations. Alternatively, if tL_1 is interpreted as a direction of maximum elongation it is not necessary that fold axes of the same age should be parallel to it. A detailed analysis of the relationship

between tL_1 and tF_1 is hindered by the later folding.

The most profound influence on the macroscopic geometry of the rocks was by the second recognizable phase of deformation (tD_2). The folds (tF_2) formed during this phase of deformation (tD_2) are observed on macroscopic and mesoscopic scales. The form of the macroscopic folding is indicated on Figure 1.2. A major westerly dipping fault breaks the continuity of the macroscopic structure between sub-areas 1 and 2 (Figures 1.2, 1.3). The mesoscopic folds (Figure 2.15a) vary in style from tight to isoclinal. Typical profiles are given in Figure 2.13D,E,F,G,H. Profiles differ depending on the lithology in which the folds are generated. Axial planes range from nearly upright to inclined and they dip at moderate to steep angles to the south or south-west (Figure 2.7c). A second schistosity tS_2 is developed parallel to the axial planes of tF_2 folds. In the hinge zones of these folds, it forms a large dihedral angle with the layering and tS_1 . The tS_2 schistosity is strongly developed in the quartzo-feldspathic lithologies as a wavy anastomosing alignment of lenticular quartz and feldspar (Figure 2.16a,b). In the mafic lithologies it is commonly not developed to the same extent (Figure 2.16a). It appears as an elongation of feldspars and ferromagnesian constituents aligned by a fine grained anastomosing layering (Figure 3.16a,b).

In the cores of the mesoscopic tF_2 folds the tS_2 schistosity commonly develops a fanned appearance and may be observed to be refracted into differing orientations in layers of differing anisotropy (Figure 2.12b). The tF_2 mesoscopic and macroscopic folds plunge at shallow to steep angles to the south-east (Figure 2.7c).

Petrographic evidence indicates that both hornblende and orthopyroxene were synmetamorphic minerals with the tD_2 phase of deformation, as both these phases have been observed forming the tS_2 schistosity.

A strong linear feature (termed for convenience tL_2), statistically co-axial with the plunges of the tF_2 fold axes (i.e. plunging towards the south-east; Figure 2.17a) is found in the transitional terrain. In Collerson et al. (1972) it was observed that the south-easterly plunging lineations are widely distributed through-

out the area (Figure 2.2) apparently lying solely within tS_1 ; and because the tS_2 schistosity was believed to be limited to the hinge zones of the tF_2 folds, the lineations were interpreted to be predominantly earlier tL_1 lineations, unrelated to tS_2 . Nevertheless, it was recognized that intersection lineations were present in the hinge regions of the tF_2 folds, where tS_2 formed a large angle intersection with the layering and with tS_1 .

As a result of recent microstructural studies on suitably oriented thin sections from the transitional terrain it has been recognized that tS_2 is more widespread than was previously thought.

Whereas it is commonly possible to determine in the field the relationship between schistosities and lineations in areas where schistosities are relatively well developed (e.g. where schistose units predominate), it is extremely difficult to determine this relationship in gneissic terrains where overprinting of one schistosity by another may be only feebly developed, as in the transitional terrain.

Therefore, in the light of the microstructural evidence it remains open whether the south-easterly plunging lineation is solely the result of intersection, is the result of intersection and extension associated with the tD_2 deformation, or is in part the earlier tL_1 lineation which has been overprinted by the tL_2 intersection lineation (Collerson *et al.*, 1972).

This problem has been recognized in other metamorphic areas. Fortunately, however, it has little significance for the correlation of the deformation episodes between the transitional and granulite facies terrains (see p. 27).

Folds (tF_3) produced during the third phase of deformation are superimposed on the macroscopic limbs of the tF_2 folds, especially in sub-area 2. They are sinistral and have been observed only on a mesoscopic scale (Figure 2.13I,J,K,L). They appear on schistosity-layering surfaces as sets of corrugations and often result in the warping of the tL_2 lineations (Figure 2.17b). The tF_3 folds plunge at moderate to steep angles to the north and south (Figure 2.7c) and their axial planes are inclined.

As in the granulite area tD_3 was followed by the development of

a new fabric in fault zones and dolerite dykes. In the case of the dolerites the igneous microstructures were not completely obliterated. The schistosity and lineation are defined by the alignment of clusters of fractured euhedral to subhedral twinned plagioclase laths surrounded by an anastomosing layering.

2.3.2 Orientation of Structural Elements

The principal structural elements in the transitional terrain are summarised in Figures 2.3, 2.7b,c, 2.10b and 2.14b. The distribution of poles to tS_1 is indicated by three great circles representing the girdle distribution of the poles of the three sub-areas (Figure 2.3). This distribution is evidently the result of re-folding about the tF_2 fold axes.

Figure 2.7c shows that the tF_3 folds have superposed on the tF_2 folds. The average trend of the axial planes of the tF_3 folds is approximately north-south and the tF_3 fold axes show a spread in this direction.

The orientation of linear structures, tL_4 , in late discordant faults and deformed dykes is shown in Figure 2.10b. The structures have a common south-easterly plunge virtually identical with that of the tF_2 structures. However, the dykes are discordant to the tF_2 structures and are not folded by them so that there is unambiguous evidence for the postulated age relationship.

2.4 STRUCTURAL FEATURES OF THE AMPHIBOLITE FACIES ROCKS

2.4.1 Structural Style

In contrast to the other main areas, the amphibolite facies area shows well developed macroscopic interference patterns. This is due to the increased importance of later generation folds (aF_3) in this area. The rocks exhibit a well defined compositional layering produced by the inter-banding of various types of acid gneisses (Figure 2.11a), rare lenses of amphibolite and pelitic schist. This compositional layering has been termed aS_0 .

The dominant schistosity, aS_1 , is parallel to the axial planes of rare mesoscopic isoclinal intra-folial folds (aF_1) of aS_0 . The

schistosity is generally due to the planar preferred orientation of the quartzo-feldspathic and ferromagnesian constituents forming a gneissic fabric in the rocks, but locally, intense anastomosing layering around lozenge-shaped xenoblasts in zones gradational to the normal gneissic fabric also contributes to aS_1 .

Two other platey schistositities, aS_2 and aS_3 , are locally developed in the hinge regions of later generation folds and parallel to their axial planes. The aF_2 folds (Figure 2.15b) vary from open to tight on both mesoscopic and macroscopic scales. Open aF_3 folds on macroscopic and mesoscopic scales produce interference patterns with the aF_2 folds.

Lineations due to the dimensional orientation of the mineral components were not observed but intersection lineations, aL_2 and aL_3 , occur where aS_2 or aS_3 cut aS_1 and aS_0 . The aL_3 lineations may sometimes also be seen to overprint aL_2 .

Deformed dykes are much less common in the amphibolite facies area, but again their linear and planar fabric produced during the aD_4 deformation, agrees with that of the associated faults (Figure 2.10c), and they cut the earlier folds.

The last recognizable phase of deformation, aD_5 , resulted in the broad warping, aF_5 , of the layering on a macroscopic scale.

2.4.2 Orientation of Structural Elements

Figure 2.3 shows that the average dip of $aS_0//aS_1$ in the area is about 15° S.W. but the wide-spread of poles indicates the interference folding by aF_2 and aF_3 . aL_2 lineations and aF_2 folds plunge gently north-west or south-east while aL_3 lineations and aF_3 folds plunge to the south (Figures 2.3 and 2.14a). aL_4 lineations in deformed dykes have southerly plunges similar to those of the aD_3 structures (compare Figures 2.10c and 2.14a). The axis for aF_5 has a westerly plunge (Figure 2.14a).

2.5 MAJOR FAULT ZONES

2.5.1 Davenport Shear

The Davenport Shear separates the granulite and transitional areas and ranges in width from less than 10 metres to more than 30 metres. The zone is composed of a central core of very fine- to medium-grained mafic to intermediate 'altered dolerite' surrounded by quartzofeldspathic mylonites and highly deformed and recrystallized gneisses. The core rocks consist of clinopyroxene, garnet, amphibole, quartz plagioclase and rutile, forming granoblastic (often slightly porphyroblastic) aggregates. Preliminary analyses undertaken on the phases are listed in Appendix 6. The compositions of the mineral phases suggest that the core rocks are 'plagioclase eclogites' (Green and Ringwood, 1967)¹.

Minor pseudotachylite forms the matrix of brecciated recrystallized ultramylonite and appears to be a later stage feature.

On the southern side of the shear the mylonites merge gradually into the gneisses of the transitional terrain. The shear is locally discordant to tF_2 folds but in general the schistosity and lineation in the shear zone is similar to that in the transitional terrain (compare Figures 2.7c and 2.18a), especially in the zone immediately adjacent to the shear. There is some suggestion that this schistosity in the transitional terrain may be the tS_2 schistosity, in which case the Davenport Shear may have been initiated along a zone of structural anisotropy caused by this schistosity.

In contrast, the schistosity in the granulites north of the shear swings abruptly into the shear at several localities (through as much as 30° in 3 metres) (Figure 2.18b). Only a very narrow zone of quartzofeldspathic mylonites and proto-mylonites, seldom wider than 1 metre (where it can be recognized) is present on the northern side of the dominant mafic to intermediate recrystallized mylonites of the shear. Nevertheless on the macroscopic scale the Davenport Shear

1. Some of the schistose dolerites occurring in the granulite facies terrain contain similar assemblages of minerals, although they are not as extensively recrystallized, and some aspects of the original dolerite mineralogy can still be observed. A detailed account of these rocks is the subject of a publication by Collerson and Milnes (in press).

appears to be parallel to the layering in the granulites (compare Figures 2.3 and 2.18a). Occasionally small isoclinal folds in the faint compositional layering of the central zone are encountered. These are sometimes re-folded by more open folds.

A faint streaking lineation is sometimes visible in the core-rock. However, in the surrounding quartzo-feldspathic mylonites, a more prominent south-easterly plunging mineral streaking lineation is developed.

2.5.2 The Woodroffe Thrust Zone

The Woodroffe thrust zone separates the granulite and amphibolite areas (Figure 2.19a). It is composed of proto-mylonites, mylonites, ultra-mylonites and pseudotachylite. All the rocks except the pseudotachylite have well developed planar anastomosing recrystallized microstructures and a very strongly developed mineral streaking lineation. The 'mylonitic' planar fabric has a point maximum distribution (Figure 2.3) indicating that the thrust dips gently to the south. Minor variations in the attitude of the strike of the mylonitic layering have been noted. One swing of the trend of the layering (Figure 1.3) is through more than 90° but this is largely topographic and is related to a strike swing of less than 40° .

The lineation plunges at a low angle to the south-south-west. Its total variation in trend is about 40° (Figure 2.3) but this variation is found over small areas and appears to be independent of variations in the strike and dip of the layering. The axis of folding of the layering lies within the lineation field so that the relationship to the lineation cannot be used to determine the age of the folding. However, field evidence suggests that the folding is concentric in character and it is believed to post-date the lineation.

Although the Woodroffe thrust zone is discordant to the layering of the granulites (Figure 1.2), the statistical plots of layering in the thrust zone are almost identical to those in sub-areas 6 and 7. Thus it may be inferred that on the regional scale the thrust zone is concordant with the layering in the granulites.

The Woodroffe thrust zone varies considerably in width from less than 17 metres to greater than 50 metres. It has a sharp contact with

the granulite facies rocks and the intensity of mylonitization increases towards the top of the thrust. A close similarity exists between the orientation of aL_3 in the amphibolite facies rocks and the plunge of the mineral streaking lineation in the thrust zone. In the granulite facies area this direction compares closely with the lineations in small faults and deformed dykes (Figure 2.10a). This suggests that the main fabric in the thrust zone post-dates the main granulite fabric. However, some evidence of repeated movement in the mylonite zone is given by brecciated blocks of disorientated mylonite surrounded by later mylonite with the usual southerly lineation.

The structural relationships of the Woodroffe Thrust appears to be comparable to other zones of intense deformation such as the Grenville Front which marks the north-western boundary of the Grenville province in Canada (Dalziel et al., 1969) and the Moine Thrust belt along the north-western margin of the Scottish Caledonides (Johnson, 1957; Christie, 1963; Dalziel and Bailey, 1968). Areas where there has been considerable controversy concerning the direction of movement of the rock masses relative to the attitude of the lineations and isoclinal folds.

2.6 CONCLUDING DISCUSSION

Structural observations in the Musgrave Ranges have been made previously by a number of authors, i.e. Wilson (1952a, 1953, 1954a, b vol.2, 1959, 1960 and 1969a) and Sprigg and Wilson (1958). Wilson (1952a, p.214) indicated that the 'charnockitic rocks' of the 'Musgrave-Warburton Block' have a N-S to NNW-SSE regional tectonic trend, although the ranges have a predominantly E-W geomorphic expression. He believed that the E-W trend was due either to 'later granitic injection' or to 'overthrusting from the SSE'. Later, however (Wilson, 1953, p.50), he showed that the 'original granitization' and emplacement of the Ernabella hypersthene adamellite 'was controlled by N-S rather than E-W tectonic trends' and he therefore concluded that the E-W topographic expression of the ranges was related to 'post-orogenic thrusting' and not to the 'original tectonic trend of the older rocks'.

Sprigg and Wilson (1958) also noted that the ranges were east-

west striking geomorphic features, although they were folded tightly on meridional axes. They regarded these north-south axes as 'normal for the ancient 'Westralian Shield' of which the area is part.

Wilson (1953, p.48-49) considered that the lineations which paralleled the (sub-meridional) axes of major and minor folds in the Ernabella area were *b*-lineations. He believed that the *b*-lineation fabrics indicated 'shearing stresses and pressure from the E or W,...' a situation which was compatible with the 'N-S orogenic setting'.

Furthermore, Wilson (1959, p.63) specifically rejects the idea that the lineation in the 'Woodroffe Thrust' (or 'Woodroffe Shear-zone') is an *a*-lineation and he considers the Woodroffe Thrust to be a strike slip fault zone ('the shear-zone is thought to represent a major transcurrent movement of considerable tectonic significance'). He believed that the granulite facies rocks had developed in response to a 'regional deep-seated E-W downwarp (possibly associated with deep-seated E-W transcurrent shearing)'. (Wilson, 1960, p.72).

Schmidt (1926) first applied quartz fabric analyses of lineated rocks to regional structural problems and found *c*-axes girdles trended parallel to the direction of tectonic transport (inferred from regional evidence). Sander (1930) concluded that in lineated quartz tectonites the direction of tectonic transport could be gauged when the quartz *c*-axes produced a singular maxima.

Martin (1935) however, challenged this conclusion and reported quartz *c*-axis girdles in rocks from southern Sweden perpendicular to both lineations and the geologically inferred direction of thrusting. These contradictory situations resulted in considerable discussion between British and Norwegian geologists concerning the direction of tectonic transport in the Caledonide thrust belt (Phillips, 1937; McIntyre, 1951; Kvalé, 1948, 1953). Further studies from the Appalachians (Balk, 1952; Brace, 1955) and from the British and Scandinavian Caledonides (Christie, 1963; Koark, 1961) reported *c*-axis patterns perpendicular to stratigraphically demonstratable directions of tectonic transport.

In the past decade it has been widely recognized that many symmetry arguments using quartz fabrics to determine the orientation of the deformation plane were improperly formulated. They were thus

invalid, since the nature of the finite strain was unknown (Dalziel et al., 1969, p.222). In many cases they were based on the assumption that monoclinic symmetry indicated biaxial strain. However, recent research in the Scandinavian Caledonides has shown that the finite strain is strongly triaxial and that the prominent mineral lineations in many metamorphic areas are developed parallel to the direction of maximum elongation in the rocks (e.g. Kvalé, 1948, 1953; Hooper, 1968; Nicholson and Rutland, 1969; Schwerdtner, 1970). The early penetrative linear and planar fabric in the granulites from the Amata area compares favourably with that of the Moine schists in Scotland or the 'Hardschiffer' of northern Sweden (R.W.R. Rutland, pers.com.) and although natural strain ellipsoids are absent from the granulites the principal penetrative lineation, gL_1 , is confidently interpreted as a lineation parallel to the direction of maximum elongation. The early folding deformation, gD_1 , is therefore regarded as being responsible for a significant amount of the elongation of the rocks. The D_4 phase of deformation (thrusting) is regarded as representing a later stage in the translation of the rock masses parallel to the direction of the principal axis of finite strain. The highly strained nature of the rocks at this stage resulted in the formation of thin recrystallization zones, now manifested as mylonites and the development of planar and linear fabrics in some of the dolerites.

The Davenport Shear and Woodroffe Thrust are regarded as essentially similar thrust fault zones on either side of the thrust slice of granulite facies rocks. The parallelism of these faults with the layering in the granulites strongly suggests that the faults were developed at an early stage in the deformation history, and this inference is supported by the polyphase deformation in the mylonites.

The Davenport Shear is made up of rocks derived from the transitional terrain and its linear structures are parallel to the tL_2 lineations in the transitional terrain. If the lineation in the transitional terrain can also be interpreted as a direction of maximum extension (cf. the gL_1 lineation in the granulite facies terrain) it is not inconceivable therefore, that the transitional terrain was thrust over the granulite facies terrain in a north-westerly direction.

The mineral streaking lineations in the Woodroffe Thrust have a north-south trend oblique to the trend of the gL_1 lineations and similar to the trend of the aL_3 lineations in the amphibolite facies terrain. This suggests that the movement direction may have been south-easterly in gD_1 but changed to northerly in D_4 .

The absence of a strong early linear fabric in the amphibolite facies terrain suggests an absence of large extensional strains and this terrain is interpreted as the Foreland to the thrust masses of the transitional and granulite facies terrains.

The structural analysis of the granulites provides no evidence of a complex tectonic history as would be expected of reworked basement. The structural sequence is readily interpreted in terms of a single orogenic cycle.

It is therefore suggested, notwithstanding the granulite metamorphism, that the granulites represent a series of cover rocks (i.e. Carpentarian sediments) rather than reworked basement (cf. Arriens and Lambert, 1969, pp.385-386).

The transitional terrain, on the other hand, may represent reworked basement since the early fold axes show very variable trends compared with the earliest lineation, tL_1 , which may indicate that the tL_1 lineation has been superposed on an earlier basement fabric.

CHAPTER 3

METAMORPHIC PETROLOGY - PETROGRAPHY

3.1 INTRODUCTION

Field relationships and petrographic features of the three groups of metamorphic rocks recognised in the Amata area are described and discussed in this chapter.

The different lithologies have been subdivided into the following compositional classes: mafic, intermediate, ultramafic, quartzo-feldspathic, quartzitic, calc silicate, pelitic and manganiferous, on the basis of mineralogical criteria. These divisions adequately describe the main compositional variations within the three metamorphic zones and they are used throughout the thesis.

3.2 METAMORPHIC MICROSTRUCTURES

In attempting to describe the microstructures¹ of the metamorphic rocks from the Amata area it became apparent that the earlier descriptive terminologies of Buddington (1939, pp.251-256), Katz (1968, pp.801-806), Moore (1970, pp.124-127) were not entirely applicable, either because they did not give adequate freedom in the description or because they had undesirable genetic overtones. For example, Buddington (1939, pp.251-253) classified the 'igneous rocks of the Adirondacks' according to the amounts of crushing recrystallisation and neo-mineralization they had suffered and proposed that they be described by the following terms: Mortar gneiss, Augen gneiss, Mylonite, Ultramylonite, Ultracataclastic mylonite, Flaser gneiss and Granoblastic gneiss. Katz (1968) adopted Buddington's terminology (with slight modification) to describe the quartzo-feldspathic granulites from Mt. Tremblant Park, Canada. He defined the 'fabrics'² of the granulites in terms of the relative amounts of deformation and recrystallisation they

-
1. Recent interpretations of the spatial distribution of grains and the nature of their interfaces with adjacent grains in metamorphic rocks have been based on metallurgical principles, established in polycrystalline aggregates. Therefore, following Vernon (1968) and for the sake of uniformity with metallurgical usage the term microstructure is used in preference to 'texture' in this thesis. 'Texture' in metallurgical description means 'preferred orientation' (Vernon, 1968).
 2. Katz (1968) uses 'fabric', 'texture' and 'microstructure' synonymously.

had suffered. He considered that the following hypothetical sequence represented the progressive modification of the granulite fabric:

Mortar → Augen → Flaser → Granoblastic

Certain aspects of this terminology, e.g. 'Mortar' and 'Augen' unfortunately have genetic ('cataclastic') connotations (see Moore 1970, p.124). They are therefore undesirable terms to use, especially when one considers that the textures are believed to have developed 'without micro-brecciation or cataclasis' (Katz, 1968, p.801). The term 'flaser' has similar genetic connotations. For example, Joplin (1968, pp.29-30) defines flaser structure as the 'term applied to rock sheared or crushed into lenticular masses or phacoids which are separated by wavy streaks of finely granulated material'.

Moore (1970) considered that 'textural' (microstructural) terminology should be:

1. descriptive
2. free from words with genetic connotations
3. unambiguous

He proposed a classification of granulite 'textures' (his term) based on the three-fold division:

1. granoblastic
2. flaser
3. mylonitic

He further subdivided granoblastic in terms of relative grain size into:

- (a) equigranular
- (b) inequigranular
- (c) seriate

To describe the grain boundary relationships observed in the three textural types he used the terms originally proposed by Berthelsen (1960) for granoblastic textures, and later modified by Katz (1968), i.e. polygonal, interlobate and amoeboid.

Unfortunately his proposed terminology did not fulfil his requirements for a descriptive textural terminology. For example, Moore's (1970) usage of the terms 'flaser' and 'mylonitic' have considerable genetic overtones despite his criticism of Katz (1968) for

the same reason. The subdivision between grain size type (b) and (c), apart from being difficult to apply, is unnecessary and only leads to ambiguity. In addition the three-fold subdivision of grain boundary relationships does not provide sufficient scope for the descriptive documentation of the predominant grain boundary types.

3.2.1 Proposed New Terminology

The microstructural terminology followed herein is considered to eliminate the ambiguities and genetic overtones inherent in the schemes of Katz (1968) and Moore (1970). In addition it is applicable not only to the granulites but also to the rocks from the transitional and amphibolite facies terrains. The new microstructural nomenclature is in part a modification of Moore's (1970) terminology and is in some regards similar to that proposed by Berthelsen (1960). It is intended to be purely descriptive and for that reason terms like 'flaser' and 'mylonitic' have been rejected.

When describing the microstructure of tectonites it is essential to state the orientation of the section being described¹. From an examination of the literature it is apparent that this is seldom considered, an omission which commonly leads to ambiguities (see Collerson and Etheridge, 1972). For example, a strongly lineated rock when viewed in a section normal to the lineation generally contains a significant proportion of equigranular grains. On the other hand in any section parallel to the lineation, significant proportions of the grains are inequidimensional, oriented with their longest dimension at low angles to the lineation. To facilitate the accurate description of the microstructures in many of the rocks being investigated, three orthogonal sections were cut.

The terminology used throughout this thesis is based on sections cut both normal to and parallel to the lineation, the orientation being specified in each case.

1. In this thesis the capital letter P, N or S following the specimen number refers to the section orientation with regard to the main linear feature in the rocks (see Figure 3.1).

The microstructures are classified into two main groups:

- (a) those with a predominantly granoblastic appearance;
- (b) those with a moderately to strongly developed (fine to medium grained) anastomosing layering which separates lozenge to ovoid shaped domains composed of single grains, or aggregates of xenoblastic¹ grains.

3.2.2 Discussion

3.2.2.1 Predominantly Granoblastic Rocks

The term granoblastic has been defined in a variety of ways:

1. 'The texture of a metamorphic rock composed of equidimensional elements'. Dictionary of Geological Terms, p.216 (American Geological Institute, 1962).
2. 'Mosaic of irregular grains or xenoblasts normally with well sutured boundaries'. Joplin (1968, p.28) (Moore, 1970, also follows this convention).
3. '... containing equidimensional generally xenoblastic crystals of approximately equal size'. Spry (1969, p.186).

Spry (1969, p.263) makes use of the term 'granoblastic elongate' to describe a texture where '... crystals tend to lie flat and elongate with their long and mean dimensions giving a foliation which is parallel to the axial surface of folds and their long dimensions parallel to the fold axis'. This usage is apparently similar to the term platy granoblastic (Katz, 1968; Moore, 1970).

In this thesis Joplin's usage of 'granoblastic' is followed. Some rocks (especially the quartzo-feldspathic varieties) have a weakly to strongly developed planar layering, defined by thin lenses of quartz. This is generally prominent in the P section. However, in some N sections the grains of certain layers exhibit a distinct dimensional preferred orientation. To describe this texture

-
1. Grains which lack crystal faces.

the terms granoblastic elongate or platy granoblastic are used.

Other rocks (although they are predominantly granoblastic) may be weakly banded (especially some of the transitional terrain quartzofeldspathic gneisses), the bands consisting of aggregates of tabular or prismatic crystals. The microstructure in these cases would be described as being 'predominantly granoblastic with lepidoblastic or nematoblastic domains'.

As was mentioned previously, Moore's (1970) subdivision of relative grain sizes into two subgroups of non-equidimensional grains, i.e. inequidimensional and seriate is not considered to be a necessary adjunct to the terminology of relative grain size. The term seriate has therefore been deleted from the new terminology, and only the terms equigranular and inequigranular¹ utilized. Berthelsen (1960, p.24) used the prefixes eu- and hemi- (granoblastic) in a similar manner.

The absolute grain sizes used to distinguish between fine, medium and coarse grained rocks are as proposed by Berthelsen (1960), viz:

1. fine; grains smaller than 1.0 mm diameter (but still visible with the naked eye);
2. medium; grains between 1.0 mm and 1.0 cm diameter;
3. coarse; grains greater than 1.0 cm diameter.

The methods of describing grain boundaries used by previous workers (Berthelsen, 1960; Katz, 1968; Moore, 1970) as mentioned above do not allow sufficient scope for adequate description. It is realized that a structural classification of grain boundaries (see Spry, 1969) is preferable. However, for a simple and easily applicable terminology, a purely descriptive approach has been utilized. Grain boundaries are classified on the basis of their shape (Figure 3.2). They can be described as being:

-
1. The definition of these two terms, taken from the Dictionary of Geological Terms are as follows: Equigranular; 'A textural term applied to rocks whose essential minerals are all of one order of size'. Inequigranular; 'A textural term applied to rocks whose essential minerals are of different orders of size.'

straight
 curved
 embayed
 scalloped
 sutured (1) lobate
 (2) serrated
 rational
 irrational

(from Spry 1969, p.19, fig.1).

With this classification it is then possible to describe boundaries in terms of several parameters.

3.2.2.2 Rocks with Anastomosing Layering

No adequate single term can be applied to these rocks without engendering genetic overtones (e.g. 'mylonitic', Moore, 1970). They are therefore best described in purely descriptive terms. The terms to describe the grain sizes, the appearance of the grain boundary relationships and the spatial distribution of the components of the anastomosing layers and diamond shaped domains can be those used above in the description of the granoblastic microstructures.

3.2.2.3 Summary

In summary, the terminology used herein is as follows: There are two broad types of microstructures; rocks are either granoblastic or display an anastomosing layering. The following terms are then used to describe each type:

- (a) Relative grain size; equigranular, inequigranular.
- (b) Absolute grain size; fine, medium, coarse.
- (c) Grain boundary shape; straight, curved, embayed, scalloped, sutured (lobate or serrated), rational, irrational.

3.3 PETROGRAPHY OF THE GRANULITE FACIES LITHOLOGIES

3.3.1 Mafic Lithologies

3.3.1.1 General Description

Mafic rocks are not as abundant as quartzo-feldspathic varieties are in the Amata area (Page 111). In the granulite facies terrain they crop out as discontinuous bands or lenses which are generally conformable with the layering and schistosity in the surrounding rocks (Figure 2.4a). Their melanocratic appearance contrasts strongly with the leucocratic nature of the quartzo-feldspathic varieties. Contacts between layers are generally sharp. Some units appear to 'thicken' and 'thin' along strike (for example at station 1862). They range in thickness from less than 1 cm to greater than 60 m and they vary in lateral extent from several metres to greater than 25 km.

The individual units are themselves commonly banded on a fine scale; intercalated mafic and ultramafic layers (e.g. specimen A325-950)¹; or leucocratic and melanocratic units (e.g. at station 1790) range in width from less than a few mm to greater than .25 m and they have sharp contacts.

In hand specimen the mafic granulites are medium to fine grained, grey to black in colour (depending on the ratio of ferromagnesian minerals to feldspar) and the major minerals are easily discernable with the aid of a hand lens.

Planar and linear fabrics are developed to varying extents in different units. They are defined either by the parallel alignment of elongate xenoblastic, or nematoblastic, grains of pyroxene, feldspar and/or hornblende (e.g. in A325-2000), by the clotting of aggregates of these phases (e.g. in A325-1115a) or by the alignment of these phases to produce a pronounced anastomosing schistosity (e.g. in A325-1848).

3.3.1.2 Mineral Assemblages

The mafic granulites are composed of varying proportions of the

1. Specimens mentioned in the text are housed in the collection of the Department of Geology and Mineralogy, University of Adelaide. Locations of specimens are given in Figure A.1.1.

following phases: plagioclase, orthopyroxene and clinopyroxene. Garnet, hornblende, scapolite, biotite and opaque oxides (e.g. magnetite, ilmenohaematite, haemo-ilmenite, ilmenite, haematite and rutile) may or may not be present depending on the host rock composition. Minerals present in accessory amounts include alkali feldspar, quartz, spinel, pyrite and apatite. Secondary garnet, clinopyroxene and amphibole in addition to sericite and epidote are present in minor amounts. However, on the basis of microstructural relationships, these phases are not believed to be related to the granulite facies paragenesis.

The mineral assemblages¹ recognised in the mafic granulites are as listed below.

1. plagioclase - orthopyroxene - clinopyroxene - hornblende - scapolite - opaques ± (biotite) ± alkali feldspar
2. plagioclase - orthopyroxene - clinopyroxene - scapolite - opaques ± (biotite)
3. plagioclase - orthopyroxene - hornblende - scapolite - opaques ± (clinopyroxene)
4. plagioclase - orthopyroxene - clinopyroxene - hornblende - garnet - opaques
5. plagioclase - orthopyroxene - clinopyroxene - garnet
6. plagioclase - orthopyroxene - clinopyroxene - garnet - opaques ± (biotite)

1. The term mineral assemblage refers to all minerals which have been observed (in polished and thin sections) to be in mutual contact with one another (Korzhinskii, 1959). In recognising the mineral assemblages, care was taken to ensure that the minerals were equilibrated during the same metamorphic event. This interpretation was mainly based on the nature of the grain contacts, i.e. they were sharp and did not display features which were suggestive of mutual reaction between phases (except for those phases which were formed by late stage retrogression). No estimate of mineral percentages is indicated in the individual assemblages. The minerals listed in parenthesis are only present in subordinate amounts. The phases present in accessory amounts are not taken into consideration in the lists of assemblages. Because of inhomogeneity in some of the lithologies more than one assemblage is often present in a given specimen.

7. plagioclase - orthopyroxene - clinopyroxene - opaques ± (hornblende)
± (biotite)
8. plagioclase - orthopyroxene - clinopyroxene - hornblende
9. plagioclase - orthopyroxene - clinopyroxene - opaques ± (biotite)
± quartz
10. plagioclase - orthopyroxene - clinopyroxene ± (quartz) ± (alkali
feldspar)
11. plagioclase - orthopyroxene - clinopyroxene - opaques - alkali
feldspar ± (biotite) ± (hornblende)

From a total of forty-eight mafic granulites examined in thin section, 46% belong to assemblage 9 and 15% to assemblage 11.

Modal analytical data for the chemically analysed mafic granulites are listed in Table 4.1. These values, together with additional visual modal estimates indicate that the major phases vary within the following ranges: plagioclase (16%-76%), orthopyroxene (5%-36%), clinopyroxene (2%-38%), hornblende (0%-14%), garnet (0%-35%), opaque oxides (0%-10%) and scapolite (0%-9%).

3.3.1.3 Microstructures

Under the microscope the mafic granulites are composed of equigranular or inequigranular granoblastic grains (Figure 3.3a,b, 3.4a,c) with straight or gently curved grain boundaries. These grains are commonly strongly polygonal and display excellently developed triple point junctions. In sections parallel to the lineation the xenoblastic grains have a weak to strong dimensional preferred orientation. In some sections the schistosity is accompanied by intercalated compositional bands (generally less than 1.0 mm wide) of elongate xenoblastic ferromagnesian and feldspathic phases (Figure 3.3b).

The original granoblastic microstructures have been modified in some rocks by the effects of later deformation (e.g. in A325-62, -542 and -1848N), resulting in the development of a fine grained anastomosing layering which engulfs and commonly penetrates the pre-existing xenoblastic grains, causing some of the grains to assume a brecciated

appearance. In some lithologies the anastomosing zones are more widely spaced. The inter-zone regions are composed of equigranular or inequigranular granoblastic aggregates of grains. The coronas occurring in some rocks are a further secondary development.

3.3.1.4 Descriptive Mineralogy

Plagioclase (An42-77) occurs in equidimensional to elongate xenoblastic grains. Grain interfaces involving plagioclase are usually straight or slightly curved; boundaries between adjacent ferromagnesian phases are usually embayed or curved. Triple point junctions are commonly developed where plagioclase grains impinge on one another. Grains commonly show undulose extinction indicating that the plagioclase has been strained. Glide or mechanical twinning on the albite and pericline laws are common. These twins appear to be wedge shaped, i.e. they taper rapidly and frequently terminate within grains. They vary in thickness from less than 0.002 mm to .01 mm. Kink bands occur, apparently unrelated to the crystallographic orientations of plagioclase. Between crossed nicols the deformation bands are readily visible because of the variation in optical orientation and hence extinction position. The deformation bands have sharp boundaries and individual bands commonly exceed 0.16 mm in width. The mechanical twins don't appear to cross the kink bands. Different sets of mechanical twins are commonly developed in adjacent bands.

The plagioclase is commonly antiperthitic. The alkali feldspar blebs are irregular in outline and distribution. They range in size from less than 0.005 x 0.018 mm to 0.16 x 0.08 mm. In some of the antiperthitic plagioclase the alkali feldspars inclusions are spindle shaped while in others they appear to be roughly ovoid although slightly irregular in outline. In some sections the blebs are haphazardly distributed within the host whereas in other sections they appear to be aligned into regular trains.

Some plagioclase grains are kinked parallel to the twin direction causing the twin lamellae to impinge on one another producing chevron shaped patterns. Kink bands are also observed

normal to glide lamellae in which cases the lamellae themselves are gently bent (Figure 3.5b).

In some sections the plagioclase grains are extensively fractured. There is some suggestion that the glide twins are related to the fracturing deformation as it is apparent that the twin lamellae stop abruptly at fracture planes. The fracture planes appear dark in plane light. This is caused by the presence of fine opaque material.

Minute needle-like inclusions are abundant in some of the plagioclase. In contrast other grains are virtually clear. The most common inclusions are acicular needles of sillimanite (?). These inclusions appear to have nucleated along plagioclase-plagioclase interfaces and also along interfaces between plagioclase and other phases. They are extremely fine grained averaging 0.002×0.020 mm in size. The needles appear to be arranged along definite crystallographic directions; for example in A325-2000P one prominent set appears to be aligned parallel to the (010) direction. Two other sets are inclined at a high angle to this direction. Inclusions of epidote (?) are also abundant in some grains. They occur as randomly oriented extremely delicate needles or angular plates.

In contrast, other mafic granulites, especially those which lack extensive coronal development around ferromagnesian phases are virtually free from such inclusions, e.g. A325-1117a and -1104a.

Orthopyroxene (both hypersthene and bronzite are identified by optical properties and analyses) is constantly found in these rocks. It is characterised by its typical pleochroism (green to pink) which ranges from extremely intense to rather weak, and also its low birefringence and straight extinction (in most sections). The following pleochroic schemes have been observed in different sections:

α	pink
β	pale yellow, green
γ	pale green
α	pink
β	pale pink
γ	pale green

α pink
 $\beta=\gamma$ pale green

with $\alpha > \beta > \gamma$ or $\alpha > \beta = \gamma$

The orthopyroxene is commonly associated with other ferromagnesian phases, e.g. hornblende, clinopyroxene and garnet. It occurs as xenoblastic grains which display straight or gently rounded interfaces with surrounding phases, notably plagioclase and hornblende (Figures 3.4b, 3.8b). These boundaries are invariably irrational. Grain sizes range from less than 0.2 x 0.2 mm to greater than 6.0 x 1.5 mm. In some sections grain sizes are distinctly bimodal and the microstructures appear to be porphyroblastic (e.g. in A325-137P).

The intensity of pleochroic colours commonly varies within individual grains, suggesting that they may be compositionally zoned (this is assuming that pleochroic colour and composition are related, see Chapter 4.3).

The orthopyroxenes commonly contain abundant opaque to slightly translucent platy or needle-like inclusions aligned parallel to (010) or (001). They are ilmenite or brookite.

Fine needle-like inclusions of rutile are present in some of the orthopyroxene grains (e.g. A325-2000P). Moore (1968) observed similar needles in orthopyroxenes from Gosse Pile. The needles have straight extinction, high birefringence colours and refractive indices greater than the surrounding orthopyroxene. Some needles are extremely elongate up to 0.16 x 0.001 mm in size. No anomalous elongation effects have been observed (cf. Griffin *et al.*, 1971).

Exsolution blebs of clinopyroxene are frequently aligned parallel with (100) of the host orthopyroxene. They are elongate and commonly reach 0.2 x 0.02 mm. They are easily distinguishable from the orthopyroxene host grains by their higher birefringence, extinction angle and optical sign. Likewise orthopyroxene exsolution lamellae are developed in clinopyroxene host grains (Figure 3.6c). In addition to these lamellae the orthopyroxene xenoblasts exhibit fine striations parallel to (100); a feature which is strongly suggestive

of polysynthetic twinning. However they are believed to be due to finely intergrown clinopyroxene. They transect grains and are seldom wider than 0.004 mm.

Coronal microstructures are frequently developed around orthopyroxene grains. They consist of clinopyroxene, pale green pleochroic amphibole and garnet (Figure 3.7a, b, c). These coronas are believed to be secondary features.

Post crystallization effects are manifest in the presence of kink bands (e.g. in A325-1152N), bent cleavage traces and undulose extinction.

Pale green to colourless non pleochroic clinopyroxene is observed in most of the mafic granulites. Chemical analyses and optical properties indicate that clinopyroxene compositions are salite and augite (see Figure 4.24). The clinopyroxenes are optically positive and have a strongly developed (100) parting. Flat-stage maximum Z^c 's ranged from 36° - 46° . The colour is often masked by the presence of abundant opaque needles or small blebs, up to 0.008×0.001 mm in size (Figure 3.7c). These inclusions are frequently aligned in clusters parallel to the (100) parting producing a distinctive banded effect. In other grains they appear to have a random distribution. In some orientations they are concentrated towards the cores of grains whereas in others they congregate along the margins. Some of the inclusions have knee-shaped outlines, a feature commonly associated with rutile. The clinopyroxene is generally xenoblastic and ranges in grain size from less than 0.1×0.1 mm to greater than 2.0×0.9 mm. It forms mosaic-like aggregates with orthopyroxene, hornblende, garnet, plagioclase and scapolite. Grain interfaces are commonly irrational and they are slightly to strongly curved. In several sections, e.g. A325-953cN and -1133N, grains are strongly embayed and intergrown with plagioclase laths, suggestive of a possible relict igneous microstructure. Rational boundaries frequently result from these intergrowths. Simple twins on (100) are well developed in some sections, e.g. A325-953cN and -1861N.

Post crystallisation deformation is manifest in the

fracturing of grains, bending of cleavage traces and the occasional development of kink bands (A325-118P).

Hornblende has been observed in contact with all the main ferromagnesian phases. It forms irregular xenoblastic to subidioblastic grains (average size 0.4 x 0.4 mm, although some grains exceed 2.5 x 1.5 mm in inequigranular granoblastic specimens) and frequently shows marked elongation in P sections, the elongation being parallel to the (110) or (010) faces. Grain interfaces are generally smooth and predominantly curved or embayed. Rational boundaries parallelling the {110} form are also commonly present. Strongly embayed boundaries express intergrowth microstructures especially with orthopyroxene (Figure 3.8b). These embayed microstructures are interpreted as preserved high interfacial energy interfaces which have been unable to achieve grain boundary equilibrium during crystallisation, rather than reaction intergrowths (cf. Binns, 1964, Fig.9, p.299).

Examples of hornblende pleochroic schemes are as follows:

α pale green
 β green
 γ brown green

and intensity $\gamma > \beta > \alpha$ e.g. A325-1117a, -137

α neutral to pale green
 β green brown
 γ brown to brown green

and intensity $\gamma > \beta > \alpha$ e.g. A325-1104a, -1169

α pale yellow
 β orange brown
 γ orange brown

and intensity $\gamma > \beta > \alpha$ e.g. A325-1105

α neutral
 β brown
 γ breen

and intensity $\gamma > \beta > \alpha$ e.g. A325-1139

Z^c's range between 16° and 22°.

Pleochroic colours are frequently difficult to discern because of the presence of hordes of minute opaque inclusions (positive identification has not been possible for these inclusions).

Coronal microstructures are commonly developed around hornblende, generally in the form of radiating grains of secondary amphibole (cummingtonite) and granular garnets.

Pale pink, polygonal xenoblastic grains of primary garnet (almandine-pyrope) occur in some assemblages. The garnets form elongated aggregates which are either monominerallic or involve other ferromagnesian constituents and felsic phases. The aggregates are generally even grained, averaging 0.2 x 0.2 mm in grain size. Interfaces between garnets are generally smoothly curved (either convex or concave) or straight, for example in A325-1105N and -949bN and -137N. Against opaque oxides and other ferromagnesian phases (e.g. in A325-1115aN) they form smooth straight or curved interfaces, whereas against feldspars the interfaces are strongly embayed. Grains are invariably extensively fractured. Some of these fractures and patches within the garnets are slightly birefringent. Fractures are also sites for concentrations of finely granular opaque oxides (predominantly magnetite although ilmenite and haematite have also been identified).

The garnets are rarely markedly poikiloblastic as in A325-949N where xenoblastic grains of green spinel and small idioblastic laths of corundum averaging 0.16 x 0.02 mm are observed as inclusions. Spinel and corundum also commonly occur in interfacial regions within garnet aggregates. The corundum grain boundaries are invariably rational and the spinel boundaries are either straight or curved. Inclusions of spinel in garnet have smooth curved interfaces and form spherical shapes.

No garnet-quartz symplectites have been observed.

Xenoblastic to subidioblastic grains of 'secondary' garnet commonly form coronal microstructures around opaque oxides, hornblende, clinopyroxene, orthopyroxene and biotite. Coronas are either monominerallic or are associated with other secondary phases, for example

clinopyroxene and amphibole (cummingtonite) (see sections A325-1848N and -953bP). Idioblastic boundaries are commonly developed where the garnets are in contact with plagioclase grains.

The coronas appear to be characteristic of the lithologies containing clouded plagioclase. In comparison, lithologies which lack coronal development are typified by clear feldspars.

As well as forming coronas, secondary garnets are aligned along grain interfaces which roughly define the attitude of the anastomosing fractures already mentioned (3.3.1.2). These features are believed to indicate that much of the secondary garnet growth could have taken place during, or in response to, the deformation (D_4 ?) which was responsible for the fracturing. Also, much of the coronal development may have occurred during this event. Similarly the development of clouded plagioclase may have taken place at this time.

Scapolite (var. mizzonite - from analysis and optical properties) occurs as colourless discrete xenoblastic polygonal grains or aggregates of grains with smooth, straight or curved boundaries. Grains are either equigranular or distinctly bimodal, e.g. averaging 0.4 x 0.2 mm and 1.0 x 0.3 mm. Low birefringent grains are distinguishable from untwinned plagioclase by their uniaxial negative optics. Their slightly elongate nature contributes to the expression of the schistosity. (100) partings are generally prominent but (110) cleavages are less distinct. In A315-1139N and -1133N, minute needle like opaque inclusions are commonly aligned parallel to (100).

The aggregates of scapolite are generally restricted to plagioclase rich areas; there is no suggestion from microstructural relationships that the feldspars are unstable with respect to the scapolite. Grain boundaries are strongly suggestive of low interfacial energies, i.e. the phases may be regarded as being in microstructural equilibrium.

Alkali feldspar occurs in two forms:

1. as discrete grains which are frequently microperthitic;

2. in antiperthite.

The former type of occurrence has only once been observed as an essential feature of the mafic rocks, e.g. A325-1133N. The alkali feldspar is untwinned and is free from needle like inclusions, c.f. plagioclase. Grains range in size up to 0.6 x 0.6 mm. Grain boundaries are smooth and gently curved. Some grains show undulose extinction.

Pseudo-myrmekitic quartz occurs as a minor constituent in the fractured feldspar grains as small irregular blebs showing undulose extinction (e.g. in A325-118P). They seldom exceed 0.16 x 0.08 mm in size. Tilley (1921) observed similar quartz in fractured feldspars from Eyre Peninsula and considered that it developed in response to a later deformational event (which was responsible for the formation of the fractured microstructure) as a result of frictional heat.

The fractured plagioclase grains showing this development are characteristically altered to sericite and epidote. Liberation of quartz could be an expected accompaniment to the retrograde plagioclase to sericite and epidote breakdown, facilitated in this by the easier movement of water through the fractured plagioclase. It seems unnecessary to invoke frictional heat as a source of energy in the non-fractured rocks.

Small subidioblastic to idioblastic laths, singly or in decussate clusters, of biotite (and possibly phlogopite) are a minor phase in some of the mafic granulites. Grain boundaries are generally smooth, straight and rational (parallel to (001)) although kink development occasionally causes deviations from this pattern.

The biotite flocks are strongly pleochroic:

α	neutral
$\beta=\gamma$	red orange
α	neutral to straw yellow
$\beta=\gamma$	deep red
α	yellow
$\beta=\gamma$	orange brown

being the most observed schemes.

Kink bands in biotite are characterised by strongly serrated axial plane traces. New grains are occasionally nucleated in these regions. The kinks are generally oriented normal to the (001) cleavage. Thin slivers of alkali feldspar occur as oriented inclusions parallel to (001) within the biotite, e.g. in A325-118P. Deformation of the biotites is also manifested by undulose extinction.

The most common accessory mineral is apatite, which occurs as idioblastic stumpy laths. Subordinate accessory phases include idioblastic to subidioblastic cloudy zircons, xenoblastic or idioblastic green spinel (the idioblastic variety occurring as needles in ilmenite) and idioblastic laths and aggregates of corundum. Some corundum occurs as inclusion in grains of ilmenite or spinel. In A325-949, coronal microstructures of corundum and spinel are prominent. The spinel and corundum are frequently surrounded by fibrous radiating coronas of a pale blue fibrous to prismatic mineral identified tentatively as margarite.

Ilmenite with varying amounts of haematite exsolution, and magnetite (showing alteration to martite parallel to (111)) are present in varying amounts in the mafic granulites.

The ilmenite and magnetite occur as xenoblastic grains (average size 1.3 x 1.3 mm) occasionally forming polygonal grano-blastic aggregates with smooth straight or gently curved interfaces. However in the same section they may be found in juxtaposition with each other as large irregular grains. Some ilmenite and magnetite grains contain long needle like blebs of spinel. Pyrite occurs rarely (e.g. in A325-121P, -158P) as idioblastic grains averaging 0.04 x 0.04 mm, as does rutile.

3.3.2 Ultramafic Lithologies

3.3.2.1 General Description

The ultramafic granulites constitute less than one percent of the granulite varieties. They are composed essentially of orthopyroxene, clinopyroxene, hornblende and phlogopite. In hand specimen they are extremely dense, medium to fine grained and distinctly

melanocratic (dark grey to grey green in colour). Many specimens exhibit a prominent parallel compositional banding, e.g. A325-2050a.

Weathered surfaces are rusty black-brown to orange-brown in colour. Individual bands rarely exceed 5 mm in width. Pyroxenes and amphiboles are discernable with the aid of a hand lens.

In the field they crop out as lensoidal intercalations within the quartzo-feldspathic granulite sequence in a similar manner to the mafic granulites. Because of the absence of felsic layers, schistosity is commonly difficult to perceive. However, with careful observation the schistosity and also a mineralogical lineation can generally be recognised.

3.3.2.2 Mineral Assemblages

In thin section the following minerals can be seen: orthopyroxene, clinopyroxene, hornblende, phlogopite, spinel, scapolite, opaque oxides, plagioclase, rutile, epidote(?), clinozoisite(?) and secondary amphibole.

The epidote group minerals and the secondary amphibole are not representative of the granulite facies paragenesis and are considered to have formed during a later event.

Assemblages of the essential phases are:

1. orthopyroxene - clinopyroxene - hornblende - opaques
2. orthopyroxene - clinopyroxene - hornblende - scapolite
3. orthopyroxene - clinopyroxene - hornblende ± (plagioclase)
4. orthopyroxene - clinopyroxene - hornblende - spinel ± (plagioclase)
± phlogopite
5. orthopyroxene - clinopyroxene - hornblende - phlogopite ±
(plagioclase) ± scapolite
6. orthopyroxene - clinopyroxene - hornblende

Visual and micrometric techniques indicate the following abundances of the major phases; orthopyroxene 30-90%, clinopyroxene 10-70%, hornblende 0-35%, spinel tr-10%, and phlogopite 0-5%.

3.3.2.3 Microstructures

Microstructures are dominated by the presence of xenoblastic pyroxene grains which form equigranular or inequigranular aggregates, best seen in the N orientation (Figure 3.8c). In the P orientation, grains are generally elongate and their prismatic nature becomes apparent. A mineral elongation-type lineation and schistosity is defined by elipsoidal clusters of inequidimensional xenoblastic grains which parallel the compositional layering. Grain boundaries are generally irrational and smoothly straight or curved to embayed. Usually there is a dominant type of grain interface in each lithology, e.g. A325-131 is dominated by straight boundaries and well developed triple point junctions whereas A325-2050c is characterised by a preponderance of curved or gently embayed grain interfaces. Examples of rare rational grain interfaces are:

- (a) in orthopyroxene-spinel, or orthopyroxene clinopyroxene aggregates the interfaces are parallel to the (010) direction in the orthopyroxene;
- (b) in hornblende-pyroxene or hornblende-spinel aggregates the interfaces involve the form {110} in the amphibole.

Inclusions of one ferromagnesian phase in another are commonly rounded to spherical in outline. However, straight or gently curved xenoblastic to subidioblastic clinopyroxene intergrowths in orthopyroxene have been observed (Figure 3.8a).

3.3.2.4 Descriptive Mineralogy

Orthopyroxene; (bronzite to enstatite - from optical properties) and clinopyroxene (both augite and diopside), which are the principal phases in the ultramafic granulites, form interlocking mosaics of xenoblastic grains. In some lithologies the grains are equidimensional, in others they are predominantly inequidimensional. Grain sizes range from an average of 0.8 x 0.8 mm up to 7.0 x 3.0 mm. Some of the largest orthopyroxenes are poikiloblastic, with angular subidioblastic to xenoblastic inclusions of clinopyroxene (Figure 3.8a).

Orthopyroxene is either strongly or weakly pleochroic, the following colours predominating:

- α pink
- β neutral to pale yellow
- γ pale yellow to pale green

Some grains are biaxial positive whereas others are negative. Deformation twins, fine lamellar twinning and kink bands are abundant features and provide ample evidence for post-crystallization deformation (Figure 3.7d). Some deformation bands exceed 0.04 mm in width.

Narrow coronas of secondary amphibole (cummingtonite(?)) secondary clinopyroxene, garnet(?) and epidote are commonly observed at orthopyroxene-plagioclase boundaries. In extreme cases the plagioclase is completely replaced by radiating fibrous cummingtonite and blades of epidote. The orthopyroxene also forms coronas where in contact with scapolite. These are generally composed of an inner core of clinopyroxene with a rim of opaque granules in epidote.

Acicular inclusions of a highly birefringent phase with refractive indices greater than the host (orthopyroxene) have been observed in orthopyroxenes from A325-2050bN and A325-2050cN. They range in size from less than 0.02 x 0.002 mm to greater than 0.2 x 0.001 mm and they are oriented in three directions at approximately 60° to one another in the (010) plane of the host (Figure 3.6d). Some are slightly curved and others are possibly helical, i.e. under high power they appear to twist as the focus is maintained. Although it is difficult to determine their extinction position because of their size relative to the thickness of the birefringent host, it appears that some show parallel extinction while others in the same host grain exhibit oblique extinction. The inclusions have tentatively been identified as rutile. They are similar in appearance to rutile inclusion in orthopyroxene identified optically and verified by microprobe from the Tomkinson Ranges by Moore (1968).

The presence of rutile inclusions in orthopyroxene was

initially suggested by Howie (1963, p.220) to account for the anomalously high TiO_2 contents shown by some pyroxenes. Moore (1968) first observed its occurrence in igneous orthopyroxenes in orthopyroxenites from the Giles Complex (central Australia). He believed that it was a high pressure exsolution feature which occurred following Ti incorporation into the pyroxene structure during the high temperature magmatic stage of the formation of the rock.

Griffin et al. (1971) recently reported anomalously elongated rutile as inclusions in garnet and orthopyroxene from eclogitic xenoliths in kimberlites and from mafic and eclogitic pods associated with certain Norwegian anorthosites. These authors suggested that the development of anomalous elongation was also favoured by specific environmental conditions, notably by exsolution at high temperatures and pressures.

Metamorphic assemblages indicate that the Amata terrain attained mineralogical equilibrium during the granulite facies metamorphism. The presence of rutile in the orthopyroxenes from certain lithologies, and its absence from others of approximately the same mineralogical (and probably chemical) composition, is interpreted to reflect subtle chemical differences in the progenitors of the ultramafic and mafic lithologies rather than slight pressure and temperature differences throughout the area.

Moore (1968) only found rutile-bearing orthopyroxene in igneous rocks (orthopyroxenites). In the Amata area it has been observed in metamorphic lithologies containing abundant other minerals including clinopyroxene, phlogopite, almandine, plagioclase, hornblende, and scapolite.

The interpretation that the rutile formed by exsolution from geochemically favourable orthopyroxenes at high pressures is not inconsistent with the high pressure environment postulated for the Amata terrain on other evidence (see Chapters 4 and 5).

The clinopyroxene occurs as pale green to colourless xenoblasts. Some grains are faintly pleochroic; neutral to pale green. Other grains are either non pleochroic or the pleochroism is masked by their

turbid appearance due to the presence of opaque inclusions. Z^c 's range from 37° to 48° . Deformation lamellae are commonly well developed.

Coronas are not common between clinopyroxene and either plagioclase or scapolite.

Hornblende is abundant in some ultramafic granulites, e.g. A325-2050c, -2050d and -952. However it is only present in minor amounts in others, e.g. A325-131. It forms sharp straight, curved or embayed contacts with orthopyroxene and clinopyroxene. Some grains measure up to 2.5×2.0 mm in size (e.g. in A325-952N). Parallel to the lineation direction some grains exceed 4.00 mm in length (e.g. in A325-952P). Although hornblende grains are frequently intergrown with orthopyroxene there is no suggestion of a reaction relationship. The evidence indicates that the hornblende and the pyroxenes crystallized contemporaneously.

The following pleochroic schemes have been observed:

α	neutral
β	green brown
γ	brown
α	neutral
β	pale green to green brown
γ	pale green brown

with intensity $\gamma > \beta > \alpha$

Some sections of amphibole are biaxial positive; others are negative. Chemical data for A325-2050c indicates that the primary amphibole (biaxial negative) is magnesium hornblende. However the positive sign in others suggests the existence also of a pargasitic amphibole.

Simple twins are occasionally observed. Inclusions of opaque oxides aligned in two directions within the form $\{110\}$ frequently mask the pleochroic colours, e.g. in A325-2050c. In other sections however, the hornblendes are free of such inclusions. Some of the longer grains exhibit undulose extinction and fine parallel mechanical twins.

Narrow coronas of cummingtonite and epidote are common at plagioclase-hornblende interfaces.

Large olive-apple green, irregular xenoblastic grains of spinel¹ (up to 1.5 x 1.5 mm in size) form 'eutectoid' to skeletal intergrowths with the ferromagnesian phases. They are isotropic and under plane light can be seen to contain haphazardly distributed blebs of ilmenite. Some of the larger grains are quite poikiloblastic and contain inclusions of orthopyroxene.

Corundum forms idioblastic to subidioblastic needles or plates up to 0.5 x 0.5 mm in size, partially or wholly enclosed by spinel. It is easily distinguished by its colourless appearance, high refractive index, uniaxial negative character, low birefringence, straight extinction and strong basal parting.

Phlogopite forms narrow subidioblastic flakes (with rational or irrational boundaries) ranging in size from 0.3 x 0.3 mm to greater than 1.2 x 0.4 mm. The pleochroism is:

α colourless

$\beta = \gamma$ orange

with the following intensity $\gamma = \beta > \alpha$

Minerals present in accessory quantities include apatite, epidote, cummingtonite, rutile, secondary garnet, clinopyroxene and opaque oxides.

Traces of scapolite and plagioclase occur as small xenoblastic grains interstitial to the ferromagnesian phases. Reaction coronas with orthopyroxene and hornblende are invariable present at grain interfaces.

1. Which are probably members of the pleonaste-hercynite group because of their colour.

3.3.3 Quartzo-feldspathic Lithologies

3.3.3.1 General Description

Quartzo-feldspathic granulites are the most commonly observed compositional varieties found in the granulite facies terrain. They occur in discrete layers which can be differentiated on the basis of compositional and microstructural characteristics. The units range in width from several millimetres to more than 10 metres (however, most are between 1 and 3 metres). They are seldom traced for any significant distance along strike because they are markedly lensoidal. Because of their relative thinness and discontinuous nature, on the scale of the field mapping it was not feasible to map unit for unit.

The quartzo-feldspathic granulites are commonly strongly lineated and they generally have a weak to strongly developed schistosity which parallels the compositional layering.

In hand specimen they are fine to medium grained. They have a greasy grey-blue to grey-green appearance on freshly broken surfaces. Some of the alkali-feldspar-rich lithologies are coloured pale yellow to grey-white. Weathered surfaces are orange brown to yellow white in colour. The zone of alteration seldom extends for more than a few millimetres.

Pyroxene, garnet, feldspar and quartz can all be easily distinguished in the hand specimen with the assistance of a hand lens.

During field mapping, four varieties of quartzo-feldspathic granulite were differentiated on the basis of hand specimen characteristics (for distribution, see Figure 1.3). These are as follows:

- (a) fine to medium grained granulite containing hypersthene and thin platy layers of quartz. They occasionally contain large lozenge shaped feldspar aggregates which are surrounded by anastomosing layers of quartz.
- (b) medium to coarse grained granulites in which ferromagnesian constituents are rare or absent.
- (c) fine to medium grained porphyroblastic garnetiferous granulite in which hypersthene may or may not be present.

(d) finely interbanded quartzo-feldspathic and mafic granulite
(Figure 2.4a).

3.3.3.2 Mineral Assemblages

Under the microscope the quartzo-feldspathic granulites are seen to consist of varying assemblages of the following primary phases: quartz, alkali feldspar, plagioclase, hypersthene, clinopyroxene, garnet, apatite, zircon, allanite and opaque oxides (dominantly magnetite). Secondary biotite, garnet, diopside, and cummingtonite are also commonly observed. Margarite is present as an alteration product of corundum and sillimanite.

The mineral assemblages which were observed in the sequence of quartzo-feldspathic granulites are listed below:

1. quartz - alkali feldspar - opaques
2. quartz - alkali feldspar - orthopyroxene - opaques
3. quartz - alkali feldspar - orthopyroxene - clinopyroxene - opaques
4. quartz - alkali feldspar - plagioclase - orthopyroxene - clinopyroxene - opaques ± (hornblende)
5. quartz - alkali feldspar - plagioclase - orthopyroxene - opaques
6. quartz - alkali feldspar - garnet - opaques
7. quartz - alkali feldspar - orthopyroxene - garnet - opaques
8. quartz - alkali feldspar - plagioclase - orthopyroxene - garnet - opaques
9. quartz - alkali feldspar - plagioclase - garnet - opaques
10. quartz - plagioclase - orthopyroxene - opaques
11. quartz - plagioclase - orthopyroxene - clinopyroxene - opaques

Perthite and mesoperthite are considered with alkali feldspar in this listing. Likewise antiperthite is considered with plagioclase. Accessory phases include apatite, zircon and allanite.

Micrometric analyses and visual estimates of the modal

composition of some of the quartzo-feldspathic granulites reveals the following abundances: quartz (20-50%), alkali feldspar, including perthite and antiperthite (0-60%), plagioclase, including antiperthite (0-70%), orthopyroxene (0-10%) clinopyroxene (0-5%), garnet (0-20%), opaques (tr-3%).

3.3.3.3 Microstructures

The quartzo-feldspathic granulites are predominantly inequigranular (in the P section); however, sections normal to the lineation contain arrays of grains which are more equigranular (see Figure 3.9a,b).

Three microstructural varieties have been recognised:

- (a) those that are granoblastic to platy granoblastic. In the P orientation these are characterised by aggregates of lenticular to platy quartz (and sometimes feldspar), e.g. Figure 3.10b. The lenticular plates are commonly more abundant in the quartz rich domains. The intervening areas consist of granoblastic aggregates of feldspar together with minor quartz and pyroxene.
- (b) those containing lozenge shaped granoblastic aggregates of feldspar in a platy granoblastic to granoblastic groundmass in which the elongate layers weakly anastomose around the coarse grained diamond shaped domains, e.g. Figure 3.10c.
- (c) porphyroblastic varieties with groundmasses consisting of platy granoblastic to granoblastic quartz, feldspar and pyroxene. The elongate tabular elements of the groundmass are commonly deflected by the porphyroblasts (e.g. Figures 3.6b, 3.10a).

The microstructures are commonly quite variable even on the scale of a single thin section (Figure 3.9c).

Absolute grain sizes range from fine to medium. More coarse grained varieties are rare, e.g. the type b, lozenge shaped aggregates.

Grain interfaces are smoothly straight, curved, embayed or

sutured, depending on the microstructural maturity¹ of the aggregates.

3.3.3.4 Descriptive Mineralogy

The individual elongate lenticular grains of quartz range up to 2.0 cm x 0.9 mm in size. They show undulose or crisp extinction. Some of the larger lenticles (up to 4 cms in length) are composed of smaller subgrains which have sharp to highly serrated subgrain boundaries normal to the direction of extension of the quartz grain. Deformation bands are common in the larger strained grains. Recrystallized grains of quartz form polygonal granoblastic arrays along subgrain interfaces, or at the margins of the lenticles. The recrystallized grains have sharp extinction, straight to serrated grain boundaries and they average 0.04 mm in diameter. Böhm lamellae are uncommon.

The alkali feldspar is never twinned and is commonly difficult to identify unless the slides are stained with sodium cobaltinitrite. X-ray diffraction studies indicate that it is in a disordered state, i.e. it has the structure of orthoclase (see Chapter 4.3). It invariably contains exsolved albite which forms stringlet, string-thread and bead perthites (Eskola, 1952, termed these hair-perthites). Ribbon-type exsolution results in the formation of mesoperthite (Figure 3.5a). The alkali feldspar occurs as irregular xenoblastic equidimensional to nonequidimensional grains with straight, curved, sutured or embayed grain interfaces. Grain sizes range between 0.1 x 0.05 mm and 0.9 x 0.4 mm although some larger grains have been observed (up to 4.6 x 1.0 mm in A325-239b). Grains commonly exhibit undulose extinction and no evidence of recrystallization has been observed. The grains of perthite and mesoperthite are surrounded by a rim of

-
1. The presently observed microstructures do not necessarily represent those which formed initially during the granulite facies metamorphism. It is believed that recrystallization and grain growth, to achieve arrays with minimum interfacial free energy, could have occurred after the granulites had crystallized while, however, cooling was still taking place. Similar interpretations of microstructures, based on grain growth in the solid state, have been made by Smith (1948, 1953, 1964), Kretz (1966), Binns (1964), Vernon (1968, 1970) and Flinn (1971), for geological materials.

orthoclase which is in optical continuity with the host and is free of any traces of exsolution.

Plagioclase (An30-37) is present in varying amounts. It forms xenoblastic grains (average size 0.4 x 0.4 mm) which are commonly intergrown with quartz and alkali feldspar. Grains are frequently elongate and are aligned parallel to the schistosity. Lozenge shaped granoblastic aggregates of grains averaging 1.2 x 0.6 mm reach 2 cm x .5 cm in size. The feldspar is commonly twinned, usually on the albite law(?), a feature which is believed to be due to deformation. Pericline twins are less commonly developed. Bleb and stringer potash feldspar exsolution is a common feature of the plagioclase. The antiperthitic plagioclase is generally twinned and the exsolved alkali feldspar blebs are commonly aligned parallel to (010) although some appear to transgress the twin orientation.

Extremely fine grained needles of sillimanite form sheaf-like clusters at grain interfaces and also occur as inclusions (e.g. in A325-1165aP,N and -907FP).

The garnets (almandine-pyrope) occur as aggregates aligned parallel to the lineation. They are dark red in hand specimen and pale pink in thin section. Analyses are given in Chapter 4.3. They occur as large idioblastic to xenoblastic porphyroblasts up to 10 x 15 mm (A325-1121P), and also as a groundmass constituents (ranging between 0.2 x 0.2 mm and 0.5 x 1.0 mm in size). They are frequently poikiloblastic with contained angular to rounded inclusions of quartz biotite, alkali feldspar, opaques, spinel and zircon. Flakes of biotite and opaque oxides are common at garnet margins - possibly indicating that the garnets are undergoing mild retrogression. There is some evidence of post or syn-tectonic crystallization in A327-76P. Small grains of quartz and feldspar occur as inclusions in the marginal zone of some idioblastic porphyroblasts.

Extremely small colourless needles of an unidentified phase are present as inclusions in garnets from A325-927N and 1175P. They range in size up to 0.1 x .002 mm. They exhibit oblique extinction, high birefringence and high refractive indices. They occur in three sets

at approximately 60° to each other. In appearance they are similar to the rutile needles identified in the orthopyroxene from A325-2050c.

Hypersthene occurs either as small isolated subidioblastic to xenoblastic, prismatic grains ranging in size from 0.13×0.06 mm to 2.0×0.7 mm, or as aggregates of grains. It is distinctly pleochroic.

α pale pink
 β pale pink-yellow
 γ pale green
 with $\gamma > \beta > \alpha$

Grains are invariably biaxial negative. Kink bands are commonly developed (A325-1114N), however there is no evidence of subgrain development or secondary crystallization. Ramifying coronas of diopside(?), secondary amphibole and garnet are common around the orthopyroxene, e.g. in A325-543P and 907fP. In some sections, only garnet constitutes the corona. Some of the coronas are up to 0.05 mm wide.

Clinopyroxene (diopside augite) is colourless to pale green. It occurs as subidioblastic to xenoblastic elongate grains which are aligned parallel with the schistosity. Grains average 0.16×0.08 mm in size. Interfaces are straight, curved or highly serrated (cf in A325-G11). Some grains are free of inclusions, others contain miriads of fine opaque blebs aligned parallel to (001). A feeble pleochroism is present in the inclusion-free grains. The pleochroic scheme is:

α pale yellow green
 β pale green brown
 γ pale green

$Z^c = 42-45^\circ$ and the intensity scheme is $\gamma > \beta > \alpha$. Shadowy lamellar deformation twins are present in some sections.

The biotite which is sometimes found associated with the primary garnet forms either as isolated flakes, up to 0.16×0.08 mm in size, or as decussate clusters. The pleochroic scheme in all cases is:

α pale yellow
 $\beta=\gamma$ light brown

with the intensity $\beta = \gamma > \alpha$

Opaque oxides form skeletal aggregates or irregular xenoblastic grains. They are frequently surrounded by narrow coronas of xenoblastic secondary garnet (e.g. A325-239bP). Magnetite (commonly with haematite along (111) crystallographic planes) and ilmeno-haematite are the most common phases. A small amount of haemo-ilmenite is present in some cases.

Margarite (after sillimanite) is present in A325-927N, and in A325-911P it is associated with corundum and green spinel. In A325-927N it forms bladed platy aggregates which pseudomorph basal sections of sillimanite (e.g. in Figure 2.3d). The individual grains range in size from 0.3 x 0.009 mm to 0.24 x 0.08 mm and some of the pseudomorphs are up to 0.7 x 0.7 mm in size. It is colourless and shows well developed (001) cleavage. Elongate sections are length slow. It is biaxial negative with $2V = 50^\circ$, maximum birefringence is in the upper first order.

A member of the hercynite-pleonaste group of spinel is commonly present as inclusions in the garnets, e.g. in A325-927N. It is dark green in colour although the intensity of colour is not constant, and isotropic. The inclusions have rounded or slightly irregular outlines.

Apatite is a virtually ubiquitous accessory phase forming sub-idioblastic to idioblastic elongate to stumpy laths up to 0.2 x 0.08 mm in size aligned parallel to the schistosity. Rounded grains of zircon are a further accessory phase in some lithologies. Their rounded shape indicates that they could be of sedimentary origin. Bladed laths of corundum are a rare inclusion associated with ilmenite and spinel in A325-911P.

3.3.3.5 Pegmatites

3.3.3.5.1 General Description

Discontinuous veins and pods of pegmatite, transgressive, or locally conformable with the regional layering and structural elements (Figure 3.11b) have been recorded from several localities in the granulite facies terrain, e.g. at stations 953, 1960 and 2096 (Figures 1.3, A.1.1). The pegmatites are medium to coarse grained and they show gradational contact relationships with the surrounding granulites. They are seldom very extensive, ranging in width from several centimetres to one metre and they have been traced for distances up to six to ten metres. They intrude both quartzo-feldspathic and mafic lithologies.

Hand specimens are leucocratic and white to pink in colour. They are composed of large, tabular feldspar porphyroblasts (up to 6.0 x 3.0 cm in size), graphically intergrown with quartz. The pegmatites are not compositionally zoned, although there appears to be an increase in grain size across the width of the veins. They are structurally isotropic in comparison to the surrounding granulites.

In Heinrichs' (1948) classification of pegmatites based on field occurrence, the veins are 'exterior-replacement bodies'.

3.3.3.5.2 Mineral Assemblages

The following assemblages have been recorded:

1. quartz - alkali feldspar - opaque oxides
2. quartz - alkali feldspar - plagioclase - tourmaline - muscovite
- garnet - zircon

One thin section of the more complex assemblage, A325-953, has been examined in detail. The minerals are present in the following volume proportions: quartz 30%, alkali feldspar 50%, plagioclase 3%, tourmaline 15%, muscovite 2% and zircon trace.

3.3.3.5.3 Microstructure

The gross microstructural relationships are presented in Figure 3.12b.

3.3.3.5.4 Descriptive Mineralogy

Quartz occurs as large graphic lenticles up to 6.0 cm in length. The lenticles are highly strained and consist of medium to coarse grained, randomly oriented, recrystallized xenoblasts with complexly sutured or smoothly embayed grain boundaries. Deformation bands are commonly present and subgrains are extensively developed. Minor secondary recrystallization of quartz is present at grain interfaces in the form of trains of minute polygonal aggregates with sharp extinction.

Microcline, microcline perthite and plagioclase (albite) are present as large irregular xenoblasts up to 2 x 1 cm in size. With the exception of the grains which have resisted recrystallization, most of the larger areas of feldspar have a saccharoidal appearance. The saccharoidal areas are composed of equigranular to inequigranular granoblastic arrays of grains averaging 0.8 x 0.8 mm in size with straight or gently curved interfaces. Triple point junctions are produced where grains impinge on one another. The larger grains show undulose extinction; in contrast, the smaller recrystallized grains display crisp extinction. Cross-hatched twinning is ubiquitously developed in the microcline and the plagioclase shows polysynthetic albite twinning.

Tourmaline (var. schorl) forms small or large irregular xenoblastic grains. Some boundaries are embayed by quartz while others are smoothly curved or slightly sutured. The grains range in size from less than 0.5 x 0.5 cm to more than 3.0 x 3.0 cm. Basal sections are non pleochroic, however other sections enable the following pleochroic scheme to be determined:

ε	pale pink
ω	dark blue green

No zoning has been observed. Granoblastic (recrystallized) grains of tourmaline are developed at quartz-tourmaline interfaces and along narrow domains which transect the larger grains. The granoblastic grains average 0.06 x 0.06 mm in size and they have straight boundaries and form aggregates with triple point junctions.

Muscovite occurs as small isolated idioblastic to subidio-

blastic flakes up to 0.32 x 0.08 mm in size or as decussate aggregates of flakes.

Small subidioblastic colourless to pale pink poikiloblastic garnets averaging 0.2 x 0.2 mm in size are commonly closely associated with the tourmaline. They contain wispy inclusions of quartz and are frequently extensively fractured. Small flakes of muscovite have been observed occupying these fractures.

Zircon is present in trace quantities. One large idioblastic crystal has been collected, however none has been observed in thin section.

3.3.4 Quartzitic Lithologies

3.3.4.1 General Description

Minor units of quartzite intercalated with the quartzo-feldspathic granulites have been found in the mapped area (Figure 1.3). They are coarse grained and crop out in a blocky or flaggy manner as relatively thin lenses up to 3 metres wide. They have a strong lithological layering defined by laminae of light grey and dark blue-grey quartz. The laminae are lensoidal and some appear to be folded. There is a strong schistosity parallel to the layering and a well-developed lineation. It cannot be stated with authority whether or not the layering is of sedimentary origin. However it is highly probably that the gross compositional interface between the quartzites and the quartzo-feldspathic granulites represents an original sedimentary surface.

3.3.4.2 Mineral Assemblages

Under the polarizing microscope the quartzites consist predominantly of quartz together with a trace of alkali feldspar and garnet (almandine).

3.3.4.3 Microstructures and Descriptive Mineralogy

Two microstructural varieties of quartzite have been recognized:

(a) A325-1891; consisting of large tabular subidioblastic to idioblastic grains of strained quartz averaging 2.0 x 1.0 cm in size with curved, embayed or serrated grain interfaces. They are composed of arrays of intricately sutured subgrains. Undulose extinction is ubiquitous and deformation bands are common, although they are relatively widely spaced. The margins of the deformation bands also are strongly serrated. In some places the material from one deformation band or grain appears to be growing into the adjacent band or grain. Arrays of small recrystallized polygonal aggregates of granoblastic grains with sharp extinction commonly develop along the grain and subgrain boundaries. However these seldom exceed 0.08 mm in width.

(b) A325-140; the typical texture of this rock is shown in Figure 3.6a. It is highly strained and is composed of wavy lenticles of quartz composed of interlocking sutured subgrains. Some of these lenticles are up to 3 cm in length. Undulose extinction is ubiquitous. The lenticles invariably exhibit intricate deformation bands. Nucleation of recrystallized grains is common at the boundaries of deformation bands, at subgrain boundaries and at the interfaces between the larger quartz lenticles. The recrystallized grains have sharp extinction and they form granoblastic polygonal arrays up to 0.4 mm wide. The individual recrystallized grains average 0.05 x 0.03 mm in size.

The alkali feldspar and garnet occur as small lensoidal grains up to 2 x 0.4 mm in size. The interfaces with the surrounding quartz act as nucleation surfaces where secondary crystallization of the quartz is initiated.

Similar microstructures to those described above have been produced experimentally in quartz by Carter et al. (1964) and Hobbs (1968). Hobbs' (1968) work indicates that stress annealing, hydrostatic annealing and syn-tectonic recrystallization can give rise to similar features. Until more detailed electron microscope and c-axis work is carried out on the Amata quartzites it is not possible to indicate whether or not the deformation and recrystallization microstructures

are the result of stress annealing or syn-tectonic recrystallization, nor is it possible to gauge the effect any pre-existing anisotropy may have had on the formation of the microstructures.

3.3.5 Manganiferous Lithologies

3.3.5.1 General Description

One outcrop of manganiferous granulite has been found during the course of the mapping (at station 2048). It is believed that the manganiferous granulites were originally manganese rich sediments.

The unit is interlayered with mafic and quartzo-feldspathic granulite. It has been traced for 30-40 metres along strike and is about 3 metres wide. It has an extremely low outcrop profile due to its pronounced tendency to weather.

Hand specimens are brown to purple in colour. Weathered surfaces are invariably black due to the presence of thin coatings of manganese oxides. Garnet and quartz are clearly visible without the aid of a hand lens on freshly broken surfaces.

3.3.5.2 Mineral Assemblages

The following assemblages have been recognised under the microscope:

1. quartz - spessartite
2. spessartite - johannsenite - opaques
3. quartz - spessartite - opaque oxide
4. quartz - spessartite - johannsenite - rhodocroisite - opaques
5. quartz - spessartite - johannsenite - bustamite - opaque oxides.

The mode of A325-2048 is presented in Table 4.1.

3.3.5.3 Microstructures

Rock microstructures are characteristically dominated by the presence of aggregates of fine to coarse grained, elongate xenoblastic grains which define a strong schistosity in some rocks. Poikiloblastic porphyroblasts of garnet are virtually ubiquitous.

3.3.5.4 Descriptive Mineralogy

Grains of pale yellow to orange, spessartite rich garnets are extremely irregular in shape and they are frequently greater than 3.6 x 3.6 mm in size. Perfectly rounded and irregular inclusions of quartz are poikilitically contained in the larger porphyroblasts. Narrow selvages of garnet are commonly observed around grains of johannsenite. These coronas average 0.03 mm in width. Trains of xenoglastic garnet are frequently elongated in the plane of the schistosity, and these are commonly microboudinaged (Johnson, 1967; Stauffer, 1967, 1970) with extensive fracturing approximately normal to the direction of extension.

Quartz occurs in large highly strained lozenge shaped grains up to 2.0 x 0.5 mm in size. Grain boundaries are either straight, curved or highly sutured. Deformation bands are prevalent. Some subgrain development and recrystallization occurs in the larger grains, especially when dislocations are present. Extinction in the quartz frequently occurs in diamond shaped domains defining areas of separate subgrain formation. Deformation bands are strongly serrated. Recrystallized grains are commonly observed growing between adjacent bands. Fine Böhms lamellae form intricate wavy patterns through the larger quartz grains. They consist of trains of very fine grained clear high relief inclusions. Böhms (1883) interpreted the inclusions to be liquid or gas filled. In A325-2048b the trains of inclusion are apparently related to dislocations in the quartz grains.

Johannsenite forms pale green to colourless non-pleochroic, xenoblastic elongate grains (with elongation ratios of up to 15:1), aligned parallel with the schistosity. Grains are biaxial positive and extinction angles of 46-48° have been measured. Grains range in size from less than 1.2 x 0.08 mm to greater than 0.6 x 0.6 mm.

The johannsenite is commonly intergrown with two other phases which occur as subidioblastic to xenoblastic grains, averaging 1.2 x 0.8 mm in size: Bustamite is colourless to pink in thin section, biaxial negative and has a 2V of approximately 40°; Pyroxmangite is colourless in thin section, biaxial positive and also has a 2V of

approximately 40° . Both phases have oblique extinction. Fine lamellar twins interpreted to have been formed by deformational processes are extremely common in these three phases.

Rhodocroisite occurs as xenoblastic masses and as coronas around manganese rich(?) magnetite. It is colourless in thin section and exhibits uniaxial negative optics. Birefringence colours are extreme. Grain sizes range up to 3.5×1.5 mm.

Opaque oxides, predominantly manganese rich (?) magnetite with plates of haematite aligned along (111), and rare inclusions of ilmenite, occur as irregular grains which reach a maximum size of 1.5×0.8 mm.

3.3.6 Calc Silicate Lithologies

3.3.6.1 General Description

Rocks derived from calc silicate progenitors have been recognised at two localities, one in the granulite facies and the other in the 'transitional' terrains. The units occur as thin lensoidal bodies interlayered with quartzo-feldspathic, mafic and ultramafic lithologies. They are conformable with the layered schistosity in the surrounding units. Their occurrence is of considerable significance as it adds weight to the argument that some, at least, of the pre-metamorphic lithologies in both areas represent former sediments.

In the hand specimen they are medium to fine grained and exhibit a weak discontinuous compositional banding due to the clotting of pyroxene or garnet in a feldspathic matrix. Without careful perusal these units can easily be identified as mafic units which have similar gross field characteristics. There is a weak schistosity (defined by the elongation of individual grains and clusters of grains) which parallels the mesoscopic banding and schistosity in the surrounding rocks.

3.3.6.2 Mineral Assemblages

- (a) Granulite facies: the primary assemblage, plagioclase - grossularite - andradite - allanite - opaque oxide, is typical.
- (b) Transitional terrain: plagioclase - scapolite - diopside - sphene.

Clinzoisite and secondary garnet represent a later alteration feature in both groups of rocks.

3.3.6.3 Microstructures

The rocks are microstructurally quite mature. They consist of a medium to fine grained, equigranular to inequigranular granoblastic mosaic of xenoblastic grains with straight and curved interfaces (Figure 3.13a); a slight degree of flattening and elongation of component species manifests the feeble schistosity. The microstructure is typical of what might be expected from metallurgical studies to result from the achievement of minimum interfacial free energy by grain growth in the solid state (Smith, 1964; Stanton, 1964).

3.3.6.4 Descriptive Mineralogy

(a) Granulite Facies Lithology

Plagioclase (An 89) is the most abundant constituent (see Table 4.1). It forms an interlocking mosaic of xenoblastic grains (ranging in size from less than 0.16 x 0.16 to greater than 2.3 x 1.4 mm), with straight, curved or embayed grain interfaces. Four, five and six sided grains are commonly observed intersecting at triple point junctions. Inclusion of plagioclase in garnet are invariably oval shaped. The grains show undulose extinction and prominent pericline and albite lamination forming a rather complex pattern. These patterns are further complicated by the superposition of high angle kink bands. There is no evidence of subgrain development along these kink bands although their traces are highly irregular.

Primary coarse grained garnet (andradite-grossularite: see analysis, Chapter 4.3) is orange brown in colour and usually isotropic. Individual xenoblasts reach 1.0 x 1.0 mm although a significant number are somewhat smaller. Some grains are embayed by plagioclase, others are completely poikiloblastic with oval enclosures of plagioclase and allanite. Most grains are usually extensively fractured.

Secondary fine grained garnet is colourless to pale pink and occurs in xenoblastic aggregates associated with granular dusty magnetite.

Allanite occurs as fresh irregular xenoblastic grains up to 0.4 x 0.2 mm in size. It is coloured yellow to pale brown, and is faintly pleochroic. The refractive index is approximately 1.75. It is biaxial positive, has high dispersion and middle second-order birefringence colours. The $2V$ is approximately 60° and it shows oblique extinction, with Z^a 36° . Two sets of lamellae twins are prominent parallel to (100) and (001). It is commonly surrounded by narrow coronas or completely replaced by decussate aggregates of clinozoisite showing anomalous berlin blue birefringence.

Magnetite occurs as irregularly distributed skeletal to sub-idioblastic grains with deeply embayed boundaries. Needle-like inclusions of corundum(?) pseudomorphed by an unidentified colourless fibrous mineral are common throughout the opaques.

(b) 'Transitional' Lithology

Plagioclase (An 78) forms small polygonal grains (average size 0.4 x 0.4 mm) with undulose extinction and prominent pericline and albite lamellae twinning. All grains are biaxial negative. Some grains are antiperthitic.

Small needles of clinozoisite(?) and zoisite are present as inclusions. These seldom exceed 0.16 x 0.008 mm.

Clinopyroxene (ferrosalite - by analysis, Chapter 4.3) occurs as small olive green, slightly pleochroic xenoblastic grains average size 0.4 x 0.4 mm. Lamellar deformation twins are common. Grain boundaries are sharp to gently curved. Maximum Z^c is 48° . Coronas of decussate or radiating clinozoisite and zoisite plates and granular garnet commonly surround the clinopyroxene grains.

Scapolite is moderately abundant, forming colourless brilliantly birefringent grains which are uniaxial negative. The grains are similar in shape to the plagioclase xenoblasts and although they are commonly in contact with the plagioclase there is no suggestion that a replacement of one by the other is not considered to be taking place. Refractive index and chemical analysis indicate that the scapolite has a different composition from that in the mafic rocks (Chapter 4.3, p.222).

Sphene is subordinate in abundance and forms small rounded

grains (seldom larger than 0.16 x 0.08 mm) or inclusions in the clinopyroxene.

3.4 PETROGRAPHY OF THE TRANSITIONAL TERRAIN LITHOLOGIES

3.4.1 Mafic Lithologies

3.4.1.1 General Description

Mafic rocks are as abundant in the area south of the Davenport Shear as they are in the granulite facies terrain.

They are fine grained and invariably melanocratic. Some show extensive quartz-feldspar veining in contrast to mafic rocks of the granulite terrain. Both porphyroblastic and equigranular varieties are present. The porphyroblastic types are characterised by the presence of easily recognisable glomeroporphyroblasts of hornblende and/or plagioclase.

Mica is rare to absent in some lithologies and abundant in others, e.g. A325-990, -1328.

The mafic rocks crop out as intermittent layers and small lenses and occasionally boudins, ranging in width from less than 0.5 metres to greater than 100 metres and in length from several metres to greater than a kilometre.

They have sharp conformable contacts with the surrounding quartzo-feldspathic gneisses (Figure 2.11b). Smaller lenses of mafic material within the gneisses (ranging in thickness from several millimetres to 20 cm) give the gneisses a distinctly banded appearance.

Schistosity (tS_1) is strongly developed. In hand specimen it is defined by the dimensional preferred orientation of clusters of felsic and mafic constituents (i.e. feldspar, hornblende, clinopyroxene and orthopyroxene), parallelling the fine scale compositional banding above mentioned.

Folds in the transitional terrain are clearly defined by the mafic units. Some of these folds are tight and intrafolial whereas others are less tightly appressed. The latter group are interpreted to have formed during the tD_2 deformation (the main phase of deformation registered in the area (see above, Chapter 2). In the hinge regions of the tF_2 mesoscopic and macroscopic folds, a faint dimensional preferred orientation (tS_2) of mafic and felsic constituents at a high or low dihedral angle to tS_0 parallel to tS_1 ($tS_0 // tS_1$) (depending on the

portion of the fold being examined) is discerned. This contrasts with the more strongly developed tS_2 in the quartzo-feldspathic gneisses.

Some mafic units display a prominent lineation (rodding, in the coarser lithologies) due to the alignment of prismatic components in the plane of the foliation.

3.4.1.2 Mineral Assemblages

The constituents of the mafic rocks as seen under the microscope are: plagioclase, hornblende, orthopyroxene, clinopyroxene, biotite, phlogopite, scapolite, alkali feldspar, opaque oxides, magnetite, ilmeno-haematite, haemo-ilmenite and rutile. Minerals present in accessory and minor amounts include quartz, corundum, spinel, apatite and zircon. As in the granulites, secondary garnet, amphibole, clinopyroxene, sillimanite(?), epidote and biotite are present as minor phases. The absence of primary garnet is in contrast to the mafic rocks of the granulite facies terrain.

The following mineral assemblages have been recognised in the thin sections examined:

1. plagioclase - orthopyroxene - hornblende - clinopyroxene - opaque oxides \pm (biotite)
2. plagioclase - orthopyroxene - clinopyroxene - opaque oxides \pm (hornblende) \pm (biotite)
3. plagioclase - orthopyroxene - clinopyroxene - hornblende - biotite
4. plagioclase - hornblende - orthopyroxene - opaque oxides \pm (biotite)
5. plagioclase - hornblende - orthopyroxene
6. plagioclase - hornblende - orthopyroxene - clinopyroxene - opaque oxides - (quartz)
7. plagioclase - hornblende \pm biotite \pm clinopyroxene - opaque oxides - (quartz)
8. plagioclase - hornblende - clinopyroxene - orthopyroxene - opaque oxides - (quartz)
9. plagioclase - orthopyroxene - phlogopite - (quartz)

10. plagioclase - orthopyroxene - clinopyroxene - opaque oxides - (quartz)
11. plagioclase - hornblende - opaque oxides
12. plagioclase - clinopyroxene - hornblende - opaque oxides
13. plagioclase - hornblende - clinopyroxene - opaque oxides - biotite
14. biotite - alkali feldspar - clinopyroxene - phlogopite

Only minerals which apparently equilibrated during the same metamorphic event are considered in the above list. The coronal minerals, i.e. secondary amphibole, garnet, clinopyroxene and biotite together with the needle-like inclusions in the feldspars, viz. sillimanite(?) have been disregarded as microstructural relationships suggest that they were the products of a later event.

Mineral assemblage (1) constitutes 56% of the sections examined (however, the proportion of the individual phases, especially the hornblende/orthopyroxene ratio, varied considerably. Twenty percent of the sections have mineral assemblages typomorphic of the amphibolite facies.

Modes of the major phases are listed in Table 4.1. Although hornblende is extremely common throughout the area, it is absent or virtually absent from some rocks that might be expected from bulk chemistry to contain it, e.g. A325-664, -909a. Likewise, although orthopyroxene is present in most rocks it is absent from some of the more hornblende rich lithologies, e.g. A325-402, -599, -6, -414.

Microstructural evidence (intergrowth textures and xenoblastic grain relationships) suggests that in rocks containing both hornblende and orthopyroxene, they apparently crystallised simultaneously.

3.4.1.3 Microstructure

In thin section the mafic rocks have some microstructural features in common with the mafic granulites (Section 2.3.1). They are typically composed of inequigranular to equigranular granoblastic aggregates of grains (Figures 3.1a,b,c and 3.15c) which range in size from coarse to fine. Porphyroblastic or glomero-porphyroblastic

(Figure 3.16b) variants are common.

Three distinct schistositys can be recognised in the microstructures of some lithologies, (e.g. A325-846, -891, -705b, -896). Two of the deformations (during which the schistositys were developed) involved the crystallization of orthopyroxene, hornblende, mica and opaque oxides.

The earliest recognisable anisotropy is a discontinuous layering and schistosity manifested by parallel lenticular aggregates of inequigranular to equigranular granoblastic hornblende, orthopyroxene, clinopyroxene, plagioclase, opaque oxides and lepidoblastic grains of mica with smooth to irregular, straight, curved or distinctly embayed interfaces. In N sections the granoblastic constituents also display some dimensional preferred orientation, even in the most polygonal looking aggregates. This layering and schistosity has been assigned the terminology $tS_0//tS_1$. tS_0 may represent a pre-existing layering and schistosity formed during the tD_{0-1} or $tD_{0-2,3}$... deformations. In the absence of recognisable original features which can be used as a benchmark or base line from which the terminology can be generated, interpretations based on early folded structures and schistositys are always subject to uncertainty.

The second microstructural development is a prominent schistosity in the hinge regions of tF_2 structures (Chapter 2). The schistosity appears in the N section as a parallelism of ovoid to lozenge shaped aggregates of hornblende, orthopyroxene, clinopyroxene, and feldspar grains with curved or straight grain interfaces. In some sections small diamond shaped domains, composed of granoblastic grains, are defined by a gently anastomosing layering (now extensively altered) (Figure 3.16b). In N sections the tS_2 layering transects the pre-existing aggregates of xenoblastic grains, which constitute $tS_0//tS_1$ at a low to moderate dihedral angle (Figure 3.16a). In the P section tS_2 is virtually parallel to the pre-existing layering and schistosity. The lineation which characterises the hinge regions of tF_2 structures is formed, or accentuated by, this intersection.

The third layering is a post crystallization fracturing. It causes moderate to strong disruption to the pre-existing grain aggregates

by the development of narrow breccia-filled anastomosing veins, up to 3 mm wide. Phases which crystallized during the earlier deformations and which are situated even some distance from the zone of fracturing are commonly extensively brecciated.

Orthopyroxene, hornblende, opaque oxides and biotite are commonly surrounded by coronal microstructures. The coronas are believed to be post tF_2 features.

3.4.1.4 Descriptive Mineralogy

Hornblende occurs as subidioblastic to xenoblastic grains depending on its abundance and the nature of the adjacent mineral phases. Prismatic subidioblastic hornblende predominates in the hornblende rich lithologies (in both P and N orientations). Glomerophyroblastic aggregates of xenoblastic hornblende commonly exceeding .5 cm in diameter, give the rock a distinctive mottled appearance. Interfaces are strongly or gently curved. Multiple twinning is common, developed parallel to (100). Amphibole cleavages are well developed. The following pleochroism has been observed (Table 3.1). Maximum Z^c 's range from 17° to 28° . Grains average 0.5 x 0.5 mm in size in most sections. However individual variants may range up to 2.0 x 1.5 mm in size. The most common interfaces are straight or gently curved. Grain boundaries are occasionally rational, e.g. in A325-523 (Figure 3.15c), the interfaces paralleling the plane containing the form {110} (cf. Vernon, 1968, 1970).

TABLE 3.1

REPRESENTATIVE PLEOCHROIC SCHEMES EXHIBITED BY
HORNBLENDES FROM THE MAFIC LITHOLOGIES

Specimen Number	α	β	γ	Intensity
A325-615b	pale yellow	green brown	brown	$\gamma > \beta > \alpha$
A325-2074	pale yellow	green	green brown	$\gamma > \beta > \alpha$
A325-403	pale green	green	dark brown green	$\gamma > \beta > \alpha$
A325-874	neutral	pale green	pale green to bluish green	$\gamma > \beta > \alpha$
A325-402	pale green	pale green	apple green	$\gamma > \beta > \alpha$

The presence of biaxial negative and positive optics, e.g.

A325-1228	negative
A325-1345	positive
A325-599	negative
A325-414	negative
A325-874	positive
A325-891	positive

indicates that both common hornblende and a pargasitic variety are present. However, they have not been observed co-existing with each other.

Many hornblendes contain miriads of (unidentified) needle-like colourless to pale green inclusions (average size 0.001 x 0.02 mm) with oblique extinction (the extinction angle being greater than that of the host amphibole), aligned parallel to {110}. They are frequently associated with granules of opaque oxide.

Pleochroic pale to dark green hornblende forms coronas of radiating small xenoblastic grains around grains of opaque oxides. These coronas are seldom wider than 0.08 mm. They are believed to be of a later generation. Coronas of a different amphibole are also common around primary hornblende. This amphibole is pleochroic colourless to pale green-blue and has parallel extinction; maximum interference colours are second order reds and it is biaxial positive. From these optical properties this mineral has been tentatively identified as cummingtonite.

The coronal hornblende and cummingtonite are believed to have developed during the same metamorphic event. However they are both unrelated to the pre- tF_2 and tF_2 parageneses.

Plagioclase (An30-80) is present in all the mafic rocks except A325-1328 in which alkali feldspar is the sole felsic constituent. Modal abundances range from 0% to greater than 60%. The plagioclase forms xenoblastic equidimensional to slightly elongate grains, averaging between 0.4 x 0.4 and 0.7 x 0.7 mm. Some rare glomeroporphyroblastic aggregates composed of xenoblastic, polygonal grains (averaging 1.0 x 1.0 mm) may reach 1.0 x 0.5 cm in size (e.g. in

A325-1228N). Grain interfaces are generally straight or curved. Triple point junctions are common especially in aggregates where plagioclase is the sole constituent. Plagioclase also occurs as small inclusions in pyroxene and amphibole. The inclusions display parallel planar interfaces with rounded corners or occur as spherical or more irregular shapes. Grain boundaries are often accentuated by trains of sillimanite(?) needles extending into the plagioclase grain as fine acicular sheafs (e.g. in A325-469P, -910N, -1264N). These apparently nucleated because of the presence of intergranular pore fluids rich in Al_2O_3 and SiO_2 and/or because the interface, being a dislocation, provided a favourable site for nucleation and grain growth. The concentration of fine grained sillimanite commonly causes the plagioclase to appear cloudy.

Undulose extinction and mechanical twinning on both the albite and pericline laws (Figure 3.5c,d) register the effects of strain in the plagioclase xenoblasts. In addition to complex twin patterns deformation bands and brecciation of the feldspar xenoblasts are not infrequent adjuncts to the effects of strain.

Antiperthite has only been observed in two sections, A325-267P and -497N. This contrasts strongly with the rather wide spread distribution of antiperthitic plagioclase among the mafic granulites.

Two varieties of mica are present; phlogopite and biotite. Their modal abundances vary considerably from a trace to more than 20%. Both form moderately to strongly pleochroic tabular subidioblastic to xenoblastic flakes up to 1.0×0.8 mm. Contacts occur with virtually all phases in the thin section including orthopyroxene (e.g. in A325-990). Rational interfaces parallel to the (001) direction of the mica are common (Figure 3.15b).

Two orientations have been observed, one parallel to the prominent layering and schistosity, the other randomly oriented, suggesting that two distinct periods of mica crystallization are represented.

The pleochroic schemes observed are:

α	straw yellow
$\beta=\gamma$	brown

α	pale yellow
$\beta=\gamma$	red brown
α	neutral
$\beta=\gamma$	black brown
α	neutral
$\beta=\gamma$	orange brown

with the following intensity: $\beta = \gamma > \alpha$

The same range of pleochroic colours is present in the hornblende rich mafic rocks as in the orthopyroxene rich varieties. This suggests that the variation in pleochroism is not influenced by changes of metamorphic grade.

The mica flakes commonly extinguish unevenly and kink bands are ubiquitous in most sections. The kink boundaries have serrated appearance and growth of minute grains (average size 0.005 x 0.005 mm) which lack optical continuity with the host grains, is evident along these boundaries. The trains of subgrains are generally aligned parallel to the axial plane schistosity, tS_2 .

Coronas of garnet or green amphibole are relatively well developed in most sections (Figure 3.17b). Biotite of secondary origin is also a coronal phase around orthopyroxene. Small zircons form rare inclusions in the biotite. They are commonly surrounded by narrow pleochroic haloes.

Hypersthene occurs as strongly cleaved irregular xenoblastic grains with curved or embayed interfaces, as equidimensional xenoblastic grains with smooth, straight or slightly curved boundaries, or as elongate grains dominated by the {100} (e.g. A325-523, Figure 3.15c) and {010} prism forms. Grain sizes range from less than 0.2 x 0.2 mm to more than 3.0 x 1.5 mm. Glomeroporphyroblastic aggregates are not uncommon. Large porphyroblasts are frequently poikiloblastic with respect to plagioclase, biotite, apatite and hornblende (e.g. A325-664N, -990N, Figure 3.15a,b).

Pleochroism is invariably intense:

α	pale pink
$\beta=\gamma$	pale green

with $\gamma > \beta > \alpha$

Although most grains are biaxial negative, some of the (presumably more magnesium-rich) varieties are optically positive.

Bent cleavage traces, kink bands and undulose extinction indicate that the pyroxenes have suffered varying degrees of post-crystallization deformation.

Ramifying coronas comprising all or some of the following phases, viz.: secondary amphibole, clinopyroxene, garnet, biotite and opaque oxides, surround the orthopyroxene as a result of reaction with plagioclase, hornblende, opaque oxides and biotite (Figure 3.17a, 3.18b). They are seldom present between orthopyroxene and clinopyroxene. Where coronal development is extreme, the large xenoblasts of orthopyroxene are subdivided into small domains and the coronas coalesce, forming a 'mesh work type' texture.

Diopside and augite are ubiquitous, forming non- to slightly pleochroic colourless to pale green xenoblastic grains. Grain boundaries are curved or embayed against orthopyroxene, hornblende and plagioclase. Grains range between 0.1 x 0.1 mm and 1.5 x 0.8 mm. Some of the larger grains are poikiloblastic with inclusions of plagioclase, hornblende, orthopyroxene and/or mica. In plagioclase-clinopyroxene aggregates triple junctions are commonly observed. The pyroxene colour is often masked by hoards of rounded to needle-like opaque exsolution(?) blebs which are commonly concentrated in the cores of grains. Multiple twins on (100) as well as fine twins on (001) (see A325-1328) are developed to varying extents. They are similar in appearance to the mechanical twins observed in feldspars and are interpreted to have formed similarly, viz. as a result of deformation. Coronas of granular garnets are common at former plagioclase-clinopyroxene interfaces. They are believed to have formed contemporaneously with the selvages around orthopyroxene, hornblende, biotite and opaque oxides.

Scapolite (var. mizzonite - from optics) forms xenoblastic grains or aggregates of grains. Contacts with other phases vary from sharp to irregular and are gently curved, straight or rarely embayed. Grains average 0.6 x 0.6 mm in size. They are commonly haphazardly

distributed with respect to the other phases although almost mono-minerallic bands occur. Needle-like inclusions produce a distinctive brown colouration in some grains. Irregular selvages of granular garnet are common at scapolite-plagioclase interfaces.

Magnetite, ilmeno-haematite and haemo-ilmenite are the typical opaque mineral assemblages. Magnetite characteristically occurs as idioblastic to xenoblastic grains (average size 0.02 x 0.06 mm) with haematite parallel to (111) (Figure 3.19c,d). Small exsolution lamellae of spinel occur in some of the magnetite (Figure 3.19a). In A325-339 fine selvages of garnet occur at ilmenite/magnetite contacts.

Ilmeno-haematite and haemo-ilmenite form either small polygonal aggregates associated with magnetite or large inequidimensional xenoblastic to subidioblastic grains with extensive haematite exsolution flames and stringers. The larger haematite lamellae frequently display secondary exsolution lamellae of ilmenite. The haemo-ilmenite and ilmeno-haematite grains exhibit mechanical twin lamellae.

Grains of rutile are common at ilmenite-magnetite interfaces. This is interpreted as due to Ti enrichment of the ilmenite by ulvö spinel which has exsolved from the magnetite during cooling and oxidation (see Chapter 4.3) and migrated to the magnetite-ilmenite interface.

Trace quantities of quartz interstitial to the major phases in a number of lithologies (e.g. A325-990, -599, -14, -10, -903, -872, -755) form small irregular grains up to 0.2 x 0.2 mm in size, with undulose extinction. Deformation bands are common. Sub-grains and secondary polygonal aggregates have been observed.

Epidote and clinozoisite are present as alteration products of plagioclase in A325-371.

With the exception of A325-990 and -1328 apatite is present only in extremely small amounts. It generally forms isolated stumpy subidioblastic to idioblastic grains and is strongly fractured. Optical figures are difficult to obtain. Minute rounded grains of zircon are present in some sections. However, this must be regarded as a rare phase. Small needle-like grains of corundum in ilmenite show well developed basal cleavages. They are commonly associated with spinel

(e.g. in A325-891). Sillimanite(?) as mentioned above (p. 40) occurs as acicular inclusions in plagioclase grains or as aggregates or sheafs of needles along plagioclase-plagioclase or plagioclase-clinopyroxene interfaces.

3.4.2 Ultramafic Rocks

3.4.2.1 General Description

A small number of ultramafic rocks have been recognised in the transitional terrain. They occur as thin lenses parallel to the layering and schistosity ($tS_0//tS_1$) in the surrounding quartzo-feldspathic gneisses, and they are believed to be closely genetically related to the mafic lithologies.

Some of the ultramafic rocks contain hornblende as the principle ferromagnesian mineral. Others contain abundant orthopyroxene and clinopyroxene.

In the hand specimen they are predominantly fine to medium grained, although larger grains are present in a few specimens. They have a characteristic dark hue, ranging in colour from shades of blue grey to green black, depending on the proportions of the different ferromagnesian constituents. Weathered surfaces are typically rusty brown in colour and the zone of intense weathering seldom exceeds 2 - 3 mm.

They have a prominent schistosity (and lineation) defined by the parallel alignment of ellipsoidal clusters of the prismatic mineral constituents.

3.4.2.2 Mineral Assemblages

Under the microscope they are seen to be composed of differing proportions of the following essential phases: hornblende, orthopyroxene, clinopyroxene, phlogopite and minor amounts of plagioclase and opaque oxides. Coronas of cummingtonite, clinopyroxene, epidote and a trace of garnet are present to varying degrees at plagioclase-ferromagnesian interfaces.

The primary metamorphic assemblages are:

1. hornblende - orthopyroxene - clinopyroxene - phlogopite
2. hornblende - orthopyroxene - clinopyroxene ± (plagioclase)
3. hornblende - orthopyroxene - clinopyroxene ± (opaque oxides) ± (plagioclase)

Mineralogical abundances determined by point counting and visual estimation are: orthopyroxene, 5%-60%; clinopyroxene, 5%-40%; hornblende, 10%-85%; phlogopite, 0%-40%; opaque oxides, tr-1%; plagioclase, 0%-5%.

3.4.2.3 Microstructures

Granoblastic, inequigranular to equigranular aggregates are typical. Grain interfaces exhibit the same variations as were noted previously for the mafic lithologies (Chapter 3.4.1.2). Xenoblastic grains of clino- and orthopyroxene, and hornblende are commonly complexly intergrown (Figure 3.20b,c). As in the granulite terrain it is thought that the three phases crystallised contemporaneously.

3.4.2.4 Descriptive Mineralogy

Orthopyroxene is present as aggregates of small xenoblastic grains complexly intergrown with hornblende, clinopyroxene and plagioclase or as large poikiloblastic xenoblasts. Grain sizes range from less than 0.2 x 0.2 mm to greater than 3.5 x 5.0 mm. Grain boundaries are either curved or deeply embayed. The pleochroism is weak to moderate, and the scheme is:

α	pale pink
β	pale yellow
γ	pale green

Some grains are optically positive whereas others are negative. Compositions thus range from enstatite to bronzite.

In A325-295N some of the orthopyroxene is present in irregular inclusions in large poikiloblastic hornblende xenoblasts (Figure 3.20c), illustrating the contemporaneous crystallisation of these phases, above mentioned. Other grains of orthopyroxene in the same slide occur as discrete individual xenoblasts not associated with hornblende.

Exsolution lamellae of clinopyroxene are commonly aligned parallel to (001) (see A325-836P).

Kink bands are prominent in some of the large xenoblasts. However there is no evidence of subgrain growth.

Hornblende is a primary phase and a significant component of some rocks, constituting as much as 85% of A325-327N. It forms large subidioblastic to xenoblastic grains which are commonly intricately intergrown with aggregates of orthopyroxene and clinopyroxene (Figure 3.20c), as already noted. Some grains are distinctly poikiloblastic and the inclusions are rounded or embayed and highly irregular in shape. Grains average 0.5 x 0.5 mm to 1.0 x 1.0 mm in size in the N section although some grains reach 1.6 x 0.5 mm in the P orientation. Triple point junctions are common especially in the monominerallic hornblende aggregates. Opaque inclusions are commonly present.

The following weak pleochroic schemes have been observed:

α pale olive green
 β pale brown green
 γ pale brown
 with $\gamma > \beta > \alpha$

α pale green
 β green brown
 γ green brown
 with $\gamma > \beta > \alpha$

α neutral
 β pale green
 γ pale green
 with $\gamma > \beta > \alpha$

α pale green
 β green
 γ brown green
 with $\gamma > \beta > \alpha$

Z^c's range from 17° to 20°.

Some grains display broad simple twins while in others the twinning is more finely laminated. Both types of twins are believed to be of mechanical type. Extinction is either crisp or undulose. Cleavage traces are frequently bent.

Clinopyroxene has the same microstructural appearance as orthopyroxene. Grains range in size from 0.3 x 0.3 mm to 3.5 x 1.6 mm. It is pale green to colourless and is frequently complexly intergrown with orthopyroxene and hornblende. Some of the intergrowths appear to be almost 'twin-like' (Figure 3.20b). Similar intergrowths have been noted previously in other granulite facies terrains by Quensel (1951) and Binns (1964), who believe them to be the result of synchronous crystallization. As mentioned above, the same interpretation has been placed on these features in the Amata rocks.

The clinopyroxene is commonly turbid due to the presence of miriads of opaque inclusions. Fine multiple twinning on (100) and (010) is considered to be the result of post crystallization deformation. Z^c 's range from 35° to 43° .

Phlogopite is present as small discrete subidioblastic laths or as aggregates of flakes which commonly engulf smaller grains of orthopyroxene, clinopyroxene and hornblende, e.g. in A325-776N. Rational boundaries with orthopyroxene parallel to (001) are common. Inclusions of phlogopite in pyroxene are either rounded or idioblastic.

The following pleochroic schemes have been observed:

α straw yellow

$\beta = \gamma$ brown

α colourless

$\beta = \gamma$ orange

with $\beta = \gamma > \alpha$

Kink bands are ubiquitous.

Reaction coronas of pale amphibole and epidote are prominent at phlogopite-plagioclase interfaces.

Traces of plagioclase (An 68) occur as small rounded grains (average size 0.1 x 0.1 mm) interstitial to the ferromagnesian constituents. Undulose extinction and albite and pericline mechanical

twins are common.

Minerals present in minor amounts include skeletal blebs of magnetite, ilmenite, haemo-ilmenite and haematite, rounded grains of spinel and irregular grains of zircon.

3.4.3 Intermediate Lithologies

3.4.3.1 General Description

The intermediate rocks have similar field characteristics to the mafic types.

In hand specimen they are melanocratic to slightly leucocratic, fine to coarse grained and commonly banded as a result of grain size and compositional differences. Quartz, feldspar, pyroxene and mica can easily be detected. The rocks are often extensively penetrated by quartzo-feldspathic veins which are either sub parallel to the regional layering or are ptygmatic. Much of the veining appears to be a pre- tF_2 feature (see Figure 2.16b). Weathered surfaces are typically rusty orange.

3.4.3.2 Mineral Assemblages

In thin section the intermediate rocks consist of plagioclase, orthopyroxene, clinopyroxene, quartz, opaque oxides, scapolite, biotite, hornblende, secondary garnet, amphibole and clinopyroxene. Apatite, spinel, corundum, epidote and sillimanite(?) are present in accessory amounts. In contrast to the mafic lithologies the intermediate rocks with one exception, A325-693, do not contain abundant hornblende. The main ferromagnesian constituents are orthopyroxene and clinopyroxene.

The following assemblages of minerals have been recognised in thin section:

1. plagioclase - orthopyroxene - quartz ± (opaque) ± biotite
2. plagioclase - orthopyroxene - clinopyroxene - quartz - opaques
3. plagioclase - orthopyroxene - quartz ± (scapolite)
4. plagioclase - orthopyroxene - quartz - clinopyroxene - opaque - scapolite

5. plagioclase - orthopyroxene - quartz - clinopyroxene - opaques - biotite
6. plagioclase - quartz - orthopyroxene - opaques
7. plagioclase - quartz - orthopyroxene - clinopyroxene - hornblende - opaques \pm biotite
8. plagioclase - quartz - hornblende \pm (biotite) \pm clinopyroxene - opaques
9. plagioclase - alkali feldspar - quartz - orthopyroxene \pm clinopyroxene - opaques
10. plagioclase - quartz - orthopyroxene - alkali feldspar - opaques

Modal content of the essential phases are visually estimated as follows: orthopyroxene 10%-45%; clinopyroxene 10%-40%; biotite 0%-5%; hornblende 0%-5%; plagioclase (and antiperthite) 15%-60%; quartz 3%-10%. Secondary amphibole, clinopyroxene and garnet range from a few percent to almost 10%.

3.4.3.3. Microstructure

The major ferromagnesian phases occur predominantly as xenoblastic grains. The microstructural appearance is dominated by the effect of the tF_2 deformation, e.g. the tS_2 schistosity. The schistosity is manifested by the preferred orientation of anastomosing elongate ellipsoidal aggregates of grains, e.g. in A325-864N, -705bN, 675bN. The pre- tF_2 layering/schistosity (i.e. $tS_0//tS_1$) is commonly obliterated by tS_2 . However, in several sections, viz. A325-727N, -705cN and -693N, remnants of the earlier schistosity can still be observed, composed of aggregates of equidimensional to inequidimensional, equigranular to inequigranular granoblastic grains, frequently parallel to a strong compositional and grain size layering (Figure 3.20a). Interstitial areas are occupied by elongate lenticles or rounded granules of quartz which commonly exhibit embayed interfaces with the xenoblastic ferromagnesian grains, e.g. in A325-258N, -538N, -1041P, 1410N.

3.4.3.4 Descriptive Mineralogy

Orthopyroxene (hypersthene and bronzite, from optics) occur as xenoblastic grains which are either equidimensional or inequidimensional. They range in size from 0.1 x 0.1 mm to more than 0.9 x 0.4 mm. Grain boundaries are either straight, gently curved or deeply embayed. Some of the deeply embayed grains exhibit rational interfaces with surrounding feldspars and ferromagnesian phases. These embayed microstructures indicate high degrees of interfacial energy (according to Smith (1948, 1953, 1964), Stanton (1964), Kretz (1967), Vernon (1968)).

The pleochroism is:

α pale pink to dark pink
 β pale green
 γ green
 with $\gamma > \beta > \alpha$

Post crystallization deformational processes have resulted in the fracturing of some grains, the development of kink bands, bent cleavage traces and the presence of undulose extinction.

Grain contacts with plagioclase are commonly indistinct due to the presence of selvages of fine grained xenoblastic garnet (Figure 3.18c), clinopyroxene and occasionally amphibole. The coronas are seldom wider than 0.05 mm.

Clinopyroxene (augite and diopside, by optics) grains are pale green to colourless and are non pleochroic. They have similar microstructural characteristics to orthopyroxene and they average 0.6 x 0.6 mm. Virtually all grains have clouded cores and they are commonly surrounded by coronas of xenoblastic garnets.

Biotite occurs intermittently as deformed subidioblastic laths (up to 0.9 x 0.4 mm in size) elongate parallel to either tS_1 or tS_2 . They are pleochroic, either:

α neutral to straw yellow
 β=γ orange to orange brown
 or
 α neutral
 β=γ foxy red brown

with the following intensity: $\beta = \gamma > \alpha$. They are frequently kinked. Some of the kink planes have a serrated appearance and show evidence of subgrain nucleation.

Long stringers of potassium feldspar are commonly aligned parallel to the biotite (001) cleavage direction.

Coronas of secondary amphibole and granular garnet occur as selvages to the biotite flakes.

With the exception of A325-693, hornblende has been observed only as an accessory phase. It forms small xenoblastic grains (averaging 0.3×0.1 mm), which are commonly clouded with opaques. When pleochroic colours can be observed, in grains free of opaque inclusions, the following scheme is present:

α	pale green yellow
β	pale green brown
γ	green to green brown

with intensity $\gamma > \beta > \alpha$

Grains are commonly surrounded by narrow coronas of subidioblastic to xenoblastic pale green secondary amphibole and xenoblastic garnet.

Scapolite has a similar refractive index to that of quartz however it is easily recognisable by its optically negative character, higher birefringence and turbid appearance. The turbidity is caused by the presence of hoards of minute translucent inclusions (of an unknown phase). It generally forms small xenoblastic grains with straight, curved or embayed grain boundaries. Although it occurs predominantly in plagioclase rich areas of sections there is no suggestion that it is an alteration product of the feldspar.

Quartz has several modes of occurrence:

- (a) as inequidimensional to equidimensional xenoblastic grains with straight or curved interfaces, undulose extinction and wavy deformation bands (which can easily be recognised by their different extinction positions either side of parallel kink planes). Some of these grains are elongate parallel to the schistosity and they have been observed up to 2.0×0.8 mm in size.
- (b) where the tS_2 schistosity is pronounced the grains of quartz

appear as wavy lenticles (up to 1.2 x 0.4 mm in size). They are extensively strained and are generally situated interstitial to the plagioclase and pyroxene grains indicating that quartz was the last phase to crystallize during the tF_2 deformational event. Grain boundaries are commonly serrated.

- (c) small granoblastic polygonal aggregates of quartz (average size 0.04 x 0.04 mm) formed by subgrain nucleation and secondary crystallization in the solid state (Hobbs, 1970) occur as marginal, or internal domains to large strained grains of quartz. Grain boundaries are straight and the grains show crisp extinction positions.

Minute needles of rutile(?) are commonly present as inclusions (e.g. A325-705b).

Plagioclase (An45 to 60) occurs as interlocking aggregates of xenoblastic grains (average size 0.6 x 0.4 mm). Some of the plagioclase is antiperthitic, e.g. A325-291, -693, -675b, -1410, -1398, -705c, -673b, -258 and -1353, containing elongate blebs of alkali feldspar which have much lower refractive indices than their host grains.

Grains commonly show curved albite and pericline (mechanical twin) lamellae and wavy extinction (due to strain). Some grains are poikiloblastic with rounded inclusions of quartz, e.g. A325-727. 'Myrmekite'-like quartz plagioclase intergrowths are a prominent feature in A325-673b.

Needle-like inclusions of epidote(?) and/or clinozoisite(?) are a common alteration product of the feldspar. Sillimanite(?) occurs as sheafs of acicular needles which are concentrated along plagioclase-plagioclase interfaces or as inclusions in plagioclase grains.

Other minerals present as accessories include apatite which forms small stumpy idioblastic to subidioblastic grains; rounded xenoblasts of zircon; subidioblastic to xenoblastic grains of spinel and corundum which frequently form inclusion in grains of ilmenite (e.g. in A325-693, -1410, -864).

Opaque oxides (predominantly magnetite, and ilmenite with

exsolved haematite) form irregular skeletal xenoblastic grains or aggregates of grain. The larger grains are commonly poikiloblastic with rounded inclusions of quartz, spinel and needles of corundum. Fine grained selvages of garnet (Figure 3.18a), together with subidioblastic to xenoblastic flakes of secondary biotite and secondary amphibole, or garnet-opaque symplectites occur along the contacts with the opaque oxides.

3.4.4 Quartzo-feldspathic Lithologies

3.4.4.1 General Description

Gneisses of quartzo-feldspathic composition occur in similar abundance to those in the granulite facies area. They crop out as discontinuous resistant dissected whale-backs, core stones and tors (Figure 2.19b). Some are lithologically inhomogeneous whereas others are homogeneous at outcrop scale. The inhomogeneous varieties show a significant compositional variation defined by the abundance of alkali feldspar relative to plagioclase, by the abundance of ferromagnesian constituents relative to quartzo-feldspathic components and by variation in grain size.

Gneissic granites containing amphibolite xenoliths crop out as a series of low, isolated whale-backs and tors in the core of a large south-easterly plunging tF_2 folded structure (Figures 1.2, 1.3).

In hand specimen the gneisses are fine to coarse grained and distinctly leucocratic. On outcrop and hand specimen scale they can be grouped into five broad divisions:

1. Strongly banded quartzo-feldspathic gneisses which have concentration of ferromagnesian constituents in bands ranging in width from a few millimetres to several centimetres. A prominent schistosity is parallel to the compositional layering. This schistosity is defined by the alignment of ellipsoidal and prismatic clusters of ferromagnesian and quartzo-feldspathic components.
2. Poorly banded quartzo-feldspathic gneisses which are poor in ferro-

magnesian constituents, have a weak widely spaced compositional banding (= layering) and a prominent schistosity. They occasionally contain thin mafic lenses aligned in the plane of the schistosity.

3. Banded quartzo-feldspathic gneisses with interlayered mafic units. These consist of alternating thin mafic lenses and quartzo-feldspathic gneiss. The mafic lenses are aligned parallel to the compositional layering in the gneisses (Figure 2.11b).
4. Garnetiferous quartzo-feldspathic gneisses which have a strong compositional banding due to alternating layers of granular xenoblastic garnets and quartzo-feldspathic phases. Some of these units are migmatitic.

The banding in types (2), (3) and (4) is occasionally accentuated by bands of pegmatite, from a few centimetres to several metres wide composed of quartz, perthite and magnetite.

5. Weakly schistose gneissic granite.

The distribution of the different gneissic types is shown diagrammatically on Figure 1.3. Because of the relative thinness and lensoidal nature of the $tS_0//tS_1$ layering it is not possible to map separate units (cf. the quartzo-feldspathic granulite in the granulite facies terrain).

3.4.4.2 Mineral Assemblages

Under the microscope the gneisses are seen to consist of combinations of the following primary constituents; quartz, microcline and orthoclase perthite, plagioclase, orthopyroxene, clinopyroxene, hornblende, biotite, garnet, sillimanite, apatite, zircon, spinel, corundum and allanite opaque oxides. Secondary products include garnet, biotite, clinopyroxene, quartz, alkali feldspar, hornblende, spinel(?) and margarite.

The following mineral assemblages have been recognised from a study of 56 thin sections of quartzo-feldspathic gneisses.

1. quartz - plagioclase \pm clinopyroxene \pm orthopyroxene - opaques

2. quartz - plagioclase
3. quartz - plagioclase - orthopyroxene - biotite - opaques
4. quartz - alkali feldspar - plagioclase ± opaques
5. quartz - alkali feldspar - plagioclase - biotite - opaques
6. quartz - alkali feldspar - plagioclase - biotite - hornblende
opaques
7. quartz - alkali feldspar - plagioclase - biotite - orthopyroxene -
opaques
8. quartz - alkali feldspar - plagioclase - biotite - clinopyroxene -
opaques
9. quartz - alkali feldspar - plagioclase - hornblende ± clinopyroxene
- opaques
10. quartz - alkali feldspar - plagioclase - orthopyroxene - opaques
11. quartz - alkali feldspar - opaques
12. quartz - alkali feldspar - clinopyroxene ± orthopyroxene ±
hornblende - opaques
13. quartz - alkali feldspar - plagioclase - almandine ± (sillimanite)
- opaques
14. quartz - alkali feldspar - plagioclase - almandine - biotite ±
(sillimanite) - opaques
15. quartz - alkali feldspar - plagioclase - almandine - corundum
- sillimanite - biotite - opaques
16. quartz - plagioclase - almandine - biotite - hornblende - opaques

Perthite (orthoclase and microcline) is included with alkali feldspar. Some of the plagioclase is antiperthitic, however it has not necessarily been differentiated as a separate phase. Minerals present in accessory amounts are not included in the lists of assemblages. Secondary 'coronal' phases likewise are disregarded as their inclusion would contravene the commonly accepted notion of the term mineral assemblage (Korzhinskii, 1959, p.5).

The most common constituents vary within the following ranges: quartz, 15-45%; alkali feldspar 0-75%; plagioclase, 0-62%; hornblende, 0-10%; biotite 0-10%; clinopyroxene, 0-6%; orthopyroxene, 0-10%; almandine, 0-20%; opaques, tr-5%.

3.4.4.3 Microstructures

Under the polarizing microscope the gneisses are either homogeneous or banded. The banding is produced by grain size and compositional differences (see above). Grain size ranges from fine to coarse (and rarely very coarse, e.g. the pegmatites). In sections normal to the lineation they are typically equigranular or inequigranular. The distribution and appearance of grain aggregates is controlled by the effects of the tD_1 and tD_2 deformations¹.

Two groups of microstructures are represented amongst the quartzo-feldspathic gneisses:

1. Microstructural arrays are dominated by xenoblastic and (to a lesser extent) lepto- and nematoblastic grains which form generally granoblastic to granoblastic-elongate aggregates (Figures 3.21a,b,c and 3.22a,b). Grain boundaries are generally curved, embayed or sutured. Smaller recrystallized grains commonly have straight or gently curved interfaces. In sections normal to the lineation, wavy lenticles of quartz and feldspar or prismatic aggregates of orthopyroxene commonly cut $tS_0//tS_1$ at small to large dihedral angles (Figure 3.22a,b).
2. Characterised by the presence of aligned lozenge shaped xenoblastic grains or aggregates of grains in a groundmass of anastomosing layers of quartz, feldspar and ferromagnesian constituents (Figure 3.22c). Grain interfaces are either curved, straight or embayed to sutured. This schistosity may be a manifestation of the tS_2 axial plane schistosity. The gneisses marginal to the Davenport Shear commonly display this schistosity.

1. It is possible also that deformations prior to tD_1 contribute to the appearance of the tD_1 microstructures.

3.4.4.4 Descriptive Mineralogy

Alkali feldspar (both orthoclase and microcline) occurs as subidioblastic to xenoblastic, equidimensional or lozenge shaped, irregularly sutured or gently curved grains. Grain sizes range from less than 0.5 x 0.3 mm to greater than 4.0 x 4.0 mm. Grains are commonly surrounded, or penetrated by, fine granoblastic recrystallized areas (e.g. in A325-698). At low magnification these areas appear to be strongly sutured. However, at greater magnification they can be seen to be composed of discrete xenoblastic smoothly bounded grains. Most grains are untwinned; others show rare Carlsbad twinning. Patch-like shadowy cross-hatched twinning has been observed in a few cases, e.g. A325-472, -396, suggesting a more ordered structure.

Micro- and mesoperthitic exsolution is commonly well developed (Figure 3.16c); string, thread and bead varieties have been observed. There appears to be a greater density of exsolution towards the cores of grains. Some of the larger xenoblasts are poikiloblastic with rounded inclusions of quartz and plagioclase. Wart-like patches of myrmekite commonly embays adjacent plagioclase. The grains of alkali feldspar are highly deformed and show undulose extinction. Mild alteration to kaolin is observed in a few sections.

Plagioclase (An22-37) occurs as angular interlocking xenoblastic and lozenge shaped grains up to 4.0 x 4.0 mm in size. These commonly show undulose extinction and have well developed albite and pericline deformation twins. Rare Carlsbad twins have also been observed. Post-crystallization deformation is also registered in the presence of bent twin lamellae and the formation of sector undulose extinction. Needle-like inclusions and grain boundary aggregates of sillimanite are present in some sections, particularly A325-882N. Some grains are distinctly poikiloblastic with rounded inclusions of quartz. Others are antiperthitic.

Strained quartz forms large sutured and embayed xenoblasts (up to 3.6 x 2.0 mm) or wavy lenticles with undulose extinction and Böhmer lamellae. The xenoblasts commonly comprise irregularly bounded subgrains. Unstrained, newly recrystallized grains (average size 0.08 x 0.08 mm) also have been observed within, or marginal to, the larger

strained xenoblasts. These recrystallized grains form fine to medium grained polygonal aggregates whose straight to gently curved interfaces contrast strongly with the intricately sutured grain boundaries of the subgrains. In some sections the quartz is completely recrystallized, e.g. A325-16B and -370, individual grains being up to 0.2 x 0.2 mm in size.

Garnet (almandine-pyrope) is present as colourless to pale pink porphyroblasts or xenoblasts in some of the gneisses (Figure 3.16c). They range in size up to 0.5 x 0.5 cm, are extensively fractured and commonly contain rounded to subidioblastic inclusions of sillimanite, quartz, spinel, opaque oxides, biotite, feldspars and corundum (Figure 3.16d). In A325-318c the inclusions display 'S' shaped trails. Small granular aggregates of garnets, opaque oxides and decussate patches of biotite occur in 'pull apart' and 'goatee' structures. Trains of granular garnets are commonly aligned parallel to the layering schistosity or the tS_2 schistosity, e.g. A325-882.

Garnet-quartz symplectites or granoblastic garnet, formed by the breakdown of opaque oxides, orthopyroxene, clinopyroxene, hornblende and biotite occur as idioblastic grains (up to 0.2 x 0.2 mm in size) or as ramifying coronas (Figure 3.17c). Traces of biotite, hornblende, quartz, opaque oxides and alkali feldspar are found throughout the coronas.

Several generations of amphibole are present. Ragged decussate aggregates or discrete prismatic subidioblastic grains up to 0.6 x 0.2 mm in size are commonly aligned parallel to the schistosity (Figure 3.18b). Moderate pleochroism is according to the following schemes:

α	pale green yellow
β	deep green
γ	deep green
α	neutral
β	olive green
γ	olive green
α	pale yellow
β	green

γ blue green

with $\gamma > \beta > \alpha$ and $Z^c 29^\circ - 34^\circ$.

Some grains are twinned along (100). Ragged intergrowths of biotite and hornblende are common (Figure 3.18b). Single and double layer coronas of garnet or garnet biotite are frequently observed.

Secondary hornblende is sporadically developed as decussate xenoblasts mantling opaque oxides (Figure 3.17d), biotite and orthopyroxene.

Biotite is common as discrete, subidioblastic to idioblastic laths (up to 0.9 x 0.4 mm in size), as decussate clusters of laths, as fine grained (averaging less than 0.08 x 0.04 mm) intergrowths with garnet, as inclusions, or as aggregates along fractures in garnet porphyroblasts, and as coronas around hornblende. It is commonly kinked and shows undulose extinction. The pleochroism is:

α yellow
 $\beta=\gamma$ red brown
 α neutral
 $\beta=\gamma$ light to dark brown
 α neutral
 $\beta=\gamma$ orange brown

Thin foliae of alkali feldspar occasionally parallel the (001) cleavage direction. Zircon inclusions display narrow pleochroic haloes.

Orthopyroxene (hypersthene) and clinopyroxene have similar microscopic expressions forming irregular prismatic xenoblastic grains which are commonly mantled by coronal phases. Grain sizes range from less than 0.2 x 0.2 mm to 4.0 x 4.0 mm. The hypersthene is weakly to distinctly pleochroic:

α pale pink
 β pale green pink
 γ pale green
 with $\gamma > \beta > \alpha$

It is commonly fractured and shows alteration along cleavages to

serpophite giving the grains a rather ragged appearance. The coronal phases include garnet, clinopyroxene(?) and a pale green to blue green biaxial negative amphibole.

Clinopyroxene is pale green to colourless, often heavily clouded with small granules of opaque oxide and frequently shows fine deformation lamellae. Z^c 's range between 37° and 40° . Grains are commonly surrounded by narrow selvages of garnet and quartz.

Minerals present in accessory or minor amounts include strongly idioblastic laths of apatite, rounded to idioblastic grains of zircon, small flakes of epidote as inclusions in the feldspars, spinel as rounded inclusions in garnet or as irregular xenoblasts associated with or including needle-like grains of corundum. Corundum forms inclusions in ilmenite grains. Sillimanite is common in the garnetiferous rocks as small needle-like inclusions in garnet or as small isolated rhombic sections with well developed (010) cleavages. It is also found in the non-garnetiferous gneisses as sheafs of needle-like inclusions, or grain boundary growths in plagioclase aggregates. Margarite has been identified as a replacement growth, associated with biotite, of sillimanite and corundum.

Skeletal opaques comprise haematite, haemo-ilmenite, magnetite, rutile and ilmeno-haematite.

3.4.5 Calc Silicate Lithologies

See Chapter 3.3.6.

3.5 PETROGRAPHY OF THE AMPHIBOLITE FACIES LITHOLOGIES

3.5.1 Mafic Lithologies

3.5.1.1 General Description

Mafic rocks intercalated with quartzo-feldspathic gneisses north of Amata (both in the Woodroffe Thrust Zone and in the quartzo-feldspathic foreland) constitute less than 1% of the observed lithologies. They occur as minor lenses which are seldom more than 30 cm in length.

In hand specimen they are medium to fine grained, melanocratic, and invariably banded parallel to the regional schistosity $aS_0//aS_1$. Coarse grained quartzo-feldspathic veining is sometimes present.

3.5.1.2 Mineral Assemblages

The following simple mineral assemblages have been recognised in the mafic rocks from north of Amata.

1. plagioclase - hornblende - opaques
2. plagioclase - hornblende - biotite - opaques - (quartz)

Plagioclase and hornblende are present in approximately equal amounts. Sphene, secondary hornblende and biotite are present in several sections, garnet and epidote are accessory phases. However, on microstructural and mineralogical criteria they are believed to represent a later paragenesis.

Modal analytical data for two specimens A325-1684 and -1748 are presented in Table 4.1.

3.5.1.3 Microstructures

In sections normal to aL_2 or aL_3 (see Chapter 2.4), the rocks are predominantly inequigranular, granoblastic to slightly nematoblastic (Figure 3.13c,d). The amphibole occurs as decussate or xenoblastic grains clustered as micro-glomeroporphyroblastic aggregates within the granoblastic groundmass.

Anastomosing trains of fine grained recrystallized hornblende

and biotite express the superposition of a schistosity later than aS_1 , e.g. in A325-1748N.

3.5.1.4 Descriptive Mineralogy

The hornblende is subidioblastic to xenoblastic with commonly well developed cleavages and partings. Grain sizes average 0.6 x 0.4 mm. Z^c 's range from 19° to 22° . Both optically positive (A325-1748N) and optically negative (A325-1684N, -1636N) grains have been observed, suggesting the presence of both common hornblende and pargasitic or edenitic varieties.

The following pleochroic schemes have been observed:

α pale yellow
 β pale green brown
 γ green to green brown

α pale yellow
 β pale blue green
 γ blue green to blue

with $\gamma > \beta > \alpha$

The blue green pleochroism exhibited by these lower grade hornblendes is in keeping with the patterns described by Binns (1964, 1969) in the Willyama metamorphic complex.

Irregular blebs of opaque oxide are commonly scattered throughout the hornblende; inclusions of sphene in some grains are surrounded by shadowy pleochroic haloes. Simple twinning is common parallel to (001). Deformational effects are manifest in the presence of multiple lamellar twins and undulose extinction.

Recrystallized hornblende prominent in A325-1748N occurs as polygonal to decussate xenoblastic grains, averaging 0.02 x 0.02 mm in size, with pleochroism:

α yellow
 β pale green
 γ pale green
 with $\gamma > \beta > \alpha$

suggesting a composition different from that of the primary hornblende.

Plagioclase (An38-45) is present as deformed xenoblasts ranging in size from less than 0.2 x 0.2 mm to greater than 0.8 x 0.8 mm. Pericline and albite deformation twins are commonly well developed. Epidote inclusions are frequent accessories and are interpreted to be an alteration product.

Quartz is a major accessory phase in some rocks forming fine grained unstrained polygonal aggregates or larger, irregular, strained xenoblasts. Grain boundaries range from straight to serrated, and grain sizes vary between 0.08 x 0.08 mm and 0.4 x 0.2 mm

There are two generations of biotite in A325-1748N, viz. fine grained decussate xenoblastic aggregates and subidioblastic laths. Pleochroism respectively, is:

α neutral
 $\beta = \gamma$ brown

 α neutral
 $\beta = \gamma$ red brown

 with $\beta = \gamma > \alpha$

There is also some evidence of subgrain nucleation in the larger kinked laths.

Pale pink to colourless garnet occurs as mosaics of irregular to subidioblastic poikiloblastic grains around xenoblastic opaque oxides (predominantly magnetite and ilmenite). Some of these coronas are up to 0.24 mm wide.

Accessory phases include stumpy laths of apatite, rounded to idioblastic grains of zircon and irregular to rounded grains of sphene. Sphene is also present as coronas around ilmenite.

In contrast to mafic rocks in the granulite and transitional terrains, sillimanite(?) needles in the plagioclase and secondary cummingtonitic amphibole around the hornblende, are both absent.



3.5.2 Quartzo-feldspathic Lithologies

3.5.2.1 General Description

The quartzo-feldspathic gneisses north of the Woodroffe Thrust crop out sporadically as low isolated whale-backs and tors. Their unsubstantial field expression strongly contrasts with the outcrop patterns displayed by the rocks of the granulite facies and the transitional terrains. There is a marked break of slope where the northern amphibolite facies gneisses grade into the Woodroffe Thrust zone. The break of slope is, in fact, a clearer demarcation between the amphibolite facies gneisses and the Woodroffe Thrust mylonites than is the field appearance of these two rock groups.

The gneisses are fine to coarse grained and highly variable in appearance. Some are strongly banded whereas others are homogeneous. Four broad groups have been differentiated on the basis of field characteristics (Figure 1.3). These are:

1. quartzo-feldspathic gneiss which is compositionally layered on a scale ranging from a few millimetres to tens of centimetres (Figure 2.11a); with a prominent schistosity defined by the alignment of ellipsoidal clusters of quartz and feldspar and the parallel alignment of platy aggregates of biotite and hornblende;
2. non-banded, coarse grained quartzo-feldspathic gneiss with large tabular or lozenge feldspars (up to 3.0 x 1.0 cm in size) in parallel alignment and a well developed anastomosing schistosity;
3. medium to fine grained gneiss with a prominent anastomosing layering surrounding small (<0.5 cm diam.) lozenge shaped porphyroblasts (or -clasts) of alkali feldspar and quartz.
4. homogeneous gneissic granite containing gneissic xenoliths (Figure 3.11a).

3.5.2.2 Mineral Assemblages

The essential minerals observed in thin section are quartz, microcline perthite, plagioclase, biotite, muscovite, hornblende, garnet and opaque oxides. Common accessory minerals include apatite,

zircon, allanite, sphene and epidote-zoisite.

The following mineral assemblages have been recorded:

1. quartz - alkali feldspar - plagioclase - biotite - garnet - opaques
2. quartz - alkali feldspar - plagioclase - hornblende - biotite - muscovite - garnet - opaques
3. quartz - alkali feldspar - plagioclase - biotite - hornblende - garnet - opaques
4. quartz - alkali feldspar - plagioclase - hornblende - opaques
5. quartz - alkali feldspar - plagioclase - garnet - biotite ± (muscovite) - opaques

Point counting and visual estimation reveal the following abundances: quartz 20-30%, microcline perthite 30-50%, plagioclase 20-30%, biotite 0-6%, muscovite 0-2%, garnet 0-8%, hornblende 0-8%, opaque oxides tr-2%.

3.5.2.3 Microstructures

The characteristic microstructures observed in the quartzo-feldspathic gneisses are depicted in Figures 3.12a and 3.23a,b. They are dominated by:

- (a) the presence of xenoblastic grains forming granoblastic arrays; and
- (b) the prominence of the compositional banding and the anastomosing layering.

The nature of the anastomosing layering is governed by the extent to which the rocks have been recrystallized and by the size of the recrystallized grains. As the Woodroffe Thrust is approached the incidence of layered anastomosing schistosity increases.

The granoblastic grains are typically inequigranular and the largest grains show interfaces which are curved, embayed or highly sutured. Finer grained recrystallized aggregates of quartz and feldspar between the larger grains commonly have straight or gently curved boundaries forming mosaics with triple point junctions.

3.5.2.4 Descriptive Mineralogy

Several stages of recrystallization of quartz are registered

in the gneisses. Quartz forms lenticular wavy aggregates or trains of small xenoblastic grains producing a layering which engulfs the porphyroblastic components. The wavy lenticles invariably display undulose extinction and range in size up to 3.6 x 1.5 mm. They are commonly composed of intricately sutured subgrains with undulose extinction. Some of the subgrains constitute recrystallization nuclei. The recrystallized aggregates of quartz average 0.08 x 0.08 mm in size and they show crisp extinction. They are commonly elongate and form straight sided polygonal shapes. A325-1744, contains secondary crystallized xenoblastic grains of quartz with highly serrated boundaries which mimic the traces of pre-existing deformation bands or subgrain boundaries.

Microcline or microcline perthite form large tabular to lozenge shaped xenoblastic and subidioblastic porphyroblasts (or -clasts) up to 3.0 x 1.5 cm in size. They have shadowy to distinct cross hatched twinning and X-ray diffraction studies (Chapter 4.3) indicates a high degree of ordering in contrast to the more disordered K feldspar of the granulites and transitional rocks. The larger grains are commonly poikiloblastic with rounded inclusions of plagioclase and quartz. Undulose extinction is common. Some grains show well developed Carlsbad twinning.

Plagioclase (An23-30) is present as subidioblastic to xenoblastic porphyroblasts and as smaller granoblastic recrystallized aggregates. It is commonly poikiloblastic with inclusion of strain-free quartz. The larger grains display albite-pericline or the combination albite-pericline-Carlsbad twins and they have undulose extinction. Some grains are normally zoned. No antiperthitic plagioclase has been observed. Wart-like embayments of myrmekite are more commonly developed in these gneisses than in those of the granulite facies or transitional terrain. Needle-like inclusions of epidote, muscovite or zoisite are ubiquitous in the larger porphyroblastic plagioclase grains.

Biotite is plentifully distributed as trains of small decussate subidioblastic flakes (average size 0.02 x 0.002 mm), intergrown with garnet, muscovite and sphene, or as larger individual flakes with its elongation parallel to the schistosity (up to 1.2 x 0.4 mm in size). It is strongly pleochroic:

α yellow
 $\beta = \gamma$ brown
 with $\beta = \gamma > \alpha$

Grain interfaces are either smoothly straight or raggedly serrated. Slivers of alkali feldspar are elongate parallel to the (001) cleavage direction. Pleochroic haloes around zircon inclusions are commonly observed.

Subidioblastic flakes of hornblende up to 0.8 x 0.4 mm in size with ragged boundaries are commonly surrounded by fine grained biotite, muscovite and garnet. Grains are biaxial negative with 2V approximately 70°. The pleochroism is:

α pale green
 β green
 γ blue green
 with $\gamma > \beta > \alpha$

Z^c's is 22° to 26°. Some grains have multiple lamellar twins, and they extinguish in an undulose fashion.

The garnet is pale pink to colourless, forms intricately fractured xenoblastic or idioblastic grains varying from 0.02 x 0.02 mm to 1.3 x 0.5 mm in size. Sub-parallel aggregates of garnet intergrown with ilmenite and magnetite frequently define a rough banding/schistosity. Symplectic intergrowths of biotite, quartz and opaque oxides with garnet are commonly observed.

Opaque oxides (magnetite, ilmeno-haematite and ilmenite) occur as irregular xenoblastic grains. They are commonly intergrown with the ferromagnesian phases and are frequently observed to be mantled by narrow selvages of pale orange sphene.

Minerals present in accessory amounts include small subidioblastic grains of apatite, zircon, allanite and sphene (showing complex deformation twin patterns) together with idioblastic needles and flakes of zoisite and epidote.

3.5.3 Pelitic Lithologies

3.5.3.1 General Description

Only one pelitic unit has been recognised in the amphibolite facies area (Figure 1.3). It crops out in a narrow schistose band inter-layered with quartzo-feldspathic gneiss and has been traced along strike for approximately 100 metres. In hand specimen the schist is compositionally layered with prominent light and dark grey bands, respectively rich and poor in feldspar. Two schistositys are clearly visible, one parallel to the banding, the other at a low dihedral angle to it. Plagioclase, biotite, garnet and muscovite are distinguishable with the aid of a hand lens.

3.5.3.2 Mineral Assemblage

The following mineral assemblage has been recognised in thin section:

plagioclase - corundum - biotite - garnet - muscovite - opaque oxides.

Zircon is present as an accessory phase.

The muscovite is possibly a component of a later paragenesis.

3.5.3.3 Microstructure

The schist consists of a fine to medium grained matrix of xenoblastic and lepidoblastic phases containing large irregular poikiloblastic porphyroblasts of garnet and corundum. Grain boundaries are either straight or curved.

3.5.3.4 Descriptive Mineralogy

Plagioclase (An₃₂) occurs in two forms:

- (a) as rounded lozenge-shaped xenoblastic grains up to 1.0 x 1.0 mm in size, showing strain extinction;
- (b) as small polygonal xenoblastic grains averaging 0.04 x 0.04 mm, with crisp extinction.

The latter are believed to be recrystallised from the highly strained lozenge shaped variety. The larger grains are commonly extensively

fractured and deformation albite twins are frequently observed.

Biotite occurs as subidioblastic clusters up to 2.0 x 2.0 mm in size and individual flakes up to 1.8 x 0.23 mm. The pleochroic scheme for the mica is:

α straw yellow
 $\beta = \gamma$ black brown
 with $\beta = \gamma > \alpha$

(001) cleavage traces are commonly deformed. Minute inclusions, presumably of zircon, are commonly surrounded by narrow pleochroic haloes.

Muscovite forms colourless idioblastic flakes clearly cross-cutting the earlier formed biotite. Flakes range in size from less than 0.08 x 0.08 mm to greater than 0.2 x 0.04 mm.

Pale pink almandine garnet porphyroblasts with well developed dodecahedral faces measure between 0.23 x 0.10 mm and 2.0 x 1.0 mm. They are commonly poikiloblastic with inclusions of biotite, plagioclase and opaque oxides.

Skeletal colourless to pale blue corundum with prominent basal parting reach a maximum size of 1.0 x 1.0 mm.

Opaque oxides (magnetite, ilmenite and haematite) occur sporadically throughout the rock as small irregular xenoblastic grains complexly intergrown with both biotite and corundum.

Zircon, sphene and apatite are irregularly distributed as accessory phases.

CHAPTER 4

METAMORPHIC PETROLOGY - CHEMICAL

4.1 INTRODUCTION

4.1.1 Previous Work

Recent research in granulite and amphibolite facies metamorphic terrains has suggested that they exhibit distinct and, to some extent, predictable geochemical differences (Ramberg, 1951; Engel and Engel, 1958, 1962; Eade et al., 1966; Heier, 1960, 1964, 1965a,b; Heier and Adams, 1965; Lambert and Heier, 1967, 1968; Fahrig et al., 1967; Sighinolfi, 1969, 1971; Whitney, 1969; Heier and Thoresen, 1971; Lambert, 1971). The more mobile elements (the granitophile elements of Rankama and Sahama, 1950), i.e. K, Rb, Th, Si and U, appear to be present in greater abundances in rocks of amphibolite facies metamorphic grade. On the other hand, the so-called siderophile elements, i.e. Ca, Mg, Fe, Mn, Ti and Sr, appear to be preferentially concentrated in higher grade rocks. These chemical changes are considered by Heier and his co-workers to take place during medium to high pressure granulite facies metamorphism. Belief that such environments are dominated by intermediate bulk chemical compositions (Green and Lambert, 1965; Ringwood and Green, 1966; Green and Ringwood, 1967) are corroborated by more recent calculations of weighted average chemical compositions of high grade metamorphic areas (Lambert and Heier, 1968; Heier and Thoresen, 1971; Lambert, 1971; Sighinolfi, 1971). Shaw (1968b, p.861) however, considered unjustified the assumption that elemental patterns typical of one series of pyroxene granulites are applicable to them all.

Previous geochemical researchers on rocks from the Musgrave Block are briefly mentioned in Chapter 1.

4.1.2 Nature of the Analysed Specimens

A suite of forty-eight rocks from the Amata area was selected for analysis. Twenty-one of these were from the granulite facies terrain, twenty from the transitional terrain and seven from the amphibolite facies terrain. Specimens for analysis were chosen to portray the

major mineralogical and textural groups recognised as a result of field mapping and detailed petrographic examination.

The location of the individual samples can be seen in Figure A.1.1.

4.1.3 Petrographic Descriptions

Petrographic descriptions of the 48 samples are listed in Appendix 1.

4.1.4 Modal Analyses

Micrometric analyses of the analysed rocks are given in Table 4.1. Modal analyses of the analysed rocks were carried out using a Swift Automatic Point Counter. Sections were stained with sodium cobaltinitrite and amaranth dye (following the methods of Chayes, 1952, and Laniz et al., 1964) to facilitate the recognition of alkali feldspar and plagioclase respectively.

4.1.5 Sample Preparation

A bulk rock sample of greater than 400 grms was crushed, sieved and portioned such that sampling errors were considered to be relatively small (see Kleeman, 1967).

Further details of the techniques of sample preparation are given in Appendix 2.

Minerals were separated using standard techniques (Appendix 2). Purities of greater than 99% were obtained.

4.1.6 Methods of Chemical Analysis

Except where indicated¹ all major elements except ferrous iron were determined by X-ray fluorescence spectrometer and flame photometer. U.S. Geological Survey standard rocks were used to gauge the accuracy of the analyses. Statistical data on the accuracy and precision of the

1. Major elements in A325-1636a, -1744 and -1748 were determined by The Australian Mineral Development Laboratories. Uranium determinations were carried out by the same organization using fluorimetric techniques.

analyses are given in Appendix 2.

Trace elements (except for uranium) were determined by X-ray fluorescence spectrographic methods.

4.2 ROCK CHEMISTRY

4.2.1 Compositional Classes of Rocks

Where present, the following compositional classes of rocks in the three metamorphic terrains have been analysed:

- (1) quartzo-feldspathic
- (2) mafic
- (3) ultramafic
- (4) pelitic
- (5) calc silicate
- (6) manganiferous

The above groups are used in preference to the classification of high grade metamorphic rocks proposed by Lambert and Heier (1968) (viz. acid, sub-acid, intermediate and basic) based on the content of SiO_2 . To have rigorously employed Lambert and Heier's (1968) subdivisions would have required the chemical analysis of all lithologies for SiO_2 . The large number of specimens examined by the author made this impracticable. Therefore, it seems preferable, in the absence of chemical analyses of all rocks described, to maintain a common terminology for the different compositional groups of rocks in both the petrological and geochemical discussions.

4.2.1.1 Compositional Abundances

The estimated abundances of the major compositional classes of rocks from the three metamorphic terrains are given below:

	<u>Granulite Facies</u>	<u>Transitional</u>	<u>Amphibolite Facies</u>
Quartzo-feldspathic	90%	90%	99%
Mafic	9%	9% ¹	<1%
Ultramafic) Calc Silicate) Manganiferous)	<1%	<1%	-
Pelitic	-	-	<1%

For comparison the estimated abundances of Lambert and Heier (1968) for the 'Musgrave Range Block' (Ernabella area?) are also presented:

	<u>Granulite Facies</u>	<u>Amphibolite Facies</u>
Acid	5%}	70-80%
Sub-acid	25%}	
Intermediate	20%}	<20%
Basic	25%}	
Hypersthene Granite	20%	
Gabbroic Anorthosite	5%	

From the above lists it is clear that the estimates of abundances of different lithological units in the 'Musgrave Range Block' are considerably different from the estimates in the Amata area (see also Collerson *et al.*, 1972). What is implied by the 'Musgrave Range Block' is uncertain, but, from its stated dimensions (1500 square miles) it would seem to include only part of the Musgrave Block of Hossfeld (1954). The implication, therefore, in Lambert and Heier (1968) that the 'Musgrave Range Block' lithologies are representative of the whole of the Musgrave Block is misleading. From passing observations in the Tomkinson and Mann Ranges (also part of the Musgrave Block, Figure 1.1) lithologies overall are more in keeping with those in the Amata area and contrast to those described by Lambert and Heier (1968).

4.2.2 Modal Composition

4.2.2.1 Granulite Facies Lithologies

Modal analyses of the twenty-one granulite facies lithologies chosen for chemical analysis are given in Table 4.1. Traces of

1. Also includes intermediate lithologies

TABLE 4.1

MODAL ANALYSES OF QUARTZO-FELDSPATHIC GRANULITES

SPECIMEN NO. A325/-	205	199	1121	1165a	77	138
Qtz.	26.31	22.56	28.87	24.72	31.72	29.81
Alk. Feld.	0.21	-	18.48 ^x	10.36 ^x	43.80	39.63 ^x
Plag.	63.88 ¹	70.98 ¹	42.57	61.43 ^{1 2}	12.49 ²	24.54 ^{1 2}
Cpx.	0.89	-	-	-	-	-
Opx.	6.59	4.78	0.78	2.17	-	3.30
Mica	0.04	0.05	-	tr	-	-
Hb.	-	-	-	-	-	-
2° Amph.	0.64	0.28	0.98	0.25	-	0.48
Op.	1.02	0.93	2.24	1.07	1.27	2.21
Gar.	0.30 ⁺	0.37 ⁺	5.90	-	10.63	-
Others	0.13	0.05	0.18	tr	0.08	0.03
Opaques Present						
Mt.	*	*	-	*	*	*
Ilm.	*	*	*	*	*	*
Hae.	*	*	*	*	*	*
Pyr.	-	-	-	-	-	-

x Perthitic Feldspar

1 Antiperthitic

2 Mesoperthitic Feldspar

TABLE 4.1

MODAL ANALYSES OF MAFIC GRANULITES

SPECIMEN NO. A325/-	83	119	105b	81	138b	60	148	121	949	1105	78	158
Qtz.	0.68	1.59	tr	1.55	-	0.56	tr	tr	-	-	0.05	-
Plag.	71.90 ¹	66.83 ¹	63.96 ¹	75.71 ¹	45.22 ¹	67.43 ¹	61.80 ¹	66.13 ¹	17.89	35.21	21.00	35.02
Cpx.	2.73	2.73	8.20	1.77	37.43	1.43	4.04	4.18	28.79	22.65	28.45	19.48
Opx.	18.96	20.03	22.37	15.74	10.06	26.29	27.98	19.39	5.52	14.08	18.97	34.44
Mica	-	0.10	0.12	tr	0.30	0.04	0.18	-	-	0.05	0.44	2.72
Hb.	-	-	-	-	0.59	-	-	-	10.70	8.34	7.24	0.27
2 ^o Amph.	1.58	2.28	2.28	2.00	0.94	1.08	2.11	2.15	4.55	1.23	8.33	2.76
Op.	2.00	2.88	1.36	1.24	4.73	1.17	2.90	5.52	0.10	2.65	6.08	3.85
Gar.	1.42 ⁺	2.58 ⁺	1.23 ⁺	1.68 ⁺	0.69 ⁺	1.91 ⁺	0.88 ⁺	2.64 ⁺	31.28	15.64	1.76 ⁺	1.18 ⁺
Others	0.74	0.99	0.49	0.31	0.05	0.09	0.13	-	1.17	0.14	7.68	0.27
Opaques Present												
Mt.	*	*	-	*	*	*	-	*	-	-	*	*
Ilm.	*	*	*	*	*	*	*	*	*	*	*	*
Hae.	*	*	*	*	*	*	*	*	*	*	*	*
Pyr.	-	-	-	-	-	-	-	*	*	-	-	-

¹ Antiperthitic⁺ Secondary Garnet

TABLE 4.1

MODAL ANALYSES OF CALC SILICATE,
MANGANIFEROUS AND ULTRAMAFIC GRANULITES

SPECIMEN NO. A325/-	2040	2048	2050c
Qtz.	-	54.03	-
Plag.	69.19	-	2.55
Cpx.	-	12.23	24.36
Opx.	-	-	52.83
Mica	-	-	1.04
Hb.	-	-	15.37
2 ^o Amph.	-	-	0.62
Op.	0.92	4.83	tr
Gar.	27.29	24.34	-
Others	2.60	4.57	3.23
Opagues Present			
Mt.	*	*	-
Ilm.	-	-	*
Hae.	-	*	*
Pyr.	-	-	-

TABLE 4.1

MODAL ANALYSES OF QUARTZO-FELDSPATHIC ROCKS
FROM THE TRANSITIONAL TERRAIN

SPEC. NO. A325/-	531	396	400	323	783	474	18	326	405
Qtz.	19.32	18.63	25.66	21.58	33.68	26.63	27.29	19.98	28.93
Alk. Feld	23.64	72.44 ^x	56.60 ^x	31.98 ^x	63.45 ^x	54.53 ^x	40.03 ^x	-	-
Plag.	39.97	-	8.63	19.52	-	14.54	27.75	57.94 ¹	61.99 ¹
Cpx.	-	1.50	0.22	-	0.45	-	-	-	5.44
Opx.	-	-	-	-	0.69	-	-	8.08	-
Mica	0.58	0.98	1.02	7.90	-	3.43	3.24	0.17	-
Hb.	-	2.91	5.00	2.31	-	-	-	-	-
2 ^o Amph.	-	-	-	-	-	0.18	-	2.27	-
Op.	2.70	1.56	1.51	5.74	1.46	0.44	1.46	3.43	0.62
Gar.	13.71	0.93 ⁺	0.09 ⁺	10.64 ⁺	0.16 ⁺	0.18 ⁺	0.05 ⁺	6.36 ⁺	1.55 ⁺
Others	0.09	1.03	1.28	0.34	0.11	0.08	0.09	1.77	1.48
Opaques Present									
Mt.	-	*	*	*	*	*	*	*	*
Ilm.	*	*	*	*	*	*	*	*	*
Hae.	*	*	*	*	*	*	*	*	*
Pyr.	-	-	-	-	-	-	-	-	-

1 Antiperthitic

x Perthitic Feldspar

+ Secondary Garnet

TABLE 4.1

MODAL ANALYSES OF MAFIC AND ULTRAMAFIC ROCKS
FROM THE TRANSITIONAL TERRAIN

SPECIMEN NO. A325/-	517	544	339	523	295	497
Plag.	36.86	35.62	30.04	34.24	3.15	53.18 ¹
Cpx.	10.49	-	14.36	11.03	9.26	19.97
Opx.	22.06	12.22	12.34	15.39	25.66	16.45
Mica	0.14	tr	0.88	-	0.09	0.31
Hb.	18.52	26.24	23.55	27.46	49.06	4.28
2° Amph.	9.85	24.11	11.40	7.46	7.75	4.10
Op.	0.73	0.07	2.71	2.55	1.18	1.06
Gar.	0.23 ⁺	-	2.65 ⁺	1.88 ⁺	0.14 ⁺	0.66 ⁺
Others	1.04	1.75	2.07	-	3.71	-
Opagues Present						
Mt.	*	*	*	*	*	*
Ilm.	*	-	*	*	*	*
Hae.	*	*	*	*	*	*
Pyr.	-	*	-	-	-	-

+ Secondary Garnet

1 Antiperthitic

TABLE 4.1

MODAL ANALYSES OF MICACEOUS MAFIC ROCKS AND
CALC SILICATE ROCK FROM THE TRANSITIONAL TERRAIN

SPECIMEN NO. A325/-	14	6	990	1328	425
Qtz.	2.03	0.13	7.13	0.22	-
Alk feld.	0.55	tr	0.19	15.01	-
Plag.	27.69	24.55	10.03	1.20	51.15
Cpx.	20.92	-	-	46.99	38.56
Opx.	-	-	18.70	-	-
Mica	40.86	3.32	53.69	29.27	-
Hb.	0.74	53.52	-	-	-
2° Amph.	0.12	5.89	6.15	4.25	-
Op.	0.86	1.99	0.06	tr	-
Gar.	6.03	10.19	1.11 [†]	0.62 [†]	0.07 [†]
Scap.	-	-	-	-	2.07
Others	0.18	0.40	2.95	1.90	-
Opagues Present					
Mt.	*	*	*	*	
Iln.	-	*	*	-	
Hae.	*	*	*	-	
Pyr.	-	-	-	-	

† Secondary Garnet

TABLE 4.1

MODAL ANALYSES OF AMPHIBOLITE FACIES LITHOLOGIES

SPECIMEN NO. A325/-	1659	1744	1636a	1684	1748	1687
Qtz.	28.50	22.58	26.80	0.69	1.61	-
Alk. feld	34.16 ^x	44.39 ^x	43.70 ^x	-	-	1.17
Plag.	31.66	25.27	20.00	34.46	28.95	45.74
Cpx.	-	-	-	-	0.61	-
Opx.	-	-	-	-	1.33	-
Bi.	3.85	3.43	5.33	0.60	1.32	40.68
Musc.	-	-	-	-	-	6.24
Hb.	-	-	-	46.10	61.95	-
Op.	1.43	0.95	1.03	7.97	4.03	2.28
Gar.	0.15	3.01	2.78	4.77	-	2.10
Others	0.25	0.36	0.36	5.41	0.20	1.79
Opagues Present						
Mt.	*	*	*	*	*	*
Ilm.	*	*	*	*	-	-
Hae.	*	*	*	*	*	*
Pyr.	-	-	-	-	-	-

^x Perthitic Feldspar

secondary amphibole, clinopyroxene and garnet are present in some rocks (cf. Himmelberg and Phinney, 1967; Griffin and Heier, 1969).

The analysed granulites contain the following assemblages:

(a) Quartzofeldspathic

quartz - plagioclase - orthopyroxene - opaques (A325-199)

quartz - plagioclase - orthopyroxene - clinopyroxene - opaques
(A325-205)

quartz - alkali feldspar - plagioclase - orthopyroxene - opaques
(A325-138, -1165a)

quartz - alkali feldspar - plagioclase - garnet - orthopyroxene
- opaques (A325-1121)

quartz - alkali feldspar - garnet - opaques (A325-77)

(b) Mafic

plagioclase - orthopyroxene - clinopyroxene - hornblende - garnet
- opaques (A325-1105, -949)

plagioclase - orthopyroxene - clinopyroxene - scapolite - opaques
(A325-78)

plagioclase - orthopyroxene - clinopyroxene ± (quartz) (A325-81)

plagioclase - orthopyroxene - clinopyroxene - opaques ± (quartz)
± (biotite) (A325-119, -83, -158, -105b, -121, -148, -60, 138b)

(c) Ultramafic

orthopyroxene - clinopyroxene - hornblende ± (plagioclase) ±
(scapolite) ± phlogopite (A325-2050c)

(d) Manganiferous

quartz - johannsenite - garnet - bustamite - pyroxmangite
(A325-2048)

(e) Calc Silicate

plagioclase - garnet - allanite (A325-2040)

4.2.2.2 Transitional Lithologies

Micrometric analyses for the twenty chemically analysed rocks from the transitional terrain are given in Table 4.1.

The following mineral assemblages are represented amongst the analysed rocks:

(a) Quartzo-feldspathic

quartz - alkali feldspar - plagioclase - garnet - opaques (A325-531)

quartz - alkali feldspar - orthopyroxene - clinopyroxene - opaques (A325-783)

quartz - alkali feldspar - plagioclase - clinopyroxene - hornblende - opaques (A325-400)

quartz - alkali feldspar - plagioclase - hornblende - opaques (A325-396)

quartz - alkali feldspar - plagioclase - biotite - hornblende - opaques (A325-323)

quartz - alkali feldspar - plagioclase - biotite - opaques (A325-18, -474)

quartz - plagioclase - orthopyroxene - biotite - opaques (A325-326)

quartz - plagioclase - clinopyroxene - opaques (A325-405)

(b) Mafic

plagioclase - hornblende - clinopyroxene - biotite - opaques - (quartz) (A325-14)

plagioclase - hornblende - opaques - (quartz) (A325-6)

plagioclase - orthopyroxene - phlogopite ± (quartz) (A325-990)

alkali feldspar - clinopyroxene - phlogopite (A325-1328)

plagioclase - orthopyroxene - clinopyroxene - hornblende - opaques (A325-497, -517, -523, -339)

plagioclase - hornblende - orthopyroxene - opaques (A325-544)

(c) Ultramafic

clinopyroxene - orthopyroxene - hornblende - (plagioclase) -
opaques (A325-295)

(d) Calc Silicate

plagioclase - clinopyroxene - scapolite (A325-425)

4.2.2.3 Amphibolite Facies Lithologies

Modal analyses for the chemically analysed amphibolite facies lithologies are given in Table 4.1. Assemblages represented include:

(a) Quartzo-feldspathic

quartz - alkali feldspar - plagioclase - biotite - garnet -
opaques (A325-1659)

quartz - alkali feldspar - plagioclase - biotite - muscovite -
garnet - opaques (A325-1636a, -1744)

(b) Mafic

plagioclase - hornblende - opaques (A325-1748)

plagioclase - hornblende - biotite - opaques - (quartz) (A325-1648)

(c) Pelitic

plagioclase - biotite - garnet - corundum - muscovite - opaques
(A325-1678)

4.2.2.4 Modal Plots

Ternary plots of quartz, feldspar and 'others', calculated from the modes of the above rocks are depicted in Figure 4.1a,b,c. It is clear that the mafic granulites form two distinct groups (Figure 4.1a), viz. a feldspar-rich and feldspar-poor group. The feldspar-rich group corresponds to those containing antiperthitic plagioclase, whereas the feldspar-poor group contains non-antiperthitic plagioclase. The mafic and quartzo-feldspathic antiperthite bearing rocks from the transitional terrain (A325-497, -326) also fall in a field towards the feldspar apex

of the ternary plot, and the remaining mafic rocks containing non-antiperthitic plagioclase plot towards the 'other' apex (Figure 4.1b).

4.2.3 Major Element Chemistry

Chemical analyses, normative values^{1,2} and Niggli numbers of the Amata rocks are presented in Tables 4.2, 4.3, 4.4 and 4.5.

4.2.3.1 Quartzo-feldspathic Lithologies

4.2.3.1.1 Granulite Facies

A detailed examination of the analyses of the quartzo-feldspathic granulites reveals that they fall broadly into three groups:

- (a) A325-205, -199 and, to some extent, -1165a are characterised by SiO_2 between 67.56 and 70.02, constant Al_2O_3 (16.4%), approximately equal CaO and Na_2O and low K_2O ranging from 0.92 to 1.94%. In all three rocks normative quartz, orthoclase, albite and anorthite are of a similar magnitude, viz. 23.6-25.9%, 5.44-11.5%, c 40% and c 20% respectively.
- (b) The two garnet bearing quartzo-feldspathic granulites (A325-1121 and -77) are also geochemically similar. SiO_2 contents are 69.1 and 71.8% respectively. They have approximately similar Al_2O_3 content and exhibit higher K_2O than Na_2O . This is manifest in relatively high normative quartz and orthoclase and lower normative albite and anorthite. In addition they have much higher normative corundum and show normative cordierite in the catanorm (cf. the other quartzo-feldspathic granulites have low amounts of normative corundum and do not possess any normative cordierite).

-
1. C.I.P.W. norms are given for all rocks to facilitate direct interfacial comparison of the bulk compositions. Mesonorms (Table 4.5) are listed for the hornblende and mica-bearing rocks from the transitional terrain and the amphibolite facies lithologies. Catanorms (Table 4.4) are presented for the granulite facies lithologies and the orthopyroxene bearing lithologies from the transitional terrain. The meso- and catanorms were calculated following the scheme proposed by Barth (1958, 1962) and modified by Kleeman, pers. comm. (Appendix 3)
 2. In the following discussion (except where otherwise stated) all normative values are C.I.P.W. norms.

TABLE 4.2
ANALYSES OF AMATA ROCKS WITH SELECTED TRACE ELEMENTS,
CALCULATED RATIOS AND NIGGLI NUMBERS

Located in the pocket at the back of Volume 2.

TABLE 4.3

C.I.P.W. NORMS OF QUARTZO-FELDSPATHIC GRANULITES

SPECIMEN NO. A325/-	205	199	1121	1165a	77	138
q	23.63	23.27	30.67	25.86	33.05	29.97
c	-	0.37	2.18	0.31	3.02	-
or	5.44	6.80	19.68	11.47	23.58	23.17
ab	40.11	40.11	24.79	41.46	25.64	30.29
an	20.57	20.12	12.69	16.11	6.54	9.22
(wo	0.49	-	-	-	-	0.20
di (en	0.25	-	-	-	-	0.09
(fs	0.22	-	-	-	-	0.10
hy (en	3.43	3.21	2.96	1.42	2.24	1.67
(fs	3.06	2.45	3.05	0.93	3.67	1.83
mt	1.49	0.96	2.22	0.93	1.44	1.86
il	0.74	0.68	1.03	0.40	0.95	0.91
ap	0.14	0.19	0.16	0.09	0.95	0.05
Total	99.57	99.15	99.42	98.97	100.21	99.36
wt % Or	8.22	10.14	34.43	16.61	42.29	36.96
wt % Ab	60.67	59.85	43.37	60.06	45.99	48.33
wt % An	31.11	30.01	22.20	23.34	11.72	14.71
wt % Q	34.16	33.16	40.52	35.82	40.17	35.92
wt % Or	7.86	9.68	26.19	14.55	28.66	27.77
wt % Ab	57.18	57.15	32.99	52.62	31.17	36.51
Σ Q,Or,Ab	69.48	70.78	75.58	70.61	82.10	83.97

TABLE 4.3

C.I.P.W. NORMS OF MAFIC GRANULITES

SPECIMEN NO. A325/-	83	119	105b	81	138b	60	148	121	949	1105	78	158
q	-	1.79	-	-	-	-	1.55	-	-	-	-	-
or	4.08	3.90	3.55	4.08	2.48	3.43	4.14	3.25	0.59	1.71	1.12	2.07
ab	36.64	32.15	28.52	39.01	25.81	35.37	24.96	32.15	12.86	15.91	12.19	16.16
an	38.56	36.91	34.29	36.35	24.34	34.51	34.74	33.30	42.76	37.26	33.17	31.05
ne	-	-	-	-	-	-	-	-	1.01	-	-	-
(wo	0.96	1.19	2.70	1.30	12.76	0.59	0.73	1.98	7.01	7.38	11.70	6.61
di (en	0.58	0.69	1.58	0.75	7.52	0.36	0.42	1.14	4.50	4.56	7.12	4.41
(fs	0.33	0.45	0.99	0.49	4.61	0.20	0.28	0.75	2.06	2.38	3.94	1.71
hy (en	7.69	10.65	15.33	5.77	6.70	13.28	17.09	12.11	-	11.08	9.93	16.18
(fs	4.34	7.04	9.64	3.81	4.11	7.26	11.60	7.97	-	5.79	5.49	6.28
ol (fo	1.56	-	0.16	3.77	2.07	1.63	-	1.85	15.91	5.58	3.36	6.57
(fa	0.97	-	0.11	2.74	1.40	0.98	-	1.34	8.02	3.21	2.05	2.81
cs	-	-	-	-	-	1.44	-	-	-	-	-	-
mt	2.16	2.70	1.28	1.29	4.41	1.44	1.68	2.65	3.76	3.49	6.10	3.06
il	1.22	1.42	0.70	0.68	1.99	0.38	1.48	1.46	1.46	1.75	2.83	2.16
ap	0.05	0.12	0.09	0.05	0.26	-	0.26	0.07	0.05	0.35	0.40	0.30
Total	99.11	99.00	98.93	100.09	98.45	99.42	98.92	100.04	99.97	100.45	99.39	99.36
wt % Or	5.14	5.35	5.34	5.13	4.72	4.68	6.48	4.73	1.05	3.12	2.42	4.20
wt % Ab	46.22	44.07	42.98	49.11	49.04	48.25	39.10	46.80	22.88	28.99	26.22	32.80
wt % An	48.64	50.58	51.68	45.76	46.24	47.07	54.41	48.47	76.07	67.89	71.37	63.01

TABLE 4.3

C.I.P.W. NORMS OF CALC SILICATE AND ULTRAMAFIC GRANULITES

SPECIMEN NO. A325/-	2040	2048*	2050c
or	-		4.91
ab	-		9.39
an	74.01		16.85
ne	1.60		-
(wo	0.64		7.60
di (en	-		5.60
(fs	0.73		1.27
wo	11.83		-
(en	-		20.62
hy (fs	-		4.67
(fo	-		18.79
(fa	-		4.69
cs	2.32		-
mt	6.52		2.48
il	2.01		1.48
ap	0.51		0.12
Total	100.18		98.47
wt % Or	-		15.75
wt % Ab	-		30.15
wt % An	-		54.10

* Not calculated.

TABLE 4.3

C.I.P.W. NORMS OF QUARTZO-FELDSPATHIC ROCKS
FROM THE TRANSITIONAL TERRAIN

SPEC. NO. A325/-	531	396	400	323	783	474	18	326	405
q	20.24	18.90	24.97	17.55	32.77	25.03	26.38	22.15	20.63
c	3.76	-	-	-	0.18	0.51	0.30	-	-
or	21.22	32.92	27.07	27.36	33.92	40.07	29.61	4.85	4.85
ab	26.74	35.62	28.94	27.08	25.55	24.79	32.41	34.19	38.50
an	12.89	4.11	8.50	12.02	4.20	5.65	7.45	25.01	27.74
(wo	-	1.62	1.53	0.50	-	-	-	0.10	2.68
di(en	-	1.02	0.87	0.28	-	-	-	0.05	1.30
(fs	-	0.50	0.60	0.20	-	-	-	0.04	1.34
hy(en	5.65	0.72	2.27	3.33	-	0.80	0.75	4.88	0.02
(fs	4.80	0.36	1.58	2.38	0.70	1.11	0.78	13.86	0.02
mt	2.31	2.07	2.35	4.86	1.67	1.20	1.44	2.78	1.42
il	1.46	0.89	1.04	2.32	0.72	0.66	0.55	1.10	0.59
ap	0.09	0.37	0.26	1.28	0.09	0.23	0.21	0.30	0.16
Total	99.16	99.10	99.98	99.17	99.81	100.05	99.86	99.31	99.26
wt % Or	34.87	45.31	41.96	41.17	53.27	56.83	42.62	7.57	6.82
wt % Ab	43.95	49.04	44.86	40.74	40.13	35.16	46.65	53.38	54.16
w. % An	21.18	5.66	13.18	18.08	6.60	8.01	10.72	39.06	39.03
wt % Q	29.68	21.61	30.83	24.38	35.52	27.84	29.84	36.20	32.25
wt % Or	31.11	37.65	33	38.01	36.77	44.58	33.50	7.92	7.57
wt % Ab	39.21	40.74	35.74	37.61	27.70	27.58	36.66	55.88	60.18
Σ Q,Or,Ab	68.78	88.23	81.00	72.59	92.42	89.85	88.52	61.62	64.46

TABLE 4.3

C.I.P.W. NORMS OF MAFIC AND ULTRAMAFIC ROCKS
FROM THE TRANSITIONAL TERRAIN

SPECIMEN NO. A325/-	517	544	339	523	295	497
q	-	-	-	-	0.78	-
or	2.36	2.01	4.55	2.78	0.41	3.31
ab	9.90	17.77	18.09	20.48	2.96	26.82
an	39.08	46.90	33.82	36.84	19.37	28.21
ne	-	-	0.24	-	-	-
(wo	5.82	3.11	10.15	8.42	9.79	9.94
di (en	3.66	2.11	6.72	5.47	6.73	6.09
(fs	1.80	0.76	2.70	2.38	2.26	3.28
hy (en	17.16	2.71	-	0.43	38.52	7.62
(fs	8.45	0.98	-	0.19	12.95	4.10
ol (fo	4.56	14.29	11.58	11.33	-	3.79
(fa	2.47	5.70	5.14	5.43	-	2.25
mt	3.33	1.80	4.31	4.93	3.74	2.26
il	0.68	0.66	1.65	0.78	1.20	0.80
ap	0.09	0.12	0.16	0.07	0.23	0.12
Total	99.37	98.91	99.10	99.51	98.94	98.59
wt % Or	4.60	3.01	8.06	4.62	1.82	5.67
wt % Ab	19.28	26.65	32.03	34.08	13.02	45.97
wt % An	76.11	70.34	59.91	61.30	85.16	48.35

TABLE 4.3

C.I.P.W. NORMS OF MICACEOUS MAFIC ROCKS AND CALC SILICATE
ROCKS FROM THE TRANSITIONAL TERRAIN

SPECIMEN NO. A325/-	14	6	990	1328	425
c	-	-	2.10	-	-
or	18.20	8.57	26.18	16.45	1.00
ab	24.65	19.03	8.29	-	6.22
an	16.03	27.73	9.82	8.41	54.49
lc	-	-	-	6.24	-
ne	2.23	4.45	-	4.03	0.30
(wo	7.00	7.78	-	22.12	14.54
di (en	4.60	4.72	-	16.93	8.19
(fs	1.90	2.64	-	2.88	5.75
wo	-	-	-	-	2.65
(en	-	-	32.73	-	-
hy (fs	-	-	7.86	-	-
(fo	10.82	9.51	1.49	12.43	-
ol (fa	4.92	5.86	0.40	2.33	-
mt	3.45	5.80	2.06	2.57	3.64
il	2.64	2.79	4.79	2.18	2.20
ap	1.84	0.40	2.86	2.37	0.58
Total	98.28	99.28	98.58	98.95	99.56
wt % Or	30.92	15.49	59.11	66.16	1.63
wt % Ab	41.86	34.39	18.72	0.00	10.07
wt % An	27.22	50.12	22.17	33.84	88.30

TABLE 4.3

C.I.P.W. NORMS OF AMPHIBOLITE FACIES LITHOLOGIES

SPECIMEN NO. A325/-	1659	1744	1636a	1684	1748	1687
q	30.21	20.26	25.40	1.33	-	-
c	-	1.01	1.02	-	-	6.76
or	26.30	40.19	37.23	5.73	10.64	32.62
ab	26.57	22.00	18.62	25.98	15.17	14.59
an	11.56	8.61	9.11	22.05	27.10	10.28
ne	-	-	-	-	1.87	10.21
(wo	0.19	-	-	8.99	10.37	-
di (en	0.10	-	-	6.87	6.58	-
(fs	0.08	-	-	1.18	3.13	-
hy (en	1.17	2.49	2.37	4.73	-	-
(fs	0.91	1.70	2.28	0.81	-	-
ol (fo	-	-	-	-	11.97	7.38
(fa	-	-	-	-	6.28	8.27
mt	1.55	1.54	1.51	14.70	3.25	4.74
il	0.95	1.33	1.23	5.64	1.99	2.72
ap	0.21	0.46	0.46	0.93	0.23	0.21
Total	99.80	99.59	99.23	98.94	98.57	97.77
wt % Or	40.82	56.76	57.32	10.66	20.11	56.75
wt % Ab	41.24	31.07	28.66	48.32	28.66	25.37
wt % An	17.95	12.17	14.03	41.01	51.23	17.88
wt % Q	36.36	24.58	31.26	-	-	-
wt % Or	31.66	48.74	45.82	-	-	-
wt % Ab	31.98	26.68	22.91	-	-	-
Σ Q,Or,Ab	83.25	82.79	81.88	-	-	-

TABLE 4.4

CATANORMS OF QUARTZO-FELDSPATHIC GRANULITES

SPECIMEN NO. A325/-	205	199	1121	1165a	77	138
q	21.76	21.71	28.55	24.13	29.40	28.19
or	5.46	6.84	20.11	11.55	23.90	23.61
ab	42.77	42.88	26.90	44.33	27.59	32.76
an	20.67	20.27	12.98	16.23	6.63	9.40
hyp	7.36	5.32	-	1.36	-	3.86
pyral	-	1.61	7.12	1.34	4.62	-
cord	-	-	1.79	-	6.02	-
ap	0.13	0.17	0.15	0.08	0.08	0.04
mag	1.08	0.70	1.64	0.67	1.05	1.36
ilm	0.08	0.51	0.77	0.29	0.71	0.49
sph	0.70	-	-	-	-	0.29
wt % Or	8.22	10.14	34.43	16.61	42.29	36.96
wt % Ab	60.67	59.85	43.37	60.06	45.99	48.33
wt % An	31.11	30.01	22.20	23.34	11.72	14.71
wt % Q	33.92	33.16	40.41	32.82	38.88	35.84
wt % Or	7.89	9.68	26.37	14.55	29.28	27.81
wt % Ab	58.19	57.16	33.23	52.63	31.84	36.35
Σ Q,Or,Ab	69.99	71.43	75.56	80.01	80.89	84.56

TABLE 4.4
CATANORMS OF MAFIC GRANULITES

SPECIMEN NO. A325/-	83	119	105b	81	138b	60	148	121	949	1105	78	158
q	-	1.13	-	-	-	-	1.09	-	-	-	-	-
or	4.05	3.91	3.54	3.99	2.53	3.38	4.16	3.22	0.59	1.70	1.15	2.06
ab	38.62	34.22	30.20	40.53	27.94	36.98	26.63	33.79	13.52	16.79	13.22	17.09
an	38.31	37.02	34.23	35.60	24.83	34.00	34.93	32.99	42.39	37.07	33.92	30.96
ne	-	-	-	-	-	-	-	-	1.18	-	-	-
di	0.05	0.20	4.14	1.46	21.96	0.56	-	1.64	11.19	11.52	18.69	9.46
hyp	12.10	19.89	25.07	9.41	11.11	20.53	30.30	19.95	-	17.07	15.98	23.14
ac	-	-	-	-	-	-	-	-	-	-	-	-
ol	3.96	-	1.05	7.33	5.92	3.12	-	4.86	26.82	11.12	8.99	12.45
ap	0.04	0.10	0.08	0.04	0.23	-	0.23	0.06	0.04	0.31	0.36	0.27
mag	1.55	1.95	0.92	0.91	3.24	1.02	1.22	1.89	2.68	2.51	4.50	2.20
ilm	-	-	-	-	-	-	0.39	-	-	-	-	-
sph	1.33	1.57	0.77	0.74	2.24	0.41	1.06	1.59	1.59	1.91	3.18	2.37
wt % Or	5.14	3.35	5.34	5.13	4.72	4.68	6.48	4.73	1.05	3.12	2.42	4.20
wt % Ab	46.22	44.07	42.98	49.11	49.04	48.25	39.10	46.80	22.87	28.99	26.22	32.80
wt % An	48.64	50.58	51.68	45.76	46.24	47.07	54.42	48.47	76.08	67.89	71.37	63.01

TABLE 4.4

CATANORMS OF CALC SILICATE AND ULTRAMAFIC GRANULITES

SPECIMEN NO. A325/-	2040	2048*	2050c
q	0.10		-
or	-		4.80
ab	3.23		9.75
an	61.42		16.49
di	4.29		12.12
hyp	-		26.21
ol	-		27.19
gross	23.38		-
ap	0.47		0.10
mag	4.83		1.75
sph	2.27		1.59
wt % Or	-		15.75
wt % Ab	4.72		30.15
wt % An	95.28		54.10

* Not calculated

TABLE 4.4

CATANORMS OF QUARTZO-FELDSPATHIC ROCKS
FROM THE TRANSITIONAL TERRAIN

SPEC. NO. A325/-	531	396	400	323	783	474	18	326	405
q	18.27	17.35	23.00	16.45	30.91	23.38	24.60	20.76	19.02
or	21.54	33.24	27.37	28.09	34.54	40.41	29.81	4.91	4.88
ab	28.82	38.18	31.06	29.51	27.62	26.54	34.63	36.79	41.13
an	13.09	4.15	8.60	12.34	4.28	5.70	7.50	25.37	27.93
di	-	1.81	1.42	-	-	-	-	-	4.31
hyp	-	2.44	5.44	6.85	0.01	0.14	0.52	8.98	0.91
pyral	12.61	-	-	-	0.79	2.25	1.31	-	-
cord	2.80	-	-	-	-	-	-	-	-
ap	0.08	0.34	0.23	1.18	0.09	0.21	0.19	0.28	0.15
mag	1.69	1.51	1.71	3.60	1.22	0.88	1.04	2.04	1.03
ilm	1.09	-	-	1.25	0.54	0.49	0.41	0.72	-
sph	-	0.99	1.16	0.74	-	-	-	0.14	0.65
wt % Or	34.87	45.31	41.96	41.17	53.27	56.83	42.62	7.57	6.82
wt % Ab	43.95	49.04	44.86	40.74	40.13	35.16	46.66	53.38	54.16
wt % An	21.18	5.65	13.18	18.09	6.60	8.01	10.72	39.06	39.03
wt % Q	28.83	21.30	30.48	24.11	35.52	27.84	29.84	36.16	32.00
wt % Or	31.49	37.80	33.60	38.14	36.77	44.58	33.50	7.92	7.61
wt % Ab	39.69	40.90	35.92	37.75	27.70	27.58	36.66	55.92	60.39

TABLE 4.4

CATANORMS OF MAFIC AND ULTRAMAFIC ROCKS
FROM THE TRANSITIONAL TERRAIN

SPECIMEN NO. A325/-	517	544	339	523	295	497
q	-	-	-	-	0.28	-
or	2.37	1.99	4.56	2.77	0.41	3.32
ab	10.54	18.66	19.24	21.69	3.15	28.58
an	39.21	46.41	33.92	36.77	19.41	28.33
ne	-	-	0.29	-	-	-
di	10.18	4.93	17.08	14.96	17.03	17.94
hyp	26.22	3.78	-	0.63	55.49	11.95
ol	8.22	22.13	19.82	18.72	-	7.26
ap	0.08	0.10	0.15	0.06	0.21	0.10
mag	2.41	1.28	3.11	3.55	2.70	1.64
sph	0.75	0.72	1.82	0.86	1.32	0.88
wt % Or	4.60	3.01	8.06	4.62	1.82	5.67
wt % Ab	19.28	26.65	32.02	34.08	13.02	45.97
wt % An	76.12	70.34	59.91	61.30	85.16	48.35

TABLE 4.4

CATANORMS OF MICACEOUS MAFIC ROCKS AND CALC SILICATE ROCKS
FROM THE TRANSITIONAL TERRAIN

SPECIMEN NO. A325/-	14	6	990	1328	425
q	-	-	-	-	-
or	18.31	8.63	26.26	20.29	1.03
ab	26.31	20.33	8.83	-	5.13
an	16.13	27.93	9.86	8.36	55.83
ne	2.65	5.27	-	4.71	1.34
kal	-	-	-	2.38	-
di	9.60	10.89	-	38.96	30.43
hyp	-	-	38.96	-	-
ol	19.90	19.29	1.06	18.95	0.54
pyral	-	-	6.39	-	-
ap	1.66	0.36	2.58	2.12	0.54
spin	-	-	1.06	-	-
mag	2.50	4.21	1.49	1.84	2.69
ilm	-	-	3.52	-	-
sph	2.92	3.09	-	2.39	2.48
wt % Or	30.92	15.49	59.10	70.82	1.67
wt % Ab	41.86	34.39	18.72	-	7.84
wt % An	27.22	50.13	22.18	29.18	90.49

TABLE 4.5

MESONORMS OF QUARTZO-FELDSPATHIC ROCKS
FROM THE TRANSITIONAL TERRAIN

SPEC. NO. A325/-	531	396	400	323	783	474	18	326*	405
q	22.19	17.66	25.01	19.87	31.11	24.02	25.18	-	18.87
or	12.81	32.34	23.72	22.38	34.04	38.88	28.56	-	4.88
ab	28.82	38.18	31.06	29.51	27.62	26.54	34.63	-	41.13
an	13.09	4.15	8.60	12.34	4.28	5.70	7.50	-	27.93
sill	6.26	-	-	-	0.30	0.85	0.49	-	-
di	-	-	-	-	-	-	-	-	3.09
act	-	3.39	2.67	-	-	-	-	-	2.28
bi	13.97	1.44	5.83	9.13	0.80	2.44	2.00	-	-
ap	0.08	0.34	0.23	1.18	0.09	0.21	0.19	-	0.15
sph	-	0.99	1.16	0.74	-	-	-	-	0.65
mag	1.69	1.51	1.71	3.60	1.22	0.88	1.04	-	1.03
il	1.09	-	-	1.25	0.54	0.49	0.41	-	-
wt % Or	24.15	44.63	38.52	35.80	52.90	55.88	41.58	-	6.82
wt % Ab	51.19	49.65	47.52	44.46	40.44	35.94	47.50	-	54.16
wt % An	24.67	5.73	13.96	19.74	6.65	8.19	10.92	-	39.03
wt % Q	37.48	21.82	33.75	29.94	35.86	29.0	30.76	-	31.83
wt % Or	20.04	37.01	29.66	31.24	36.35	43.2	32.32	-	7.63
wt % Ab	42.48	41.17	36.59	38.81	27.79	27.8	36.92	-	60.55
Σ Q,Or,Ab	63.82	88.18	79.79	71.76	93.07	89.40	88.37	-	64.88

* Not calculated

TABLE 4.5

MESONORMS OF MAFIC ROCKS FROM THE TRANSITIONAL TERRAIN

SPECIMEN NO. A 325/-	517	544	339	523	295*	497*
q	1.10	-	-	-		
ab	10.54	15.82	13.67	15.93		
an	-	1.08	20.35	18.38		
act	19.09	0.74	13.88	10.78		
tsch	58.82	68.00	20.36	27.58		
anth	3.40	-	-	-		
eden	-	9.06	19.36	18.43		
bi	3.79	3.18	7.30	4.43		
ap	0.08	0.10	0.15	0.06		
sph	0.75	0.72	1.82	0.86		
mag	2.41	1.28	3.11	3.55		
wt % Or	-	-	-	-		
wt % Ab	100.00	93.27	38.77	44.95		
wt % An	-	6.73	61.23	55.05		

* Not calculated

TABLE 4.5

MESONORMS OF MICACEOUS MAFIC ROCKS AND CALC SILICATE ROCK
FROM THE TRANSITIONAL TERRAIN

SPECIMEN NO. A325/-	14	6	990	1328*	425
q	0.07	-	14.28	-	-
or	2.20	-	-	-	1.03
ab	30.72	22.95	8.83	-	4.98
an	16.13	15.93	-	-	55.83
neph	-	-	-	-	1.07
sill	-	-	3.45	-	-
cor	-	-	-	-	-
di	-	-	-	-	29.48
act	18.00	1.93	-	-	-
tsch	-	18.00	14.79	-	-
anth	-	-	9.05	-	-
eden	-	19.72	-	-	1.91
bi	25.78	13.80	42.01	-	-
ap	1.66	0.36	2.58	-	0.54
sph	2.92	3.09	1.49	-	2.48
mag	2.50	4.21	3.52	-	2.69
wt % Or	4.65	-	-	-	1.67
wt % Ab	61.23	57.59	100.00	-	7.63
wt % An	34.11	42.41	-	-	90.70

* Not calculated

TABLE 4.5
MESONORMS OF AMPHIBOLITE FACIES LITHOLOGIES

SPECIMEN NO. A325/-	1659	1744	1636a	1684	1748	1687
q	29.56	20.58	25.84	1.66	-	-
or	24.65	37.16	34.23	-	-	15.53
ab	28.64	23.65	20.22	28.92	15.06	28.74
an	11.75	8.73	9.33	22.06	21.85	10.40
neph	-	-	-	-	-	4.28
sill	-	1.67	1.71	-	-	-
cor	-	-	-	-	-	7.46
act	-	-	-	17.61	17.49	-
tsch	-	-	-	1.62	8.19	-
eden	-	-	-	-	15.48	-
bi	3.28	5.67	6.20	9.62	17.14	27.93
ap	0.19	0.42	0.43	0.88	0.21	0.19
sph	0.27	-	-	6.51	2.21	-
mag	1.14	1.12	1.11	11.12	2.36	3.46
il	0.53	0.99	0.93	-	-	2.01
wt % Or	38.90	54.51	54.67	-	-	29.30
wt % Ab	42.57	32.69	30.43	55.28	39.39	51.10
wt % An	18.53	12.80	14.90	44.72	60.61	19.61
wt % Q	38.20	27.21	34.36	-	-	-
wt % Or	29.51	45.51	42.17	-	-	-
wt % Ab	32.30	27.29	23.47	-	-	-
Σ Q,Or,Ab	82.85	81.39	80.29	-	-	-

(c) A325-138 is characterised by high SiO_2 , approximately equal amounts of Na_2O and K_2O and lower Al_2O_3 (13.5%) than the other groups. It has high normative quartz, orthoclase and albite. Normative corundum is absent.

4.2.3.1.2 Transitional Rocks

The analysed quartzo-feldspathic rocks from the transitional terrain exhibit a far greater range of compositions than the quartzo-feldspathic granulites. On the basis of major oxide variation, four chemically different specimens or groups of samples can be recognised:

- (a) A325-783, -474, -18
- (b) A325-531
- (c) A325-405, -326
- (d) A325-400, -323, -396

To some extent these divisions are related to petrological subdivisions of the group.

The range of compositions is considered unlikely to be due to biased selection of the granulite samples, as care was taken to ensure that representatives of all petrologically different lithologies were analysed. It is believed to indicate that rock compositions were initially more variable in the transitional terrain.

Normative corundum is present in A325-474, -18, -783 and -531. Cata-normative cordierite is present in A325-531 together with a large amount of normative pyralspite (12.61%) which is present also in smaller amounts in A325-474, -18 and -783. In the mesonorm calculations, excess Al_2O_3 is manifest in the formation of normative sillimanite in A325-531, -18, -474 and -783.

Low K_2O and relatively high CaO in A325-405 and -326, results in much lower normative orthoclase and higher normative anorthite than in the other transitional terrain gneisses. This is the reason for the absence of modal alkali feldspar in these lithologies (cf. perthite in the other transitional quartzo-feldspathic lithologies).

4.2.3.1.3 Amphibolite Facies

The quartzo-feldspathic gneisses from the amphibolite facies

terrain exhibit some of the geochemical features of both the granulite and transitional terrain quartzo-feldspathic rocks. Silica ranges from 76.4-72.5% and K_2O is more abundant than Na_2O .

The group is characterised by greater amounts of normative orthoclase than anorthite, as would be expected from consideration of the potash and lime contents.

4.2.3.1.4 Plots of Normative Quartzo-feldspathic Components

The compositional fields of the analysed quartzo-feldspathic lithologies from the granulite facies, transitional and amphibolite facies areas are indicated by plots of weight percent normative (C.I.P.W. meso- and cata-) quartz-orthoclase-albite and orthoclase-albite-anorthite.

These values of Q, Or, Ab (recalculated to 100%) are plotted onto the anhydrous base of the tetrahedron SiO_2 - $NaAlSi_3O_8$ - $KAlSi_3O_8$ - H_2O (Luth, Tuttle and Jahns, 1964) (Figures 4.2.1a, 4.2.2a, 4.2.3a). The quaternary isobaric minimum and the quaternary isobaric eutectic are plotted for 0.5 kb and 10 kb water pressure. The normative values of Or, Ab and An are plotted onto the feldspar projection of the system $KAlSi_3O_8$ - $NaAlSi_3O_8$ - $CaAl_2Si_2O_8$ - SiO_2 (Figures 4.2.1b, 4.2.2b, 4.2.3b). The position of the low temperature trough in the system (after Kleeman, 1965) is also shown.

Catanorm values for the granulites and mesonorm values for the transitional and amphibolite facies lithologies have been plotted. C.I.P.W. normative positions also are given. It is clear that the positions of the C.I.P.W. and meso-normative Q, Or, Ab are slightly different. This is because in the mesonorm calculation, K_2O in biotite and hornblende has been satisfied before the formation of orthoclase, whereas in the C.I.P.W. norm all K_2O is assumed to be present as orthoclase. Hence the displacement of the (C.I.P.W.) Q, Or, Ab value towards the orthoclase apex away from the quartz-albite side of the quartz-albite-orthoclase ternary plot. This discrepancy between the theoretical (C.I.P.W.) and actual (meso-normative) positions of rocks containing biotite and hornblende in the ternary system has been commented on previously by Barth (1966), Rutland and Sutherland (1967)

and Parslow (1969).

Tuttle and Bowen (1958) found that there was a close correspondence between the minimum melting point at low water vapour pressures, and the position of the 571 analysed rocks in Washington's Tables (1917) which had greater than 80% normative Q + Or + Ab. As a result of this coincidence they concluded that magmatic liquids were involved in the genesis of granitic rocks.

The different groups of quartzo-feldspathic rocks from the Arata area have variable contents of Q + Or + Ab (Table 4.3). Only A325-138 and -77 in the granulite facies and A325-1659 in the amphibolite facies plot close to the field considered by Tuttle and Bowen (1958) to be typical of granitic rocks, and hence close to the minimum melting point in the system Q-Ab-Or-H₂O. A325-1744 and A325-1636a from the amphibolite facies and several rocks from the transitional terrain plot towards the Or apex well away from the minimum melting curve and the field of granitic compositions, a feature which may be the result of potash metasomatism.

The relatively broad spread of plots in Figures 4.2.1a, 4.2.2a and 4.2.3a suggests that it is unlikely that crystal melt equilibria had any large effect on the genesis of the rocks (cf. Barth, 1969).

The Ab-Or-An plots give a far better indication of the overall variations of bulk rock composition and of a possible melt origin. Kleeman (1965) indicated that 'there is a closer correlation between the average granite composition and the low temperature trough in the Or-Ab-An-SiO₂ system than there is between the 'average' granite composition and the minima in the Or-Ab-SiO₂ system'.

From Figure 4.2.1b it is clear that the majority of the quartzo-feldspathic granulites plot away from the low temperature trough. It is significant to compare the relationship of A325-1121, -138 and -77 to the minimum melting curve in the system Q-Ab-Or. This suggests that the quartzo-feldspathic granulites were not apparently directly influenced by 'magmatic' processes.

With reference to Figure 4.2.2a for the transitional terrain, A325-396, -783 and -474 all lie in the orthoclase field away from the minima. However, from Figure 4.2.2b it can be seen that they fall in

the region of the low temperature trough. Similarly in Figure 4.2.3a A325-1636a and -1744 both plot in the Or field away from the minima, however in Figure 4.2.3b it is clear that they also are located within the low temperature trough.

These data indicate that at least some lithologies in the transitional terrain and amphibolite facies terrain approach minimum melting compositions in the 'granite system'. None of the quartzo-feldspathic granulites, however, approach such a composition.

A marked linearity of the normative plots for high grade metamorphic rocks in the projection Or-Ab-An has been reported by Katz (1969) for quartzo-feldspathic and hypersthene granulites from Mont Tremblant Park and for 'charnockites' from Arendal and Langby (Barth, 1969): See Figure 4.3.

Barth (1969) explains the broad spread and general trend from plagioclastic (or antiperthitic) to mesoperthitic (and perthitic) compositions as being due to original heterogeneity of the progenitors (of the quartzo-feldspathic rocks) rather than to any differentiation trend.

The apparent trend towards low melting compositions (Figure 4.3) emphasises the fact that during high grade metamorphism the melting temperature of granite may be exceeded causing partial melting to commence.

Trends displayed in Figure 4.3 by the Amata rocks however are believed to be compositional lines. They do not depict evolutionary trends (cf. Katz, 1969) but rather show chemical variation due to heterogeneity of the progenitors of the different groups.

Evidence of partial melting is nevertheless present in the granulite facies area, i.e. from the presence of quartzo-feldspathic pegmatite veins. These veins post date the gL_{2-3} lineation (Figure 3.11) and they are believed to have been formed during a later metamorphic event.

Cooray (1969, p.979) has indicated that the existence of pegmatites in granulite facies terrains is not uncommon. He explains them as being the result of local partial melting of the quartzo-feldspathic components of the granulites. The fact that partial melting is

manifest in the quartzo-feldspathic granulites and not the mafic granulites is ascribed to the quartzo-feldspathic lithologies having lower melting points than the Ca-femic lithologies.

4.2.3.2 Mafic Lithologies

4.2.3.2.1 Granulite Facies

The mafic granulites exhibit distinct variations in bulk chemistry, notably in their silica and alumina contents (Table 4.2). Only A325-119 and -148 are quartz normative. The remainder develop olivine as a normative and diopside as a cata-normative constituent. Normative nepheline, indicating marked under-saturation of SiO_2 , is present only in A325-949.

The absence of diopside in the catanorm of A325-148 and its presence in the C.I.P.W. norm can be explained by the fact that sphene is a normative mineral in the catanorm (it is not made in the C.I.P.W. norm). Lime is combined with excess titania to form sphene before the formation of diopside. In A325-148 no lime remains after the titania has been satisfied hence formation of diopside is impossible.

With the exception of A325-138b, -78 and -158, the mafic granulites have extremely high alumina (between 17.06 and 22.00%). This feature is believed to be a characteristic of the parent rocks of the mafic granulites (see Chapter 5).

The normative feldspar content of the mafic granulites allows the recognition of two distinct groups, Table 4.6.

It is apparent from Table 4.6 that the mafic granulites containing antiperthitic plagioclase have much higher normative orthoclase and albite than the granulites with non-antiperthitic plagioclase. This suggests that availability of potash may have governed the presence or absence of antiperthitic plagioclase (see also Sen, 1959).

4.2.3.2.2 Transitional Rocks

The mafic transitional terrain rocks exhibit greater variations in bulk composition than the granulites with equivalent silica contents (Table 4.2).

Two broad groups can be differentiated:

TABLE 4.6

NORMATIVE FELDSPAR CONTENT OF THE MAFIC GRANULITES

SPECIMEN NO. A325/-	or	ab	an
<u>Antiperthitic Plagioclase</u>			
83	4.08	36.64	38.56
119	3.90	32.15	36.91
105b	3.55	28.52	34.29
81	4.08	39.01	36.35
138b	2.48	25.81	24.34
60	3.43	35.37	34.51
148	4.14	24.96	34.74
121	3.25	32.15	33.30
<u>Non-antiperthitic Plagioclase</u>			
949	0.59	12.86	42.76
78	1.12	12.19	33.17
1105	1.71	15.91	37.26
158	2.07	16.16	31.05

- (1) A325-497, -517, -544, -339 and -523 with potash contents less than 0.8% and Niggli k values between 0.1 and 0.19;
- (2) A325-990, -1328, -14 and -6 with potash ranging from 1.5-4.4% and Niggli k values from 0.23-0.76.

The term broad is used advisedly as it is recognized that both groups are compositionally variable with regard to other components.

The erratic variations of normative feldspar, quartz, the feldspathoids and the peraluminous minerals for the same rocks in the three schemes of norm calculation serve to indicate the intrinsic difficulties in applying any one normative calculation scheme to a suite of rocks as compositionally heterogeneous as those described above.

For example, A325-990 has 7% modal quartz. In the C.I.P.W. and catanorm schemes the rock is calculated as being undersaturated with SiO_2 whereas in the mesonorm calculation 14% quartz is formed. The author is aware that modal and normative mineralogies should not necessarily correspond. However, differences such as those mentioned are considered to indicate some of the problems involved in applying normative calculation schemes to rocks of unusual composition.

4.2.3.2.3 Amphibolite Facies

The amphibolite facies mafic lithologies A325-1684 and -1748 differ markedly in their contents of TiO_2 , Fe_2O_3 and MgO , Table 4.2. With approximately equal SiO_2 , A325-1684 is quartz normative whereas A325-1748 is undersaturated and contains normative olivine and nepheline. In A325-1684 normative mineral content is influenced by high TiO_2 which combines with iron to form ilmenite. This results in a decrease of normative ferromagnesian minerals allowing a small amount of excess silica to remain after the formation of feldspar. In the mesonorm calculation, sphene is produced instead of ilmenite. Potash is utilized for the formation of biotite instead of orthoclase. The minerals being formed containing potash, viz. actinolite, tschermakite and biotite, contain less SiO_2 than would be required to form orthoclase, and excess silica therefore again remains as normative quartz.

The undersaturated nature of A325-1748 and the presence of normative nepheline is directly attributable to the slightly higher content of Al_2O_3 , and much higher FeO/Fe_2O_3 ratio. Once the alkalis have been satisfied with alumina and silica to form feldspar, excess lime combines with silica magnesia and ferrous iron to form diopside. To satisfy the formation of other ferromagnesian minerals an amount of normative feldspar releases silica thus resulting in the formation of feldspathoids.

4.2.3.3 Ultramafic Lithologies

The ultramafic rocks from the granulite facies area and the transitional terrain, A325-2050c and -295 respectively, have marked differences in their contents of silica, alumina, alkalis and magnesia (Tables 4.2, 4.3, 4.4 and 4.5). For example, A325-2050c is olivine normative and A325-295 is slightly saturated in SiO_2 . The latter also contains lower alkalis and slightly lower alumina and therefore has less normative feldspar than A325-2050c.

4.2.3.4 Calc Silicate Lithologies

Both of the analysed calc silicate rocks (A325-2040 and -425) contain normative wollastonite and abundant amounts of normative anorthite. They both have high Niggli c values which is a reflection of their lime-rich nature.

4.2.3.5 Manganiferous Granulite

Due to the curious chemical composition of A325-2048 (Table 4.2), it was not feasible to calculate a normative mineralogical composition. Niggli values were, however, calculated. The effect of the high MnO is manifest in the fm value of 75.8. The short-comings of the Niggli scheme for inter-compositional correlation or comparison are apparent when extreme rock compositions are considered. As the value of fm is calculated by the expression:

$$fm = \frac{\text{mol.prop.}(Fe_2O_3 + FeO + MnO + MgO) \times 100}{\text{mol.prop.}(Al_2O_3 + Fe_2O_3 + FeO + MnO + MgO + CaO + Na_2O + K_2O)}$$

it is clearly apparent that rocks with high contents of MgO, MnO or Σ Fe oxides will have approximately the same fm value. For general use however (as MnO rich rocks are quite rare), the Niggli system is quite useful for reducing weight per cent data to numbers based on molecular content.

4.2.3.6 Oxidation Ratios

4.2.3.6.1 General

The oxidation ratio of Chinner (1960, p.186) i.e. the molecular percentage $(2\text{Fe}_2\text{O}_3 \times 100)/(2\text{Fe}_2\text{O}_3 + \text{FeO})$, has been used as an index of the oxidation state of the analysed rocks. The ratio is a direct indication of the percentage of total iron in the ferric state.

The oxidation ratios of the Amata rocks are listed in Table 4.2. It can be seen that the granulites have more variable oxidation ratios (11.0-95.2) than either transitional (15.0-47.4) or amphibolite facies rocks (20.38-53.7).

The range of oxidation ratios of the Amata granulites is similar to the range of 17.56-99.21 displayed by the Mont Tremblant granulites (calculated from Table 2, Katz 1969) and the range (22.7-100.0) of Grenville Schists from Ontario (Hounslow and Moore, 1967). Haematite bearing assemblages from the above two localities extend to higher values than those reported from Glen Clova by Chinner (1960), viz. 6.1-74.8.

The mineralogical reflection of oxidation ratios has been emphasised by several workers. Chinner (1960, p.187) found that amongst the Glen Clova pelitic gneisses the magnetite-ilmenite bearing gneisses have oxidation ratios between 0 and 14, the magnetite-haematite bearing gneisses have oxidation ratios in excess of 43 and that the ilmenite-magnetite-haematite bearing gneiss has a ratio of 37.0. Essentially similar relationships are shown by the Amata rocks (Tables 4.1 and 4.2).

Fletcher (1971) showed that in a layered two pyroxene amphibolite from Parham, Ontario, the modal percentage of magnetite is directly related to the oxidation ratio (see Figure 5, p.1074). He also showed that the garnet-bearing and the pyroxene-bearing (hornblende free) mafic assemblages have higher oxidation ratios (37.2 and 40.3, and

27.7-35.9 respectively) than the hornblende-bearing assemblage (14.7-24.1).

4.2.3.6.2 Relationship between Oxidation Ratio and Rock Composition

Chinner (1960, p.188) observed a marked correlation of MnO and total Fe (as Fe_2O_3) with the oxidation ratios in a number of Glen Clova pelitic gneisses. Hounslow and Moore (1967), however, reported no such correlation in the Grenville schists. Nevertheless, both groups of rocks have similar extensive ranges of oxidation ratios.

No linear relationship between the oxidation ratios and the contents of MnO and total Fe was observed for the total populations of specimens from the three metamorphic terrains in the Amata area (Figures 4.4 and 4.5). For the individual chemical classes of rocks, only the mafic granulites show a positive correlation (Figures 4.4a and 4.5a).

To test the significance of the correlation in the mafic granulites, the correlation coefficient and statistic t were computed (Table 4.7).

TABLE 4.7

STATISTICAL DATA FOR THE CORRELATION OF THE OXIDATION RATIO WITH MnO AND TOTAL Fe AS Fe_2O_3

	r_{xy}	n	$df(n-2)$	t	p
(a) Oxidation Ratio/MnO					
Mafic Granulites	0.4689	12	10	1.68	near 0.1 certainly at the 0.2 level
(b) Oxidation Ratio/ ΣFe as Fe_2O_3					
Mafic Granulites	0.5674	12	10	2.18	near 0.05 certainly at the 0.1 level

$$r = \frac{\Sigma xy}{\sqrt{\Sigma x^2 \cdot \Sigma y^2}}$$

$$\Sigma x^2 = \Sigma X^2 - \frac{(\Sigma X)^2}{n}; \quad \Sigma y^2 = \Sigma Y^2 - \frac{(\Sigma Y)^2}{n}$$

$$\Sigma xy = \Sigma XY - \frac{(\Sigma X \cdot \Sigma Y)}{n}$$

$$\text{Statistic } t = \frac{r\sqrt{n-2}}{\sqrt{1-r^2}}$$

p is the probability;

r is the correlation coefficient

n is the population

df is n-2, i.e. the number of degrees of freedom.

From Table 4.7 it can be seen that there is a greater correlation between the oxidation ratio and total Fe than between the oxidation ratio and MnO. The null hypothesis (that the pairs of samples xy are drawn at random from a larger population in which the correlation between xy is zero, i.e. there is no correlation) does not hold at p = 0.10 level for total Fe and p = 0.20 level for MnO. It can therefore be seen that there is a slight positive correlation in the mafic granulites.

Chinner (1960) considered that the correlation between the oxidation ratio and the content of manganese oxide and total iron, supported his hypothesis that the different oxidation ratios are a pre-metamorphic feature and are partially influenced by sedimentary processes. However, in other areas, undoubted metasediments fail to show such correlation (Hounslow and Moore, 1967).

The correlation between total iron and MnO, with the oxidation ratio in the mafic granulites cannot be due to sedimentary processes if the igneous origin of the mafic granulites, postulated elsewhere (Chapter 5) is correct. It seems likely, indeed, that it is an igneous feature established in the intrusive mafics prior to their metamorphism to mafic granulites.

4.2.3.6.3 Mobility of Oxygen

Numerous workers have suggested that the mobility of oxygen is low in rocks undergoing metamorphism (e.g. Rankama and Sahama, 1950; James, 1955; Thompson, 1957; Chinner, 1960; Mueller, 1960, 1961a), and this is supported by the wide range of oxidation ratios in the granulites. This implies steep gradients in the μ_{O_2} between adjacent lithological units. It may be argued, therefore, that these units have remained relatively closed to oxygen during the metamorphism (cf. Taylor and

Epstein, 1962). The smaller range of oxidation ratios of the transitional and amphibolite facies rocks may be a consequence of their generally lower and less variable oxygen fugacities. It is felt, however, that this does not necessarily reflect more open system conditions.

4.2.3.6.4 Variation of Oxidation with Metamorphic Grade

A tendency for $\text{Fe}_2\text{O}_3/\text{FeO}$ ratio to decrease with increasing grade of metamorphism has been suggested by Shaw (1956) and Miyashiro (1958 and 1964) for rocks of pelitic composition, due to the progressive reduction of constituent minerals (Miyashiro, 1964), the oxygen released being dissipated as CO_2 which has a higher mobility than oxygen.

Miyashiro (1958, 1964) found also that the $\text{Fe}_2\text{O}_3/\text{FeO}$ ratio varies with the metamorphic grade of basic lithologies and he attributed this variation to diffusion of the 'reducing fluid' from the associated pelitic rocks. The amount of reduction (hence the $\text{Fe}_2\text{O}_3/\text{FeO}$ ratio in the pelitic units was found to be different from that in the basic units.

At grades of metamorphism higher than those described by Shaw (1956) and Miyashiro (1958, 1964), orthogneisses of the Stark Complex (granulite facies) in the Adirondack Highlands, U.S.A. were found by Buddington *et al.* (1963) to have an $\text{Fe}_2\text{O}_3/\text{FeO}$ ratio of 0.23, whereas orthogneisses of similar composition, but of lower grade (the Diana Complex amphibolite facies) were found to have a ratio of 0.73¹. They considered that the differences in the degrees of oxidation were most likely to be the result of metamorphic, rather than igneous, influences.

Eade *et al.* (1966) working on a large population of samples from New Quebec, Canada, similarly showed that the $\text{Fe}^{2+}/\text{Fe}^{3+}$ ratios were higher in granulite facies terrains than amphibolite facies terrains.

No major differences in the oxidation ratios of rocks of similar bulk composition, metamorphosed at different grades, are found in the Amata area (Table 4.2). Nor were they found by Heier (1960, p.163) in equivalent grade rocks from Langøy, northern Norway.

1. Chinner's Oxidation Ratios calculated for the two complexes are as follows: Diana Complex, 39.1; Stark Complex, 25.1.

4.2.3.7 A.C.F. and A.K.F. Diagrams

4.2.3.7.1 General

A.C.F. diagrams (Figure 4.6a,b,c,d) and, where suitable¹, A.K.F. plots (Figure 4.7a,b,c,d), were constructed, following the rules outlined by Eskola (1939, p.347) and Winkler (1965) to represent the compositions and parageneses of rocks belonging to the different metamorphic groups. From these plots (Figure 4.6a,b,c) it is apparent that the quartzo-feldspathic granulites and gneisses are generally situated towards the A-C side of the ternary plot, away from the MgO, MnO, FeO apex. The rocks of mafic compositions, on the other hand, are located towards the A-F side.

4.2.3.7.2 Comparison with 'Average' Rocks

The generalised fields of some average rock compositions (Table 4.8) are shown for comparison in Figures 4.6d and 4.7d. In the absence of modal analyses for these rocks, no correction could be applied to Fe_2O_3 and FeO for the opaque oxides and to CaO for sphene. Albee (1952) drew attention to the fact that comparison of composite or average analyses of rocks with single metamorphic rocks was not a reliable basis for discerning the effect of chemical changes during metamorphism. The average rocks have not been included for this purpose. They have been included merely to give an indication of the composition of lithologies and suites of lithologies which on the assumption of isochemical metamorphism would possibly have been the antecedents of the sequence of rocks under consideration.

It can be seen that the mafic and quartzo-feldspathic rocks from the Amata area correspond closely with the fields of basic igneous or acid igneous (or arkosic) lithologies respectively.

Because of the presence of unequivocal meta-sedimentary lithologies throughout the area, e.g. quartzite, pelitic schists, calc silicate and manganiferous lithologies it is considered not unreasonable to assume that most of the quartzo-feldspathic rocks were derived from sedimentary (possibly arkosic) progenitors.

1. Certain rock compositions (i.e. most of the mafic lithologies and certain of the quartzo-feldspathic granulites and gneisses) can not be depicted on A.K.F. plots, as a negative value for A ($Al_2O_3 + Fe_2O_3 - Na_2O + CaO + K_2O$) is obtained.

TABLE 4.8

ANALYSES OF AVERAGE IGNEOUS ROCKS

SPECIMEN NO.	A	B	H	C	D	E	F	G
SiO ₂	51.2	47.2	50.19	54.20	66.27	72.08	69.15	63.58
Al ₂ O ₃	15.9	15.8	17.58	17.17	15.39	13.86	14.63	16.67
Fe ₂ O ₃	2.9	3.2	2.84	3.48	2.14	0.86	1.22	2.24
FeO	8.0	8.0	7.19	5.49	2.23	1.67	2.27	3.00
MgO	6.2	7.0	7.39	4.36	1.57	0.52	0.99	2.12
CaO	9.9	10.1	10.50	7.92	3.68	1.33	2.45	5.53
Na ₂ O	2.4	3.2	2.76	3.67	4.13	3.08	3.35	3.98
K ₂ O	0.7	1.4	0.40	1.11	3.01	5.46	4.58	1.40
TiO ₂	1.6	2.4	0.75	1.31	0.66	0.37	0.56	0.64
MnO	0.17	0.16	0.25	0.15	0.07	0.06	0.06	0.11
P ₂ O ₅	0.21	0.48	0.14	0.28	0.17	0.18	0.20	0.17
H ₂ O ⁺	0.8	1.0	-	-	-	-	-	-

- A Average Tholeiitic Basalt and Dolerite; Mason (1967, p.227)
 B Average Alkali Basalt and Dolerite; Mason (1967, p.227)
 H Average High Alumina Basalt; Kuno (1960)
 C Average Andesite; Nockolds (1954, p.1019)
 D Average Rhyodacite and Rhyodacite Obsidian; Nockolds (1954, p.1014)
 E Average Calc Alkali Granite; Nockolds (1954, p.1012)
 F Average Adamellite; Nockolds (1954, p.1014)
 G Average Dacite and Dacite Obsidian; Nockolds (1954, p.1015).

TABLE 4.8
ANALYSES OF AVERAGE SEDIMENTARY ROCKS

SPECIMEN NO.	1	2	3	4	5	28
SiO ₂	76.37	70.00	66.7	58.9	69.69	70.4
Al ₂ O ₃	10.63	8.20	13.5	16.7	13.53	14.2
Fe ₂ O ₃	2.12	2.50	1.6	2.8	0.74	1.7
FeO	1.22	1.50	3.5	3.7	3.10	0.8
MgO	0.23	1.90	2.1	2.6	2.00	0.5
CaO	1.30	4.30	2.5	2.2	1.95	0.6
Na ₂ O	1.84	0.58	2.9	1.6	4.21	5.7
K ₂ O	4.99	2.10	2.0	3.6	1.71	1.6
TiO ₂	0.41	0.58	0.6	0.78	0.40	0.3
MnO	0.25	0.06	0.1	0.09	0.01	0.01
P ₂ O ₅	0.21	0.10	0.2	0.16	0.10	0.07
H ₂ O ⁺	-	-	-	-	-	4.0

- 1 Average Arkose; Pettijohn (1957)
- 2 Average Sandstone from platforms; Wedepohl (1969)
- 3 Average Greywacke; Pettijohn (1963)
- 4 Average Shale from geosynclines; Wedepohl (1969)
- 5 Average Franciscan Greywacke; Taliaferro (1943)
- 28 Analcime-rich Crystal Vitric Tuff; Coombs (1965)

4.2.4 Trace Element Chemistry

4.2.4.1 General

The following trace elements were determined during the course of this study: Rb, Sr, Zr, Ca, La, Th and U. Their values are listed in Table 4.2. Techniques employed in their determination are given in Appendix 2.

4.2.4.2 Rubidium and K/Rb Ratio

4.2.4.2.1 Introduction

The K/Rb ratios in terrestrial igneous and metamorphic rocks have been the subject of considerable research and discussion by petrologists and geochemists during the last two decades.

Arhens et al. (1952) first recognised the significance of the K/Rb ratios in igneous rocks and proposed that the ratio has a constant value of 90 in all except pegmatites where it is less. Taylor et al. (1956) confirmed the trends established by Arhens et al. (op.cit) but amended the average value to 240. Subsequently, Taylor (1960), Heier and Adams (1964) and Taylor (1965) have established that, in general, continental igneous rocks are characterised by K/Rb ratios between the limits of 160 and 300 with a median value of 230.

Recent studies of mafic and ultramafic igneous rocks by Gast (1965), Tatsumoto et al. (1965), Erlank et al. (1968) and Hart (1969) have drawn attention to the anomalously high K/Rb ratios (1000-2000) exhibited by the oceanic tholeiites and some continental intrusive rocks with tholeiitic affinities, e.g. Bushveld (Erlank et al., 1968). The high ratios have been interpreted as being a primary magmatic phenomena related to the source material of the magma.

Silicate phases (e.g. garnet, pyroxene and mica) occurring in xenoliths or as xenocrysts in kimberlites and other mafic igneous rocks (Griffin and Murthy, 1968, 1969; Philpotts and Schnetzler, 1970 - see Table 4.9) have much lower K/Rb ratios than are normally found in igneous rock suites with high K/Rb ratios.

Studies by Hart and Aldrich (1967), Erlank et al. (1968), Griffin and Murthy (1968, 1969), Philpotts and Schnetzler (1970) and

Murthy and Griffin (1970) on the K/Rb ratios (Table 4.9) of amphiboles and plagioclase (phases which are stable in the upper mantle) have emphasised the importance of their control on the K/Rb ratio in the upper mantle, as both these phases may have a high K/Rb ratio. Partial melting of mantle material containing significant amounts of these species could therefore result in the production of magmas with high initial K/Rb ratios.

In differentiated igneous rock suites it has been noted that K and Rb appear to undergo fractionation, with the result that K/Rb ratio decreases in the more quartzo-feldspathic members. As a result certain highly fractionated rocks such as alkali granites and pegmatites commonly exhibit ratios less than 160 (Taylor et al., 1956; Heier and Taylor, 1959).

Shaw (1968a) quantified the above fractionation relationships for 21 igneous rock suites by covariance analysis of their potassium and rubidium contents. He recognised three trends:

- (1) The main trend with K/Rb ratios of 160-300.
- (2) The oceanic tholeiite trend with high K/Rb ratios.
- (3) The hydrothermal trend with low K/Rb ratios extending from 150 to 20.

He emphasised the mineralogical control of these trends.

Differences of K/Rb ratios between groups of high grade metamorphic rocks have been investigated by Lambert and Heier (1968), Whitney (1969), Sighinolfi (1969, 1971), Lambert (1971) and Heier and Thoresen (1971). These authors all found that granulite terrains, and especially the medium-high pressure granulite terrains, have higher K/Rb ratios than the amphibolite facies areas. Following Heier (1960, 1964, 1965a) and Shaw (1968a), they suggested that these patterns of K/Rb distribution are the result of fractionation of effects within the crust, Rb becoming concentrated relative to K in the lower grade rocks and depleted relative to K in the higher grade lithologies.

Rubidium was analysed in the Amata rocks to see if such a pattern was present. It was considered that the distribution of K/Rb ratios may have been a criterion for recognising whether or not the

TABLE 4.9
SOME COMMON VALUES OF K/Rb IN ROCK FORMING MINERALS

REFERENCE	BIOTITE	AMPHIBOLE	PYROXENE	K FELDSPAR	PLAGIOCLASE	GARNET	PHILOGOPITE
Demin and Khitarov (1958)	(4) 82-196						
Sen et al. (1959)	(6) 40-76	(2) 1200, 1400		(4) 147-255			
Zartman (1964)	(16) 29-115			(7) 148-415	(2) 382, 847		
Hart and Aldrich (1967)	(14) 35-470	(50) 100-5000	(2) 243, 670		(2) 280, 342		
White (1966)	(9) 65-129			(16) 245-554			
Stueber (1969)			(9) 67-714				
Lange et al. (1966)	(16) 35-219			(16) 108-620			
Heier (1966)				(5) 560-784	(6) 780-2100		
Rhodes (1969)				(70) 65-589			
Griffin et al. (1967)		(9) 295-2570					
Virgo (1966)					(21) 65-780		
Griffin and Murthy (1968, 1969)		(3) 171-2530	opx (4) 142-229 cpx (18) 105-982			(12) 114-318	(1) 280
Whitney (1969)	(42) 87-214						
Philpots and Schnetzler (1970)	(1) 158	(5) 1000-9758	opx (2) 273-415 cpx (9) 194-966	(1) 470	(11) 281-2890	(1) 213	(2) 192, 224
Murthy and Griffin (1970)					(15) 568-2941		

The number in parenthesis refers to the number of specimens

transitional rocks were retrograded granulites. Heier and Thoresen (1971, p.98) found that the retrograded granulites on Langøy had similar K/Rb ratios to the granulites and they interpreted both suites as being originally the same rock. They concluded therefore that 'retrogression does not noticeably affect the trace element concentrations' between granulites, and granulites that have suffered later retrogression.

4.2.4.2.2 Presentation of Results

From Table 4.2 it can be seen that the rubidium contents of the major rock types in the Amata area are highly variable. Average values are listed in Table 4.10.² The weighted average rubidium contents of the granulite facies, transitional and amphibolite facies rocks (Table 4.11) (viz. 44 p.p.m., 163 p.p.m. and 230 p.p.m. respectively) are higher than the estimated crustal abundances of rubidium (15 p.p.m. and 100 p.p.m. respectively) in the lower and upper continental crust (Hurley, 1968).

Log-log plots of %K ($K^+ 1.33\text{\AA}$) against p.p.m. Rb ($Rb^+ 1.49\text{\AA}$) for each of the different metamorphic groups are given in Figure 4.8.

From Table 4.11 it can be seen also that the weighted average K/Rb ratio for the granulite facies (quartzo-feldspathic and mafic) lithologies is considerably higher than for the transitional and amphibolite facies rocks. These K/Rb values conform to the patterns established elsewhere in granulite and amphibolite facies terrains, viz. in the Australian Shield (Lambert and Heier, 1968); in the Valle Strona, Western Alps (Sighinolfi, 1969); in the Adirondacks, U.S.A. (Whitney, 1969) and in Lofoten Vesterålen, Norway (Heier and Thoresen, 1971).

The range of K/Rb ratios for the quartzo-feldspathic and mafic rock types (the most abundant rocks in the three areas and, therefore, those with the most significant effect on the weighted average K/Rb ratio) are listed in Table 4.12.

Following the method of Shaw (1968a) linear regression analyses¹

-
1. This method was also followed by Sighinolfi (1969) for granulite and amphibolite facies rocks from Valle Strona.
 2. See pocket at back of Volume 2.

TABLE 4.11

WEIGHTED AVERAGE CHEMICAL COMPOSITION
OF THE AMATA AREA, MUSGRAVE RANGES

	GRANULITE FACIES	TRANSITIONAL TERRAIN	AMPHIBOLITE FACIES
SiO ₂	67.75	66.48	69.07
Al ₂ O ₃	15.78	15.03	14.94
Fe ₂ O ₃	1.12	1.64	1.09
FeO	2.67	2.64	1.90
MgO	1.66	0.88	0.88
CaO	3.62	3.28	2.29
Na ₂ O	3.90	3.33	2.65
K ₂ O	2.34	4.37	5.81
TiO ₂	0.45	0.60	0.63
MnO	0.12	0.11	0.09
P ₂ O ₅	0.05	0.17	0.16
%K	1.94	3.63	4.82
Trace Elements in p.p.m.			
Sr	333.0	235.6	212.5
Rb	44.0	163.0	229.8
Th	3.4	16.1	104.2
Zr	145.2	310.5	-
Ce	55.6	165.2	-
La	27.7	72.6	-
U	0.4	0.8	-
Rb/Sr	0.176	1.08	1.59
(Th/K) x 10 ⁴	1.96	6.38	19.92
K/Rb	628.1	310.3	202.9
(U/K) x 10 ⁴	0.21	0.17	-

TABLE 4.12
 RANGE OF K/Rb RATIOS FOR AMATA QUARTZO-FELDSPATHIC
 AND MAFIC ROCK TYPES

Quartzo-feldspathic		
Granulite Facies	363(A325-1121)	1046(A325-205)
Transitional	151(A325-18)	486(A325-326)*
Amphibolite Facies	178(A325-1636a)	232(A325-1659)
Mafic		
Granulite Facies	244(A325-949)	2293(A325-60)
Transitional	Bi poor	317(A325-544)
	Bi bearing	120(A325-14)
Amphibolite Facies	431(A325-1684)	604(A325-1748)

* Exception A325-405, K/Rb 1583

were made of the K and Rb data from the quartzo-feldspathic, mafic and ultramafic classes of rocks, separately, and from those classes combined from the different metamorphic environments.

The analyses of covariance were undertaken to test the hypothesis that the K/Rb ratios from the different metamorphic suites are, or are not, drawn from a single larger population, i.e. to see whether or not the K/Rb ratios trends differ between the three groups of metamorphic rocks.

The method clearly shows (see below, p.166) the influence of mineralogy on the K/Rb ratios of the different compositional classes of sample, thus emphasizing the necessity to weight data when determining the average K/Rb ratios for metamorphic terrains.

Details of the statistical methods and a summary of data used in the construction of the regression lines in Figure 4.9a and c are given in Appendix 5.

A single line, the reduced major axis (R.M.A.) was calculated (following Sighinolfi, 1969) in place of the two regression lines for the quartzo-feldspathic and mafic lithologies in the granulite facies and transitional terrains (Figure 4.9b,d) and for the total granulite, transitional and amphibolite facies populations (Figure 4.10a).

The R.M.A. represents the major axis of the correlation surface for each pair of regression lines. The data used in their construction are given in Appendix 5.

To test for significance and to compare the slopes of the reduced major axes, Miller and Kahn (1962, p.124) propose that the following equations should be used:

$$Z = \frac{K_1 - K_2}{\sqrt{S_{K_1}^2 + S_{K_2}^2}}$$

and (slightly modified)

$$Z^1 = \frac{y_0(K_1 - K_2) + (b_1 - b_2)}{\sqrt{S_{K_1}^2(y_0 - y_1)^2 + S_{K_2}^2(y_0 - y_2)^2}}$$

In the first expression, the significance of regression coefficients of the reduced major axes is tested. In the second expression, both

regression coefficients and intercepts are tested. Results of these tests are tabulated in Table 4.13. The values of Z are taken from standard normal tables (i.e. tables of the normal distribution function).

TABLE 4.13
SIGNIFICANCE OF THE REDUCED MAJOR AXES

	Z	Confidence Level
Granulite/Transitional	0.12	90%
Granulite/Amphibolite	-1.19	23.4%
Transitional/Amphibolite	-1.65	9.9%
	Z ¹	
Granulite/Transitional	-2.31	2%
Granulite/Amphibolite	0.79	42.96%
Transitional/Amphibolite	1.48	13.88%

The absolute values of Z (Table 4.13), i.e. 0.12, 1.19 and 1.65, indicate that the expected difference between $(K_G - K_T)(K_G - K_A)$ and $(K_T - K_A)$ is larger than that observed when drawing pairs of samples from a homogeneous population 90%, 23.4% and 9.7% of the time respectively. In addition, a distance larger than $0.90\%K$, $0.04\%K$ and $0.22\%K^1$ would be expected between the slopes of the three R.M.A.'s (i.e. G-T, G-A, T-A), 2%, 43% and 13.9% of the time.

Therefore the null hypothesis that the slopes of the R.M.A.'s are drawn at random from a larger population is corroborated only in the case of the granulite facies and transitional terrains. It can therefore be concluded that only the granulite facies and transitional facies rocks behave as a single population with regard to K/Rb but the granulite-amphibolite and the transitional-amphibolite facies rocks do not.

This suggests that the K/Rb distribution pattern in the amphibolite facies rocks is **different** from that in the granulite and transitional lithologies. This is due possibly to the limited number of samples in the amphibolite facies population ($n = 6$) compared with the

1. This is the difference in %K between each pair of R.M.A.'s at a given p.p.m. Rb (or y).

other populations. Alternatively, it is possibly a real effect due to differences in metamorphic grade.

These results are at variance with those of Sighinolfi (1969, p.352) who, after carrying out a similar regression analysis of covariance, concluded that both the amphibolite and granulite series behave as single populations with regard to the K/Rb ratio. The reduced major axes of the Sighinolfi (1969) data are included for comparison in Figure 4.10b.

It can be seen (Figure 4.10b) that the R.M.A. slopes for Whitney's (1969) paragneiss and granitic gneiss data from the Adirondacks have different orientations both from those of Sighinolfi (1969) and from the Amata rocks. This is interpreted as being the result of mineralogical control. The steeper slopes of Whitney (1969) are the result of not including mafic lithologies in the population. Mafic lithologies generally have high K/Rb ratios (e.g. the Amata values other than the quartzo-feldspathic lithologies - Table 4.2), thus they tend to weight the population towards generally higher ratios, although the individual samples have lower total contents of K and Rb.

It is therefore important to realise that the trend of the reduced major axis in a mixed unweighted population of lithologies does not represent the average K/Rb ratio for that population, but only a trend. For example, in Figure 4.10a, the amphibolite facies R.M.A. lies between that of the granulite and that of the transitional terrain, although the amphibolite facies weighted average K/Rb ratio is less than that of both the granulite and transitional terrains, i.e. 203, (cf. 628 and 310 - Table 4.11).

This emphasises the importance of weighting K/Rb ratios in terms of the areal abundance of the lithologies involved when calculating the average K/Rb ratio of any given terrain. Such weighting methods have been followed by Eade *et al.* (1966), Lambert and Heier (1968), Lambert (1971) and Sighinolfi (1971).

The K/Rb ratios in the quartzo-feldspathic and pelitic assemblages clearly decrease with increasing %K content (Figure 4.11a,b,c). A similar relationship is demonstrated by Shaw (1968), Whitney (1969), Sighinolfi (1970) and Sheraton (1970).

Figure 4.11a, however, shows that no such relationship is manifest in the mafic granulites. This is interpreted as indicating that the mafic granulites behaved in a manner different from the quartzo-feldspathic granulites during metamorphism as regards the distribution of K and Rb.

These different patterns of behaviour of K and Rb are also depicted by the correlation coefficients (Table A.5.1) determined during the analysis of covariance. There is a high degree of correlation in the quartzo-feldspathic granulites ($r_{xy} = 0.9895$) whereas there is virtually no correlation between K and Rb in the mafic granulites ($r_{xy} = 0.2645$).

These data indicate that while the hypothesis of fractionation of K and Rb may be applicable to the quartzo-feldspathic granulites to account for their K/Rb ratios, it does not appear to be valid for the mafic lithologies. It is therefore possible that the K/Rb ratios of the mafic granulites are to some extent manifestations of original compositional differences - perhaps igneous features (see also Chapter 5) preserved during isochemical metamorphism.

The somewhat limited data for the mafic rocks in the transitional and amphibolite facies terrains indicate that the K/Rb ratio decreases as %K increases. This fractionation effect is believed to indicate that in the more hydrous transitional and amphibolite facies environments the metamorphism was not isochemical.

4.2.4.2.3 Mineralogical Control of the K/Rb Ratios

The mineralogical variation in rocks from the different metamorphic groups has a significant effect on the slopes of the R.M.A.'s for the different bulk compositions (Figure 4.9b,d).

For example, the R.M.A. of the mica poor transitional mafic rocks differs greatly in slope from that of the mica bearing mafic rocks. It is therefore significant that the (mica free) hornblende bearing rocks have higher K/Rb ratios than those that contain only abundant mica. As hornblende has a high K/Rb content (see Table 4.9) an increase in its modal content will result in an increase in K/Rb ratio of the total rock (see Hart, 1968). Biotite, on the other hand, is characterised by lower K/Rb ratios as biotite has the ability to concentrate Rb relative to K. Hart (1968) stresses the fact that biotite would contribute more Rb to

the total rock composition than hornblende, therefore lower K/Rb ratios would result.

Shaw (1968a) considered that the greatest control on the K/Rb ratios of the common igneous rocks would come from the modal proportion of biotite and hornblende.

Erlank et al. (1968) believed that the high K/Rb ratios of the Bushveld rocks were due to the fact that the plagioclases discriminated against the entry of Rb^+ into their structures. They believed that K^+ (1.33Å) preferentially entered Na^+ (0.97Å) sites and this excluded Rb^+ (1.49Å). Similarly, Philpotts and Schnetzler (1970) considered that plagioclase is a greater potential control on the high K/Rb ratios of anorthosites than either hornblende or mica. They considered that as the anorthite content of plagioclase decreases K^+ increases at the expense of Rb^+ (for the same crystallo-chemical reasons as discussed in Erlank et al., 1968) and hence K/Rb increases.

Gill and Murthy (1970) found that antiperthitic plagioclases from the Nain anorthosite have higher K/Rb ratios than the non-exsolved types and considered that the substitution of Rb for Na instead of for K in plagioclase is not inconceivable on geochemical grounds as the Rb^+ is 10% larger than the K^+ ion and Rb compounds have lower melting points, heats of fusion and lattice energies.

Murthy and Griffin (1970) found that metamorphic plagioclases (mainly from amphibolite facies rocks) have low K/Rb ratios whereas plagioclases from gabbroic rocks and anorthosites have higher K/Rb ratios. They considered that the low K/Rb ratios of the plagioclases from the amphibolite facies rocks reflect the absence of 'plagioclase fluid equilibration processes'. They considered the higher K/Rb ratios in granulite facies rocks to be the result of partial fusion and dehydration (Lambert and Heier, 1968) with plagioclase liquid equilibration taking place causing an increase in the concentration of Rb in the postulated liquid phase.

Plots of K against K/Rb, using Virgo's (1966) and Murthy and Griffin's (1970) data suggest that there are no significant differences in the K/Rb ratios between the plagioclases of quartzo-feldspathic granulite and those of amphibolite facies rocks (Figure 4.11d). There-

fore, plagioclase liquid equilibration may not have played a significant role in the genesis of the higher K/Rb ratios of the granulites.

Although no data are available for the plagioclases from the Amata granulites, it is possible that the relatively high K/Rb ratios displayed by some of the mafic granulites are of a primary (possibly igneous) nature. It seems unlikely that the K/Rb of orthopyroxene and clinopyroxene have had much effect on the high K/Rb ratios (see Table 4.9) of the mafic granulites. It is more likely that the plagioclase in these mafic rocks influences the K/Rb ratio. A325-2050c has minor plagioclase and is composed predominantly of orthopyroxene, clinopyroxene and amphibole, and displays a low K/Rb ratio (229), whereas A325-60, with a K/Rb ratio of 2293, does not contain hornblende and is composed predominantly of orthopyroxene and plagioclase.

TABLE 4.14

K/Rb RATIOS OF ANTIPERTHITE AND 'NORMAL'
PLAGIOCLASE-BEARING MAFIC GRANULITE

SPECIMEN NUMBER	A325/-	K/Rb
<u>Antiperthitic Plagioclase</u>		
83		1245
119		1015
105b		1060
81		1736
138b		1516
60		2293
148		1263
121		302
<u>'Normal' Plagioclase</u>		
949		244
78		1213
1105		669
158		257

From Table 4.14 it can be seen (with two exceptions, A325-121 and A325-78) that antiperthitic plagioclase bearing mafic granulites have higher K/Rb ratios than those with 'normal' plagioclase. This is considered to corroborate Gill and Murthy's (1970) findings regarding the K/Rb ratios of antiperthitic and non-antiperthitic plagioclase in the

Nain anorthosite. It strongly suggests that the K/Rb ratios in the Amata mafic granulites are an initial igneous feature.

4.2.4.2.4 Evidence for Crustal Fractionation

The K/Rb ratios displayed by the Amata rocks appear to conform to the worldwide pattern (viz. higher K/Rb ratios in granulite facies terrains, cf. amphibolite facies terrains). However, whether or not they are the result of crustal fractionation processes is a matter of contention. For example, errors may be involved in the calculation of the weighted averages, due to inaccurate estimation of the volume percentage of the different rock compositions.

To determine unequivocally whether or not such a fractionation process takes place, it would be necessary to examine only rocks which were originally of exactly the same bulk composition, and which can be traced from one metamorphic grade to another. This point was emphasised by Taylor (1965) who considered (p.196) that 'evidence is lacking for the migration of elements on a large scale....during metamorphic processes.' He considered that this is '....due to the difficulty of finding....large bodies of rock of identical composition' which can 'be traced through several metamorphic facies.'

In the Amata area the metamorphic suites are fault bounded, precluding the possibility of tracing units from one metamorphic grade to another. Therefore the K/Rb ratios of the different metamorphic grades can not be rigorously compared.

Nevertheless, within the individual metamorphic terrains, e.g. the granulite facies terrain, some lithologies (i.e. the quartzofeldspathic) have apparently been influenced by fractionation processes, whereas others have not (i.e. the mafic granulites). As the average compositions for the different terrains are weighted towards quartzofeldspathic compositions, it can be surmised therefore, that fractionation processes have influenced the weighted K/Rb values in the individual metamorphic terrains. It is not possible however, to say whether or not the three terrains represent an original crustal succession.

The low ratios of K/Rb in transitional rocks, cf. the granulite facies lithologies, possibly indicate that they are not a suite of

retrograded granulites, cf. Heier and Thoresen (1971, p.98).

4.2.4.3 Strontium and Rb/Sr Ratio

The average strontium contents of the major rock compositions have been calculated from the values listed in Table 4.2. These average values, together with their standard deviations are presented in Table 4.10.

The quartzo-feldspathic granulites have higher average strontium contents (viz. 326 p.p.m.) than either the quartzo-feldspathic rocks from the transitional or amphibolite facies areas (viz. 217 p.p.m. and 213 p.p.m. respectively). The mafic granulites and transitional mafic lithologies have virtually identical strontium contents (viz. 397 p.p.m. and 401 p.p.m. respectively). They contrast strongly with the mafic amphibolite facies rocks which have an average content of only 131 p.p.m. The reason for the high value in transitional mafic suite is undoubtedly due to the inclusion of A325-1328 (1793 p.p.m.). If this value is omitted the average value becomes 262 p.p.m.

The weighted average content of strontium in the granulites is higher than that present in the transitional or amphibolite facies rocks (Table 4.11), as the average values have been weighted towards quartzo-feldspathic compositions.

The strontium value (333 p.p.m.) for the Amata granulite facies terrain compares favourably with the value given by Lambert and Heier (1968) for the 'Musgrave Range block' granulites (viz. 340 p.p.m.). The average values for the transitional and amphibolite facies terrains (viz. 236 p.p.m. and 213 p.p.m. respectively) are decisively lower, however, than the strontium value quoted by Lambert and Heier (1968), viz. 400 p.p.m. for amphibolite facies rocks. They compare more favourably with the value for the Cape Naturaliste amphibolite facies terrain (viz. 190 p.p.m.).

The value of the Amata granulites is considerably lower than the average strontium content of the Bahia and Langöy granulites, viz. 543 p.p.m. (Sighinolfi, 1971) and 572 p.p.m. (Heier and Thoresen, 1971), respectively.

Heier and Thoresen's (1971) data indicates that strontium is more

concentrated in granulite facies than amphibolite facies rocks. This pattern is emulated by the Amata suite. However, this is contrary to the pattern established by Lambert and Heier (1968) for the 'Musgrave Range block'. The lower grade rocks quoted by Lambert and Heier (1968) may thus not be a truly representative sample.

The average contents of strontium in the Amata rocks are significantly lower than the estimated abundances of Sr in the upper and lower continental crust (Hurley, 1968), viz. 400 p.p.m. and 500 p.p.m. respectively. The value for the Amata granulites is however, similar to the weighted average content of the Canadian Precambrian shield, viz. 340 p.p.m. (Shaw *et al.*, 1967) and the African Precambrian basement (Hurley, 1968), viz. 305 p.p.m.

Hedge and Walthall (1963) and Hamilton (1964) drew attention to the possibility that deeper crustal rocks could have similar Rb/Sr ratios to those present in mantle material.

Heier (1964) suggested that, concomitant with an increase in the K/Rb ratio in high grade rocks (i.e. granulites) during metamorphism, there should be a decrease in the Rb/Sr ratio. Lambert and Heier (1968), on the basis of more detailed data, confirmed that such a pattern existed in the Musgrave Ranges (Ernabella area?), i.e. lower Rb/Sr ratios in the granulite facies than the amphibolite facies lithologies. A similar relationship was demonstrated by Heier and Thoresen (1971) in the Lofoten Vesterålen province of northern Norway.

From Tables 4.2 and 4.10, and also from the log-log plots of rubidium against strontium (Figure 4.12a,b,c) it is apparent that the Rb/Sr ratios of the granulite facies rocks, with the exception of the quartzo-feldspathic granulites with more Na_2O than K_2O , are lower than in rocks of similar composition from the lower grade terrains.

The mafic transitional rocks containing significant quantities of micas plot in a completely different field to that of the mafic rocks containing minor or no plate silicates (Figure 4.12b). This is an undoubted reflection of the higher content of rubidium and (with the exception of A325-6) strontium present in the mica-bearing rocks. Except for A325-1328, this suite of mica-bearing lithologies is also characterised by higher Rb/Sr ratios than are found in the other mafic

groups. It is considered that there may be intrinsic differences which may possibly reflect a different pre-metamorphic parentage for the two groups (see below, Chapter 5).

Average values of Rb/Sr for the major rock compositions are given in Table 4.10 and the weighted average ratio for the three metamorphic units are listed in Table 4.11.

Table 4.15 has been included for the comparison of the Rb/Sr ratios from the Amata granulites with those of other granulite facies terrains. The weighted average for the Amata granulites (0.176) is much greater than either the Bahia or Lofoten Vesterålen averages of 0.094 and 0.120 respectively. The Amata value is close to the estimates given by Faure and Hurley (1963) for the continental crust (viz. 0.20), however it is lower than the estimate for the upper parts of the continental crust (viz. 0.25). It is also much higher than the Rb/Sr ratio calculated from the estimates of lower crustal rubidium and strontium given by Hurley (1968), viz. 0.03.

The higher weighted average Rb/Sr in the Amata granulites could be the result of strontium depletion. This may be the reason for the lower strontium in the Amata and Ernabella granulites, compared to values from other medium to high pressure granulite facies terrains.

Lambert and Heier (1968) have suggested that strontium may have been lost by the Fraser Range granulites during metamorphism. However, Arriens and Lambert (1969, p.383), on the basis of Lambert and Heier's (1968) evidence, 'do not believe that there was any large net gain or loss of Sr on a regional scale during metamorphism up to granulite facies'.

Nevertheless, the Amata data could indicate that a net loss of strontium has in fact occurred in the granulite facies terrain.

Plots of potassium against Rb/Sr (Figure 4.12d,f,g) clearly demonstrate that the Rb/Sr ratio decreases as the potassium content decreases in each of the metamorphic groups (cf. Heier, 1964; Sighinolfi, 1971). From Figure 4.12 it is apparent that the above relationship is more strongly developed in the quartzo-feldspathic than in the mafic granulites. This apparently anomalous relationship of the mafic granulites is similar to their pattern of behaviour when potassium is

TABLE 4.15
Sr/Rb DATA FROM HIGH GRADE METAMORPHIC TERRAINS

Metamorphic Terrain	Acid	Sub-Acid	Intermediate	Basic	Weighted Average
Southern Bahia, Brazil ¹	0.209	0.077	0.093	0.046	0.094
Ernabella Area, ² Musgrave Ranges	0.96	0.32	0.17	0.01	-
Fraser Range, Western Australia ²	4.92	0.40	0.57	0.08	-
Eyre Peninsula, ² South Australia	1.79	0.74	-	0.46	-
Lofoten-Vesterålen ³	-	-	-	-	0.120

1. Sighinolfi (1971)
2. Lambert and Heier (1968)
3. Heier and Thoresen (1971)

plotted against K/Rb (Figure 4.11a). It is considered to be further evidence for isochemical recrystallization of the mafic granulites as distinct from a more open system 'fractionation' in the quartzo-feldspathic lithologies.

From Figures 4.12e,h,i the relationship between calcium and the Rb/Sr ratio can be seen. In all rock compositions (except the mafic granulites, see Figure 4.12h) there is a trend of decreasing Rb/Sr ratio with increasing calcium. The relationship is explained by the fact that Sr^{++} (1.18Å) enters the eight co-ordinated Ca^{++} (0.99Å) position in plagioclases irrespective of the fact that the Sr-O bond is more ionic than the Ca-O bond. Taylor (1965) interprets this to be the result of fractionation processes.

The trends displayed by the Amata rocks clearly indicate that calcium rich rocks have abundant calcium sites in feldspars for strontium substitution, hence they have high strontium contents and consequently low Rb/Sr ratios. On the other hand, the rocks that are poor in calcium have few sites for strontium substitution, thus a low content of strontium and hence high Rb/Sr ratios.

4.2.4.4 Zirconium

From Table 4.2 it is clear that the quartzo-feldspathic (and pelitic) rocks have generally higher zirconium contents than the mafic lithologies, and the granulite facies rocks have lower zirconium contents than the surrounding lower grade lithologies. The average values (Table 4.10) exhibited by the mafic granulites (viz. 32 p.p.m.) and quartzo-feldspathic granulites (viz. 158 p.p.m.) are below the values quoted by Sighinolfi (1971) for basic and acid to sub-acid compositions in the southern Bahia province (viz. 114 p.p.m. and 195 to 244 p.p.m. respectively). The weighted average¹ zirconium contents for the Amata granulite facies (145 p.p.m.) and transitional terrains (viz. 311 p.p.m.) (Table 4.11) are not appreciably different from the patterns reported by other workers from rocks of equivalent metamorphic grade (Table 4.16).

1. The weighted average Zr content of the amphibolite facies terrain was not calculated, as insufficient data were available.

However, they are slightly lower than the average value for the Canadian Shield of 400 p.p.m. (Shaw *et al.*, 1967).

TABLE 4.16
AVERAGE ZIRCONIUM CONTENTS IN GRANULITE AND AMPHIBOLITE
FACIES ROCKS FROM OTHER AREAS

Source	Granulite Facies	Amphibolite Facies
Heier and Thoresen (1971)	144 p.p.m.	128 p.p.m.
Sighinolfi (1971)	222 p.p.m.	-
Lambert and Heier (1968)	310 p.p.m.	250 p.p.m.

Taylor (1965, pp.164-166) in briefly summarizing the geochemical behaviour of zirconium, stressed its ability to form separate phases (e.g. apatite and zircon). He also considered that it could be expected to substitute for Ti^{4+} , and combine with Ti^{4+} in substituting for Fe^{3+} during the crystallization of early igneous phases.

The behaviour of zirconium in igneous rock has been studied by numerous workers, in particular Havesy and Würstlin (1934), Wager and Mitchell (1951), Degenhardt (1957), and Brooks (1969), who have all confirmed the progressive enrichment of Zr with differentiation.

The behaviour of the Ti/Zr ratio with respect to Ti content is depicted graphically in Figure 4.13. The distribution pattern does not appear to be highly significant although several features are worthy of note:

1. The Ti/Zr ratio is much lower in the quartzo-feldspathic and alkali rich mafic rocks, for similar values of Ti. This suggests a trend of increasing zirconium in the more alkaline rocks (similar to the conclusions of the igneous workers).
2. The mafic granulites exhibit a smaller range of Ti/Zr (95.6-308) than the mafic transitional rocks (19.29-3083).

It can be concluded therefore, that the mafic granulites are a more homogeneous group with regard to the distribution of Ti and Zr than the transitional mafic rocks. This homogeneity could be the result of

several causes, acting separately or in concert; i.e., the different behaviour of the mafic rocks in the two terrains during the metamorphism; the result of original differences in composition of the mafic precursors of the transitional and granulite facies terrains.

4.2.4.5 Cerium and Lanthanum

4.2.4.5.1 Presentation of Data

Cerium was determined in all specimens excepting A325-1105 and -60, where it was below detection. Lanthanum however, was found to be below detection limits in the majority of the mafic granulites, several of the mafic rocks from the transitional terrain, quartzo-feldspathic granulites and the ultramafic granulite (A325-2050c). Values are tabulated in Table 4.2.

The average cerium contents of the mafic¹ and quartzo-feldspathic rocks, and their weighted averages² are given in Tables 4.10 and 4.11. Lanthanum was only averaged for the quartzo-feldspathic compositions. The average values are listed in Table 4.10. No weighted average lanthanum value was determined for the different terrains due to lack of adequate data.

The data presented in Tables 4.2, 4.10 and 4.11 clearly indicate that cerium is less abundant in the quartzo-feldspathic and mafic granulite facies rocks than it is in the rocks of the transitional terrain. Where data for lanthanum were available they showed a similar pattern. The few cerium and lanthanum values determined in amphibolite facies rocks suggests a similar distribution to that present in the transitional terrain.

The relationship between cerium and lanthanum is depicted graphically in Figure 4.14a. From this figure it is clear that cerium (except in A325-1165a) is present in greater concentrations than lanthanum. The La/Ce ratio greater than 1.00 in A325-1165a is attributed to an anomalous lanthanum or cerium value.

-
1. The average cerium value for the mafic granulites was computed without the inclusion of A325-1105 and -60.
 2. Only the weighted averages of the granulite facies and transitional terrain rocks were computed. Data was inadequate to allow calculation of the weighted average for the amphibolite facies terrain.

The relative concentration of (Ce + La) appears to be related to lithology. For example, the quartzo-feldspathic, mica-rich mafic, calc silicate and pelitic rocks have significantly higher contents of (Ce + La) than the mica-poor mafic rocks.

4.2.4.5.2 Correlation between Cerium, Lanthanum and Major Elements

No simple, sympathetic variation patterns of these rare earth elements with any of the major elements can be observed, although to some extent higher (Ce + La) are found in the more potassic rocks. A325-2040 is, however, an exception to this pattern with (Ce + La) 314 p.p.m. and %K only 0.03%.

The behaviour of the rare earth elements (REE) and major oxides in the Skaergaard intrusion and in several New England granites has recently been commented on by Haskin and Haskin (1968) and by Buma et al. (1971) respectively.

Haskin and Haskin (1968) observed that fluctuation of REE concentrations were greatest for the lightest REE and found that they could be compared with the behaviour of some of the major elements, e.g. Si and K. However, any similarity was strictly qualitative and there was no simple variation between the rare earth elements and any of the single major elements.

Buma et al. (1971) observed a trend of higher Al_2O_3 , CaO and MgO with higher La/Yb ratios in several New England sub-alkaline granites. However, they concluded that there was 'no close geochemical coherence of the REE with any major element'.

4.2.4.5.3 Influence of Mineralogy on Cerium and Lanthanum Distribution

The distribution patterns of the REE in rock forming minerals has been discussed by a number of workers. Gavrilova and Turanskaya (1958) commented on the rare earth content of monozite and apatite in granites. Fleischer (1965) reiterated the fact that the lanthanides, while tending to form independent mineral species, e.g. monozite and xenotime, were also present in minor quantity in phases such as apatite, sphene, garnet and zircon. Haskin et al. (1966) showed that sphene could contain at least 0.2-0.4% REE. Fleischer and Altschuler (1969),

as a result of a detailed study of the REE content of the accessory phases monazite, sphene and apatite, with a view to elucidating the geological environment in which they formed, showed the ability of sphene and apatite to concentrate the light REE such as those from La to Nd. Buma et al. (1971) found that while zircons contained large amounts of the heavy rare earth elements they also showed significant concentrations of the lighter ones.

Condie and Lo (1971) working on the geochemistry of the Precambrian Lake batholith, Wyoming, reported that the accessory (apatite and zircon) accounted for the major REE contribution in the rocks, however, plagioclase too, was enriched in the light REE, especially La, Ce and Sm.

The preceding review of REE distributions in rock forming minerals, although pertinent to igneous rocks, is included because of the woeful lack of data on metamorphic rocks.

From Figure 4.14b there appears to be a close correlation between zirconium and (Ce + La). This evidence, in the light of results of workers on igneous rock suites, strongly suggests that the light REE components (Ce + La) in the Amata terrain are mainly concentrated in accessory phases which contain minor amounts of zirconium, e.g. sphene, zircon and apatite.

From Table 4.2 it can be seen that P_2O_5 (presumably contained in apatite) is high in certain rocks enriched in (Ce + La), e.g. A325-990 and -1328. But, conversely, high values of (Ce + La) are found in rocks containing negligible P_2O_5 , viz. A325-2040 and -1687, suggesting that this is by no means a simple mineralogical relationship. It is concluded therefore that, as in igneous rock suites, the light REE are mainly concentrated in a number of accessories.

4.2.4.5.4 Fractionation of the REE

Taylor (1962) proposed that the REE distribution in the crust is indicative of a general fractionation pattern, the lighter rare earths being enriched in the upper crustal rocks. The postulated and actual behaviour of the rare earth elements during igneous fractionation was said, and found to be, towards an increase in the total REE concentration

(Taylor, 1965; Haskin et al., 1966). The observed enrichment of the light REE (La; Ce; Sm) in crustal rocks according to Taylor (1965) was the result of the preferential incorporation of rare earth with larger ionic radii into the liquid phase during liquid-solid equilibration.

Buma et al. (1971) asserted that garnet-bearing rocks in the lower crust (e.g. charnockites) could have been responsible for the depletion of the heavy REE from certain upper crustal granites; garnet preferentially incorporating heavy rare earths.

Little work has been done on REE distribution in metamorphic rocks. However Green et al. (1969) contended that: 'there was little or no fractionation of the rare earth element group with increasing metamorphic grade from amphibolite to granulite facies'.

The limited data available for cerium and lanthanum from the Amata area shows that these lighter rare earths are more abundant in the amphibolite facies and transitional rocks than the granulite facies rocks, a fact which could be the result of fractionation (cf. Green et al., 1969).

Concerning the possibility of fractionation within the granulites, it was noted previously (p.111) that the quartzo-feldspathic granulites form two distinct groups:

- (i) those with antiperthite;
- (ii) those with perthite and mesoperthite.

It is perhaps significant that the (La + Ce) ranges are completely different for the two groups:

- (i) A325-205, -199 and -1165a; (La + Ce) 7, 42, 31 p.p.m. respectively.
- (ii) A325-1121, -77 and -138; (La + Ce) 158, 115, 142 p.p.m. respectively.

Such a pattern might have arisen as a result of fractionation during the granulite facies metamorphism, or alternatively, it may reflect original compositional differences in the precursors of the quartzo-feldspathic granulites.

To resolve this question it would be necessary to have complete REE analyses of these quartzo-feldspathic granulites to determine whether there is a corresponding increase in the heavy REE as the

lighter REE decreases.

The limited data from the Amata area thus appears to contradict the conclusions of Green et al. (1969).

The data from the Amata area regarding the distribution of REE between the three metamorphic terrains do not necessarily mean that these terrains, now juxtaposed, were contiguous during metamorphism. Their significantly different (La + Ce) values may merely indicate the level in the crust at which metamorphism took place. It cannot be ascertained whether the apparent depletion of Ce and La from the Amata granulite terrain contributed to the increase in (La + Ce) in the mapped transitional rocks, as the age relationship between the three blocks is unknown.

4.2.4.6 Thorium and Uranium

The effect of high grade metamorphic processes on the distribution of thorium and uranium in crustal rocks has been the subject of considerable research and speculation. Heier (1962), Heier and Adams (1965), Lambert and Heier (1967, 1968), Fahrig et al. (1967), Lambert (1971) and Smithson and Heier (1971) have all investigated the distribution of these elements in amphibolite and granulite facies terrains. They invariably found a general depletion of thorium and uranium in the granulite facies terrains (especially those consisting of medium to high pressure granulites) relative to surrounding amphibolite facies terrains. Heier and Adams (1965) found that the metamorphic transition from amphibolite facies, through low pressure to medium and high pressure granulite facies conditions was marked by a general decrease in the Th/U ratio. However, Fahrig et al. (1967), after investigating amphibolite facies and hornblende granulite facies rocks (low pressure granulites) from New Quebec, Canada, believed that uranium was more highly fractionated than thorium as the grade of metamorphism increased, causing the Th/U ratio to increase.

Both groups of authors agreed that uranium values were subject to greater variation than thorium values due to the ease with which uranium could be oxidised to form the uranyl complex ion. This ion, because of its greater solubility, could then easily be removed, either

during the dehydration associated with the high grade metamorphism or as a result of surface weathering (Richardson and Adams, 1963).

Thorium was sought in the Amata rocks, and was detected in most specimens from the transitional terrain (the exceptions being A325-783 and -326) and all specimens from the amphibolite facies terrain. However, it was below the limit of detection in many of the granulites.

Uranium determinations were carried out fluorimetrically by A.M.D.E.L. on selected quartzo-feldspathic lithologies from the different metamorphic terrains. The degree of precision of the uranium determinations was much greater than was obtained for thorium by XRF. Therefore, although traces of uranium were present in several specimens, viz. A325-199, -1165a, -783, thorium was not detected.

TABLE 4.17

Th AND U RANGES IN THE QUARTZO-FELDSPATHIC
AND MAFIC LITHOLOGIES FROM THE AMATA AREA

		Granulite Facies Terrain	Transitional Terrain	Amphibolite Facies Terrain
Quartzo- feldspathic	Th	n.d. - 9	n.d. - 1	9 - 249
	U	0.3 - 0.6	0.6 - 1.0	2.0
Mafic	Th	n.d. - 4	0.4 - 17	1 and 7

n.d. = not detected; values in p.p.m.

The fairly limited data, summarized in Table 4.17, indicate that amongst the quartzo-feldspathic compositions the granulite facies rocks have lower uranium values than either the transitional or amphibolite facies lithologies. Thorium values are generally low in the quartzo-feldspathic granulite facies and transitional lithologies, and they are significantly higher in the amphibolite facies lithologies. The pattern is less clear for the mafic compositions, thus providing additional evidence for the contrasting metamorphic histories of some of the mafic and quartzo-feldspathic lithologies, i.e. fractionation may have occurred in the quartzo-feldspathic rocks before the mafic rocks were emplaced.

Although the granulites have generally lower thorium contents (0-9 p.p.m.) than are present in the lower grade rocks, one calc silicate

lithology, A325-2040, from the granulite terrain contains 42 p.p.m. thorium. In this rock the thorium is believed to be contained in accessory allanite, which constitutes 2.60% of the mode (Table 4.1).

The extent to which the distribution pattern of thorium and uranium in the Amata granulite facies, transitional and amphibolite facies lithologies is due to fractionation (as is suggested by Heier and Adams, 1965; and others) is not certain.

It is clear from Figures 4.15a,b and c that no linear relationship exists between the two variables thorium and potassium. Comparing the $\text{Th/K} \times 10^4$ ratios for the quartzo-feldspathic compositions (Table 4.2) it can be seen that the granulites extend to lower values than the amphibolite facies gneiss. However, there is a considerable degree of overlap. Similar $\text{Th/K} \times 10^4$ relationships were reported by Heier and Adams (1965) and Lambert and Heier (1968).

Average values of thorium and uranium have not been calculated due to the incomplete nature of the data. Average values of thorium and uranium from other high grade terrains and shield areas have, nevertheless, been included (Table 4.18) for comparison with the ranges presented in Table 4.17.

TABLE 4.18

AVERAGE Th, U VALUES FROM OTHER HIGH GRADE METAMORPHIC TERRAINS

	Th	U
<u>Musgrave Ranges</u> ¹		
(Granulite Facies)	2.1	0.4
(Amphibolite Facies)	11	1.0
<u>Cape Naturaliste</u> ¹		
(Granulite Facies)	35.0	2.5
(Amphibolite Facies)	23.0	1.5
<u>New Quebec</u> ²		
(Granulite Facies)	7.1	0.8
(Amphibolite Facies)	9.6	1.3
<u>Langby</u> ³		
(Granulite Facies)	0.93	0.39 ^a
	4.09	0.88 ^b
(Amphibolite Facies)	9.39	1.22 ^c
	26.48	3.45 ^d
<u>S.E. Mysore Precambrian Shield</u> ⁴		
(Amphibolite Facies)	24.83	3.61
<u>Canadian Precambrian Shield</u> ⁵	10.3	2.45

1. Lambert and Heier (1968)
2. Fahrig *et al.* (1967)
3. Heier and Adams (1965)
4. Narayanaswamy and Venkatasubramanian (1969)
5. Shaw (1968b)

- a high granulite facies
- b low granulite facies
- c high amphibolite facies
- d low amphibolite facies

TABLE 4.19

Th/U RATIOS FOR SEVERAL QUARTZO-FELDSPATHIC ROCKS
FROM THE AMATA AREA

SPECIMEN NO.	Th/U	METAMORPHIC GRADE
A325-1121	15	Granulite Facies
A325-400	14	Transitional Zone
A325-474	43	
A325-1659	5	Amphibolite Facies

Only four pairs of data were available for the calculation of Th/U ratios. The ratios (Table 4.19) for the granulite facies and transitional rocks are very much higher than those presented by Lambert and Heier (1968) for rocks of approximately equivalent composition from the Ernabella area. The sole Th/U ratio (4.5) for the amphibolite facies gneiss (A325-1659) is much lower than for the granulite specimen and the transitional rocks, thus possibly indicating that more depletion of uranium relative to thorium has taken place in the granulite facies and transitional terrains than in the amphibolite facies terrain. On the basis of this admittedly very limited data, the pattern displayed by the Amata rocks is similar to that suggested by Fahrig *et al.* (1967) and contrasts with the pattern established by Heier and Adams (1965) and Lambert and Heier (1968). The distribution of thorium and uranium, then, in these Amata rocks could possibly be the result of fractionation associated with the metamorphic processes.

4.3 MINERAL CHEMISTRY4.3.1 General

Complete and partial major element analyses of forty-eight ferromagnesian silicates, fourteen opaque oxides, four scapolites and twelve alkali feldspars are given in Tables 4.20 to 4.27. Structural formulae¹, calculated on the basis of 6, 23, 24, 22 and 32 oxygen anions for the pyroxenes, amphiboles, garnets, micas and feldspars respectively are listed together with relevant molecular ratios. Details of the analyses and the tables in which they are listed are presented in Table 4.28.

TABLE 4.28

DETAILS OF CHEMICAL ANALYSES

MINERAL SPECIES	NUMBER OF ANALYSES FOR EACH METHOD		TABLE
	XRF/CLASSICAL	ELECTRON PROBE	
Orthopyroxene	13	1	4.20
Clinopyroxene	4	12	4.21
Amphibole	5	2	4.22
Garnet	6	-	4.23
Mica	5	1	4.24
Rutile	-	1	4.25
Haematite	-	4	4.25
Magnetite	-	4	4.25
Ilmenite	-	5	4.25
Scapolite	-	4	4.26
Alkali Feldspar	12	-	4.27

Analyses were undertaken by a combination of X-ray fluorescence and wet chemical methods on mineral fractions separated by magnetic and heavy liquid techniques, or by electron microprobe. The latter technique was deemed necessary as separation of phases was often precluded due to:

- (1) the presence of abundant inclusions of opaque oxides (e.g. in the clinopyroxene);

1. Structural formulae were computed by the University of Adelaide IBM 6400 computer using a programme written by Dr. A.W. Kleeman (Department of Geology and Mineralogy, University of Adelaide).

TABLE 4.20
ORTHOPYROXENE ANALYSES

(Located in the back pocket of Volume 2)

TABLE 4.21
CLINOPYROXENE ANALYSES

(located in the back pocket of Volume 2)

TABLE 4.22
HORNBLLENDE ANALYSES

SPECIMEN NO. A325/-	2050c	949*	1105*	523	339	6	1684
SiO ₂	45.30	38.92	40.11	41.26	41.98	42.41	41.87
Al ₂ O ₃	13.21	16.70	15.09	14.24	13.21	12.46	12.16
Fe ₂ O ₃	2.11	n.d.	n.d.	2.91	2.83	4.87	5.77
FeO	3.83	9.00	10.61	9.28	8.83	9.71	11.48
MgO	18.06	12.92	11.62	12.27	12.43	12.13	9.72
CaO	12.18	11.87	12.07	11.44	11.81	10.89	11.10
Na ₂ O	0.04	n.d.	n.d.	2.35	1.78	2.68	1.73
K ₂ O	1.80	n.d.	n.d.	1.45	2.19	1.67	1.53
TiO ₂	1.65	3.14	3.77	1.15	2.26	1.58	0.96
MnO	0.10	0.04	0.05	0.17	0.17	0.15	0.32
P ₂ O ₅	-	n.d.	n.d.	-	-	-	0.10
L.O. Ignit.	0.75	n.d.	n.d.	3.23	2.33	1.58	3.03
Total	99.11	92.59	93.33	99.75	99.87	100.13	99.77
STRUCTURAL FORMULAE (BASED ON 23 OXYGEN ATOMS)							
Si	6.387	5.904	6.080	6.147	6.199	6.237	6.331
Al ^{IV}	1.613	2.096	1.920	1.853	1.801	1.763	1.669
Al ^{VI}	0.578	0.889	0.776	0.648	0.499	0.397	0.499
Fe ³⁺	0.223	-	-	0.326	0.315	0.539	0.657
Fe ²⁺	0.451	1.142	1.345	1.156	1.091	1.194	1.452
Mn	0.012	-	-	0.021	0.021	0.019	0.041
Mg	3.789	2.921	2.626	2.725	2.736	2.659	2.191
Ca	1.837	1.929	1.960	1.826	1.869	1.716	1.798
Na	0.011	-	-	0.679	0.510	0.764	0.507
K	0.323	-	-	0.276	0.413	0.313	0.295
Ti	0.175	0.358	0.430	0.129	0.251	0.175	0.109
Z	8.000	8.000	8.000	8.000	8.000	8.000	8.000
X	2.171	1.929	1.960	2.781	2.791	2.794	2.601
Y	5.228	5.316	5.182	5.006	4.913	4.983	4.948
mg	84.7	71.8	66.0	64.4	65.7	60.3	50.5

* Micro-probe analyses by AMDEL

Mg = 100.Mg/(Mg + Fe³⁺ + Fe²⁺ + Mn)

TABLE 4.23
GARNET ANALYSES

(Located in the back pocket of Volume 2)

TABLE 4.24
MICA ANALYSES

SPECIMEN NO. A325/-	1328	14	990	6*	2050c	1687
SiO ₂	40.35	39.73	40.70	36.19	42.00	35.07
Al ₂ O ₃	15.52	14.30	14.50	14.63	13.94	19.11
Fe ₂ O ₃	0.86	-	0.97	-	-	2.98
FeO	8.32	12.83	8.19	13.88	4.89	16.27
MgO	20.21	14.64	17.89	14.30	23.33	9.95
CaO	0.15	1.08	0.45	n.d.	0.26	-
Na ₂ O	0.14	0.06	0.24	n.d.	0.25	0.19
K ₂ O	9.74	8.71	9.00	8.78	9.97	9.56
TiO ₂	3.46	3.94	4.82	4.28	3.27	2.81
MnO	0.08	0.10	0.09	0.04	0.05	0.23
P ₂ O ₅	-	0.15	0.06	-	-	-
L.O. Ignit.	1.57	3.51	2.48	-	2.18	3.60
Total	100.40	99.59	99.39	92.10	100.14	99.77
STRUCTURAL FORMULA (BASED ON 22 OXYGEN ATOMS)						
Si	5.619	5.824	5.684	5.558	5.798	5.269
Al ^{IV}	2.381	2.176	2.316	2.442	2.202	2.731
Al ^{VI}	0.167	0.295	0.070	0.207	0.067	0.653
Fe ³⁺	0.090	-	0.113	-	-	0.337
Fe ²⁺	0.969	1.573	0.861	1.783	0.565	2.044
Mn	0.009	0.012	0.011	0.005	0.006	0.029
Mg	4.195	3.199	3.724	3.274	4.801	2.228
Ca	0.022	0.170	0.067	-	0.038	-
Na	0.038	0.017	0.065	-	0.067	0.055
K	1.730	1.629	1.603	1.720	1.756	1.832
Ti	0.362	0.434	0.506	0.494	0.340	0.317
Z	8.000	8.000	8.000	8.000	8.000	8.000
X	1.791	1.816	1.736	1.720	1.861	1.888
Y	5.793	5.514	5.285	5.763	5.778	5.609
mg	79.7	66.9	79.1	64.7	89.4	48.0

mg = 100.Mg/(Mg + Fe³⁺ + Fe²⁺ + Mn)

*Micro-probe analysis by AMDEL

TABLE 4.25

MICRO-PROBE ANALYSES OF HAEMATITE

SPECIMEN NO. A325/-	115	18	500	538
TiO ₂	3.3	11.8	11.3	12.17
ΣFe as Fe ₂ O ₃	101.5	85.0	79.5	90.8
ΣFe as FeO	91.3	76.5	71.5	81.7
MnO	0.05	0.23	0.10	0.16
MgO	-	-	-	-

Molecular
% Hae 93.8 76.12 75.9 76.1

MICRO-PROBE ANALYSES OF MAGNETITE

SPECIMEN NO. A325/-	18	43	6	538
TiO ₂	-	0.20	0.75	0.15
ΣFe as Fe ₂ O ₃	107.7	101.2	102.4	107.7
ΣFe as FeO	96.9	91.1	92.2	96.9
ΣFe as Fe ₃ O ₄	103.4	97.9	99.1	103.4
MnO	-	0.03	-	0.02
MgO	-	-	-	-

MICRO-PROBE ANALYSES OF ILMENITE

SPECIMEN NO. A325/-	115	18	6	500	538
TiO ₂	45.9	46.4	46.4	43.9	44.4
ΣFe as FeO	46.4	46.3	47.3	51.0	51.9
MnO	0.60	2.7	0.40	0.50	0.70
MgO	-	-	0.20	-	-

Molecular
% Ilm 94.66 97.90 93.97 87.36 87.29

MICRO-PROBE ANALYSES OF RUTILE

SPECIMEN NO. A325/-	115
TiO ₂	97.4
FeO	0.20

Analyst: AMDEL

TABLE 4.26

PARTIAL ANALYSES OF SCAPOLITE

SPECIMEN NO. A325/-	425	192	78	564
SiO ₂	46.85	48.56	46.21	46.60
Al ₂ O ₃	27.40	24.56	24.38	27.97
EFe as Fe ₂ O ₃	0.06	0.10	0.22	0.29
CaO	16.09	16.65	16.65	16.23
Na ₂ O	2.43	2.97	4.85	2.97
TiO ₂	<0.02	-	-	0.03
SO ₃	0.06	5.85	4.03	4.65
Cl	0.40	0.10	~ 0.10	0.05

(2) the fact that some species were only present in minor amounts and insufficient rock was available to facilitate the separation of adequate quantities for chemical analysis.

Details of the separation and analytical techniques are given in Appendix 2.

4.3.2 Relationship of Mineral Chemistry to Whole Rock Chemical Ratios

4.3.2.1 Oxidation Ratio

The following discussion concerns the effect of the lithological oxidation ratio on:

1. the relative modal distribution of various mineral species;
2. the behaviour of selected molecular ratios.

Chinner (1960), in a detailed study of the petrology and geochemistry of the Glen Clova pelitic gneisses, showed that the fugacity of oxygen controlled to a large extent, the mineralogy and mineral chemistry of the gneisses.

Himmelberg and Phinney (1967) demonstrated that partial pressure of oxygen is also an important variable at higher grades of metamorphism (i.e. hornblende granulite facies), in establishing FeO/FeO + MgO molecular ratios of biotite, thus confirming the experimental predictions of Wones and Eugster (1965).

Butler (1969) showed that in the presence of the buffer assemblage magnetite-haematite, orthopyroxene compositions are solely a function of pressure and temperature. However, in the absence of haematite, their composition could be more variable because the chemical potential of oxygen is more variable. He considered the variation in the composition of orthopyroxene to be explained by the following relationship: $\mu_{\text{OPX}}^{\text{OPX}} / \mu_{\text{(FeSiO}_3\text{)}}^{\text{(FeSiO}_3\text{)}}$ varied directly and μ_{O_2} inversely with the mole fractions of FeSiO₃ (Fe²⁺/Fe²⁺ + Mg) at any given pressure and temperature.

From a detailed study of the geochemistry of coexisting biotite and Ca-amphibole in the Gällivare iron formation, Sweden, Annersten (1968) showed the extent to which oxygen pressure controls the mineral chemistry of these coexisting phases. He attributed the following

trends in the ferromagnesian silicates to be the result of an increase in the partial pressure of oxygen (determined from the nature of the coexisting iron and iron titanium oxides):

1. Mg/Mg + Fe²⁺ increased;
2. Ti decreased;
3. greater variation in hornblende oxidation ratios compared to biotite ratios.

Based on experimental studies, Wones and Eugster (1965) showed the influence of oxygen fugacity on the stability of biotite. Ernst (1966) demonstrated that ferro-tremolite is unstable as P_{O_2} is increased but that its stability field is extended if Mg is introduced into the system. Similarly, Gilbert (1966) hydrothermally investigated the stability relations of ferro-pargasite and demonstrated that Fe²⁺ \rightleftharpoons Mg substitution is caused by both temperature and oxygen fugacity; pargasite being stable at higher temperatures than ferropargasite. Hsu (1968) delineated the upper and lower stability limits of almandine and showed that they are strongly dependent on P_{O_2} . More recently, Keesmann et al. (1971) greatly extended the upper stability limit of almandine at high pressures (up to 20 Kb) when low oxygen fugacities were maintained. The influence of a third component on the stability of the opaque oxides was examined by Lindsley (1962, 1963), who found that because of the solubility of ilmenite in haematite, haematite tended to be stabilised at lower oxygen pressures.

To examine the extent to which the oxygen content influenced the mineralogy of the Amata rocks, the 'relative modal percentages' (Chinner, 1960, p.189) of the major mineral phases were plotted against rock oxidation ratios (Figures 4.16.1 to 4.16.7). The opaque oxides (Figures 4.16.3, 4.16.6a and 4.16.7a) exhibit a slight positive correlation with oxidation ratio. However, no correlation exists for the silicate phases. These results contrast strongly with those from the Glen Clova gneisses (Chinner, 1960, p.190, Figure 5), where distinct correlations exist between the 'relative modal percentages' of ferromagnesian silicates and the oxidation ratios.

Chinner (1960) considered that the modal variation in the Glen

Clova gneisses is directly the result of increasing rock oxidation ratio. However, he considered that the increasing modal abundance of the opaque oxides, with increasing oxidation ratio, is in part the result of an increase in the total iron content of the rocks.

It is demonstrated (p.150) that there is no strong correlation between total iron (as Fe_2O_3) of the Amata rocks and their 'oxidation ratios' (the mafic granulites show a slight correlation). It is therefore unlikely that an increase in total iron accounts for the weak opaque oxide-oxidation ratio correlation in the Amata rocks.

The molecular $\text{FeO}/\text{FeO} + \text{MgO}$ and $\text{MgO}/\text{MgO} + \text{FeO}$ ratios of the following mineral phases from the Amata area, orthopyroxene, clinopyroxene, amphibole, mica and garnet, are plotted against the oxidation ratios of their host rocks (Figures 4.17.1 to 4.17.3 and 4.18.1 to 4.18.3). These data reveal that the ratios are independent of control by the oxygen fugacity of the host rocks which may be influenced by the grade of metamorphism, bulk rock composition or opaque oxide assemblages. Chinner (1960), Butler (1969), Reinhardt (1968), Bard (1970) and others, in marked contrast, report a close correlation between the degree of oxidation and the above molecular ratios: $\text{Fe}^{2+}/\text{Fe}^{2+} + \text{Mg}$ decreasing and $\text{Mg}/\text{Mg} + \text{Fe}^{2+}$ increasing with increasing P_{O_2} .

Bard (1970, p.127) claims that 'a positive correlation can be shown to exist between:

1. the 'oxidation degree' of the amphibolite (i.e. $100\text{Fe}^{3+}/\text{Fe}^{3+} + \text{Fe}^{2+}$);
2. the ratio of $100\text{Mg}/\text{Mg} + \text{Fe}^{2+}$ of the hornblendes;
3. the paragenesis of the opaques.

By reference to Bard (1970, Figure 5, p.128), however, it is clear that little if any correlation exists between oxidation ratio and $\text{Mg}/\text{Mg} + \text{Fe}^{2+}$. This supports the contention suggested for the Amata rocks, that the Mg/Fe^{2+} ratio is not directly related (in all cases) to the rock oxidation ratio and may more directly be related to the rock $\text{Mg}/\text{Mg} + \text{Fe}^{2+}$ ratio (see below).

This apparent abnormality in the behaviour of the $\text{Mg}/\text{Mg} + \text{Fe}^{2+}$

and the $\text{Fe}^{2+}/\text{Fe}^{2+} + \text{Mg}$ ratios in the Amata minerals is perhaps reflected also in the decreasing $100\text{Mg}/\text{Mg} + \text{Fe}$ of the host rocks with increasing oxidation ratio (Figures 4.19.1 to 4.19.3). This suggests that these anomalous trends in the minerals are influenced, to some extent at least, by host rock composition and are apparently independent of prevailing oxygen fugacity.

That the mineral Fe^{2+}/Mg and Mg/Fe^{2+} ratios are not directly influenced by rock oxidation state is further corroborated by plotting the $\text{Fe}^{3+}/\text{Fe}^{3+} + \text{Fe}^{2+}$ ratios for the different mineral phases (where separate Fe^{2+} determinations permit) against the oxidation ratios of their respective host rocks (Figure 4.20). On the basis of the available data it is apparent that the two vary independently of one another and also of the nature of the coexisting opaque oxide phases.

Chinner (1960, p.206) considered that the assemblages:

1. magnetite-haematite
2. ilmenite-magnetite

are univariant at fixed temperature and pressure, the oxidation state of each rock determining the composition of the constituent minerals during metamorphism. On the other hand, he considered that the assemblage magnetite-ilmenite-haematite is invariant. Variations in the oxidation ratios therefore result in variation of the proportions of opaque oxides or ferromagnesian silicates, the compositions of the minerals remaining essentially constant.

The assemblage magnetite-haematite however was shown by Eugster and Wones (1962) and others to exert a buffering action on the activity of oxygen and FeO at constant pressure and temperature. Varying μ_{O_2} during metamorphism merely results in the formation of variable amounts of oxides and the effect of μ_{O_2} on the composition of the coexisting ferromagnesian silicates is thus small. Hence, the dependence of the $\text{Fe}^{3+}/\text{Fe}^{3+} + \text{Fe}^{2+}$ ratios of minerals is not directly related to the oxidation states of their host rocks.

The above data from the Amata rocks suggests that P_{O_2} may also have been limited by the buffering action of other assemblages, in addition to magnetite and haematite (cf. Chinner's, 1960, interpretation for the magnetite-ilmenite-haematite assemblages).

The behaviour of manganese (expressed as $Mn/Mn + Fe^{2+} + Mg$) in both garnet and amphibole appears to vary directly with the rock oxide ratio (Figures 4.21.1a and b). This pattern has been described previously in pelites by Chinner (1960, p.192) and Hounslow and Moore (1967, p.26), and has been found experimentally by Hsu (1968). Müller and Schneider (1971), in a detailed study of garnets from a variety of rock types, have also confirmed that the manganese content of the garnets is strongly dependent on the oxygen fugacity of the system in which they crystallised. To the author's knowledge the relationship between oxidation ratio and $Mn/Mn + Mg + Fe^{2+}$ in amphiboles has not been recognised previously. The $Mn/Mn + Mg + Fe^{2+}$ ratio for orthopyroxene, clinopyroxene and mica from Amata does not vary significantly with rock oxidation ratio (Figures 4.21.2, 4.21.3).

4.3.2.2 $Mg/Mg + Fe^{2+}$ Ratio

It was stated above that the $Mg/Mg + Fe^{2+}$ ratios in the Amata minerals are not apparently influenced by rock oxidation ratios. A close correlation, however, is revealed between this ratio in orthopyroxene, clinopyroxene, hornblende and mica and the same ratio in their host rocks (Figures 4.22.1, 4.22.2, 4.22.3). Garnet shows only a weak correlation (Figure 4.22.1b).

The strong control by host rock Fe^{2+} and Mg contents on the $Mg/Mg + Fe^{2+}$ ratio of constituent mineral phases (particularly hornblende) has been demonstrated also by Miyashiro (1958), Shido and Miyashiro (1959), Binns (1965a), Leake (1965), Kanisawa (1969), Sen (1970) and Ray (1970).

Figure 4.22.3a and b shows the positions of Amata hornblendes compared with hornblendes from other high grade metamorphic terrains. The plots indicate that the Amata hornblendes and host rocks, from both the granulite and transitional terrains, are more magnesium rich than in other granulite facies areas.

Sen (1970) uses the similarity of these ratios in the rocks and minerals as strong evidence to favour the amphibole being of primary origin. On microstructural evidence it is probable that hornblendes from the Amata granulite and transitional terrain are also primary.

4.3.2.3 Mn/Mn + Mg + Fe²⁺ Ratio

It has been stated above (p.196) that manganese distribution in the Amata garnets and amphiboles correlates with the prevailing oxygen fugacity. No such relationship was found for the pyroxenes or micas. However, it was found that there is a direct relationship between the Mn/Mn + Mg + Fe²⁺ for individual co-existing pyroxenes and the same ratio for the rocks (Figure 4.23.1a,b), and that, for a given value for the host rock, the ratio for the granulite facies ortho- and clinopyroxenes is lower than that for similar minerals from the transitional terrain.

Manganese partition in the pyroxenes is clearly directly related to the manganese content of their host rocks, but there is also possible correlation with metamorphic grade. Similar plots for mica, amphibole and garnet also show a direct relationship between host rock and mineral Mn/Mn + Mg + Fe²⁺ (Figure 4.23.2).

4.3.3 Systematic Mineral Chemistry

4.3.3.1 Orthopyroxenes

4.3.3.1.1 Nomenclature

The terminology of Deer et al. (1962) is employed for the classification of the orthopyroxenes. Figure 4.24 displays compositions plotted in terms of end-member components, enstatite, wollastonite and orthoferrosilite. The enstatite values range between 71.4 and 54.0, all are hypersthene except A325-949 which has the composition of bronzite. The mg values (i.e. 100Mg/Mg + Fe³⁺ + Fe²⁺ + Mn, Table 4.20) also demonstrate their narrow compositional range; i.e. 74.2-54.4 (granulite facies terrain) and 59.0-69.0 (transitional terrain). This relatively narrow range of compositions perhaps reflects their host rock chemistry, i.e. all analyses were from mafic to ultramafic rocks. In contrast, however, the basic granulites from Quairading, Davidson (1968) and the Kondapalli basic charnockites Leelanandam (1967) exhibit much wider (78.1-37.7) and smaller (57.3-47.7) ranges respectively.

4.3.3.1.2 Chemistry

Chemical analyses are listed in Table 4.20.

The orthopyroxenes display a trend of increasing content of enstatite with increasing $Mg/Mg + Fe^{2+}$ ratios of their host rocks, supporting the relationship demonstrated above (Figure 4.22.2b). Leelanandam (1967, p.160) on the other hand believes that orthopyroxene compositions are independent of the Fe^{2+}/Mg ratio of their host rocks.

MnO ranges between 0.14 and 0.95 wt. %. This is comparable to the range displayed by the Kondapalli and Quairading orthopyroxenes (0.11-0.90%) and (0.25-0.75%) respectively. However, these values are generally less than those of the Broken Hill pyroxenes (0.61-1.64%). The higher content of MnO in orthopyroxenes than in co-existing clinopyroxenes indicates that MnO favours the orthopyroxene structure (Davidson, 1968, p.243). It was previously demonstrated (p.197) that the $Mn/Mn + Mg + Fe^{2+}$ ratio of orthopyroxene varies directly with the $Mn/Mn + Mg + Fe^{2+}$ ratio of the respective host rocks (Figure 4.23.1b). This confirms Binns' (1965b, p.572) suggestion that host rock MnO content influences the content of MnO in orthopyroxene.

TiO_2 contents range as follows: 0.14 to 0.21% (granulite facies) and 0.05 to 0.33% (transitional terrain). The range for the granulites is smaller than for orthopyroxenes from Kondapalli, 0.10 to 0.43%; and Madras, 0.10 to 1.78% (Leelanandam 1967, Table II); Broken Hill, 0.18 to 0.48% (Binns 1965b, Table III) and Quairading 0.12 to 0.41% (Davidson 1968, Table 2). Kuno (1954) and Murty (1964a,b) believed that high contents of titania in orthopyroxenes is responsible for the intensity of their pleochroic schemes. However, this explanation has subsequently been discounted by Howie (1963, 1964, 1965), Binns (1965b) and Burns (1966).

From Figure 4.25a it can be seen that the amount of titanium in the Y group of cations varies inversely with the ferric/ferrous ratio of the orthopyroxene. The degree of oxidation of the pyroxene thus has some control on the amount of titanium in the crystal lattice.

The CaO contents are low, ranging from 0.29 to 1.01%. In contrast to the findings of Binns (1962, 1965b), Howie and Smith (1966), Leelanandam (1967a) and Davidson (1968), the orthopyroxenes co-existing

with clinopyroxene do not increase in calcium content as the total iron content increases (Table 4.20).

Alkali contents are low and, with the exception of A325-990, soda predominates over potash. The higher potash in A325-990 is interpreted to be a reflection of host rock control, A325-990 containing abundant K_2O (4.43%, Table 4.2) and the only co-existing ferromagnesian phase being phlogopite.

The alumina contents range between 2.30% and 6.50%, most of the aluminium being present in tetrahedral co-ordination (i.e. in the Z cation group). Six-fold co-ordinated aluminium is generally present only in small quantities (0.000 to 0.115 atoms per formula unit - Table 4.20). There is no significant difference in total Al_2O_3 content and the relative amounts of Al^{IV} and Al^{VI} in the orthopyroxenes from the granulite and transitional terrains.

There is no simple relationship between Al^{IV} substitution for Si^{IV} and the degree of oxidation of the orthopyroxenes (Figure 4.25b). Substitution of $2Fe^{2+}$ for $2Al^{3+}$ and Al^{IV} for Si^{IV} are extremely variable between the different pyroxenes and are not simply related to control by the ferric-ferrous ratio of the orthopyroxene.

The relationship between the host rock $Fe^{2+}/Fe^{2+} + Mg$ ratio and the Al_2O_3 , Al^{IV} and Al^{VI} contents of the Amata orthopyroxenes is shown in Table 4.29. The garnet bearing (granulite facies) assemblages conform to the proposals of Banno (1964) (see below). However, the orthopyroxenes from the other assemblages and metamorphic terrains display a more variable distribution pattern with regard to Al_2O_3 , Al^{IV} and Al^{VI} . The variable nature of Al^{IV} and Al^{VI} is attributed to variation in the Si^{IV} content of the pyroxenes. The reason for the decrease in Al_2O_3 with decreasing $Fe^{2+}/Fe^{2+} + Mg$ in the orthopyroxene from the Hb-opx-cpx-plag assemblages (contrary to Banno's trend) is unknown.

The Amata orthopyroxenes from both the granulite and transitional terrains are more aluminous than other high grade orthopyroxenes from Broken Hill, Quairading, Lützow-Holmbukta and West Uusimaa (compare Table 4.20 with Table 4.30).

TABLE 4.29

Al_2O_3 , Al^{VI} and Al^{IV} CONTENTS OF ORTHOPYROXENES AND HOST ROCK
 $\text{Fe}^{2+}/\text{Fe}^{2+} + \text{Mg}$ RATIOS

SPECIMEN NO. A325/-	Orthopyroxene			Host Rock $\text{Fe}^{2+}/\text{Fe}^{2+} + \text{Mg}$
	Al_2O_3	Al^{VI}	Al^{IV}	
Opx-cpx-hb-plag assemblage (Transitional Terrain)				
523	2.75	0.007	0.113	0.3042
517	2.57	0.015	0.099	0.3021
339	2.61	0.027	0.090	0.2957
295	2.34	-	0.102	0.2305
Opx-cpx-hb-garnet assemblage (Granulite Terrain)				
949	6.56	0.115	0.172	0.3018
1105	3.02	0.018	0.116	0.3311
Opx-cpx-plag assemblage (Granulite Terrain)				
138b	2.78	0.013	0.112	0.3879
81	2.36	0.010	0.095	0.3635
119	2.35	-	0.107	0.4013
121	2.30	-	0.103	0.3818
60	2.40	0.027	0.077	0.3134

TABLE 4.30

Al_2O_3 CONTENTS OF ORTHOPYROXENES FROM HIGH GRADE
METAMORPHIC ROCKS

SOURCE	AREA	RANGE OF Al_2O_3 in wt %
Binns (1965b)	Broken Hill	0.23 - 2.05
Davidson (1968)	Quairading	0.83 - 1.84
Banno <u>et al.</u> (1963)	Lützow-Holmbukta	0.21 - 1.62
Saxena (1969)	West Uusimaa Complex	0.20 - 0.50
Leelanandam (1967a)	Kondapalli	1.34 - 5.40
Leelanandam (1967a)	Madras	0.96 - 5.76
Sadashivaiah and Subbarayudu (1970)	Kondavidi	2.31 - 8.66
Sen and Rege (1966)	Saltora	1.25 - 3.12
Lovering and White (1969)	Delegate	2.19 - 3.95

However, similar high alumina contents have been reported from the various Indian granulite facies terrains, viz. Kondapalli, Madras, Saltora and Kondavidi, and also from granulite facies inclusions in the Delegate basic pipes.

The high contents of Al_2O_3 in orthopyroxenes from granulites were believed by Eskola (1957) to be the result of crystallization under high pressure. Boyd and England (1960) confirmed that it is possible for appreciable quantities of Al_2O_3 to enter the structure of enstatite at high pressure. Boyd and England (1964), MacGregor and Ringwood (1964) and Skinner and Boyd (1964) showed that as pyrope became a stable phase, the Al_2O_3 content of co-existing enstatite decreased. Banno (1964) considered that the maximum content of Al_2O_3 in orthopyroxene would be present when it co-existed with garnet. He interpreted the Al_2O_3 content to be controlled by:

1. the physical conditions;
2. the $Fe^{2+}/Fe^{2+} + Mg$ ratio of the host rock (i.e. he found higher

Al_2O_3 contents in rocks with lower $Fe^{2+}/Fe^{2+} + Mg$ ratios);

3. the presence or absence of clinopyroxene.

The highly aluminous orthopyroxenes from certain ultramafic intrusions, from ultramafic nodules and xenocrysts in basic igneous extrusives are similarly attributed to crystallization under high pressures (Table 4.31).

TABLE 4.31

Al_2O_3 CONTENT OF ORTHOPYROXENES FROM HIGH PRESSURE ULTRAMAFIC INTRUSIONS, AND FROM NODULES AND XENOCRYSTS IN BASIC IGNEOUS EXTRUSIVES

SOURCE	AREA	RANGE OF Al_2O_3 IN WT % $^{2+}$
Green (1964)	Lizard Intrusion	2.05 - 6.59
Kornprobst (1969)	Beni Bouchera Intrusion	3.27 - 5.93
Moore (1971)	Gosse Pile Intrusion	2.56 - 4.01
Binns <u>et al.</u> (1970)	New England	3.45 - 8.03
Aoki (1971)	Itinome-gata Crater, Japan	2.43 - 4.60

Howie (1964) in contrast, considered that the highly aluminous orthopyroxenes (7.21% Al_2O_3) in hornfelses from Belhelvie, Scotland, were formed because of the peraluminous nature of their host rocks rather than as the result of crystallization under high pressures. He further demonstrated (1965, p.320) that the alumina content of orthopyroxenes from regional high grade metamorphic rocks was directly related to the availability of alumina in the environment of crystallization.

Binns (1965b, p.574) believed that the alumina content of the Broken Hill orthopyroxenes depend on both host rock chemistry and the nature of the co-existing phases, i.e. he suggested that the more aluminous pyroxenes co-exist with the more sodic plagioclase.

From Table 4.2 it can be seen that the Amata mafic rocks contain medium to high contents of Al_2O_3 . However, apart from providing an aluminous environment, the alumina variation in the orthopyroxenes is not controlled by the alumina contents of the respective host rocks

(Table 4.32).

TABLE 4.32

 Al_2O_3 CONTENT OF HOST ROCKS AND ORTHOPYROXENES

SPECIMEN NO. A325/-	Al_2O_3 HOST ROCK	Al_2O_3 OPX
339	16.83	2.61
105b	18.76	2.33
81	21.65	2.36
295	7.75	2.34
138b	14.39	2.78
326	16.70	2.37
990	12.11	3.17
119	20.49	2.35
1105	17.06	3.02
523	17.99	2.75
517	16.68	2.57
121	19.05	2.30
60	20.15	2.40
949	18.64	6.56

Values in wt %

It is concluded, therefore, that high pressures, together with the nature of the co-existing phases, are responsible for the high Al_2O_3 contents of the Amata orthopyroxenes from both the granulite facies and transitional terrain. This supports Moore's (1971) conclusions concerning orthopyroxenes from the Gosse Pile intrusion west of Amata.

4.3.3.2 Clinopyroxenes

4.3.3.2.1 Nomenclature

The clinopyroxene analyses when plotted in terms of their end member components, En, Wo and Fe (Figure 4.24) with one exception fall either side of the salite-augite boundary. Specimen A325-425 has the composition of a ferrosalite (using the terminology of Deer *et al.* 1962). The mg values of the salites and augites range between 60.5 and 78.8 and the value of the ferrosalite is 42.5, indicating its much lower magnesium content.

4.3.3.2.2 Chemistry

The titanium contents are variable, ranging between 0.23 and 0.71% TiO_2 in the transitional terrain clinopyroxenes and between 0.17 and 1.21% TiO_2 in the granulite facies clinopyroxenes. The titanium content of the clinopyroxenes does not vary directly with the TiO_2 contents of their host rocks (compare Tables 4.2 and 4.21).

The $\text{MnO}/\text{MnO} + \text{MgO} + \text{FeO}$ molecular ratio of the clinopyroxenes, however, does vary directly with the same ratio in their host rocks and the plots for the different metamorphic groups fall into two distinct fields (as for the orthopyroxenes), Figure 4.23.1a suggesting control by host rock composition or metamorphic grade dependence.

The influence of the host rock $\text{Mg}/\text{Mg} + \text{Fe}^{2+}$ ratio and oxidation ratio on the composition of the clinopyroxenes was demonstrated above.

Alkali determinations (where available) show soda to be in excess of potash.

The clinopyroxenes have high contents of Al_2O_3 , ranging from 2.63 to 8.35% (Table 4.21). These Al_2O_3 contents parallel the high values in co-existing orthopyroxenes. They indicate that Al_2O_3 has a greater affinity for the clinopyroxene structures. With the exception of A325-523 and -14, they contain higher contents of aluminium in tetrahedral than in octahedral co-ordination. The anomalous values are the result of higher contents of Si^{IV} occupying Z sites. The absence of Al^{VI} in A325-295 parallels a similar deficiency in the co-existing orthopyroxene. It is considered to be the result of the low content of Al_2O_3 in the host rock (7.75%).

The alumina contents of the Amata granulite facies clinopyroxenes (4.03-8.35%) range to higher values than do the alumina contents of the clinopyroxenes from the transitional terrain (2.63-5.47%). However, both groups are significantly more aluminous than the pyroxenes from Broken Hill, West Uusimaa and Quairading (Table 4.33). The values from the transitional zone are more comparable with the values from Indian granulite facies terrains (Table 4.33).

TABLE 4.33

Al_2O_3 CONTENTS OF CLINOPYROXENES FROM OTHER
GRANULITE FACIES LITHOLOGIES

SOURCE	AREA	RANGE OF Al_2O_3 IN WT %
Binns (1965b)	Broken Hill	1.16 - 3.14
Saxena (1969)	West Uusimaa	0.60 - 1.20
Davidson (1968)	Quairading	1.54 - 2.38
Leelanandam (1967a)	Kondapalli	2.87 - 5.79
Leelanandam (1967a)	Madras	2.00 - 5.94
Sen and Rege (1966)	Saltora	1.74 - 4.64
Lovering and White (1969)	Delegate	3.86 - 6.72

The values from the Delegate granulite inclusions more closely compare with the Amata granulite facies clinopyroxenes.

It is considered that the content of Al^{VI} in certain silicate structures is influenced directly by pressure. Thompson (1947) considered that aluminium in four-fold co-ordination is controlled by temperature. White (1964, p.885) recognised that the distribution of aluminium between the tetrahedral and octahedral sites of clinopyroxenes is dependent on the physical conditions of their formation and therefore varies with metamorphic grade. He showed that eclogite facies clinopyroxenes are characterised by aluminium in six-fold co-ordination whereas granulite facies pyroxenes contain approximately equal amounts of Al^{IV} and Al^{VI} .

Aoki and Kushiro (1968) investigated the validity of this relationship for clinopyroxenes from various environments by plotting Al^{VI} against Al^{IV} . Their data show that eclogitic and igneous clinopyroxenes are distributed into two distinct fields. This suggests that aluminium abundance in octahedral or tetrahedral sites is dependent to a large extent on the environment of crystallisation. They also found that the distribution of octahedral and tetrahedral aluminium in clinopyroxenes from granulites and nodules in igneous rocks is more variable and occupies the field between the eclogitic and igneous extremes. They considered that these distributions are directly

related to the presence of significant amounts of Ca Tschermak's component ($\text{CaAl}_2\text{SiO}_6$), the amount of Tschermak's molecule ($\text{CaMgAl}_2\text{SiO}_6$) being a measure of the Al in four-fold co-ordination (White (1964).

Plots of Al^{VI} against Al^{IV} for the Amata clinopyroxenes (Figure 4.26) reveal (with two exceptions, A325-295 and -138b) that the distribution of Al^{VI} against Al^{IV} is similar to that of other granulite facies clinopyroxenes. The less aluminous nature of the clinopyroxenes from the transitional rocks is shown in the plots. From Figure 4.26 it is also apparent that the range of $\text{Al}^{\text{VI}}/\text{Al}^{\text{IV}}$ ratios is more extensive for the transitional terrain clinopyroxenes than for those from the granulites. If the suggestions of Aoki and Kushiro (1968) are valid, then it can be concluded that the pressure-temperature environment of the granulite facies rocks was more restricted than was that of the transitional rocks. However, the high content of Ca Tschermak's component in the crystal structure demonstrates that both groups of rocks crystallized under moderate to high temperature and pressure.

4.3.3.3 Hornblendes

4.3.3.3.1 Nomenclature

Leake's (1968)¹ nomenclature is employed for the classification of the Amata hornblendes. The following groups are recognised: common hornblende, pargasitic hornblende, and hastingsitic hornblende. Details are listed in Table 4.34.

-
1. Although the Amata amphibole analyses are recalculated on the 23(0) basis (following Binns' 1965a proposals), Leake's nomenclature derived from analyses computed on the basis of 24(OH, 0) is followed. It is considered that the assumptions made in the 23(0) method are valid.

These assumptions concern the existence of hydrogen deficiencies. According to Binns (1965a, p.317), such deficiencies are rarely encountered in rocks with high ferrous to ferric ratios as the environment is not sufficiently oxidizing to form oxy-hornblende.

TABLE 4.34

NOMENCLATURE OF THE AMATA HORNBLENDES

CLASSIFICATION	SPECIMEN NUMBER
ferroan pargasitic hornblende	A325-523
magnesian hastingsitic hornblende	A325-1684
titaniferous ferroan pargasitic hornblende	A325-339
ferroan pargasitic hornblende	A325-6
magnesio hornblende	A325-2050c
titaniferous pargasitic hornblende	A325-1105
titaniferous pargasitic hornblende	A325-949

4.3.3.3.2 Chemistry

The chemical variability of the hornblendes is expressed by the relationship between Al^{IV} and Na + K atoms per formula unit and by the relationship between Al^{IV} and $Al^{VI} + Fe^{3+} + Ti$ (Figure 4.27b and a). With the exception of A325-2050c, which contains less $Al^{VI} + Fe^{3+} + Ti$ and less alkali in the X site than the other amphiboles, the hornblendes exhibit an increase of Na + K and a decrease of $Al^{VI} + Fe^{3+} + Ti$ with increasing Al^{IV} . This is attributed to Al^{IV} substitution for Si.

Figure 4.27c (after Gilbert, 1966) approximates to the solid solutions within the pargasite-hastingsite series by showing the variation between the ratios $Fe^{3+}/Al^{VI} + Fe^{3+}$ and $Fe^{2+}/Fe^{2+} + Mg$. These ratios vary regularly in the Amata hornblendes and the analyses plot diagonally across the figure. Hornblende A325-2050c, with the highest Mg/Fe^{2+} ratio plots closest to the pargasite corner.

The alumina content of the hornblendes is quite variable. Al^{VI} and Al^{IV} atoms are more abundant in the hornblendes from the mafic granulites, viz. A325-1105 and -949 (Figure 4.28a) than in the other analysed hornblendes.

Leake (1965, p.311; 1971, p.397) suggested that the high content of Al^{VI} in amphibole is directly a result of crystallization under high pressure, as is thought to be the case also with high Al^{VI} in the clinopyroxenes (see above, p.205).

The nature of the co-existing minerals in the Amata granulites, the high contents of Al^{VI} in clinopyroxenes and orthopyroxenes, and the high content of pyrope and grossularite molecules in garnet A325-1105 (i.e. 32.05 py, 14.18 gross) suggest that the granulites crystallized under high pressures. Therefore the high content of Al^{VI} in two of the granulite facies hornblendes (Figure 4.28a) is probably the result of high pressures.

Figure 4.28b shows the distribution of hornblendes from high pressure rocks (mostly eclogites but including one 'garnet free' charnockite). All lie well above Binns' field of Broken Hill granulite facies hornblendes. On the other hand some hornblende analyses (amphibolite facies) taken from Bard (1969) lie within this field.

Leake (1965, p.1312) considered that the commonly observed low content of Al^{VI} in granulite facies amphiboles (i.e. at Broken Hill) 'supports the view that the most important difference between the conditions of the amphibolite facies and those of the granulite facies is temperature and not pressure'.

The content of Al_2O_3 in the host rocks is an important factor governing the content of Al_2O_3 in mineral phases (Leake, 1965). The ultramafic granulite A325-2050c contains hornblende with less Al^{VI} and Al^{IV} than the other two granulite facies hornblendes (Table 4.22). This is believed to be due to the low content of alumina in the host rock (Table 4.2) and the greater volume of hornblende in the rock which had to be satisfied with this low content of alumina (Table 4.1).

The presence of primary hornblende, rich in Al^{VI} , in some of the Amata mafic granulites associated with orthopyroxene, clinopyroxene, plagioclase and opaques indicates that under certain conditions hornblende can be stable in medium to high pressure granulite facies regimes, and suggests that the Amata (and possibly other Musgrave Range) granulites represent much deeper crustal segments than are represented in other granulite facies terrains, e.g. Broken Hill or Quairading.

If it is a valid deduction that Al^{VI} in hornblende indicates high pressures, then it follows that the Amata area hornblendes in the transitional and amphibolite facies terrains formed at lower pressures than the hornblendes from the granulite facies terrain.

The titanium content of the Amata hornblendes varies with metamorphic grade. The granulite facies hornblendes (except for A325-2050c)¹ are richer in titanium than the hornblendes from the amphibolite facies and transitional terrain. This is consistent with findings from other areas (i.e. Shido and Miyashiro, 1959; Engel and Engel, 1962b; Binns, 1965a; Leake, 1965; Leelana dam, 1970a; Davidson, 1971). The relationship appears to be independent of host rock control (See Table 4.2). There appears to be a direct relationship between titanium content in the Y group and the $Al^{IV}/Al^{IV} + Si$ ratio (Figure 4.28c).

Leake (1965, p.301) proposed that higher temperatures of crystallization favoured higher contents of titanium in amphiboles.

Binns (1965a and 1969) correlated the higher titanium in certain metamorphic hornblendes with Al^{IV} substitution for Si^{IV} and Harry (1950) considered that Al^{IV} substitution for Si^{IV} in amphiboles is directly related to an increase in temperature of crystallization.

The range of pleochroic colours characteristic of hornblendes of different metamorphic grades is considered by Deer (1938), Engel and Engel (1962b) and others to be due to the introduction of titanium into the hornblende lattice as temperature increases. Binns (1965a, p.312-313) showed that blue-green hornblende contain higher Fe^{3+} and lower

-
1. Hornblende A325-2050c contains less titanium than hornblendes from the other mafic granulites. However, the titanium content of their host rocks are similar (Table 4.2). Petrographic study (Chapter 3.3.2.4) indicates the presence of elongate rutile needles in the co-existing orthopyroxene of -2050c. This is thought to indicate that during crystallization of the ultramafic unit (perhaps pre-metamorphic crystallization), titanium was concentrated in the orthopyroxene which, theoretically, would have been the first phase to crystallize. During the ensuing metamorphic events high pressures caused the exsolution of rutile from the orthopyroxene (see also Moore, 1968; Griffin *et al.*, 1971). This removed Ti preferentially from the system and hornblende crystallized with an unusually low titanium content for granulite facies amphiboles. Titanium was not available for the formation of ilmenite; the only opaque in rock A325-2050c being a trace of magnetite.

titanium than brown hornblende. The colours of the green and green-brown hornblendes are thought to vary depending on the proportion of Fe^{3+} to titanium. Davidson (1971, p.351-352) also concluded that colour variation in hornblende depends on the relative amounts of Fe^{3+} , Fe^{2+} and Ti. However, he was unsure which type of energy-exchanging process caused the mineral colour.

In the Amata area the blue green amphibolite facies hornblende (A325-1684) is characterised by low Ti^{3+} and high Fe^{3+} (viz. 0.109 and 0.657 ions respectively) whereas the brown granulite facies hornblendes (A325-1105 and -949) have high Ti^{3+} contents (0.430 and 0.358 ions respectively). The green to brown green hornblendes from the transitional terrain (A325-523, -339 and -6) range in Ti^{3+} from 0.129 to 0.251 and in Fe^{3+} from 0.315 to 0.539. This distribution provides evidence that there is a temperature difference between the three metamorphic terrains.

The alkali content of the Amata hornblendes is variable. Na^+ is greater than K^+ in the transitional and amphibolite facies hornblendes (see also Binns, 1965a). No alkali determinations are available for the granulite facies amphiboles (except -2050c) and it is therefore not known if this pattern is typical of these hornblendes as well. Binns' (1965a) and Davidson's (1971) data suggest that it is. The ultramafic hornblende A325-2050c contains a lower content of Na^+ than the other hornblendes. This is partially balanced by an increase in the K^+ and Ca^{2+} content of the X group (Table 4.22). Leelanandam's (1970, p.478) observation that ' Na_2O is greater than K_2O in hornblendes from ultrabasic charnockites' contrasts with the observations from the Amata region, i.e. A325-2050c.

The wide range of mg values ($\text{Mg}/\text{Mg} + \text{Fe}^{3+} + \text{Fe}^{2+} + \text{Mn}$), viz. 50.5 to 84.7 is attributed to extensive Mg-Fe substitution in the Y group (see also Davidson, 1971, p.350).

The ferric/ferrous ratios of the amphiboles vary inversely with both the Ti content of the Y site and also with the $\text{Al}^{\text{IV}}/\text{Al}^{\text{IV}} + \text{Si}^{\text{IV}}$ ratio of the Z site (Figures 4.29a and b). These figures show that:

1. Fe^{3+} ions appear to enter the amphibole structure in inverse proportion to Ti ions;

2. The amount of Al^{IV} substitution for Si^{IV} apparently increases with decreasing hornblende ferric/ferrous ratio (cf. Annersten, 1968, p.393).

It was demonstrated above (p.196) that the hornblende and the host rock $\text{Mg}/\text{Mg} + \text{Fe}^{2+}$ ratio varies inversely with host rock oxidation ratio and that there was a direct relationship between hornblende $\text{Mg}/\text{Mg} + \text{Fe}^{2+}$ ratio and that of their host rocks. It is apparent that the ferric/ferrous ratio in the hornblendes is not simply a function of the host rock oxidation ratio (Figure 4.20b) and the relationship between Al^{IV} and Si^{IV} is therefore considered to be controlled by an interplay of a number of different factors.

The above data are consistent in most respects with the results of other investigations of grade dependent hornblende compositional variation (Shido and Miyashiro, 1959; Engel and Engel, 1962a; Binns, 1965a, 1969; Leake, 1965; Bard, 1970). For example:

1. $\text{Mg}/\text{Mg} + \text{Fe}$ ratio is controlled by the host rock chemistry;
2. Ti increases with increasing grade;
3. Al^{IV} increases as Si^{IV} decreases;
4. both Ti and Fe^{3+} appear to control hornblende pleochroic colours.

The Amata hornblendes, however, appear to differ from other hornblendes in their $\text{Al}^{\text{IV}}/\text{Al}^{\text{VI}}$ contents. The granulite facies hornblendes contain higher contents of Al^{VI} than were found by Binns (1965a) and Davidson (1971). This is interpreted as direct evidence for extremely high pressures during the granulite facies metamorphic events in the Musgrave Block.

4.3.3.4 Garnets

4.3.3.4.1 Nomenclature

The garnet analyses were recalculated into the standard end-member molecules following the method suggested by Ringwood (1968) and they are listed in Table 4.23. Three of the garnets are from quartzofeldspathic lithologies, viz. A325-77 and -1121 (granulite facies) and A325-531 (transitional granulite to amphibolite facies); one is from a

calc silicate unit in the granulite terrain, viz. A325-2040, and A325-1105 is from a mafic granulite. A partial analysis of A325-2048 from a manganiferous unit is also presented.

The results indicate that the garnets from the mafic and quartzo-feldspathic units are either almandine-pyrope-grossular (A325-1105 and -1121) or almandine-pyrope (A325-77 and -531), with 48.96-55.31% almandine, 32.05-43.71% pyrope and 0.00-14.18% grossular. Only minor amounts of andradite and spessartine are present (Table 4.23). Garnet A325-2040 is predominantly grossularite (49.44%) and andradite (36.86%), with also a significant amount of almandine molecule (11.35%). The manganese and calcium contents of A325-2048 reflect abundant spessartine, with lesser amounts of grossularite and/or andradite.

Garnet compositions from other granulite facies rocks are given for comparison in Table 4.35. The Amata pyralspites range to higher pyrope values and contain less almandine than the Broken Hill, Moldanubicum or Madras granulites. However, they have less almandine than the Delegate garnet granulite.

TABLE 4.35

END-MEMBER MOLECULES OF GARNETS FROM HIGH GRADE METAMORPHIC ROCKS
FOR COMPARISON WITH AMATA GARNETS

SOURCE	Alm	Sp	Py	Gross	And
Broken Hill; Binns (1965b) Table IV	48.8-67.2	2.7-17.9	3.6-13.5	9.5-27.4	0.0-3.0
Moldanubicum; Matějovská (1970) Table 3	55.8-77.8	0.9-5.3	11.0-32.6	0.0-2.9	3.4-9.9
Madras; Howie and Subramaniam (1956) Table II	58.5-77.6	0.4-2.5	12.7-38.0	0.0-14.6	0.0-6.6
Delegate; Lovering and White (1969) Table 10	37.9	1.0	41.7	12.9	6.5

4.3.3.4.2 Cell Dimensions

The unit cell dimensions listed in Table 4.23 are strongly influenced by the calcium content of the garnets (see also Binns, 1965b; Leelanandam, 1970b).

The cell dimensions in two of the garnets (A325-2048 and -2040) were not determined accurately because the high angle reflections (10, 4, 0) (10, 4, 2) and (8, 8, 0) were highly smeared. It was therefore not possible to delineate the $K\alpha_1$ and $K\alpha_2$ reflections. Both Hobson (pers.comm.) and Whittle (1968) have observed similar features in garnets from Connemara, Eire, and from the Otway Basin respectively.

The smeared reflections in the garnets are similar to the anomalous 'side bands' which occur in the powder patterns of certain alloys. Daniel and Lipson (1943, 1944) considered that they are caused by modulation of the lattice parameter in the direction of the cubic axes. Hargreaves (1951) believed that they are produced by phase transformation through nucleation and grain growth.

It is significant to note in the present study that the garnets which display this phenomenon are (1) not members of the pyralspite group, (2) have high contents of andradite, and (3) are not zoned in Mn, Fe or Ca¹. If the anomalous reflections are the result of modulation of the lattice parameters, as has been suggested by the work on alloys, then it is reasonable to presume that the modulation must have been initiated only in garnets of certain composition.

Dalziel and Bailey (1968) has shown that garnet lattices can distort under the influence of tectonic processes. It is possible therefore, that the side bands are the result of modulation in garnet of particular compositions, under the influence of tectonic processes.

4.3.3.4.3 Chemistry

The pyralspite analyses have been plotted in Figure 4.30, in terms of the following proportions: Mn + Fe²⁺, Ca²⁺ and Mg²⁺. The field of granulite facies compositions (from White, 1969) is shown for comparison. The Amata pyralspites form two groups, viz. (1) those

1. Probe scan performed by A.M.D.E.L.

from the quartzo-feldspathic lithologies with low contents of Ca^{2+} , and (2) the more lime-rich garnet (A325-1105) from the mafic granulite, thus indicating the effect of host rock compositional control.

Similarly, high MnO in garnet A325-2048 appears to be directly influenced by the large MnO content of the host rock (see also Atherton, 1965). Chinner (1960, Fig.14) demonstrated that the molecular ratio $\text{MnO} \times 100 / \text{MnO} + \text{FeO}$ of the Glen Clova garnets increases sharply with increasing oxidation.

In the Amata garnets, where oxygen fugacities are low, the $\text{Mn}/\text{Mn} + \text{Mg} + \text{Fe}^{2+}$ ratios of the garnets appear to be independent of the rock oxidation state. However, at higher oxygen fugacities, as shown above, there is a pronounced increase in the $\text{Mn}/\text{Mn} + \text{Fe} + \text{Mg}$ ratio of the garnets (see also Chinner, 1960; Mueller and Schneider, 1971). Hsu (1968) comes to similar conclusions as the result of his experimental work on the system Al-Mn-Fe-Si-O-OH.

Huckenholz and Yoder (1971, Figure 1) demonstrated that the andradite content of garnets is directly influenced by the oxidation state of the environment in which the garnet crystallized. The andradite content of A325-2040 and the oxidation state of its host rock display a close agreement with the trend depicted by the above authors. It is therefore considered that high oxygen fugacity and an iron-rich environment are responsible for the high andradite content of A325-2040.

High contents of TiO_2 are not uncommon in andradite-rich garnets and the high TiO_2 content of A325-2040 indicates an abundance of schorlomite molecule. The low total of the analysis of this garnet is thought possibly to be due to the presence of significant amounts of zirconium¹.

White (1959, p.300) noted the rarity of garnets in the composition range $\text{An}_{63}\text{Gr}_{37}$ to $\text{An}_{45}\text{Gr}_{55}$, and considered that this indicates the existence of an immiscibility gap in the calcium garnet series. The grossularite garnet from the Amata area (A325-2040), and a similar garnet from the Mt. Davies area (Barnes, 1968, Table V) with the composition $\text{And}_{46}\text{Gross}_{35.6}\text{Py}_{5.7}\text{Alm}_{12.4}\text{Spess}_{0.2}$, discount this allegation of

1. This was revealed qualitatively during the X.R.F. analysis

immiscibility.

Their compositions can perhaps be accounted for by the experimental work of Huckenholz and Yoder (1971) who showed that under anhydrous conditions the stability range of andradite becomes more extensive and, at pressures above 10 Kb, it overlaps the stability field of grossularite. They attributed the 'absence' of andradite or andraditic garnets in peridotites and high grade metamorphic rocks to the lower oxygen fugacities in these rocks rather than to unfavourable chemical composition, e.g. absence of adequate iron or calcium. The absence of andraditic garnets in the oxygen deficient mafic and quartzofeldspathic rocks supports their conclusions.

The local maintenance of high oxygen fugacities in the Amata region dominated in general by low to moderate P_{O_2} 's is evidence for the limited mobility of O_2 , even under granulite facies conditions, a condition which may be general¹.

4.3.3.5 Micas

4.3.3.5.1 Nomenclature

Following the method of Foster (1960), the octahedrally coordinated elements (i.e. Mg^{2+} , Mn^{2+} , Fe^{2+} , Al^{3+} , Fe^{3+} and Ti^{4+}) were recalculated from the structural formulae of the analysed micas (Table 4.24) and plotted on a ternary projection (Figure 4.31). Three of the specimens, A325-990, -2050c and -1328, are shown by this technique to be phlogopite, and the remainder are biotite; A325-6 and -14

-
1. The author has found only two other reports of high andradite contents in granulite or 'eclogite' facies garnets:
 1. Subramaniam (1956, p.328) describes a grossularite of the following composition: Alm 9 Spess 1.5 Py 2 Gross 69 And 18 from an anorthite-garnet-clinozoisite-corundum rock in the Sittampundi Complex.
 2. Bhattacharyya *et al.* (1970) describe garnets from the Srikakulam 'charnockites' containing Alm 37.8-60.4, Sp 0.5-4.9, Py 11.6-19.2, Gross 0.0-1.85, And 23.6-42.7.
-

are Mg biotites and A325-1687 is an Mg:Fe biotite¹.

4.3.3.5.2 Chemistry

These compositional differences reflect the variable Mg/Fe ratios of the micas. It was shown above (p.196) that the Mg/Fe²⁺ ratio of the host rock varies directly with that ratio in the mica. Thus, the most magnesian phlogopite is from an ultramafic granulite and the most ferruginous biotite is a constituent of a mica schist.

The silica contents of the micas are variable. It is considerably lower in the iron rich Mg:Fe biotite A325-1687 than the others. Alumina is approximately the same in the phlogopites and Mg biotites however it is greater in the Mg:Fe biotite. MnO is lowest in the phlogopite from the ultramafic granulite A325-2050c, slightly higher in the micas and phlogopites from the transitional terrain and greatest in the biotite from the amphibolite facies terrain. The content of TiO₂ is generally higher in the Mg biotites and phlogopites than in the Mg:Fe biotite.

Low values of MnO and high values of TiO₂ have previously been reported in micas by Leelanandam (1970a, p.484), Bhattacharyya (1970, p.686) and Matejovská (1970, p.255) from high grade terrains.

It has been shown above for the pyroxenes and amphiboles that MnO is generally lower and TiO₂ generally higher in the granulite facies minerals than in those from the other two terrains and it was suggested that these variations may have been grade dependent, i.e. TiO₂ increasing as temperature increases (Harry, 1950; Leake, 1965). The same interpretation is considered valid for the micas.

1. Ferrous iron was not determined separately for A325-14 and -2050c because of insufficient sample, nor was it determined for A325-6 (a probe analysis). Total iron was calculated as FeO. The presence of minor amounts of ferric iron (unaccounted for) is not considered to significantly alter the Al³⁺ + Ti⁴⁺ + Fe³⁺ + Mn²⁺ + Fe²⁺ : Mg ratio, although it would alter the Mn²⁺ + Fe²⁺ : Al³⁺ + Fe³⁺ + Ti⁴⁺ ratio. The Fe²⁺ values from the calculated structural formulae are therefore used to determine the Fe²⁺ + Mn²⁺ value.

4.3.3.6 Opaque Oxides

4.3.3.6.1 General

The following opaque oxides are recognised in the Amata metamorphic rocks: magnetite, ferrian ilmenite, haemo-ilmenite, ilmeno-haematite and rutile¹. No ulvospinel has been observed in the magnetite, however, spinel exsolution (Figure 3.19a) and martite alteration (Figures 3.19c,d and 4.32d) are occasionally present. The magnetite occurs either as euhedral to subhedral grains (Figures 3.19a,c,d and 4.32b,d) or as thin plates parallel to the (001) basal direction in larger grains of ilmeno-haematite or haemo-ilmenite² (Figure 4.33a,b,c). Magnetite grains surrounded by Fe-Ti oxides are mantled by narrow zones of ferrian ilmenite which are free of haematite exsolution (Figures 3.19c, 4.32b,c,d and 4.33d,e,f). Patches of rutile are frequently developed in these regions. Similar haematite free zones adjacent to magnetite have been observed by Hubaux (1956), Basta (1960), Maucher and Rehwald (1961), Vaasjoki and Heikkinen (1963), Krause (1965) and Kretschmar and McNutt (1971). It is commonly held that such zones are formed by ilmenite enrichment of the surrounding phases, the ilmenite being derived by the oxidation of the ulvospinel component in originally titaniferous magnetites.

The haematite (titan-haematite) exsolution features of the ilmeno-haematite and haemo-ilmenite grains are variable, in both volume and type. Exsolution lamellae (Figures 3.19b and 4.32c) are either parallel to (001) of their host grains (coherent exsolution, Brett (1964) or they occur as randomly oriented angular to rounded blebs (Figure 4.32a) and lamellae which frequently thicken at grain interfaces, due to coalescence (Brett's non coherent exsolution). Several types of exsolution are often present within a single grain (Figure 4.32b).

-
1. The Fe and Fe-Ti oxide terminology proposed by Buddington *et al.* (1963, p.140) is used throughout this thesis.
 2. These lamellae are considered by Buddington *et al.* (1963) and Buddington and Lindsley (1964) to be formed by the subsolidus reduction and exsolution of Fe_2O_3 (in solid solution).
-

4.3.3.6.2 Chemistry

Partial analyses of four 'haematites' and five 'ilmenites' from grains of ilmeno-haematite or haemo-ilmenite, together with four analyses of magnetite and one analysis of rutile are listed in Table 4.25.

Details of the rocks containing the analysed opaques are as follows:

1. mafic granulite, A325-115;
2. garnetiferous quartzo-feldspathic gneiss, transitional terrain, A325-500;
3. quartzo-feldspathic gneiss, transitional terrain, A325-43;
4. gneissic granite, transitional terrain, A325-18;
5. amphibolite, transitional terrain, A325-6.

The magnetites are remarkably free of titanium and do not appear to be zoned in that component (Figure 4.33c,f). Magnetites with low contents of TiO_2 have been reported previously from metamorphic rocks by Marmo (1959), Vaasjoki and Heikkinen (1963), Abdullah and Atherton (1964), Abdullah (1965), and Kretschmar and McNutt (1971). Vaasjoki and Heikkinen (1963) considered that the low content of TiO_2 in metamorphic magnetites is the result of the unmixing of magnetite and ilmenite from homogeneous magnetite-ilvospinel solid solutions during slow cooling.

In comparison, Binns (1965b, Table VII) listed TiO_2 contents from 3.8 to 8.7 wt % in magnetites from the Broken Hill amphibolites and granulites.

Abdullah and Atherton (1964) and Abdullah (1965) considered that the amount of TiO_2 in magnetite, coexisting with ilmenite, is dependent on the grade of metamorphism, the amount increasing with increasing metamorphic grade. Data presented by Marmo (1959) and the present study demonstrate that this is not always valid.

The low content of MnO in the Amata magnetites agrees with the observations of Abdullah and Atherton (1964) and Buddington and Lindsley (1964) regarding the content of manganese in metamorphic magnetite.

The analytical data indicates that the ilmenites are richer in MnO than their co-existing magnetites (see also Buddington and Lindsley, 1964).

The distribution of Ti and Fe in ilmeno-haematite and haemo-ilmenite is shown (Figures 4.33c,f and b,e respectively). The analytical data have been recalculated to molecular percent ilmenite and haematite following the method of Carmichael (1967a). Ilmenite and haematite exsolution lamellae have compositions varying from Ilm_{98} , Haem_2 to Ilm_{87} Haem_{13} and Haem_{94} Ilm_6 to Haem_{76} Ilm_{24} respectively.

Manganese is more abundant in the ilmenite phase of haemo-ilmenite and ilmeno-haematite grains. Bolfa et al. (1961) have reported the contrary.

Lovering and Widdowson (1968) showed that the MgO content of ilmenite in a variety of rocks (e.g. kimberlites, gabbros, eclogites) was related to the MgO/FeO ratios in their host rocks. They found similar MgO contents in ilmenites from gabbros and high grade metamorphic rocks and concluded that the amount of MgO in ilmenite was independent of both pressure and temperature. At Amata, magnesium is above detection limits only in ilmenite A325-6 (0.2 wt % MgO). When this value is plotted against its host rock MgO/FeO ratio the point falls above the regression line of Lovering and Widdowson (1968) but close to the position of the Mampong amphibolite-eclogite and Ernabella granulite. The host rock A325-6 is a lower grade assemblage than the Ernabella granulite. The limited data from Amata therefore supports Lovering and Widdowson's hypothesis.

4.3.3.6.3 Application of Experimental Systems

The synthetic studies of Lindsley (1962, 1963) and the practical application of these results by Buddington and Lindsley (1964) demonstrated that the compositions of the following solid solution series, magnetite-ülvospinel and haematite-ilmenite could be used to estimate the temperature and oxygen fugacity of their formation. It had been shown that total pressure had negligible effect on the oxide composition and therefore could be neglected, thus reducing the variance of the system to two. Several factors had to be considered in

applying the experiment work to natural rock systems:

1. the Fe-Ti oxides equilibrated contemporaneously during the crystallization of their host rocks;
2. ilmenite may have been lost from the magnetite at subsolidus temperatures and therefore the ulvospinel component of the magnetite would be underestimated;
3. the effect of other components, i.e. MnO and MgO on the oxygen fugacity-temperature stability ranges of the oxides was not known; it was thought that their presence would cause the fugacity and temperature estimates to be more inaccurate.

By plotting Amata magnetites with less than 10% ulvospinel and co-existing ilmenites with compositions $\text{Ilm}_{98}\text{Haem}_2$ to $\text{Ilm}_{87}\text{Haem}_{13}$ on an extrapolation of Lindsley's (1963, Figure 5) diagram temperature estimates are from less than 500 to 550°C for the ilmenite-magnetite pairs A325-18, -6 and -538 at oxygen fugacities ($-\log_{10} f_{\text{O}_2}$)²⁴ to approximately 18. These estimates probably indicate the subsolidus equilibration temperatures. The lower titanium content of the magnetites (caused by oxidation of the ulvospinel component during cooling) and the MnO content of the ilmeno-haematites and haemo-ilmenites possibly causes these estimates to be inaccurate. Binns (1965b) and Buddington and Lindsley (1964) obtain higher estimates of temperature for the opaque phases in the Broken Hill and Adirondack high grade metamorphics, viz. 600-670°C and 550-665°C respectively.

Temperature estimates for the formation of ilmeno-haematite and haemo-ilmenite in the present study range between 700-500°C, for compositions which lie on the solvus constructed by Kretschmar and McNutt (1971, Fig.7). Aberrant values which do not plot on the solvus are possibly the effect of variable oxygen fugacities over small areas.

It is possible that the opaque oxides in the Amata rocks developed in the following manner. The first opaque oxides to form are probably titaniferous magnetite and ferrian ilmenite. On cooling, after the ilmenite-haematite solvus has been intersected, ilmeno-haematite and haemo-ilmenite are probably formed and ulvospinel in the magnetite is believed to undergo oxidation resulting in the development

of TiO_2 -poor magnetite. Further oxidation of the magnetite is believed to result in the formation of martite.

In the final stages of cooling the ilmeno-haematites are thought to have been reduced slightly forming the thin slivers of magnetite parallel to the (001) basal plane. This pattern of oxide formation conforms to other paragenetic sequences described in other high grade terrains by Buddington and Lindsley (1964) and Kretschmar and McNutt (1971).

4.3.3.7 Scapolite

4.3.3.7.1 General

Partial analyses of scapolite from the Amata area are listed in Table 4.26. Three of these are from mafic granulites (A325-192, -78 and -564) and the fourth (A325-425) is from a calc silicate unit (see Chapter 3.4.5) in the transitional terrain. These analyses and the refractive indices (given in Table 4.36) indicate that the scapolites are mizzonitic to meionitic with meionite contents ranging from 63 to 86%. The mean refractive indices of scapolites from the mafic granulites are significantly lower than the N_m values for scapolites from the Delegate Pipe two pyroxene granulites (1.583 and 1.582 - Lovering and White, 1964, Table 7), but is comparable with refractive indices (1.571-1.576) listed for other scapolites from garnet-clinopyroxene granulites.

Petrographic study suggests that the scapolites are in textural equilibrium with plagioclase and are primary in origin.

-
1. Scapolite of secondary origin has been reported from mafic granulites by Leelanandam (1967b). He considers that it formed through the alteration of plagioclase by an increase in the fugacity of CO_2 , Cl_2 and/or SO_3 after the main phase of granulite facies metamorphism.

TABLE 4.36

REFRACTIVE INDICES OF SCAPOLITES FROM THE AMATA ROCKS

ROCK TYPE	SPECIMEN NO. A325/-	ω	ϵ	N_m
Mafic Granulite	192	1.588	1.564	1.576
	77	1.585	1.559	1.572
	564	1.591	1.562	1.577
	909a	1.584	1.559	1.571
	1345	1.590	1.567	1.578
Calc Silicate	425	1.578	1.557	1.567

N_m Mean Refractive Index

4.3.3.7.2 Chemistry

The range of compositions referred to above is manifested also in the chemical analyses. A325-425, from a calc silicate, is richer in Cl_2 than the scapolites from the mafic granulites. However, the scapolites from the mafic granulites are richer than A325-425 in SO_3 as in other high grade rocks (von Knorring and Kennedy, 1956; Lovering and White, 1964, 1969; Wilson, 1969b). Several analyses of these scapolites are listed in Table 4.37 for comparison.

The abnormally low SO_3 content of A325-425 could be interpreted as follows: if the transitional rocks are a suite of retrograded granulites, sulphur could have been lost during retrogression (cf. Wilson 1969b). Alternatively, it could simply be a function of lower partial pressures of SO_3 in that unit due to its different origin and bulk composition.

4.3.3.8 Alkali Feldspars

The alkali feldspars were investigated by both chemical and X-ray techniques to determine:

- (a) the chemical variability of the feldspars in the different metamorphic groups;
- (b) the variation in structural state.

4.3.3.8.1 Chemistry

Analyses of the alkali feldspars and their cation contents (calculated on the basis of 32 oxygen atoms) are listed in Table 4.27.

TABLE 4.37

PARTIAL ANALYSES OF SCAPOLITE; FROM THE LITERATURE

SPECIMEN NO.	a	b	c	d
SiO ₂	47.52	45.40	43.21	51.10
Al ₂ O ₃	25.21	27.33	27.75	25.10
Fe ₂ O ₃	-	0.25	-	0.33
FeO	0.30	0.27	0.32	0.12
CaO	15.48	16.55	18.27	12.54
Na ₂ O	4.52	3.40	2.66	5.38
TiO ₂	-	0.01	<0.10	0.05
SO ₃	4.17	5.10	5.58	0.11
Cl	0.06	0.17	<0.02	1.42

- a Von Knorring and Kennedy (1956)
 b Wilson (1969b)
 c Lovering and White (1969)
 d White (1959)

They are plotted in terms of their molecular end member components on the standard ternary diagram (Figure 4.34). The compositions range from 51.2% to 81.3% orthoclase. Two of the feldspars, viz. A325-138 and -1165a are significantly richer in albite and anorthite than the other feldspars, as reflected by their mesoperthitic nature. Of the rarer feldspar components, celsian contents range from 0.3 to 1.2% and small quantities of rubidium and strontium feldspar also are present.

4.3.3.8.2 Structural State

(a) Method of study

The separated feldspars were finely ground and mixed with a small amount of silicon (as an internal standard). Smear mounts were prepared and irradiated with filtered $\text{CuK}\alpha$ radiation. The X-ray diffraction charts were indexed and cell dimensions computed¹.

Petrological observations concerning the crystal type and degree of homogeneity of the feldspars were verified by the diffractometer data. For example, an estimate of the degree of order was obtained from the nature of the (131) doublet, following the methods of Goldsmith and Laves (1954). Likewise, the presence of a peak at $27.94^\circ 2\theta$ (the (002) albite peak) indicated that many of the feldspars are not homogeneous.

In the majority of the charts the (131) and ($1\bar{3}1$) positions could not be identified with certainty because the spacing was too close. It was therefore not possible to use the relationship $12.5(d_{131} - d_{1\bar{3}1})$ of Goldsmith and Laves (1954) to accurately estimate the degree of ordering of the feldspars. The structural state of the feldspars was, however, obtained from two relationships:

- (a) the c^*/b^* method of Jones (1966);
- (b) the function Δbc , after Stewart and Ribbe (1969) and Crosby (1971).

The values of c^*/b^* were calculated from the cell refinement data and not from the ratio of $2d_{040}/d_{002}$ as was suggested initially by Jones. The c^*/b^* ratios were plotted on Figure 4.35 to determine the degree of ordering. The values obtained are listed in Table 4.38. The most ordered phases are those from the amphibolite facies gneisses and the least ordered are from the transitional and granulite facies rocks.

1. For method, see Appendix 2.

TABLE 4.38

DETERMINATION OF TRICLINICITY BY c^*/b^* METHOD

SPECIMEN NO. A325/-	c^*	b^*	c^*/b^*	DEGREE OF ORDER
1121	0.15470	0.07699	2.0094	0.232
77	0.15435	0.07715	2.0007	0.522
1165a	0.15468	0.07699	2.0091	0.242
1328	0.15456	0.07690	2.0099	0.220
323	0.15455	0.07700	2.0071	0.299
531	0.15444	0.07703	2.0050	0.360
783	0.15471	0.07702	2.0087	0.254
400	0.15437	0.07713	2.0014	0.493
18	0.15433	0.07718	1.9996	0.583
474 ⁺	0.15443	0.07706	2.0040	0.395
1640*	0.15400	0.07719	1.9951	0.915
1659*	0.15407	0.07721	1.9955	0.860
1744*	0.15416	0.07726	1.9953	0.860
1659+*	0.15417	0.07720	1.9970	0.850

⁺ homogenized

* triclinic

The direct cell parameter data of the alkali feldspars are listed in Table 4.39. The c and b cell dimensions are plotted on Figure 4.36 which is based on Crosby's (1971) adaptation of the b - c plot used by Wright and Stewart (1968). The lengths of the bars represents the standard errors of the individual determinations.

The structural states of the alkali feldspars are defined by the value of Δbc (Figure 4.36). From the figure it can be seen that the Δbc values range from 0.72 to 1.0. The absolute positions of the feldspars on Figure 4.36 compare favourably with their distribution in Figure 4.35.

Petrological evidence, the broadening of the (131) peak and the rejection of a number of peaks from the cell refinement calculation suggests the presence of a variety of differently ordered feldspars among single samples. Therefore the structural states of the alkali feldspars are in reality only approximations.

In the refinement of the powder diffraction data the alkali feldspars with intermediate structural states are treated as having only monoclinic symmetry, regardless of their triclinic component (Wright and

TABLE 4.39

DIRECT CELL REFINEMENT OF POTASSIUM FELDSPARS

SPEC. NO. A325/-	a(Å)	b(Å)	c(Å)	INTERAXIAL ANGLE	CELL VOLUME (Å ³)	STANDARD ERROR 2θ	REFLECTION MEASURED/ ACCEPTED	D.F.
1121	8.5663	12.2988	7.1920	β 115 59.976	719.1809	0.01579	29/24	20
77	8.5843	12.9621	7.2074	β 115 59.260	720.8825	0.01434	20/18	14
1165a	8.5772	12.9894	7.1916	β 115 58.793	720.2632	0.01781	25/21	17
1328	8.5267	13.0042	7.1949	β 115 56.522	717.4029	0.01616	29/22	18
323	8.5815	12.9873	7.1991	β 115 59.937	721.1439	0.01309	25/19	15
531	8.5906	12.9829	7.2059	β 116 1.856	722.1557	0.01986	21/22	17
783	8.5902	12.9838	7.1940	β 116 2.442	720.9149	0.01514	29/24	20
400	8.5821	12.9649	7.2070	β 115 59.440	720.7973	0.01495	14/14	10
18*	8.5728	12.9648	7.2148	α 90 26.388 β 116 5.086	719.7757	0.01633	24/19	13
474 [†]	8.5297	12.9760	7.2021	α 88 4.378 β 115 57.577	716.7112	0.01881	19/18	14
1640*	8.5724	12.9661	7.2287	α 90 33.918 β 116 2.161 α 87 46.322	721.3670	0.01416	24/15	9
1659*	8.5626	12.9617	7.2197	α 90 38.022 β 115 58.038 α 87 46.167	719.8269	0.01505	26/18	12
1744*	8.5671	12.9680	7.2258	α 90 9.285 β 116 6.097 α 86 44.520	719.5085	0.01624	28/16	10
1659*	8.5360	12.9625	7.2103	α 90 35.971 β 115 53.902 α 87 54.794	717.1913	0.02031	23/19	13

[†] Homogenized
* Triclinic

Stewart, 1968). The transition between ordered and disordered structural states has been shown by Stewart and Ribbe (1969) to have considerable overlap such that no unique positions can be delineated.

The alkali feldspar compositions were also determined from the direct cell data, using the determinative graphs of Wright and Stewart (1968, Figure 1a). The results are listed in Table 4.40.

TABLE 4.40

COMPARISON OF COMPOSITIONS OF ALKALI FELDSPARS

SPECIMEN NO. A325/-	% K From feldspar	% Or Analysis	% Or by a(\AA) method	% Or by volume
1121	12.57	81.3	89.0	86.0
77	12.44	78.1	93.5	90.0
1165a	7.94	51.7	91.0	89.0
1328	no data	no data	81.0	81.0
323	11.30	70.3	91.5	90.0
531	12.66	76.0	95.0	91.0
783	9.70	59.7	95.0	90.0
400	11.66	65.0	92.0	90.0
18	9.07	53.0	90.0	89.0
474 ⁺	12.72	77.2	80.0	80.0
1659	13.02	76.7	89.0	88.0
1640	no data	no data	90.0	92.0
1659 ⁺	no data	no data	83.0	81.0
1744	no data	no data	88.5	89.0
138	8.11	51.2	no data	no data
396	9.48	54.4	no data	no data

⁺ homogenized

For feldspar A325-474, the composition derived from the a \AA method agrees with that derived from the cell volume method. The sample was homogenized for 7 days at 1000°C. The general lack of agreement in other feldspars indicates that the majority have slightly anomalous cells. A325-1328, -1640 and -1744 do not plot on Figure 4.36, probably due to this anomalous nature of the cell dimensions.

The salient features which emerge from this study of the Amata alkali feldspars are:

1. the alkali feldspars from the transitional and granulite facies rocks are disordered;
2. there is evidence to suggest a range of disordering in some of

TABLE 4.41

ESTIMATED APPROXIMATE MINIMUM TEMPERATURES OF EQUILIBRATION FOR
PERALKALINE CONDITIONS AT 7kb*

SPECIMEN NO. A325/-	% Or	T°C
1121	89.0	590
77	93.5	525
1165a	91.0	563
Mean Temperature		559°C
1328	81.0	670
323	91.5	550
531	95.0	490
783	95.0	490
400	92.0	555
18	90.0	575
Mean Temperature		555°C

* Assuming a mean structural state for the disordered feldspars
of $\Delta bc = 0.82$

- the feldspars;
3. the feldspars from the high grade rocks are predominantly orthoclase microperthites and mesoperthites;
 4. highly ordered microcline perthites occur in the amphibolite facies gneisses.

These features are typical of the alkali feldspars from high grade metamorphic rocks elsewhere (Eskola, 1952; Heier, 1957, 1960; Binns, 1964; Leelanandam, 1967c; Ohta and Kizaki, 1966; Suwa, 1968; Crosby, 1971).

The structural state of alkali feldspars is governed by the degree of ordering of fourfold co-ordinated aluminium in the tetrahedral lattice sites (Stewart and Ribbe, 1969). Disordered monoclinic alkali feldspar is believed to change into the more ordered triclinic form due to this Al-Si ordering. There is little general agreement however concerning the mechanics of this process and the effects of variable physical and chemical conditions (Laves and Goldsmith, 1961).

Heier (1961) believed that the higher temperatures of the granulite facies are responsible for the disordered orthoclase structure and enables the entry of greater amounts of sodium into the lattice. This accounts for the development of mesoperthites in the granulite facies lithologies and suggests that the transitional feldspars are formed at lower temperatures than those from the granulite facies.

Goldsmith and Laves (1954) established the approximate temperature of 500°C for the inversion of triclinic feldspar to its monoclinic polymorph. Heier (1957, 1961) considered that the transformation takes place at pressures and temperatures slightly below the upper boundary of the amphibolite facies. Recently, Steiger and Hart (1967, p.114) placed the temperature of the transition at 350-400°C as a result of a study of heat flow data from the aureole of a Tertiary quartz monzonite stock. Independently, Wright (1967) examined the same group of rocks and concluded that 375±50° was the upper stability limit of microcline.

By analogy, therefore, it is likely that 375±50° was the maximum temperature of recrystallization of the alkali feldspars in the Amata

amphibolite facies gneisses.

Conversely, this temperature may be regarded as the minimum temperature attained during the equilibration of the alkali feldspars in the transitional gneisses. The granulite facies feldspars presumably equilibrated at a slightly higher temperature. The feldspars in the transitional and granulite facies rocks (Figures 4.35 and 4.36, Tables 4.38 and 4.39) show a wide range of disordered states. This range may result from either:

- (a) variable temperatures during metamorphism; or
- (b) variable rates of cooling and hence degrees of ordering; or
- (c) compositional differences in the alkali feldspars (MacKenzie and Smith, 1961).

The latter two possibilities are considered to be the most probable; it is difficult to imagine such diversity of maximum temperatures that would initiate degrees of ordering over the range 0.232 to 0.522 (in specimens A325-1121 and -77 respectively) in rocks of similar metamorphic grade.

If certain assumptions are made, an estimate of the minimum exsolution temperature of the alkali feldspars can be determined from Crosby (1971, Fig. 2). In this figure is plotted the partial binodal curve for the Or-Ab system at 7Kb with a structural state of $\Delta bc = 0.82$ for peralkaline conditions, following the method of Waldbaum and Thompson (1969) and Thompson and Waldbaum (1969). The results for the Amata feldspars are given in Table 4.41. Although these must only be regarded as approximate temperature estimates, the means compare favourably with the estimated minimum exsolution temperature of the Whiteface Mountain charnockite, 588°C (Crosby, 1971). The values are also close to the temperature range, deduced from oxygen isotopes by Wilson *et al.* (1970), viz. $510\text{-}575^{\circ}\text{C}$ for the equilibration of the plagioclase-magnetite pair in the Ernabella granulites.

4.3.4 Element Distribution among Co-existing Minerals

4.3.4.1 General

This study has been undertaken for several reasons:

- (a) to determine whether pairs of co-existing ferromagnesian silicates behave as ideal binary mixtures of different elements;
- (b) to see if the chemical systems are equilibrated between pairs of minerals;
- (c) to examine the influence of:
 - (i) other components in the minerals;
 - (ii) host rock composition
 on the values of the distribution coefficients;
- (d) to provide comparative data with other high grade metamorphic terrains;
- (e) to determine whether the physical condition of crystallization can be gauged from the values of the distribution coefficients.

4.3.4.2 Theoretical Aspects

The application of thermodynamic principles to the study of the distribution of elements in co-existing metamorphic mineral assemblages was initially suggested by Ramberg (1944) and Ramberg and De Vore (1951). The basic theories behind the partitioning of elements in co-existing mineral pairs and their application to petrological problems have been reviewed by many workers (Kretz, 1959, 1960, 1961, 1963, 1964; Mueller, 1960, 1961; Bartholomé, 1962; Binns, 1962; Davidson, 1968; Saxena, 1968d,e; Grover and Orville, 1969; Ray and Sen, 1970; Mueller et al., 1970; Grover and Orville, 1970). From these, and other investigations especially in high grade metamorphic rocks, it has been demonstrated that component elements are systematically distributed between co-existing mineral phases when the rocks have been equilibrated

The distribution coefficient of an element X_A between two co-existing mineral phases α and β , for an ideal solution, can be written:

$$\frac{X_A^\alpha}{1 - X_A^\alpha} \cdot \frac{1 - X_A^\beta}{X_A^\beta} = \exp - \Delta G/RT = K_{D_{A-B}}^{\alpha-\beta}$$

where X_A is the mole fraction of an element A/A+B. Trace components in minerals can be assumed to be dilute solutions and they obey Henry's Law¹. The distribution of trace elements can therefore be expressed as

$$K_{D_\gamma}^{\alpha-\beta} = \frac{\text{concentration of } \gamma \text{ in } \alpha}{\text{concentration of } \gamma \text{ in } \beta}$$

where γ is any given minor or trace component, e.g. Mn.

The terminology used by Saxena (1968d) is followed throughout this section (Table 4.42).

TABLE 4.42

SUMMARY OF EXPRESSIONS USED IN DEFINING ELEMENT DISTRIBUTIONS

X_A^α	concentration expressed as mole fractions of A in phase α . $X_A = A/A+B$
$K_{D_{(A-B)}}^{\alpha-\beta}$	distribution coefficient for the exchange reaction $A_\beta + B_\alpha \rightleftharpoons A_\alpha + B_\beta$
K_D	distribution coefficient (abbreviated form)
$K_{D_A}^{\alpha-\beta}$	distribution coefficient when α and β are not treated as binary solutions

Mole fractions of elements used for the calculation of the distribution coefficients in the following discussion are given in Appendix 7.

1. This states that the activity of a component is proportional to its concentration.

4.3.4.3 Distribution of Fe^{2+} and Mg^{2+}

4.3.4.3.1 Orthopyroxene-Clinopyroxene Pairs

The computed distribution coefficients $K_{D(\text{Fe}^{2+} - \text{Mg})}^{\text{opx-cpx}}$ and $K_{D(\text{Mg} - \text{Fe}^{2+})}^{\text{opx-cpx}}$ are listed in Table 4.43. The relationship of

TABLE 4.43

DISTRIBUTION COEFFICIENTS INVOLVING PYROXENE PAIRS

SPECIMEN NO. A325/-	$K_{D(\text{Fe}^{2+} - \text{Mg})}^{\text{opx-cpx}}$	$K_{D(\text{Mg} - \text{Fe}^{2+})}^{\text{opx-cpx}}$
Transitional Terrain		
339	1.596	0.627
295	1.353	0.739
523	1.359	0.736
517	1.360	0.736
Granulite Facies Terrain		
81	1.234	0.810
138b	1.292	0.774
119	1.479	0.595
1105	1.184	0.844
121	1.541	0.649
60	1.337	0.747
949	1.298	0.771

Mean $K_{D(\text{Fe}^{2+} - \text{Mg})}^{\text{opx-cpx}}$ values

Transitional Terrain $\bar{x} = 1.417$ (\bar{x} = arithmetic mean)
 $s = 0.119$ (s = standard deviation)

Granulite Facies Terrain $\bar{x} = 1.366$
 $s = 0.178$

Mean $K_{D(\text{Mg} - \text{Fe}^{2+})}^{\text{opx-cpx}}$ values

Transitional Terrain $\bar{x} = 0.710$
 $s = 0.055$

Granulite Facies Terrain $\bar{x} = 0.741$
 $s = 0.089$

$Fe^{2+}/Fe^{2+} + Mg$ for the pyroxene pairs is depicted graphically in Figure 4.37. The range of values for the two distribution functions is much wider in the pairs from the granulite facies terrain than from the transitional terrain (Table 4.43). These values are compared with K_D values from other high grade terrains in Table 4.44. The comparison between $K_D^{opx-cpx}$ values is also shown in Figure 4.38 by plotting $Fe^{2+}/Fe^{2+} + Mg$ (orthopyroxene) against $Fe^{2+}/Fe^{2+} + Mg$ (clinopyroxene).

The average $K_D^{opx-cpx}$ values of the Amata granulite facies $(Mg - Fe^{2+})$ (0.741) and transitional pyroxene pairs (0.710) are higher than the established values for co-existing metamorphic pyroxenes. Kretz (1961, 1963) showed that the range for 25 high grade pyroxene pairs varies between 0.508 and 0.647 '(with one anomalous value of 0.74)'. A similar variation has subsequently been demonstrated by Saxena (1968d), viz. 0.501 to 0.647. The values from Amata are more comparable with the values for pyroxenes from igneous rocks, e.g. 0.654 to 0.857 (Kretz, 1961). They also fall within the range of values listed by Kretz (1963) for pyroxenes from Scottish mafic and ultramafic 'metamorphic' rocks, viz. 0.588-1.022. O'Hara (1961) regarded these rocks as being granulite facies, but Bowes *et al.* (1961) interpreted them as layered ultrabasic intrusive igneous rocks. They considered that the high K_D values reflected the preservation of igneous features.

The apparently anomalous K_D values for the Amata pyroxenes may result from the calculation of total iron as FeO in the clinopyroxene analyses (see Ray and Sen, 1970). Saxena (1968a, 1969), however, calculated iron in this manner. The $K_D^{opx-cpx}$ values computed from his data (Table 4.44) range from values normally associated with igneous crystallization to those associated with metamorphic crystallization (i.e. $K_D \approx 1.8$, calculated from Kretz, 1963).

Influence of host rock chemistry on distributing coefficients

From Figure 4.39a and b it is apparent that $K_D^{opx-cpx}$ $(Fe^{2+} - Mg)$

varies independently of both rock oxidation ratio or rock $\text{Fe}^{2+}/\text{Fe}^{2+} + \text{Mg}$ ratio. Similarly $K_D^{\text{opx-cpx}}_{(\text{Mg} - \text{Fe}^{2+})}$ is independent of rock $\text{Mg}/\text{Mg} + \text{Fe}^{2+}$

(Figure 4.39c). However, the grouping of the $K_D/\text{rock } \text{Fe}^{2+}/\text{Fe}^{2+} + \text{Mg}$ (and rock $\text{Mg}/\text{Mg} + \text{Fe}^{2+}$) for the granulite facies in a field distinct from that depicting the transitional terrain is apparent in Figure 4.39b and c. This is possibly due to mineralogical differences between the two groups. Saxena (1968d) commented on the influence of co-existing minerals on the K_D function.

Dependence of K_D on Temperature and Pressure

Based on the tenet that pyroxene pairs behave as ideal binary solutions, Kretz (1961) and Bartholomé (1961, 1962) independently reached the conclusion that K_D and K_P^1 are temperature dependent functions². Furthermore, Kretz (1963) tentatively proposed that $\ln K_D^{\text{opx-cpx}}_{(\text{Mg} - \text{Fe}^{2+})}$ is a linear function of $1/T$ and pressure³.

Similarly, Saxena (1968d,e) stressed the relation between $K_D^{\text{opx-cpx}}_{(\text{Mg} - \text{Fe}^{2+})}$ with temperature (and pressure) and he was of the opinion (like Kretz, 1961, 1963) that the different values for K_D in metamorphic and igneous pairs (Saxena, 1968d, p.300) are a function of temperature mainly and not of bulk composition. The anomalous K_D values for the Amata pyroxene pairs, suggests that if they are truly temperature dependent, then they crystallized at higher temperatures than the other metamorphic pyroxenes.

In spite of the apparent abnormality of the Amata values, it is noteworthy that 'aberrant' K_D values have been reported previously

-
1. The function of K_P is the partition coefficient in Bartholomé's equation for equilibrium condition, i.e. $(\text{Fe}^{2+}/\text{Mg})_{\text{opx}} = (\text{Fe}^{2+}/\text{Mg})_{\text{cpx}} \times K_P(T)$.
 2. Ramberg and De Vore (1951) had previously intimated that the distribution function of Mg and Fe in olivine-pyroxene pairs may be used as a geological thermometer.
 3. Kretz (1963, p.782-783) contended that the effect of pressure on the K_D could not be fully evaluated without a more detailed appreciation of the ΔH and \sqrt{E} of the mineral species, where ΔH was the enthalpy and \sqrt{E} was defined as $\partial \mu^E / \partial P$.

from the Musgrave Block (Tomkinson Ranges). For example, Barnes (1968) registered values ranging from 0.65 to 0.75 for co-existing pairs from pyroxene granulites and Moore (1971) lists $K_D^{\text{opx-cpx}}(\text{Mg} - \text{Fe}^{2+})$ ranging between 0.79 and 0.91¹ for 'syntectonically annealed' pyroxenes from orthopyroxenites and websterites.

Moore (1971, p.243) considered that these rocks have 'textures akin to those found in high grade metamorphic rocks'. During annealing, if the following ion exchange reaction takes place between the pyroxene pairs: $\text{Mg}_{\text{opx}} + \text{Fe}_{\text{cpx}} \rightleftharpoons \text{Fe}_{\text{opx}} + \text{Mg}_{\text{cpx}}$ (Kretz, 1961) then, from thermodynamic theory the K_D value should reflect the physio-chemical conditions of the rocks at the time of their crystallization. Moore's annealed rocks were probably 'equilibrated' during the final equilibration of the surrounding granulites. Therefore the values of $K_D^{\text{opx-cpx}}(\text{Mg} - \text{Fe})$ obtained by Moore for the annealed orthopyroxenites and websterites could be regarded as having been controlled by metamorphic recrystallization (a fact not emphasized by Moore (1971)), possibly in response to tectonic deformation².

1. In computing K_D Moore (1971) used the expression

$$X = \frac{\text{Mg}}{\text{Mg} + \text{Fe}^{2+} + \text{Fe}^{3+}}$$

Davidson (1968) computed a similar distribution coefficient using $X = \frac{\text{Fe}^{2+} + \text{Fe}^{3+}}{\text{Fe}^{2+} + \text{Fe}^{3+} + \text{Mg}}$ and found that the

K_D values were invariably lower than those determined from the function where $X = \frac{\text{Fe}^{2+}}{\text{Fe}^{2+} + \text{Mg}}$, i.e. they were dispersed towards the

range of igneous pyroxene values. Moore's calculated values are notably biased in the same direction. The $K_D^{\text{opx-cpx}}(\text{Mg} - \text{Fe}^{2+})$ values calculated from Moore's data should therefore be slightly less than the values he quotes and would be more comparable with the Amata data.

2. It has been shown from experimental studies and from natural examples that minerals can re-crystallize (or anneal) as a result of deformation. If, during this process ion exchange reactions are established between coexisting pairs of annealing minerals, the resulting K_D value would in part be due to the deformation. The effect of deformation in initiating recrystallization and therefore possibly ion exchange reaction has not previously been considered.

The approximate temperatures for the crystallization of the Amata pyroxenes (based on Kretz, 1963, Fig.3) are as follows:

- (a) granulite facies - approximately 1150°C;
- (b) transitional - approximately 1050°C.

High crystallization temperatures were suggested previously on the basis of other evidence.

The validity of using K_D to estimate temperatures of crystallization has been questioned by several workers. Binns (1962) found that the K_D values of the Broken Hill pyroxene pairs are not univariant at constant temperature and pressure but are dependent on host rock composition. Similarly Davidson (1968) found that the Quairading pyroxenes failed to follow the pattern predicted by Mueller (1960) and Kretz (1961, 1963). He suggested that the pyroxene structures were not ideal solutions with respect to Fe^{2+} and Mg as was intimated by the pyroxene equilibrium exchange model. The partitioning of Fe^{2+} and Mg between pyroxene pairs was considered by him to be not only a function of temperature and pressure but to be also dependent on the changing absolute activities of Fe^{2+} and Mg in the equilibrium exchange. Therefore the K_D values should vary with the Fe^{2+}/Mg ratio of the pyroxenes.

Explanation of these 'variations of K_D within groups of samples which equilibrated at more or less the same temperature have not yet been satisfactorily explained' (Ray and Sen, 1970, p.63). Discussion has been wide ranging. It has principally been concerned with the detailed examination of the cation distribution in orthopyroxenes and the nature of the mixing of Fe^{2+} and Mg, i.e. whether it was ideal or not.

Mueller (1962), Matsui and Banno (1965), Banno and Matsui (1966) demonstrated that solid solutions may exhibit a non ideal behaviour due to the presence of sub lattices (or energetically different sites). Furthermore, Banno and Matsui (1966) were able to show that Binns' (1962) Broken Hill data could be explained by such an explanation. Ghose and Hafner (1967), by using the Mossbauer technique, found that the degree of $Mg^{2+} - Fe^{2+}$ order in metamorphic pyroxenes is higher than in volcanic ones. They considered that 'it is by no means certain that orthopyroxenes behave as ideal solutions'. Nazifiger and Muan (1967)

found experimentally that pyroxene solid solutions were practically ideal with respect to Mg and Fe²⁺. However, Burns (1968) found from the compositional variations of crystal-field stabilization energies for various orthopyroxenes, that the series does not conform with the criteria for ideal solution behaviour.

Grover and Orville (1969) considered that the partitioning of cations between co-existing phases is a function of:

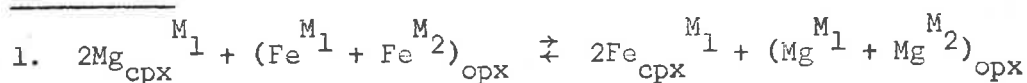
- (a) the number of energetically distinct cation sites in each phase together with the exchange of free energies between the intra-crystalline sites;
- (b) the inter-phase exchange energy;
- (c) the temperature;
- (d) the composition.

They proposed a single-site double-site model¹ to account for the Fe²⁺ - Mg distribution between both natural and experimental pyroxenes at different temperatures.

The assumption proposed by Grover and Orville (1969) that co-existing pyroxenes exhibit ideal mixing between both M₁ and M₂ sites is questioned by Mueller *et al.* (1970). They consider that the single-site - single-site model of Kretz (1963), which assumes that the pyroxenes are ideal solutions of their component end members, provides a better fit of the data than the distribution lines proposed by Grover and Orville (1970), especially for Fe-rich pyroxenes.

Grover and Orville (1970, p.1362) in reply consider that intra-crystalline site fractionation will introduce minimal non ideal effects on the inter-crystalline Mg/Fe fractionation and therefore defend their proposals.

Principally from the work of Virgo and Hafner (1969) it was established that ion exchange in orthopyroxenes is a rapid process and that it takes place between temperatures of 480°C to 1000°C. Saxena and Ghose (1971) provided experimental data on the distribution of



$Mg^{2+} - Fe^{2+}$ between the M_1 and M_2 structural sites in orthopyroxenes at elevated temperatures. They found that orthopyroxene crystalline solutions are basically non ideal in the temperature range 500 to 800°C and that this non ideality decreases with increasing temperature.

There is no universal agreement concerning the nature of the factors controlling Fe^{2+} and Mg mixing in pyroxene pairs (and therefore the extent to which K_D is temperature dependent). It is felt that the overall similarity of K_D values registered by the Amata pyroxene pairs and those from the Tomkinson Ranges is of some significance.

The close similarity between the K_D values is rather important in the light of the tectonic setting of the Musgrave Block (i.e. it is regarded as a segment of deep crust) metamorphosed under extreme granulite facies pressure-temperature conditions. If the K_D values are dependent on the prevailing physical conditions (as has been indicated previously) the implications are that the environment of crystallization of the pyroxene pairs in the Musgrave Block was fundamentally different from those belonging to other granulite facies terrains (e.g. Turner, 1968, p.364). Furthermore, the different mean values of K_D from the granulite and transitional rocks suggests that, irrespective of the nature of the factors which govern the K_D values, these factors were significantly different in these two areas; particularly as both groups of pyroxenes exhibit similar ranges of mg values (Tables 4.20 and 4.21). Apart from temperature differences, another possible explanation is the association of the transitional pyroxene pairs with hornblende in contrast to the granulites where hornblende is generally absent. Saxena (1968c) emphasises the importance of the co-existing mineralogy on the nature of the partition coefficient.

Moore (1971, p.252) considered that the syntectonically annealed rocks from Gosse Pile were 'deformed soon after crystallization at temperatures close to the solidus'. In this thesis it has been shown that the mafic granulites (from which the pyroxene pairs were obtained) were isochemically metamorphosed. Their bulk compositions are remarkably similar to those of high alumina and alkali olivine basalts (see below, Chapter 5). The high K_D values may possibly reflect similar crystallization of these rocks close to the solidus, thus assuming that

TABLE 4.44

 $K_D^{\text{opx-cpx}}(\text{Fe}^{2+} - \text{Mg})$ and $K_D^{\text{opx-cpx}}(\text{Mg} - \text{Fe}^{2+})$ VALUES FROM OTHER HIGH GRADE TERRAINS

SOURCE	n	$K_D^{\text{opx-cpx}}(\text{Fe}^{2+} - \text{Mg})$	$K_D^{\text{opx-cpx}}(\text{Mg} - \text{Fe}^{2+})$
Ganon Range Iron Formation; Butler (1969)	28	1.81 average	
Kondapalli charnockites; Leelanandan (1967a, 1968)	8	1.8 - 2.3	
Madras charnockites; Leelanandan (1967a, 1968)	10	1.7 - 2.0	
Saltora charnockites; Sen and Rege (1966)	4	1.6 - 1.8	
West Uusimaa Complex Saxena (1969)	6	1.46 - 1.94	
Varberg, Sweden; Saxena (1968a)	5	1.36 - 1.76	
Mont Tremblant; Katz (1970)	2	1.36 and 1.96	
Quairading; Davidson (1968, 1969)	12	1.70 - 1.87	
Norway garnetiferous peridotites; O'Hara and Mercy (1963)	4		0.41 - 0.51
Madras basic granulites; Ray and Sen (1970)	11		1.515 - 0.642
Adirondacks pyroxene amphibolites; Engel et al. (1964)	6		0.510 - 0.568
Broken Hill; Binns (1962, 1965b)	7		0.502 - 0.610
Kondapalli; Leelanandan (1967a)	6		0.499 - 0.546
Madras charnockites; Howie (1965)	6		0.508 - 0.600

they were originally igneous. Although Kretz (1963) considers such anomalously high K_D values as at Amata to represent disequilibrium conditions, microstructural evidence from the granulites (see Chapter 3) suggests that the assemblages were initially in chemical and textural equilibrium (Kretz, 1966).

4.3.4.3.2 Orthopyroxene-Hornblende and Clinopyroxene-Hornblende Pairs

The distribution of Fe^{2+} and Mg in the pyroxene-amphibole pairs is expressed in the form of the following distribution coefficients:

$K_D^{px-hb}_{(Fe^{2+} - Mg)}$ and $K_D^{px-hb}_{(Mg - Fe^{2+})}$ (Table 4.45). These distribution

patterns are represented diagrammatically in Figure 4.40. The values have a wide range of variation for both clinopyroxene-hornblende and orthopyroxene-hornblende pairs. The K_D values for the orthopyroxene-hornblende pairs compare favourably with the average values and range from other high grade areas (Table 4.46). However, with respect to the clinopyroxene-hornblende pair, the Amata values have a much wider range than elsewhere.

It is agreed by petrologists that such variability is the result of a number of possible influences:

- (a) the assemblages are not in equilibrium;
- (b) ionic substitution has occurred (e.g. $Al^{IV} \rightleftharpoons Si^{IV}$), changing the chemical potential of the end members (Saxena, 1968e);
- (c) $X_{Fe^{2+}}^{px}$ or Mg or X_{Fe}^{hb} or Mg may be influenced by the concentration of a third element in the lattice of one or both of the minerals.

Saxena (1968e) discussed some of these possibilities and he regards b and c as being related to the controlling influence of 'intensive parameters', e.g. oxygen fugacity. These parameters may directly effect the equilibrium exchange reaction. Aspects of the effect of oxygen fugacity on the rock and mineral chemistry have been discussed in detail above (Chapter 4.3.2.1).

The range of $K_D^{opx-hb}_{(Fe^{2+} - Mg)}$ in the mineral pairs from the transitional terrain (A325-339, -523) is greater than in the pairs from

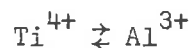
the granulite facies terrain (A325-949, -1105). This suggests that the factors which control the K_D were significantly different in the transitional terrain from those in the granulite facies terrain with regard to the $x_{Fe^{2+}}^{opx}$ or H_b value. These factors may be related to disequilibrium in the former group or to a difference in temperature.

Appreciation of the distribution of Fe^{2+} and Mg between amphiboles and other ferromagnesian minerals has not developed to the stage reached in the study of the orthopyroxene-clinopyroxene pairs. Several workers, however, have considered the possibilities and their results are summarised below.

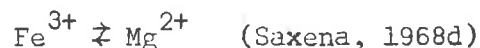
Ramberg (1952, 1954) suggested that the Fe^{2+}/Mg ratio in silicate structures increases with increase in the ratio of the four fold co-ordinated elements, i.e. Al^{IV}/Si^{IV} . Saxena (1968d) examined this as a possible explanation for the variation in K_D^{opx-hb} . He

considered that the effect on the K_D of Al^{IV}/Si^{IV} variation in hornblende is nullified if similar variation in the concentration of Al occurs in the orthopyroxene phase. Instead, he suggested variation in the K_D^{opx-hb} values are caused by intracrystalline exchanges in

the hornblende structure; highly charged, or trivalent, ions in the octahedral sites (e.g. Fe^{3+} , Ti^{4+} , Al^{3+}) being replaced by a divalent ion (e.g. Mg^{2+} and Fe^{2+}). To maintain electrical neutrality the following substitutions were postulated to take place:



or



However, Ray and Sen (1970) believed that the concentration of Al^{IV} in the hornblende structure was a major controlling influence, coupled with minor effects in either the pyroxene or hornblende phase produced by $Ca \rightleftharpoons Fe^{2+}$ and $Fe^{3+} \rightleftharpoons Fe^{2+}$ substitution. They considered that if the effects of these influences are accounted for then Fe^{2+} and Mg distribution in pyroxene-hornblende pairs can be explained using a model based on the theoretical concept of ideal mixing between the two mineral species.

TABLE 4.45

DISTRIBUTION COEFFICIENTS FOR PYROXENE HORNBLLENDE PAIRS

SPEC. NO. A325/-	$K_D^{\text{opx-hb}}$ (Fe ²⁺ - Mg)	$K_D^{\text{cpx-hb}}$ (Fe ²⁺ - Mg)	$K_D^{\text{opx-hb}}$ (Mg - Fe ²⁺)	$K_D^{\text{cpx-hb}}$ (Mg - Fe ²⁺)
339	1.682	1.054	0.595	0.949
523	1.171	0.862	0.854	1.160
949	0.884	0.681	1.132	1.469
1105	1.210	1.022	0.827	0.979

TABLE 4.46

DISTRIBUTION COEFFICIENTS FOR PYROXENE-HORNBLLENDE PAIRS FROM
OTHER GRANULITE FACIES AREAS

AREA	SOURCE	$K_D^{\text{opx - hb}}$ (Fe ²⁺ - Mg)	$K_D^{\text{cpx - hb}}$ (Fe ²⁺ - Mg)
Lapland	Eskola (1952)	1.16	0.68
Sudan	Howie (1958)	1.12	0.60
Kondapalli } Madras }	Leelanandan (1970)	1.13 1.36	0.60 0.76
Adirondacks	Engel <u>et al.</u> (1964)*	1.13	0.61
Broken Hill	Binns (1965a,b)*	1.36	0.74
West Uusimaa Complex	Saxena (1969)	0.79 - 1.30	0.54 - 0.75
Varberg	Saxena (1968a)	0.85 - 1.20	0.48 - 0.72
Quairading W.A.	Davidson (1971)	0.99 - 1.50	

* Data from Leelanandan (1970)

CHAPTER 5

CONDITIONS OF METAMORPHISM AND THE ORIGIN OF THE
MAFIC AND ULTRAMAFIC ROCKS

5.1 PARTIAL PRESSURES

In order to postulate the origin of the metamorphic rocks in the Amata area it is necessary to attempt to estimate the variables which have governed the crystallization of the different mineral assemblages. These variables are temperature, load pressure¹, fluid pressure and composition, and chemical potential of the gas and fluid phases.

The Amata granulite facies terrain and, to a minor extent, the transitional terrain contain mineral assemblages which are virtually anhydrous. Biotite and hornblende are very rare constituents of some assemblages, the main ferromagnesian minerals being orthopyroxene and clinopyroxene. On the other hand hydrous assemblages are extensively developed throughout all of the amphibolite facies terrain and the majority of the transitional terrain, orthopyroxene being present in the transitional terrain as a whole, only in minor amounts. Variation in the degree of hydration apparent in the Amata rocks suggests the importance of water and water pressure variability as influential factors in the development of the rock parageneses. Considerable discussion has taken place concerning the role of water in metamorphic processes (Yoder, 1952, 1955; Greenwood, 1961; Althaus, 1968; Fry and Fyfe, 1969; Fyfe, 1970; Touret, 1971) and it has been shown that the stability fields of minerals are considerably influenced by the effect of varying water pressure.

The effect of varying water pressure has, perhaps, nowhere been more extensively considered than in attempted explanations for the complex intermingling of amphibolite facies lithologies with hornblende bearing and hornblende-free granulites. Gjelsvik (1952) and

-
1. To avoid confusion (see Althaus, 1968) when referring to the pressures prevailing during metamorphism it is desirable that the terminology used should be unambiguous. The terminology followed herein is based on the usage of Fyfe *et al.* (1958) and Burnham (1967). Load Pressure (P_{load} , P_{total} , P_t or P_l); the pressure due to the weight of the superincumbent load of rock. Fluid Pressure (P_{fluid} or P_f) '... is the pressure exerted on or by the fluid phase and is the sum of the partial pressures of all its component species' (Burnham, 1967, p.36).

Poldervaart (1953) considered that the amphibolite facies assemblages associated with granulite facies rocks formed under conditions of similar temperature and load pressure but markedly different water pressure (Yoder, 1952).

Engel and Engel (1960) believed that the transition from amphibolite to granulite facies in the Emeryville-Colton area of the northwest Adirondacks 'evolved along gradients in temperature (and water pressure (?))'.

Buddington (1963), in the absence of evidence that the Adirondack rocks had undergone extensive retrogression concluded that the primary mineralogy, the temperature and load pressure, together with variable water pressure were collectively responsible for the complex isograd patterns; the rocks acting as closed systems with respect to their water contents.

De Waard (1966) similarly interpreted the high ratio of hornblende bearing rocks in granulite facies terrains (e.g. the Adirondack highlands) as being due to the activity of closed water deficient systems (Yoder, 1952, 1955), which produced conditions under which the reactants and products of boundary reactions could coexist. He believed that the rocks behaved as closed systems because they had low permeability. The effect of water released during the dissociation reactions, coupled with the P_w (his term water pressure(?)), produced a broad state of water pressure and temperature where hornblende could crystallize in equilibrium with orthopyroxene bearing assemblages.

Banno et al. (1963) stressed that host rock composition influenced the differing abundances of hornblende or biotite in granulite facies assemblages from Lützow-Holmbukta, Antarctica.

Wynne-Edwards (1967) interpreted the marked variation in mineral assemblages throughout the Westport map-area to be due to variable temperature and P_{H_2O} during the metamorphism (see also Currie, 1971).

Dawes (1970) considered that the interplay of water content, water pressure and host rock composition contributed to the crystallization of hydrous and anhydrous assemblages in the Tasiussaq gneiss complex, south Greenland.

A somewhat more cautious attitude is that of Sen and Ray (1971, p.292), viz. '... that our understanding of.....the interplay of physical and chemical variables that determines whether we should have pyroxene granulite or hornblende pyroxene granulite is rather incomplete'. They discounted variable water pressure as a viable agent to account for the presence or absence of hornblende in rocks in close proximity and as an alternative explanation they considered that the chemical potential of SiO_2 controlled the stability of hornblende and orthopyroxene. They considered that the presence of free quartz in rocks which were free of hornblende, or which contained only minor amounts of that phase indicated that ' μ_{SiO_2} was at least equal to G_{SiO_2} ' i.e. the rocks were saturated with SiO_2 and hence hornblende should have disappeared (see also Parras, 1958, p.114). The silica saturation was believed to have been caused by contamination from anatectic 'granodioritic' melts.

The intermingling of essentially anhydrous lithologies containing orthopyroxene and free quartz with more hydrous lithologies containing hornblende or hornblende plus orthopyroxene (but which lack quartz) in the Amata transitional terrain strongly suggests that the presence or absence of an excess of silica may influence the stability of orthopyroxene and hornblende in these rocks. However, it is unlikely that any one factor acts independently in influencing the development of a regular isograd pattern or an isograd reversal situation, and hence an irregular distribution of assemblages belonging to a variety of metamorphic facies. A more plausible explanation would be that it is the total 'assemblage of variables' including the chemical potential of components, temperature, load pressure, water pressure and the availability of fluid phases which governs the formation of particular assemblages. Nevertheless, it may be possible with further examination of the evidence to suggest the factors which are regarded as the most significant.

No direct evidence of anatectic melting concomitant with the granulite facies metamorphism, or at least concomitant with the g_{L_1} lineation has been recognised in the Amata area although temperatures exceeded those at which muscovite is stable, viz. approximately 700°C

at 5 kilobars (Althaus et al., 1970; Storre and Karotke, 1971) (see also below). Under hydrous conditions at such temperatures and pressures anatexis would presumably have taken place. It is therefore concluded that the granulites are generally anhydrous and crystallized under conditions of $P_{H_2O}^1 < P_{load}$.

In the transitional and amphibolite facies terrain there is abundant evidence of melt phases suggesting that water contents were generally higher than in the granulite facies terrain, e.g. there is extensive quartzo-feldspathic veining in the mafic units (of the transitional terrain) and quartzo-feldspathic pegmatites parallel the major lithological layering, together with migmatitic segregations in some localities. Bodies of gneissic granite containing xenoliths are also recognised. Although P_{H_2O} is believed to have been higher than in the granulite facies terrain, it is uncertain whether it is in fact less than, or equal to P_{load} .

5.2 PHYSICO-CHEMICAL CONDITIONS AS INDICATED FROM BULK ROCK AND MINERAL CHEMISTRY

In the light of earlier evidence to the effect that oxygen influence on mineral content and mineral composition is insignificant (Chapter 4.3.2.1) it is thought unlikely that P_{O_2} need be considered as an intensive variable (except possibly in the case of A325-2040 and -2048) in the metamorphic development of the Amata rocks. In addition, because of the demonstrated limited mobility of oxygen, predominantly in the granulite facies terrain but also in the other terrains, there must have been considerable gradients of oxygen fugacity on a small scale between intercalated units, supporting the probability that metamorphism in the granulite facies terrain was isochemical.

The strong negative correlation of $Mg/Mg + Fe^{2+}$ (rock) against

-
1. It is assumed that $P_{H_2O} \approx P_f$, although in the vicinity of calc silicate units CO_2 may have been significant.

the same ratio for the silicate minerals (except for garnet) indicates that the Mg and Fe^{2+} contents of the bulk rock control the $\text{Mg}/\text{Mg} + \text{Fe}^{2+}$ ratio in the constituent mineral phases. It is suggested for the Amata area at least, that it is this ratio and not necessarily oxygen fugacity that is responsible for the Fe^{2+} and Mg distribution between the silicate mineral phases.

Figure 4.39c shows that the same ratio ($\text{Mg}/\text{Mg} + \text{Fe}^{2+}$) also strongly influences the pattern of distribution of the $K_D^{\text{opx-cpx}}$'s.

It was clearly demonstrated (Figure 4.23) that the manganese contents (expressed as $\text{Mn}/\text{Mn} + \text{Mg} + \text{Fe}^{2+}$) of the pyroxenes, micas, amphiboles and garnets are influenced directly by the manganese content of the host rocks. There was also some indication that this may be a grade dependent relationship. For example, in the pyroxene plot (Figure 4.23.1a and b) the transitional terrain pyroxenes lie in a field above that of the granulite facies pyroxenes. Likewise, for both hornblende (Figure 4.23.2a) and mica (Figure 4.23.2b) the granulite facies species exhibit lower $\text{Mn}/\text{Mn} + \text{Mg} + \text{Fe}^{2+}$ ratios than those from the transitional or amphibolite facies terrain. The distributions are probably related to the differing physico-chemical environments in which the metamorphic rocks crystallized.

Evidence for the high pressure nature of the environment of crystallization of the granulite facies and transitional terrains is provided principally by the pyroxenes but also by the amphiboles. As was discussed previously (p.201) the high content of alumina in the orthopyroxenes, although it may be controlled to some extent by the availability of alumina in the environment (Howie, 1964), is believed to indicate that the rocks crystallized under high pressure (Eskola, 1957; Boyd and England, 1960). Further evidence for the high pressure (and possibly high temperature) nature of the environment (Moore, 1968; Griffin *et al.*, 1971) is provided in the presence of rutile exsolution needles in the orthopyroxenes of A325-2050c and -990 from the granulite facies and transitional terrains respectively (see above, Chapter 3.3.2.4 and 3.4.14).

High contents of alumina are also shown by the clinopyroxenes (p.204) although the transitional terrain clinopyroxenes are in general

less aluminous than those from the granulite facies terrain. It was shown that the range of Al^{VI}/Al^{IV} were more extensive for the transitional terrain than for the granulite facies terrain. From Aoki and Kushiro (1968) this suggested that the pressure-temperature environment of the granulite facies rocks is more restricted than that of the transitional rocks. Moderate to high temperatures and pressures were also indicated by the presence of significant amounts of Ca-Tschermak's molecule in the pyroxenes.

Leake (1965, 1971) suggested that the high content of Al^{VI} in amphibole was directly the result of crystallization under high pressure. It was shown above (p.207) that the Amata hornblendes from the two mafic granulites A325-949 and -1105 contain significantly higher contents of Al^{VI} than the hornblendes from the transitional terrain. If Leake's interpretation is valid (and evidence from other ferromagnesian phases indicates that it is) then it is reasonable to interpret the granulite facies metamorphism as being in a different (higher) pressure regime than the metamorphism in the transitional and amphibolite facies terrains. In addition, the high content of Al^{VI} in the Amata granulite facies hornblendes, compared to hornblendes from other granulite facies terrains, indicates that the metamorphism may have been at higher pressures than in other granulite facies metamorphic terrains; the transitional terrain may be more comparable with these.

Indications of the temperature distribution in the three metamorphic terrains are provided by the distribution of titanium in the hornblendes (Leake, 1965) and also in the micas. Titanium is higher in these minerals from the granulite facies terrain than from the other two terrains. Similarly, pleochroism differences in the hornblendes from the three grades reflect the variation in titanium (and also ferric iron) suggesting that temperature varied.

In the discussion on distribution coefficients (Chapter 4.3.4.3.1) it was shown that the $K_D^{opx-cpx}$ values for the Amata granulite facies and transitional terrain co-existing pyroxenes are anomalously higher than values from other granulite facies terrains

Table 4.44). The values are similar to those given by Moore (1971) from the annealed rocks of Gosse Pile which he interpreted to be due to crystallization close to the solidus. It is shown below (Chapter 5.4) that most of the Amata mafic rocks are remarkably similar in bulk and trace element chemistry to igneous rocks and a probable origin is as igneous intrusions. The approximate temperature estimates of crystallization of the Amata pyroxenes (from Kretz, 1963, Figure 3) are:

granulite facies	1150°C
transitional	1050°C

Both these temperatures are below the solidus (see Figure 5.1).

If these temperature estimates are valid then they may represent a preserved igneous feature of the pyroxenes (Bowes *et al.*, 1961) or they may indicate that metamorphic temperatures were extreme in both the granulite facies and transitional terrains. If igneous intrusion was contemporaneous with the metamorphism they could be the result of both these factors.

Estimates of final equilibration temperatures of the metamorphic rocks are provided by the opaque oxides and the alkali feldspars. For the granulite and transitional terrains, the opaque oxides indicate temperatures ranging from 500-700°C. Studies of the alkali feldspar structural states indicate a maximum temperature of 375°C ± 50°C for the amphibolite facies terrain. The minimum exsolution temperature of the alkali feldspars in the transitional and granulite facies terrains are estimated to be 555°C and 559°C respectively.

5.3 INFERRED TEMPERATURE AND PRESSURE CONDITIONS OF METAMORPHISM FROM EXPERIMENTAL STUDIES

If, for the primary metamorphic assemblages, equilibrium is assumed, experimental data relating to certain critical mineral reactions, or mineral stability fields, can be utilized to evaluate the temperature and pressure regimes under which the rocks were metamorphosed. A pressure-temperature plot of pertinent data is presented in Figure 5.1.

The slope in pressure-temperature space of the alkali feldspar solvus is an important parameter in any construction of a high grade

metamorphic grid (Morse, 1970). De Waard (1967a,b, 1969) recognised the significance of the occurrence of mesoperthite in granulite facies rocks in the Adirondack Mountains and used an extrapolation of the alkali feldspar solvus (deduced by Orville, 1963) to estimate the lower limiting conditions of granulite facies metamorphism.

De Waard however failed to realize that the anorthite content of alkali feldspar had a significant effect on the position of the solvus. Yoder, Stewart and Smith (1956, 1957) and Carmichael (1963) for the Ab-Or-An-(H₂O) system showed that the curvilinear surface of the solvus rose abruptly from the Ab-Or join towards An. This suggested that exsolution of An-rich alkali feldspars occurred at high temperatures.

Morse (1968) also drew attention to the fact that the height and slope of the solvus altered with the addition of anorthite, the crest rising steeply with increasing content of anorthite until it intersected the ternary feldspar solidus. Studies on mesoperthite from the Kiglapait layered intrusion, Labrador (Morse, 1968) showed that the feldspar formed at an effective P_{H₂O} of at least as low as 500 bars; a water pressure in accord with the anhydrous nature of the rocks. He (Morse) suggested that calcic mesoperthite would be formed at very much higher temperatures, in the order of 1000°C.

Morse's (1970) plot of the critical line of the alkali feldspar solvus is portrayed in Figure 5.1 curve 7. The value of dT/dP for the solvus crest at the Ab-Or join is 18.33°C/Kbar. This contrasts with 14°C/Kbar determined by Yoder, Stewart and Smith (1957), 10°C/Kbar found by Orville (1963) and 13.47°C/Kbar found by Thompson and Waldbaum (1969). The equation for the curve is $PKbar = 0.0545T^{\circ}C - 34.82$.

The intersection of the critical line with the andalusite-sillimanite curves of Richardson, Gilbert and Bell (1969) and Althaus (1969), and with the kyanite-sillimanite curve of Richardson, Bell and Gilbert (1968) and Althaus (1969) gives the minimum temperature for the assemblage sillimanite-hypersolvus alkali feldspar irrespective of anorthite content.

In the Amata rocks mesoperthite and micropertthite are present

in the quartzo-feldspathic lithologies from the granulite facies and transitional terrains. Mesoperthite has not been observed in quartzo-feldspathic gneisses from the amphibolite facies terrain. This suggests that amphibolite facies pressure - temperature conditions are to the left of curve 7 (Figure 5.1) and the conditions for the granulite facies and transitional terrains are at higher temperatures to the right of it.

It has been indicated above (p.) that there is no evidence for anatexis contemporaneous with the granulite facies metamorphism although temperatures are estimated to have been such that, had the environment been sufficiently hydrous, partial melting would have occurred (as in the transitional and amphibolite facies terrains).

Melting curves are plotted in Figure 5.1 showing: the liquidus for anhydrous granite (W.C. Burnham, pers.comm.; curve 2d); the liquidus for granite with 2% water (Tuttle and Bowen, 1958; curve 2c); the solidus for wet granite (Luth et al., 1964; curve 2a; Boettcher and Wyllie, 1968; curve 2b).

Curves 2a and 2b give the approximate minimum temperatures of beginning of melting in the amphibolite facies and transitional terrains (based on the assumption that the terrains are hydrous environments) and curve 2d gives the approximate upper limit of metamorphism in the granulite facies terrain. The minimum temperature for the occurrence of rocks containing hypersolvus alkali feldspar is given by curve 7. Metamorphism in the granulite facies and transitional terrains must have taken place between curve 7 and 2d and 2c respectively and conditions for the amphibolite facies metamorphism would be to the left of curve 7 between curves 2a and 2b.

Considerable disagreement exists between the results of various attempts to determine the position of the triple point for the Al_2SiO_5 polymorphs. The various determinations have recently been reviewed by Zen (1969). The triple points determined by Richardson, Gilbert and Bell (1969) and Althaus (1969) are plotted on Figure 5.1 (1b and 1a). The kyanite-sillimanite boundaries shown in Figure 5.1 are those determined by Richardson, Bell and Gilbert (1968) and Althaus (1969). It can be seen that the curve deduced by Richardson, Bell and Gilbert

lies at slightly lower pressures and higher temperatures than that constructed by Althaus.

The presence of sillimanite (or sillimanite altering to margarite) in rocks of suitable composition in both the granulite facies and transitional terrain demonstrates that the pressure-temperature conditions were such that mineral reactions were taking place to the right of the kyanite-sillimanite univariant curves (Figure 5.1, curves 1a and 1b). The absence of sillimanite from the amphibolite facies terrain¹ demonstrates that the stability field of this facies must be to the left of curves 6a and 6b. The intersection of curve 6a with the beginning of melting curves 2a and 2b takes place at 3.5 Kbar and 670°C and 4.6 Kbar and 700°C respectively. These pressure-temperature conditions probably represent approximate conditions for the metamorphism in the amphibolite facies terrain.

Muscovite is absent from the granulite facies terrain and transitional terrain, although it is present in certain lithologies from the amphibolite facies terrain. The reaction:

muscovite + quartz \rightleftharpoons K feldspar + sillimanite + water

experimentally determined by Evans (1965), Burnham and Shade (1968), Althaus *et al.* (1970), curve 6a, and Storre and Karotke (1971), curve 6b Figure 5.1 indicates that temperatures are in excess of approximately 700°C in both the granulite and transitional terrains, whereas, temperatures below this figure pertain for the amphibolite facies terrain.

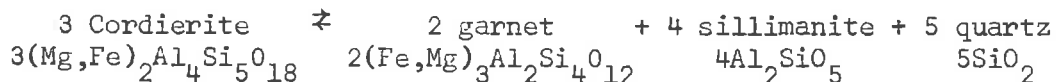
The upper stability limit of hornblende in the presence of excess water, determined by Nishikawa *et al.* (1971) is shown in Figure 5.1 (curve 3). Hornblende occurring (rarely) with orthopyroxene in the granulite facies terrain and (abundantly) in the transitional terrain is believed in both cases to be of primary origin. The virtual absence of hornblende in the granulite facies lithologies implies temperatures greater than the abovementioned hornblende breakdown curve, viz. 1000°C (see Figure 5.1). This is unlikely because such a temperature is also

1. In Collerson *et al.* (1972) sillimanite was reported as a constituent of a pelitic schist from the amphibolite facies terrain; more recent petrological studies indicate that this is in fact corundum.

greater than the granite anhydrous liquidus. It is probable, therefore, that the appropriate hornblende breakdown curve is one appropriate for $P_{H_2O} < P_{load}$, at lower temperatures, thus testifying to the earlier postulation of $P_{H_2O} < P_{load}$ conditions for the granulite facies terrain.

Cordierite is not present in any of the gneisses from the Amata area. Nor is it present in the Tomkinson Ranges (Goode and Krieg, 1965; Barnes, 1968; Moore, 1970b; Goode, 1970). However, it is recognised in granulite facies lithologies from the Ernabella area of the Musgrave Ranges (Wilson, 1954b). Its absence from the amphibolite facies terrain in the Amata area is interpreted to be due to the absence of suitable lithologies or to insufficient sampling.

The presence of almandine-pyrope containing inclusions of sillimanite and quartz in some of the gneisses from the transitional terrain is of considerable petrogenetic significance (Currie, 1971), as it indicates that cordierite was once probably present. It is shown experimentally by Richardson (1968), Hirschberg and Winkler (1968), and Hensen and Green (1969, 1970, 1971) that cordierite breaks down with increasing pressure to the assemblage garnet, sillimanite and quartz, by the following reaction:



The experimentally determined upper stability limit of Mg-cordierite (Schreyer and Yoder, 1964, p.333) and Fe-cordierite (Fe-cordierite + sillimanite \rightleftharpoons almandine + sillimanite + quartz, Richardson, 1968, p.478) are shown in Figure 5.1 (curves 5a and 5d). Hensen and Green (1969, 1971) have pointed out that the stability field of cordierite is reduced by decreasing the Mg/Mg + Fe²⁺ ratio. Curves showing the dependence of cordierite stability on the rock Mg/Mg + Fe²⁺ ratio (Hensen and Green, 1971) are shown in Figure 5.1 (curves 5b and 5c for Mg/Mg + Fe²⁺ ratios of 0.70 and 0.30 respectively) to illustrate this point. The negative $\Delta P/\Delta T$ slope for cordierite (Figure 5.1) indicates that its stability field decreases as the temperature increases.

Metamorphic conditions in the granulite facies and transitional

terrains are evidently outside the stability field of cordierite. It is not however suggested that the same stability fields should apply to both terrains as the stability of cordierite is dependent on many variables including temperature, pressure, water pressure and $Mg/Mg + Fe^{2+}$ ratio.

The anhydrous stability curve of Mg-cordierite (5a) provides a very approximate estimate of the lower boundary temperatures and pressures in the granulite facies terrain. The rocks in this terrain believed to be potentially capable of containing cordierite (A325-1121 and -77) have $Mg/Mg + Fe^{2+}$ ratios of 0.44 and 0.37 respectively. If the curves of Hensen and Green can be applied to these rocks then the metamorphism of the granulite facies terrain probably took place above a curve drawn parallel with 5c (curve 5e). The intersection of curve 5e with the feldspar critical line (7) implies that temperatures in the granulite facies terrain probably exceeded $800^{\circ}C$ (the pressure at that temperature being 8.7 Kbars).

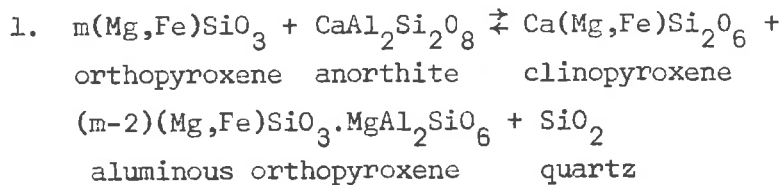
Schreyer and Yoder (1964) demonstrated that the stability of Mg-cordierite is confined to a more limited pressure-temperature field in the presence of excess water. Evidence suggests that the transitional terrain is a higher P_{H_2O} environment, therefore there is limited validity in applying the anhydrous experimental determinations of cordierite stability to estimate the conditions of metamorphism. From the mineral chemistry however, it is likely that temperatures (and pressures(?)) in the transitional terrain were generally lower than in the granulite facies terrain.

The experimental investigations under subsolidus conditions which have established the mineral assemblages formed in rocks of basaltic and granitic composition at high temperatures and pressures (Green and Lambert, 1965; Green and Ringwood, 1967; Green, 1967; Ito and Kennedy, 1971) can be used to interpret the physical conditions of formation of lower crustal rocks (i.e. granulite facies lithologies).

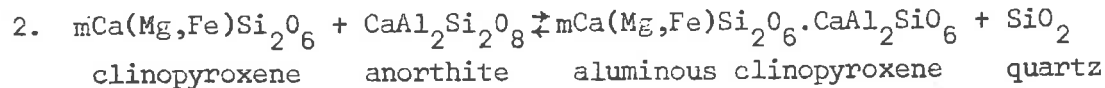
The experiments which have been performed under anhydrous conditions have shown, for basaltic compositions, that with increasing pressure, low pressure plagioclase + pyroxene ± olivine assemblages are changed through pyroxene + garnet + plagioclase ± quartz assemblages

to eclogitic compositions consisting of garnet + clinopyroxene and quartz. The mineralogical changes which take place are extremely complex, involving garnet, plagioclase and pyroxene solid solution series (Green and Ringwood, 1967). The idealized reactions which have been shown to take place with increasing pressure are summarized by Green and Ringwood (1967) and Green (1970).

They involve the increasing solubility of Al_2O_3 in both orthopyroxene:

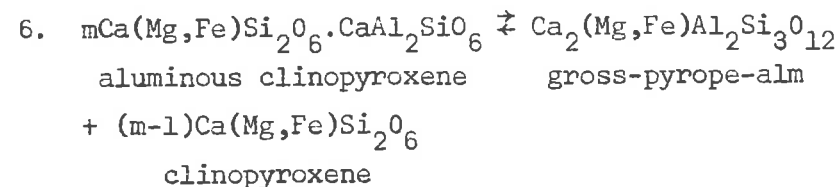
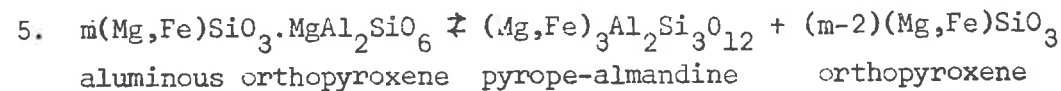
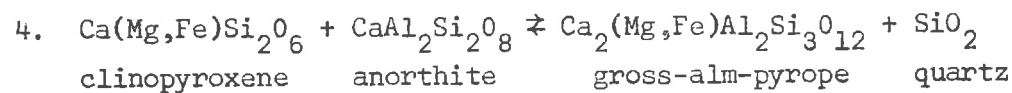
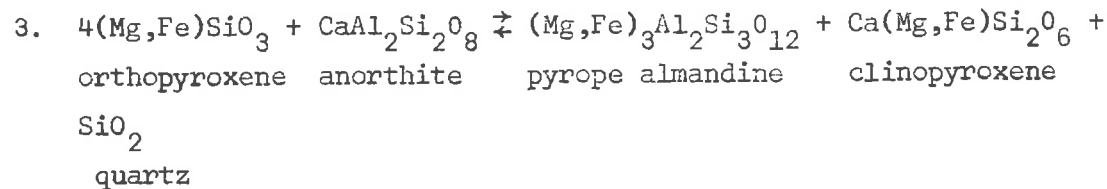


and clinopyroxene:



and an increase in the albite content of the co-existing plagioclase.

With increasing pressure garnet forms due to reaction between the pyroxene and the anorthite content of the plagioclase:



The plagioclase continues to become more sodic with increasing pressure.

The subsolidus boundaries marking the first appearance of garnet in a variety of experimentally investigated lithologies are plotted in Figure 5.1. Curve 4a is for adamellite (Green and Lambert, 1965), 4b is for quartz tholeiite (Green and Ringwood, 1967) and 4d is for olivine tholeiite (Ito and Kennedy, 1971).

The majority of the analysed mafic granulites are compositionally similar to Kuno's (1960) high alumina basalts (see below Chapter 5.4). They consist of plagioclase, aluminous orthopyroxene, aluminous clinopyroxene and opaques. No primary garnet has been recognized although garnet is occasionally present as a coronal phase. The data indicates that at least at the time of the metamorphism of the high alumina basalts pressures and temperatures were to the right of curve 4c and were probably above 5e. It is unlikely that temperatures exceeded approximately 1000°C as temperatures in excess of this would probably have resulted in at least some partial melting of the quartzo-feldspathic granulites. If the temperature indicated by the average $K_D^{\text{opx-cpx}}(\text{Mg} - \text{Fe}^{2+})$ value of the co-existing pyroxene pairs from the mafic granulites, viz. 1150°C is a valid estimate it is unlikely to be a metamorphic temperature and it is more likely to be a preserved high pressure igneous feature of the pyroxenes.

Although pyrope-almandine bearing quartzo-feldspathic granulites are present in the Amata area (Chapter 3.3.3.2) none contain the primary assemblage quartz + plagioclase + alkali feldspar + orthopyroxene + clinopyroxene + garnet; the assemblage produced experimentally by Green and Lambert (1965) in anhydrous adamellite at high pressures and temperatures. In Figure 5.1 curve 4a marks the first appearance of garnet in the assemblage quartz + alkali feldspar + plagioclase + orthopyroxene + clinopyroxene, an assemblage recognized amongst the quartzo-feldspathic granulites in the present study. It can be inferred therefore, that the granulite facies metamorphism took place to the right of curve 4a and probably in or close to the pressure-temperature field defined for the mafic granulites with high alumina basalt composition.

The coronas of clinopyroxene and garnet which are developed around the pyroxenes in the granulite facies rocks are probably formed as a result of (a) cooling or (b) increasing pressure, under anhydrous

conditions, following solidification (see also Griffin, 1971). Because of this garnet forming reactions given in Figure 5.1, curves 4a and 4d are crossed.

However, the garnet coronas around opaque oxides and biotite, and the amphibole coronas; (a) associated with coronal clinopyroxene and garnet or (b) occurring as selvages around orthopyroxene, which are commonly developed in the transitional terrain are remarkably similar to the retrograde amphibolite facies assemblages developed in the granulite facies rocks of Lofoten Vesteraålen, Norway (Griffin and Heier, 1969). It is probable that they formed in the Amata rocks in response to the reactions and conditions described by Griffin and Heier, (1969, pp.98-110), viz. oxidation of biotite accompanied by hydration of pyroxene to amphibole.

Conclusions

Using the experimental data discussed above, probable pressure-temperature fields at which metamorphism in the granulite facies and amphibolite facies terrains occurred are indicated in Figure 5.1. It is estimated that granulite facies metamorphism took place at load pressures between 8 and 9 Kbars, temperatures between 950 and 1000°C and under conditions of $P_{H_2O} < P_{load}$. The estimates of temperature are similar to those suggested by Moore (1970b) and Goode (1970) for the metamorphism of the granulites in the Tomkinson Ranges. However, the estimate of pressure is lower than those suggested by the above authors, viz. 10 Kbars and 10 to 12 Kbars respectively. Metamorphism in the amphibolite facies terrain occurred under conditions of higher P_{H_2O} than in the granulite facies terrain, at temperatures and pressures of 650°C and 4 Kbars respectively. It is more difficult to place pressure-temperature limits on the conditions of metamorphism in the transitional terrain. However, there is evidence to suggest that it took place at variable but higher P_{H_2O} and slightly lower load pressure and temperature than in the granulite facies terrain.

5.4 ORIGIN OF THE MAFIC AND ULTRAMAFIC ROCKS

5.4.1 General

The determination of the original nature of mafic and ultramafic rocks which have been subjected to high grades of metamorphism is a controversial problem. The relevant literature is voluminous and diverse. This is an attempt to resolve this problem in the Amata area.

One feature which has appeared in the literature relates to confusion in the commonly used terminology ortho- and para- (amphibolite), to differentiate between mafic rocks of an igneous origin from those whose precursors were sedimentary. For example, are metamorphosed mafic tuffs to be regarded as ortho- (Leake, 1964) or para-mafic rocks (Van de Kamp, 1968, 1970)? In this thesis, to avoid possible confusion, the suggestions of Miyashiro (1968) have been followed, i.e. descriptions of general or specific antecedents are given and the terms ortho- and para- are not used, except where quoting from other works.

Most of the previous research into this field has been concerned with the study of the origin of amphibolites, sensu stricto. Engel and Engel (1962a) when referring to the Colton amphibolites in the Adirondack gneiss complex use the term in its broader sense. These rocks are in reality hornblende bearing mafic granulites, modal orthopyroxene being ubiquitous. In the present study also, many of the rocks concerned are mafic granulites. Occasional amphibolites are found in the transitional terrain and in the amphibolite facies terrain.

5.4.2 Previous Work on the Origin of Metamorphosed Mafic Rocks

Researchers have mainly used chemical trends or specific element content (both major and trace) in an attempt to distinguish between amphibolites derived from basic igneous antecedents and those of sedimentary origin (Engel and Engel, 1951, 1953, 1962a; Lapadu Hargues, 1953; Poldervaart, 1953; Evans and Leake, 1960; Walker et al., 1960; Leake, 1963, 1964; Eckelmann, and Poldervaart, 1957; Wilcox and Poldervaart, 1958; Heier, 1962; Shaw and Kudo, 1965; Van de Kamp, 1968, 1969, 1970; Orville, 1969; Karlsbeek and Leake, 1970; Smithson et al., 1971; Holdhus, 1971; Misra, 1971). The use of chemical criteria was

often found difficult because of modifications of the original composition of the rocks due to metamorphism (Adams and Barlow, 1910; Tilley, 1957; Orville, 1969).

Walker et al. (1960), in an extensive study, examined field, mineralogical and textural features, major and minor element contents and rock magnetic properties in an attempt to distinguish between amphibolites derived from igneous sources and those derived from calc-magnesian sediments. They concluded that diagnostic differences could be discerned (especially trace element) if the rocks had not been metasomatically altered.

The banded or 'striped' nature of mafic metamorphic rocks (Wilcox and Poldervaart, 1968; Walker et al., 1960) or their association with metasedimentary rocks (Heier, 1962) was thought to be indicative of a sedimentary origin. The work of Evans and Leake (1960) in Connemara, Eire however has demonstrated that amphibolites of igneous derivation, modified by metamorphism can often display a well developed banded appearance. Similarly, Ghaly (1969) considered that metamorphic differentiation, simultaneous solution, recrystallization and mechanical differentiation initiated by tectonic deformation, were responsible for the commonly observed segregation banding in Scottish Lewisian mafic to felsic schists and gneisses.

Shaw and Kudo (1965) in a preliminary study of the differences between 'ortho- and para-' amphibolites, used multivariant statistical techniques in an attempt to overcome the problems associated with the comparison of chemical data using single variant methods. They successfully distinguished between the two types of amphibolites with the aid of calculated discriminant functions. These are positive and negative for meta-igneous rocks and meta-sediments respectively. They recognized that tuffaceous sediments, depending on their degree of reworking, could display geochemical characteristics of either group. In addition, they found that metasomatically altered amphibolites could exhibit compositional characteristics of either group. Smithson et al. (1971) showed that metasomatically formed amphibolites derived from calc silicate metasedimentary rocks exhibited generally the geochemical characteristics of amphibolites of igneous origin. However, they could

be distinguished by their titania contents.

The significance of the titania content has been stressed also by Wilcox and Poldervaart (1958) and Walker et al. (1960). They believed that titanium was more concentrated in the amphibolites derived from basalts and dolerites rather than in those derived from calc-pelite mixtures. In addition, Misra (1971) has shown that the titanium content and their degree of iron enrichment could be used to separate the two main groups of amphibolites.

Evans and Leake (1960), Leake (1963, 1964), Van de Kamp (1968, 1969, 1970), Karlsbeek and Leake (1970) and Holdhus (1971) considered that amphibolites derived from carbonate-clay mixtures or other sedimentary rocks could be discerned from those derived from igneous rocks by examining the different variation trends of certain elements (calculated as Niggli numbers).

Techniques using Niggli numbers (especially those of Evans and Leake, 1960; and Leake, 1963, 1964) are not proof of an igneous or sedimentary parentage of the metamorphosed mafic rocks (see, for example Orville, 1969; Smithson et al., 1971). However, they can provide useful information relating to the origin of the metabasic rocks if they are used in conjunction with structural data and further chemical criteria. These techniques have not been used extensively in high grade terrains. To the author's knowledge the only work of such a nature has been carried out by Leake (1963) on the Colton 'amphibolites', and by Sen and Ray (1971) on the Madras mafic granulites.

5.4.3 Origin of the Amata Mafic Rocks

5.4.3.1 Major Element Data

In the following discussion major elements from the bulk rock analyses are recalculated as Niggli numbers (Table 4.2). They are then treated according to the methods advocated by Evans and Leake (1960) and Leake (1963, 1964). The minor and trace element data are discussed in the light of the findings of Van de Kamp (1968, 1969, 1970).

The relationship between Niggli c and mg (as in Leake, 1964) is depicted graphically in Figure 5.2a and b. The mafic and ultramafic granulites plot along a field which closely defines the trend of

variation of the Karroo dolerites (Leake, 1963; Van de Kamp, 1968). A similar distribution is portrayed by the amphibolites and the non-micaceous mafic rocks from the amphibolite facies area and transitional terrain. In contrast, the micaceous mafic rocks from the transitional terrain exhibit a rather erratic distribution pattern (Figure 5.2b). The plots of al-alk against c (Figure 5.3a and b) show similar differences. Although the plots of micaceous mafic rocks (mentioned above) occupy the field characteristic of igneous rocks their plots are extremely variable.

The relationships defined by these figures are also demonstrated graphically by means of the ternary plot of 100 mg, c and al-alk recalculated to 100% (Figure 5.4a and b). The trends of variation of the Amata mafic and ultramafic rocks roughly parallel the trend of the Karroo dolerites. The micaceous mafic rocks once again display a scattered distribution pattern. None of the plots of analyses, however, fall along variation trends for limestone or dolomite-pelite mixtures. From Figures 5.2, 5.3 and 5.4 it is concluded that the evidence favours an igneous derivation of the mafic rocks from either intrusives, extrusives or pyroclastics, with the possible exception of the micaceous varieties.

5.4.3.2 Trace Element Data

A detailed account of the trace element geochemistry of the Amata area is given in Chapter 4.2.4. The following discussion is concerned only with aspects pertinent to the problem being investigated.

The ultramafic and mafic rocks in which mica is not abundant have low rubidium values (p.p.m.), ranging from:

- (a) 1.3 to 30.1 (granulite facies)
- (b) 4.7 to 14.3 (transitional)
- (c) 18.7 to 24.7 (amphibolite facies)

These values are well below the rubidium abundance levels in impure pelites (average 100 p.p.m.) given by Van de Kamp (1970). The micaceous mafic rocks have high rubidium contents ranging between 61.3 and 291.0 p.p.m., and consequently lower K/Rb ratios than the other mafic rocks. The ultramafics also have low K/Rb ratios. The low ratios

in the micaceous rocks is caused by the high concentration of rubidium in the potassium rich plate silicates. The K/Rb ratios of the majority of these mafic rocks are typical of certain basalts and intrusive basic igneous rocks.

A distinction between the mafic rocks can also be made on the basis of the rubidium/strontium ratio. The non-micaceous rocks (except for A325-2050c) have ratios which are typical of basic to intermediate igneous rocks (see Table 5.1 for comparison).

- (a) 0.004 to 0.053 (granulite facies)
- (b) 0.042 to 0.155 (transitional)
- (c) 0.140 to 0.190 (amphibolite facies).

However, the micaceous rocks (except for A325-1328, which has an abnormally high Sr content, Table 4.2) display ratios which are atypical of such igneous rocks (Table 5.1).

The ratio of lanthanum to cerium has been used by Van de Kamp (1968, 1969, 1970) as a distinguishing property for the different mafic rocks. He considered that amphibolites derived from pelite-carbonate mixtures have La/Ce ratios greater than 0.4. Table 5.2 shows the average values and ranges of values of the La/Ce ratio of common rock types including some high grade metamorphics. The La/Ce ratios displayed by the Amata rocks are:

- (a) 0.055 to 0.255 (granulite facies)
- (b) 0.201 to 0.381 (mica-free transitional)
- (c) 0.035 to 0.336 (micaceous transitional)
- (d) not determined (amphibolite facies)

It can therefore be seen that all the rocks under discussion have La/Ce ratios below 0.4. The range for the micaceous mafic rocks is similar to the non micaceous transitional rocks. Therefore, if Van de Kamp's (1968, 1969, 1970) suggestions regarding the La/Ce ratio are valid, the present data indicates that the micaceous mafic rocks were unlikely to have been derived from pelite-carbonate mixtures.

5.4.3.3 Field Evidence

Field evidence for the origin of the mafic and ultramafic rocks in the Amata area has in most cases been completely obliterated by the

TABLE 5.1

MEAN RUBIDIUM/STRONTIUM VALUES IN COMMON ROCK TYPES

Rock Type	Mean Rb/Sr
Diorites and andesites	0.18
Basic Igneous Rocks	0.07
Shales	0.50
Limestones	0.008

TABLE 5.2

La/Ce AVERAGE VALUES AND RANGES OF VALUES OF VARIOUS ROCK TYPES

Rock Type	La/Ce
Average of Granitic Rocks ¹	0.53
Average of Intermediate Rocks ¹	0.52
Gabbro, Basalt ²	0.14-0.42
Shale ²	0.39-0.72
Limestone ²	0.50
Greywacke ²	0.73
Ortho amphibolites ²	0.02-0.25
Para amphibolites ²	0.03-0.32
Amphibolite Facies Intermediate Gneiss ³	0.49
Amphibolite Facies Quartzo-feldspathic Gneiss ³	0.35
Granulite Facies Dioritic Granulite ³	0.44
Granulite Facies Intermediate Granulite ³	0.40
Granulite Facies Mangerite ³	0.46-0.53

1. Values computed from data given by Herrmann, A.G. p.11 (1969).
2. Values computed by Van de Kamp (1968) from data given by Haskin et al. (1966).
3. Values computed from data given by Green et al. (1969).

deformational events which have affected all the metamorphic zones (Collerson et al., 1972). The mafic and ultramafic units can seldom be traced along strike for any great distances. With the exception of minor occurrences in the granulite sequence they have sharp contacts with the surrounding quartzo-feldspathic gneisses. Structural evidence suggests that the mafic units have been effected by all the major folding deformations. They are often truncated by faults (Figure 1.3). The mafic granulites are not veined with quartzo-feldspathic material nor do they display any signs of brecciation. In contrast, the mafic transitional zone lithologies are frequently veined and often contain brecciated zones which have been re-cemented with quartzo-feldspathic phases. Because of the poor outcrop to the north of Amata the intimate field relations of the minor amphibolite units which occur there are not known to any extent. However, it has been recognised that they are lensoidal and have sharp contacts with the quartzo-feldspathic gneisses.

In the granulite facies terrain, it has been possible to recognise differing degrees of structural complexity in the geometry of the mafic units. The postulated sequence in order of decreasing structural complexity is given in Table 5.3.

TABLE 5.3

STRUCTURAL SEQUENCE RECOGNISED IN THE MAFIC GRANULITES

(1) Thin discontinuous lenses occasionally showing slightly gradational boundaries. Well developed planar and linear fabrics. Conformable with the regional layering.
(2) Discontinuous layers and lenses, sharp boundaries, conformable with regional layering. Well developed planar and linear fabrics.
(3) Mafic unit up to 60 metres thick, layered appearance, marginal magnetite and haematite rich zones - may be a differentiated basic intrusive. Well developed linear and planar structural elements. Slightly transgressive to regional layering. Folded by gD_4 deformation.
(4) Transgressive mafic granulites, sharp contacts, weakly developed schistosity and lineation. In comparison the surrounding rocks have strongly developed schistosity and lineation.

This sequence reflects the degree of involvement in the structural history of the mafic rocks. It supports the proposal that different periods of igneous intrusion took place throughout the deformational history. Most of the mafic granulites analysed have the characteristics of 2 and 3 (Table 5.3).

5.4.3.4 Discussion

In the discussion on trace elements (Chapter 4.2.4) it was suggested that the mafic granulites did not appear to have suffered the same geochemical history as the quartzo-feldspathic granulites. This difference is based principally on fractionation evidence, viz. the distribution of K/Rb, Rb/Sr, and the content of $\Sigma\text{La Ce}$. Distinct 'trends' were recognised in the quartzo-feldspathic granulites but no such distribution trends were found in the mafic granulites. It was suggested that the metamorphism of the quartzo-feldspathic rocks may have involved the fractionation of certain elements to produce these patterns. The absence of fractionation trends in the mafic granulites strongly favours the suggestion that they were intruded into the granulite facies terrain after the geochemical trends had been established in the quartzo-feldspathic granulites.

The chemical, field and mineralogical evidence strongly favours an igneous origin for the mafic and ultramafic granulites. Fewer data are available for the transitional and amphibolite facies terrain mafic and ultramafic rocks, but it is suggested that they also had precursors. Whether or not they were pyroclastics is not known. The antecedent or antecedents of the micaceous mafic rocks is not known. However, it is unlikely that they were derived from pelite-carbonate mixtures (see p.264).

5.4.3.5 Nature of the Igneous Parent

It has been demonstrated above that the mafic granulites and possibly the other mafic rocks (excluding the micaceous varieties) are probably derived from basic igneous precursors. An attempt is now made to indicate the type of basic magma constituting these intrusives.

The non-alkaline nature of the mafic granulites (except for

A325-949) is shown by an alkali-silica plot (Figure 5.5a). The analyses plot midway between basalts of tholeiitic composition and those that are dominantly alkaline. By analogy, Kuno (1960) found that by plotting Al_2O_3 against alkalies, for differing silica contents, the high alumina basalts lie in a field midway between the alkali and tholeiitic basalts.

Seven of the twelve mafic granulites have high alumina contents (17.06 to 22.00%). This feature, together with their silica and alkali values, and their normative composition, strongly favours the suggestion that they are geochemically similar to Kuno's high alumina basalts. The mafic granulites A325-138b, -1105, -78 and -158 plot in the field of tholeiitic basalts (Kuno, 1960, p.127, Fig. 3). With the exception of A325-1105 they have much lower alumina contents (14.39% to 14.90%). A325-949 has a curious composition with low alkali and silica and high alumina contents. It is also slightly nepheline normative (Table 4.3) which, together with its position on the alkali-silica plot, classifies it as slightly alkaline.

Analyses of mafic granulites (and 'basic charnockites') from other high grade terrains are presented in Table 5.4. Excluding A325-78, -158 and -138b it is apparent that the Amata mafic granulites are in general much more aluminous than mafic granulites from other high grade terrains, except for M.G. 10, from the West Uusimaa Complex, Finland (Parras, 1958).

The mafic rocks from the transitional and amphibolite facies terrain are widely distributed on the silica-alkali plot (Figure 5.5b). The micaceous mafic rocks, as is to be expected, are dominantly alkaline. They are undersaturated in silica and, with the exception of A325-990, are leucite and/or nepheline normative. Whether or not these compositions are inherited from a source igneous rock or magma is unknown.

Three of the non-micaceous rocks from the transitional terrain are similar to tholeiite basalts. A325-339 has affinities with alkali basalts, i.e. normative nepheline and olivine. The amphibolite facies mafic rocks are geochemically similar to both alkali and tholeiitic basalts. Both ultramafic rocks analysed are regarded as possible early differentiates from either tholeiitic or high alumina basalt.

TABLE 5.4

ANALYSES OF MAFIC GRANULITES FROM OTHER GRANULITE FACIES TERRAINS

SPECIMEN NO. M.G./-	1	2	3	4	5	6	7	8	9	10	11	12
SiO ₂	47.89	48.99	48.37	50.84	48.50	49.42	47.14	47.88	45.00	48.02	48.39	51.60
Al ₂ O ₃	14.63	14.61	16.57	14.36	14.88	14.93	14.98	14.22	16.62	22.11	12.83	16.59
Fe ₂ O ₃	1.85	1.79	2.64	3.98	2.38	1.50	1.72	1.73	6.05	0.20	2.83	0.50
FeO	11.20	8.62	10.42	9.64	11.48	11.53	11.48	12.36	8.97	8.28	11.63	6.37
MgO	7.41	10.89	7.00	5.71	8.66	6.14	8.27	6.35	7.24	4.14	6.85	14.42
CaO	11.54	12.58	9.27	10.66	9.44	10.45	12.41	10.23	9.50	11.76	11.84	8.03
Na ₂ O	2.19	1.36	2.58	2.85	2.01	2.68	1.17	2.47	2.76	2.70	2.09	1.32
K ₂ O	0.58	0.15	0.24	0.41	0.34	0.56	0.16	0.51	0.96	1.15	0.45	0.48
TiO ₂	1.56	0.34	2.01	1.04	1.18	1.20	1.00	2.95	2.40	0.85	2.08	0.37
MnO	0.25	0.20	0.20	0.19	0.23	0.23	0.28	-	0.31	0.07	0.33	0.08
F ₂ O ₅	0.14	0.02	0.41	0.16	0.21	-	-	0.40	-	0.47	0.17	-
H ₂ O ⁺	0.72	0.26	0.11	0.26	0.38	0.94	1.01	0.23	-	-	0.59	0.30
H ₂ O ⁻	0.03	0.03	-	0.08	0.15	0.30	0.21	0.07	-	-	0.06	0.04
Total	99.99	99.84	99.82	100.18	99.84	99.38	99.83	99.40	99.81	99.75	100.19	100.22

- 1 Average least altered amphibolite, Colton Area; Engel and Engel (1962a)
- 2 Mafic band, Wilmington Complex; Ward (1959)
- 3 Hornblende-Hypersthene-Plagioclase Gneiss, Arendal District, Norway; Bugge (1943)
- 4 Mafic Charnockite, Sudan; Howie (1958)
- 5 Pyroxene Granulite, Madras, India; Howie (1955)
- 6 Hornblende Pyroxene Granulite, Madras; Sen and Ray (1971)
- 7 Hornblende Pyroxene Granulite, Madras; Sen and Ray (1971)
- 8 Hornblende-Pyroxene-Plagioclase Granulite, Bunker Bay, W.A.; Prider (1945)
- 9 Basic Charnockite, Varberg, Norway; Quensel (1951)
- 10 Basic Charnockite, West Uusimaa Complex, Finland; Parras (1958)
- 11 Basic Granulite, Koddigvarri, Lapland; Eskola (1952)
- 12 Basic Granulite, Sotajoki, Lapland; Eskola (1952).

From the above discussion it can be concluded that:

- (1) most of the mafic rocks were derived from igneous progenitors;
- (2) chemical data strongly favours high alumina basalt (granulite terrain), tholeiitic basalt (granulite and transitional terrain) and alkali and tholeiitic basalt (amphibolite terrain north of Amata) to be the major magma types.

If these are valid deductions then evidence is strong that the different metamorphic terrains possibly represent distinct metamorphic blocks and that at least during the intrusion of the mafic rocks, they were not in the same tectono-igneous environment.

CHAPTER 6

CONCLUDING DISCUSSION

Structural, petrological and geochemical data have been presented in this thesis and some conclusions have already been drawn. The following discussion elaborates conclusions concerning the evolution of the three metamorphic terrains in the Amata area.

From mineralogical and geochemical evidence it is apparent that the three metamorphic terrains in the Amata area, viz. the granulite facies, amphibolite facies and transitional terrain, were metamorphosed under differing physical conditions. The following estimates of pressure and temperature are proposed:

- (i) granulite facies; P_{load} - between 8 and 9 kilobars, temperature - 950 to 1000°C, with $P_{H_2O} < P_{load}$;
- (ii) amphibolite facies; P_{load} and temperature - approximately 4 kilobars and 650°C respectively, and P_{H_2O} approximately equal to P_{load}
- (iii) transitional terrain; it is suggested, with less certainty, that the transitional terrain was metamorphosed at varying but higher P_{H_2O} and slightly lower P_{load} and temperature than the granulite facies terrain.

The three metamorphic terrains are considered to have been metamorphosed initially under different pressure-temperature conditions. There is no evidence to suggest that the transitional terrain is an area of retrograded granulites.

The coronas around the primary metamorphic phases in the granulite facies and transitional terrains are believed to have resulted from cooling of the rocks at fairly constant pressure.

It is apparent that the three metamorphic terrains form structurally unique blocks exhibiting geometrical features which differ in both style and orientation. The contrasting physical conditions referred to above are likely to have been responsible for large rheological differences in the respective terrains, and thus are thought to account for the varying responses to some of the deformational episodes (Holland and Lambert, 1969). For example, the

abundant development of folds during D_2 in the transitional and amphibolite facies terrains may be a reflection of the more hydrous nature of the environment (cf. the granulite terrain).

There is a probable relationship between the deformational event responsible for gL_1 and that responsible for tL_2 . These lineations probably reflect the directions of extension of the metamorphic blocks prior to the D_4 phase of thrusting on the Woodroffe Thrust and Davenport Shear. These faults, however, were probably initiated at an early stage in the deformational history of the area; a belief supported by the polyphase deformation in the mylonites.

Different weighted average contents of thorium, potassium, strontium and rubidium in the three terrains are probably the result of crustal fractionation. Evaluation of this proposition is complicated by the fact that the three metamorphic terrains have apparently been brought into their present spatial relationship subsequent to the crustal fractionation. No original crustal section is therefore preserved.

Evidence suggests that fractionation occurred in the quartzofeldspathic but not in the mafic granulites. Lambert and Heier (1968) and Lambert (1971) believed fractionation in high grade rocks to be the result of dehydration and partial melting. Although there is ample evidence for anatexis in the transitional and amphibolite facies terrains, there is no evidence for partial melting in the granulite facies terrain (at least contemporaneously with gD_1). It is probable therefore, that if the quartzofeldspathic granulite sequence was dehydrated and partially melted, this took place prior to gD_1 at an early stage of the orogenic cycle when heat flows were extreme. This is not inconsistent with the interpretation of the origin of the granulites in the Amata area as being the result of the metamorphism of a series of cover rocks (of predominantly arkosic composition). The mafic lithologies were probably intruded as sills after the regional dehydration and were isochemically metamorphosed, retaining their original major and trace element geochemistry. The close approximation of the composition of many of the mafic rock to those of high alumina basalts also supports this view.

In contrast to the granulite facies terrain, the mafic rocks in the transitional terrain display trends which suggest that fractionation with respect to rubidium, strontium and potassium has taken place. Some of these mafic rocks at least, are believed to be of igneous derivation. It is, therefore, likely that they were intruded prior to the establishment of the geochemical trends during metamorphism in the transitional terrain. If these trends were produced during tD_2 , the main folding deformation, then fractionation in the granulite terrain occurred earlier than in the transitional terrain. It may therefore, be purely fortuitous that similarity in the behaviour of the granulite facies and transitional populations was recognised from the R.M.A. analysis of the K/Rb data.

The metamorphic terrains thus represent three separate crustal units, close enough in space for some correlation of deformations to be possible, yet sufficiently distant to have developed distinct geochemical and petrological characteristics, brought into juxtaposition by late movements along the Woodroffe Thrust and Davenport Shear.

PETROGRAPHIC DETAILS OF ANALYSED ROCKS

Rock specimens and thin sections referred to in the text of this thesis are housed in the collections of the Department of Geology and Mineralogy, University of Adelaide. Their field numbers are prefixed by A325/-. Locations of specimens are given in Figure A.1.1. Petrographic features of specimens analysed during the course of this study are presented below. Modal analyses are presented in Table 4.1.

A.I.1. Granulite Facies Lithologies

A325-83. Two-pyroxene plagioclase granulite (mafic granulite).

Microstructure: Medium to fine grained inequigranular granoblastic; grain boundaries straight, curved or slightly embayed.

Minerals Present: Essentially the same mineralogy as A325-81 except that no 'myrmekitic' plagioclase is present. Plagioclase grains are complexly twinned under the albite and pericline laws and are commonly deformed.

A325-119. Two-pyroxene plagioclase granulite (mafic granulite).

Microstructure: Fine grained equigranular granoblastic; grain boundaries curved, straight or slightly embayed. Widely spaced anastomosing fractures are interpreted to be the result of post crystallization deformation.

Minerals Present: Consists of predominantly hyperthene and anti-perthitic plagioclase together with minor amounts of clinopyroxene, a trace of quartz and opaque oxides. Coronas of clinopyroxene, secondary amphibole and garnet surround the orthopyroxene grains. Garnet also occurs around opaque oxides. The plagioclase xenoblasts are extensively deformed; twin lamellae are bent and disrupted. Grains adjacent to the anastomosing fracture zones are commonly brecciated. Sillimanite needles occur as inclusion in plagioclase grains or along grain boundaries. Corundum is present in trace amounts.

A325-105b. Two-pyroxene plagioclase granulite (mafic granulite).

Microstructure: Inequigranular granoblastic; grain interfaces are predominantly curved.

Minerals Present: The rock consists of antiperthitic plagioclase (average size 0.6 x 0.6 mm), hypersthene and clinopyroxene. The pyroxenes range in size from less than 0.2 x 0.2 mm to greater than 1.2 x 0.8 mm. Pericline and albite twinning are well developed in the plagioclase grains and some grains show undulose extinction. Minor amounts of quartz, opaque oxides and biotite (α pale yellow, $\beta=\gamma$ red brown) are also present. Coronas of pale amphibole commonly surround grains of orthopyroxene. Opaque oxides are generally mantled by coronas of amphibole and/or biotite. Sillimanite needles occur along grain boundaries.

A325-81. Two-pyroxene plagioclase granulite (mafic granulite).

Microstructure: Medium to fine grained inequigranular granoblastic; grain boundaries straight or curved.

Minerals Present: Consists predominantly of antiperthitic plagioclase (average size 1.5 x 1.5 mm), twinned under the pericline and albite laws, with prominent undulose extinction. Minor intergrowths with quartz characterises some of the plagioclase grains. Mafics comprise orthopyroxene and clinopyroxene; the latter being the subordinate phase (average size 0.7 x 0.7 mm). The orthopyroxene is surrounded by coronas of clinopyroxene, secondary amphibole and garnet. Opaque oxides are present in small amounts.

A325-138b. Two-pyroxene plagioclase granulite (mafic granulite)

Microstructure: Fine grained, inequigranular granoblastic; grain boundaries straight or curved. Rock penetrated by narrow sub parallel shear zones.

Minerals Present: Consists of approximately equal proportions of ferromagnesian and felsic phases. Clinopyroxene is the dominant

ferromagnesian phase (average size 0.2 x 0.2 mm), it is heavily clouded with opaques and commonly contains exsolved orthopyroxene lamellae. Hypersthene is present in subordinate amounts. Narrow coronas of intensely pleochroic biotite (α pale yellow, $\beta=\gamma$ bright red) surround opaque oxides, as do coronas of granular garnet. Evidence of deformation is registered to a greater extent in the feldspars than in the pyroxenes. Green brown to brown hornblende are present in small amounts. The opaque oxides occur either as discrete grains or as symplectic intergrowths with the silicates. Apatite is present in trace amounts.

A325-60. Two-pyroxene plagioclase granulite (mafic granulite).

Microstructure: Inequigranular granoblastic; medium to fine grained; extensive development of post crystallization anastomosing fracture patterns.

Minerals Present: The rock is extensively deformed and has essentially the same mineralogy as A325-105b.

A325-148. Two-pyroxene plagioclase granulite (mafic granulite).

Microstructure: Inequigranular granoblastic with straight or curved grain boundaries.

Minerals Present: Essentially the same as A325-105b except that sillimanite needles are absent. Apatite is present as an accessory phase.

A325-121. Two-pyroxene plagioclase granulite (mafic granulite).

This rock is essentially the same as A325-105b.

A325-949. Garnet two-pyroxene plagioclase granulite (mafic granulite).

Microstructure: Equigranular granoblastic; grain boundaries straight, curved or slightly embayed.

Minerals Present: Similar mineralogy to A325-1105 except that clinopyroxene is more abundant than orthopyroxene (Table 4.1). Coronal

secondary amphibole is extensively developed around orthopyroxene and brown hornblende. Sillimanite needles are common in the plagioclase grains and also along grain interfaces. Irregular grains of green spinel and elongate laths of corundum are conspicuous.

A325-1105. Garnet two-pyroxene granulite (mafic granulite).

Microstructure: Fine grained equigranular granoblastic; grain boundaries smoothly straight or curved.

Minerals Present: Composed of xenoblasts of plagioclase, garnet, hypersthene, clinopyroxene, brown hornblende and opaque oxides. Small amounts of apatite and biotite are also components. The plagioclase grains are remarkably free of inclusions. They commonly display well developed triple point junctions. Deformation twins are common.

A325-78. Two-pyroxene hornblende scapolite plagioclase granulite (mafic granulite)

Microstructure: Equigranular granoblastic; curved or embayed grain boundaries.

Minerals Present: Consists of round to angular grains of hypersthene, (up to 1.0 x 0.7 mm in size), heavily clouded clinopyroxene (up to 1.0 x 0.3 mm in size), hornblende with green brown pleochroic colours and xenoblastic grains of plagioclase (average size 0.5 x 0.4 mm). The plagioclase grains are commonly twinned under albite and pericline laws and they have undulose extinction. Minerals present in minor amounts include scapolite and biotite (α yellow, $\beta=\gamma$ orange red). Clinopyroxene, secondary amphibole and garnet form coronas around orthopyroxene and opaques. Plagioclase grains are heavily clouded with needle-like inclusions of sillimanite and plates of epidote. Pyroxene and plagioclase grains are commonly fractured and have bent cleavage traces and twin planes.

A325-158. Two-pyroxene biotite plagioclase granulite (mafic granulite).

Microstructure: Equigranular, fine grained granoblastic; grain

boundaries straight or curved. Penetrated by narrow shear zones.

Minerals Present: Composed of xenoblastic grains of hypersthene, clinopyroxene (average size 0.7 x 0.7 mm), and plagioclase. Biotite (α pale yellow, $\beta=\gamma$ deep red brown), brown green hornblende, opaque oxides are present in subordinate amounts. The rock is extensively deformed, with the development of undulose extinction in the plagioclase grains and kink bands in the biotite. Coronas of pale green amphibole surround orthopyroxene and biotite. Apatite and sillimanite are present in accessory amounts.

A325-205. Quartz feldspar pyroxene granulite (quartzo-feldspathic granulite).

Microstructure: Inequigranular granoblastic elongate; straight or curved grain boundaries.

Minerals Present: Consists predominantly of antiperthite and quartz. Grain size range is from less than 0.2 x 0.2 mm to greater than 2.0 x 0.5 mm. The ferromagnesian phases are hypersthene together with a trace of clinopyroxene, biotite and fibrous pale green amphibole. The latter phase occurs as coronas around orthopyroxene. Apatite is present in accessory amounts.

A325-199. Quartz feldspar pyroxene granulite (quartzo-feldspathic granulite).

Microstructure: Inequigranular granoblastic-elongate; curved or embayed grain boundaries.

Minerals Present: Essentially the same mineralogy as A325-205 except that clinopyroxene is absent.

A325-1121. Quartz feldspar garnet granulite (garnetiferous quartzo-feldspathic granulite).

Microstructure: Inequigranular granoblastic-elongate; curved, embayed or sutured (lobate) grain boundaries.

Minerals Present: Consists of irregular poikiloblastic porphyroblasts

of garnet (almandine-pyrope) (up to 3.0 mm in diameter) as well as smaller, groundmass garnets (average size 0.2 x 0.2 mm), platy elongate quartz, stringlet and bead perthite, plagioclase (with albite and pericline twins) and hypersthene. Zircon and apatite are present in trace amounts.

A325-1165a. Quartz feldspar pyroxene granulite (quartzo-feldspathic granulite).

Microstructure: Inequigranular granoblastic elongate; curved, embayed or sutured grain boundaries.

Minerals Present: Consists of quartz, perthitic alkali feldspar, mesoperthite, antiperthite, hypersthene and opaque oxides. In the N and P sections some of the quartz occurs as lenticles surrounded by equigranular granoblastic quartz and feldspar. Some of the quartz lenticles exceed 1.7 cm x .2 mm. The quartz is strained and is frequently recrystallized. Albite and pericline twinning is common in the plagioclase. Some feldspars contain needle-like inclusions of sillimanite and show slight alteration to white mica and calcite. Hypersthene occurs as rounded to prismatic grains (average size 0.24 x 0.16 mm), often slightly altered to pale green amphibole. Apatite is present in trace quantities.

A325-77. Quartz feldspar garnet granulite (garnetiferous quartzo-feldspathic granulite).

Microstructure: Porphyroblastic with an inequigranular granoblastic groundmass. Pronounced dimensional preferred orientation in the groundmass produced by elongate lenticles and aggregates of quartzo-feldspathic components. Curved, straight or sutured grain boundaries.

Minerals Present: Consists of large poikiloblastic xenoblasts of garnet (up to 2.0 x 1.5 mm in size) in a groundmass composed of interlocking xenoblastic grains of recrystallized quartz (average size 0.1 x 0.06 mm) alkali feldspars and mesoperthite (up to 1.0 x 1.0 mm in size). Opaques occur in trace amounts.

A325-138. Quartz feldspar pyroxene granulite (quartzo-feldspathic granulite).

Essentially the same as A325-1165a except that the feldspars are not altered.

A325-2040. Grossularite anorthite granulite (calc silicate granulite).

Microstructure: Medium grained, equigranular granoblastic; grain boundaries curved, embayed or sutured.

Minerals Present: Consists of plagioclase (anorthite), andradite-grossularite garnet, opaque oxides, allanite and clinozoisite. Average grain size 0.8 x 0.8 mm. Deformation twins extensively developed in the plagioclase grains. Granular secondary garnets surround some of the opaque oxides. The clinozoisite occurs in fine grained decussate aggregates.

A325-2048. Garnet clinopyroxene quartzite (manganiferous granulite).

Microstructure: Inequigranular elongate-granoblastic; grain boundaries straight, curved or sutured.

Minerals Present: The rock has a distinctly banded appearance. It consists of highly strained quartz, spessartine, johannsenite, bustamite, pyroxmangite and opaque oxides. Some of the pyroxenes are surrounded by coronas of orange spessartine garnet.

A325-2050c. Two-pyroxene hornblende granulite (ultramafic granulite)

Microstructure: Medium to fine grained, inequigranular granoblastic. Some porphyroblasts distinctly poikiloblastic. Grain interfaces curved or embayed.

Minerals Present: The rock consists of orthopyroxene, clinopyroxene, hornblende, and a trace of plagioclase. The hornblende has the following pleochroic scheme (α neutral, β pale green brown, γ pale brown). Both hornblende and clinopyroxene are heavily clouded with opaque oxides. Needles of rutile are ubiquitous in the orthopyroxene. Plagioclase shows albite and pericline twinning. Coronas of pale green amphibole are

developed around the orthopyroxene grains when they are in contact with plagioclase.

A.I.2. Transitional Terrain Lithologies

A325-517. Hornblende two-pyroxene plagioclase rock.

Microstructure: Inequigranular granoblastic; grains have curved or straight boundaries.

Minerals Present: Orthopyroxene, clinopyroxene and plagioclase (average size 0.5 x 0.3 mm) together with large porphyroblasts (up to 3.0 x 3.0 mm in diameter) of strongly pleochroic (green to green brown) hornblende. Plagioclase has well developed undulose extinction and complex deformation twin patterns. Clinopyroxenes are clouded with opaque granules. Opaque oxides and biotite are present in minor amounts. Narrow coronas of pale green amphibole surround the orthopyroxene, hornblende and opaque oxides.

A325-544. Hornblende orthopyroxene plagioclase rock.

Microstructure: Deformed inequigranular granoblastic; grain boundaries are straight, curved or embayed.

Minerals Present: Composed of orthopyroxene, green brown pleochroic hornblende and plagioclase (average grain size 0.7 x 0.4 mm). Hornblende and plagioclase are frequently deformed, resulting in the formation of kinks, deformation twins and undulose extinction. Opaque oxides are minor constituents. Coronas of fibrous pale green secondary amphibole surround orthopyroxene and hornblende.

A325-339. Hornblende two-pyroxene plagioclase rock.

Microstructure: Inequigranular granoblastic; grain boundaries are either straight or curved.

Minerals Present: The rock is composed of orthopyroxene, clinopyroxene and plagioclase (average size 0.4 x 0.4 mm), together with strongly pleochroic hornblende (average size 1.0 x 0.7 mm) and minor amounts of

opaque oxides and biotite. Apatite, sphene and sillimanite are present in trace quantities. Coronas of pale green secondary amphibole and granular opaques surround the orthopyroxene and hornblende grains.

A325-523. Hornblende two-pyroxene plagioclase rock.

Microstructure: As for A325-339.

Minerals Present: Consists of large subhedral to anhedral grains of hypersthene (up to 2.9 x 1.5 mm in size), smaller polygonal aggregates of clouded pale green diopside, large green pleochroic hornblende porphyroblasts (up to 5.0 x 3.5 mm), polygonal grains of plagioclase (average size 1.0 x 1.0 mm) and opaque oxides. The plagioclase shows undulose extinction and complex deformation twins. Coronas of secondary amphibole surround the hypersthene, hornblende and opaque oxides. Minor sillimanite occurs in the plagioclase as fine needle-like inclusions.

A325-295. Hornblende two-pyroxene rock.

Microstructure: Inequigranular to equigranular granoblastic; some grains poikiloblastic; grain boundaries curved or embayed.

Minerals Present: Composed of a granular aggregate of hypersthene, clinopyroxene, green pleochroic hornblende (average size 1.0 x 1.0 mm), minor amounts of plagioclase (with inclusions of clinozoisite) opaque oxides and a trace of biotite and secondary garnet. Coronas of fibrous secondary amphibole are commonly developed at orthopyroxene- and hornblende-plagioclase contacts.

A325-497. Two-pyroxene hornblende rock.

Microstructure: Inequigranular granoblastic; grain boundaries straight, curved or distinctly embayed.

Minerals Present: Consists of hypersthene (commonly with schiller structure) and clinopyroxene in approximately equal amounts (average size 0.7 x 0.7 mm), green brown to brown pleochroic hornblende (average size 1.4 x 1.4 mm), antiperthitic plagioclase (average size 1.5 x 1.5 mm) with pericline and albite twins. Minor phases include

biotite and secondary garnet. Coronas of secondary amphibole are commonly developed around orthopyroxene grains.

A325-14. Clinopyroxene garnet biotite plagioclase rock.

Microstructure: Inequigranular, granoblastic to lepidoblastic; straight, curved or sutured grain boundaries.

Minerals Present: Consists of aggregates of clinopyroxene (average size 0.7 mm diameter) with finely developed polysynthetic twinning, idioblastic to subidioblastic garnets (average size 1.0 mm diameter), deformed laths of biotite, plagioclase exhibiting albite and pericline twinning, recrystallized aggregates of quartz, hornblende and opaque oxides. Accessories include apatite and zoisite.

A325-6. Hornblende plagioclase biotite rock.

Microstructure: Inequigranular, weakly nematoblastic, distinctly banded, either straight or sutured grain boundaries.

Minerals Present: Consists dominantly of hornblende (average size 1.5 x 0.4 mm), plagioclase (average size 0.4 x 0.4 mm), biotite (up to 1.0 x 0.4 mm) and opaques. Some of the larger grains of hornblende are surrounded by equigranular polygonal aggregates of secondary (?) hornblende. Garnets occur as fine granular intermittent rims around opaques, biotite and hornblende.

A325-990. Hypersthene phlogopite plagioclase rock.

Microstructure: Inequigranular, lepidoblastic to granoblastic; grain boundaries are straight or serrated.

Minerals Present: Consists of hypersthene (up to 1.5 mm in diameter) often poikiloblastic, phlogopite with well developed kink bands, plagioclase subidioblastic to idioblastic grains with deformation twinning and undulose extinction (containing needle-like inclusions of sillimanite), quartz as small grains with undulose extinction and also as sutured granoblastic aggregates, marginal to or penetrating the undulose grains. Accessories include apatite, zircon and rutile. The latter occurs as inclusions in orthopyroxene.

A325-1328. Diopside phlogopite K-feldspar rock.

Microstructure: Inequigranular granoblastic to lepidoblastic, with curved, often slightly embayed grain boundaries.

Minerals Present: Consists of diopside (average size 0.7 x 0.4 mm), occasionally poikiloblastic with well developed multiple twins, orthoclase showing undulose extinction, large deformed laths of phlogopite up to 1.6 x 0.2 mm in size, and aggregates of apatite grains (average size 0.4 x 0.2 mm).

A325-425. Calc silicate rock.

Microstructure: Inequigranular granoblastic.

Minerals Present: Consists of diopside (up to 1.2 mm in diameter), plagioclase showing strong deformation twinning (average size 0.4 x 0.4 mm) and scapolite. Additional phases are sphene and zoisite. The latter mineral occurs either as needle-like inclusions in plagioclase or as narrow coronas around the polygonal clinopyroxene grains.

A325-531. Quartz two-feldspar garnet gneiss.

Microstructure: Inequigranular granoblastic; strongly developed schistosity.

Minerals Present: Consists predominantly of elongate ribbons of quartz with undulose extinction and recrystallized polygonal zones, wavy lenticular aggregates of feldspar, 'stringlet' perthite and plagioclase. Grain sizes range from 1.5 cm x 2.0 mm to less than 0.04 x 0.04 mm. Garnets are large (ranging from 1.0 x 1.0 mm to 7.0 x 5.0 mm) and commonly poikiloblastic with inclusions of quartz, biotite, plagioclase and sillimanite. Opaques commonly contain laths of corundum. Biotite with red brown pleochroism is a minor constituent. Accessory apatite is present in trace quantities.

A325-396. Hornblende clinopyroxene quartzo-feldspathic gneiss.

Microstructure: Inequigranular; strongly developed lineation manifest in granoblastic texture in the N section and lenticular or platey

granoblastic texture in the P and S section. Grain boundaries are highly sutured.

Minerals Present: Consists of large lenticular grains of quartz (up to 3.0 mm long in the N section) with undulose extinction, polygonal recrystallized quartz occurs in zones through, and marginal to the larger strained grains. Perthite occurs as irregular angular grains with prominent stringlet-type exsolution and slight development of shadowy cross-hatched twinning. Hornblende occurs as ragged green pleochroic grains. Pale green diopside occurs in minor amounts as small subhedral grains. The hornblende is commonly surrounded by aggregates of brown to orange brown biotite. Both hornblende and opaque oxides are surrounded by coronas of granular garnet. Apatite, sphene and zircon occur in trace amounts.

A325-400. Hornblende quartzo-feldspathic gneiss.

Microstructure: Inequigranular to equigranular platy granoblastic; curved, embayed or sutured grain boundaries.

Minerals Present: Essentially the same mineralogy as A325-396 except that plagioclase forms irregular discrete grains with some development of albite twinning. Shadowy cross-hatched twinning developed in the alkali feldspars. Stringlet, bead and rod perthites developed.

A325-323. Hornblende biotite quartzo-feldspathic gneiss.

Microstructure: Inequigranular to equigranular lozenge shaped grains surrounded by anastomosing layers forming diamond shaped domains; strongly developed schistosity; lineation more weakly defined; grain boundaries straight or serrated.

Minerals Present: Highly strained quartz, perthite and plagioclase occur as lozenge shaped grains often with recrystallized margins and sutured boundaries. Quartz is also present as long recrystallized lentils (a component of the anastomosing layers). Mafics consist of biotite and green hornblende, both surrounded by granular garnet. Trains of biotite and granular garnet also define the anastomosing layers. Zircon is present in accessory amounts.

A325-783. Orthopyroxene bearing quartzo-feldspathic gneiss.

Microstructure: Inequigranular granoblastic; grain boundaries curved, embayed or sutured.

Minerals Present: Consists predominantly of highly strained quartz (average size 0.4 x 0.4 mm) and perthitic alkali feldspar (average size 0.6 x 0.6 mm). The strained domains in the quartz have sutured boundaries and undulose extinction. Stringlet, rod and ribbon perthite is present. Minor constituents include hypersthene, clinopyroxene and opaque oxides and the orthopyroxene. Minerals present in accessory amounts include apatite, zircon and allanite.

A325-474. Biotite quartzo-feldspathic gneiss.

Microstructure: Inequigranular granoblastic; sutured and embayed grain boundaries.

Minerals Present: Composed of anhedral grains of perthitic alkali feldspar, plagioclase, quartz, laths of biotite and granular opaque oxides. Minor constituents include euhedra of zircon and apatite. Quartz occurs either as strained grains or mosaics of small recrystallized grains. Most of the perthite is bead or stringlet-type. The quartz generally occurs interstitial to the anhedra of feldspar. Plagioclase grains contain needle-like inclusions of sillimanite.

A325-18. Gneissic granite.

Microstructure: Inequigranular, allotriomorphic granular.

Minerals Present: The rock consists predominantly of perthitic alkali feldspar and plagioclase (average size 0.4 x 0.4 mm). Quartz occurs either as unstrained granular aggregates between the feldspar grains or as larger grains (average size 0.3 x 0.3 mm) with undulose extinction. Biotite occurs as irregular laths and yellow dark brown granules of opaque oxides. The perthitic alkali feldspar displays bead and stringlet types of exsolution. Shadowy cross-hatched twinning is well developed. Plagioclase is commonly twinned under the albite law. Myrmekite is developed around the margins of the plagioclase grains. Accessories

include apatite and zircon.

A325-326. Orthopyroxene plagioclase quartzo-feldspathic gneiss.

Microstructure: Inequigranular granoblastic; grain boundaries range from straight to embayed.

Minerals Present: The rock consists predominantly of strongly deformed xenoblastic antiperthitic plagioclase (average size 0.4 x 0.4 mm), with complex deformation twins and undulose extinction. Quartz occurs as large aggregates with undulose extinction. The margins of these grains are often recrystallized to a granular mosaic of unstrained polygonal grains. The principal ferromagnesian component is hypersthene (average size 0.4 x 0.2 mm). It is commonly surrounded by narrow coronas of granular garnets and sometimes fibrous secondary amphibole. Opaque oxides and biotite are also present. The former phase is frequently mantled by selvages of garnet and the latter by secondary amphibole. Needle-like idioblastic inclusions of sillimanite occur in the plagioclase grains and along some grain boundaries. Other minerals present in trace amount include apatite and clinozoisite.

A325-405. Clinopyroxene plagioclase quartzo-feldspathic gneiss.

Microstructure: Equigranular to inequigranular granoblastic; grain boundaries range from straight to embayed.

Minerals Present: The main felsic constituents of the rock are antiperthitic plagioclase and quartz. Diopside is the major mafic phase. The plagioclase and quartz grains average 1.0 mm in diameter and are deformed. Quartz grains show undulose extinction and recrystallization zones while complex twin patterns are developed in the feldspar. Twin lamellae are commonly bent. The clinopyroxene grains average 0.1 x 0.3 mm and are commonly surrounded by granules of epidote. Granular selvages of garnet are sometimes present around opaque oxides. Minerals present in trace amounts include corundum, allanite and sphene.

A.I.3. Amphibolite Facies Lithologies

A325-1659. Biotite garnet quartzo-feldspathic gneiss.

Microstructure: Medium to fine grained, inequigranular, granoblastic to porphyroblastic; grain boundaries variable.

Minerals Present: Composed of xenoblastic grains of alkali feldspar, plagioclase and quartz (grain sizes range from less than 0.08 x 0.08 mm to greater than 5.0 x 3.0 mm) together with decussate biotite (pleochroic α neutral to $\beta = \gamma$ brown green), symplectic idioblastic to xenoblastic garnet and skeletal opaque oxides form sub-parallel aggregates. Carlsbad and grid-iron twinning is common in the alkali feldspars. Some plagioclase grains display wart-like growths of myrmekite. The majority of the quartz occurs as unstrained recrystallized grains. Accessories include sphene, apatite, zircon and epidote.

A325-1744. Biotite garnet microcline quartzo-feldspathic gneiss.

Microstructure: Medium to coarse grained, extremely large porphyroblasts up to 2.0 x 3.0 cm in size surrounded by irregular lenticular anastomosing layers composed of lepidoblastic and granoblastic elements. Grain shapes are variable.

Minerals Present: Similar mineralogy to A325-1659 and 1636a.

A325-1636a. Biotite garnet quartzo-feldspathic gneiss.

Microstructure: Porphyroblastic with groundmass composed of thin anastomosing layers of recrystallized grains and decussate aggregates of biotite flakes; grain boundaries are curved or sutured.

Minerals Present: Essentially the same mineralogy as A325-1659 with the exception that microcline is perthitic and muscovite is present as an additional phase.

A325-1684. Amphibolite.

Microstructure: Fine grained inequigranular granoblastic; grain boundaries curved or sutured.

Minerals Present: Principal constituents are slightly deformed

hornblende (α pale yellow, β pale blue green, γ blue green) and plagioclase (with well developed albite and pericline twins). Minerals present in subordinate amounts include biotite (α neutral, $\beta=\gamma$ brown), strained and commonly recrystallized sphene and garnet (coronas around skeletal opaques). Accessories include apatite, zircon and epidote.

A325-1748. Amphibolite.

Microstructure: Fine grained inequigranular granoblastic; strongly deformed; grain boundaries are curved.

Minerals Present: Consists predominantly of xenoblastic grains of deformed hornblende, pleochroic (α pale yellow, β pale green brown, γ green to green brown) (average size 0.6 x 0.6 mm), surrounded by polygonal aggregates of recrystallized hornblende (?). Plagioclase occurs in smaller amounts and shows signs of deformation, with the development of complex twin patterns, undulose extinction and bent twin lamellae. Minerals present in subordinate amounts include garnet, biotite (which is also kinked and recrystallized), quartz and clinopyroxene.

A325-1687. Biotite garnet corundum schist.

Microstructure: Medium to fine grained, porphyroblastic rock with a xenoblastic and lepidoblastic groundmass. Grain boundaries are straight or curved.

Minerals Present: Plagioclase, biotite (α pale green, $\beta=\gamma$ brown black), muscovite, corundum, garnet and opaque oxides. The muscovite apparently crystallized later than the biotite; both occur either as discrete laths or as decussate clusters. Some incipient recrystallization of the biotite is present along kink boundaries. Garnet and corundum occur as poikiloblastic porphyroblasts.

TECHNIQUES

A.2.1. Sample Preparation for Analysis

Fresh 400 gm slabs of each of the rocks to be analysed were cut into 3.0 x 3.0 cm cubes to facilitate crushing. They were then ground with carborundum and washed with distilled water in an ultrasonic cleaner for 5 to 10 minutes. They were then allowed to dry thoroughly.

The cubes were crushed to fragments about 5 mm in diameter by means of a fly press (with stainless steel plates) making sure no loss resulted. The samples were then crushed in a Siebtechnik mill using a chrome steel grinding vessel¹ until the powder was finer than 120 mesh.

The samples were thoroughly homogenized by rolling them on sheets of glazed paper for 10 minutes. They were then divided by means of a perspex hopper-type sample splitter into 50-70 gm samples for bulk and trace element analysis. 10 gm grab samples were further crushed using a 10 ml capacity tungsten carbide grinding vessel in the Siebtechnik mill. The resulting powder was used for X-ray spectrographic and wet chemical analysis.

The powder remaining after the portions for whole rock analysis had been removed were prepared for mineral separation by washing them in water and decanting off the dust fraction. When the samples were finally dust free they were rinsed in acetone and dried.

A.2.2. Mineral Separation

Mineral separations were carried out using standard techniques. Most separations were performed on the -120 + 180 mesh fraction. Highly magnetic minerals were removed by a hand magnet. The samples were then roughly separated by passing them through a Frantz Isodynamic Separator. Relatively pure concentrates of garnet, hornblende, orthopyroxene and clinopyroxene were obtained by gravity settling using

¹ The vessel was reported by its distributors to have the following composition: 0.12% V, 0.3% Si, 1.7% C, 12.0% Cr, 85.53% Fe.

Clerici's solution. In some instances the concentrates so obtained were further purified by repeated passes through the Frantz Separator. Alkali feldspars were purified from the Frantz concentrates by means of tetrabromoethane. Relatively pure mica concentrates were generally obtained directly from the Frantz. In all cases it was necessary to hand pick samples to achieve purities sufficient for analysis, viz. 99%.

The purified mineral fractions were washed in distilled water, dried and ground to a fine powder in the tungsten carbide Siebtechnik mill vessel.

A.2.3 Chemical Analysis

A.2.3.1 Major Elements - X.R.F.

Major elements, with the exception of FeO and Na₂O were analysed using X-ray fluorescence techniques (X.R.F.). Operating conditions are listed in Table A.2.1. Rock and mineral samples were fused with a lithium borate-lanthanum oxide mixture to produce a glass disc (cf. Norrish and Chappell (1967), Norrish and Hutton (1969)). They were analysed against an artificial standard 'FS 11' (supplied by C.S.I.R.O. Division of Soils, Adelaide, S.A.). The analytical techniques of Norrish and Hutton (1969) were followed during the analyses. U.S. Geological Survey standard rocks were repeatedly analysed with the Amata samples as a check on accuracy. Their analyses and calculated standard deviations are listed in Table A.2.2.

A.2.3.2 Na₂O

Sodium was determined using an EEL flame photometer. The samples were digested with hydrofluoric and perchloric acid in platinum crucibles following the method of Riley and Williams (1959). Blanks were run with all digestions to check for contamination. Standard solutions of Na₂O were used to calibrate the flame photometer.

Nine separate digestions were carried out on BCR-1 to check the precision of the digestion method. The following results were obtained:

$$\bar{x} = 3.39\% \text{ (cf. the average value given by Flanagan (1969))}$$

$$3.31\%$$

$$s = 0.082$$

TABLE A.2.1
OPERATING CONDITIONS FOR X.R.F. MAJOR ELEMENT ANALYSES

Element Determined	Primary Radiation	kV	mA	Analysing Crystal	Line	2θ	Counter	E.H.T.	Position
Si	Cr	60	40	P.E.T.	$K\alpha_1$	79.17	flow prop.	390.5	2
Al	Cr	60	40	P.E.T.	$K\alpha_1$	115.11	flow prop.	396.0	2
Ca	Cr	40	20	LiF ₂₀₀	$K\alpha_1$	113.20	flow prop.	385.0	1
Ti	Cr	40	20	LiF ₂₀₀	$K\alpha_1$	86.25	flow prop.	381.0	1
Σ Fe	Cr	60	40	LiF ₂₀₀	$K\alpha_1$	57.60	flow prop.	382.0	1
K	Cr	40	21.5	P.E.T.	$K\alpha_1$	20.69	flow prop.	387.0	2
P	Cr	60	40	G.E.	$K\alpha_1$	110.8	flow prop.	407.0	2
Mn	Mo	40	25	LiF ₂₀₀	$K\alpha_1$	63.05	flow prop.	379.0	1
Mg	Cr	60	40	A.D.P.	$K\alpha_1$	106.44	flow prop.	415.0	2

TABLE A.2.2
CHEMICAL ANALYSES OF STANDARD ROCKS BY X.R.F.

	G-2				GSP-1				BCR-1				DTS-1			
	Av.*	\bar{x}	n	S	Av.*	\bar{x}	n	S	Av.*	\bar{x}	n	S	Av.*	\bar{x}	n	S
SiO ₂	69.19	68.73	5	0.29	67.27	66.84	3	0.11	54.48	54.37	5	0.35	40.45	39.98	6	0.36
Al ₂ O ₃	15.34	15.34	5	0.09	15.11	15.33	3	0.01	13.65	13.61	5	0.11	0.55	0.27	6	0.11
Fe ₂ O ₃ (Total Fe)	2.76	2.67	5	0.00	4.33	4.24	3	0.00	13.50	13.49	5	0.17	8.85	8.75	6	0.20
MgO	0.78	0.97	5	0.04	0.95	1.01	3	0.11	3.28	3.51	5	0.15	49.80	50.11	6	0.35
CaO	1.98	1.91	5	0.06	2.03	2.04	3	0.03	6.95	6.98	5	0.10	0.15	0.09	6	0.03
K ₂ O	4.51	4.58	5	0.11	5.48	5.64	3	0.08	1.68	1.76	5	0.03	0.02	0.04	6	0.04
TiO ₂	0.53	0.52	5	0.00	0.69	0.70	3	0.00	2.23	2.31	5	0.02	0.02	0.04	6	0.00
MnO	0.03	0.06	5	0.01	0.04	0.07	3	0.00	0.17	0.21	5	0.02	0.12	0.16	6	0.01
P ₂ O ₅	0.14	0.12	5	0.03	0.28	0.29	3	0.01	0.36	0.35	5	0.02	0.01	0.01	6	0.00

* Compiled by Flanagan (1969)

\bar{x} Arithmetic mean calculated from analyses by the author

n Number of analyses

S Standard deviation

Solutions of the digested rocks were diluted to concentrations of less than 10 p.p.m. Na_2O , as the range 1-10 p.p.m. was found to give the optimum results on the flame photometer. To check the precision of the dilution method, seven dilutions of the same solution were carried out with the following results:

\bar{x} 3.40% Na_2O
s 0.04

The following Na_2O values were determined for the U.S.G.S. standard rocks (average values from Flanagan (1969) are given in parentheses):

G-2 4.11% (4.15%)
GSP-1 2.87% (2.88%)
DTS-1 not detected (0.04%)

A.2.3.4 FeO

Ferrous iron was determined by titration against a KMnO_4 solution (standardized against sodium oxalate). The rock and mineral samples were rapidly digested in a boiling mixture of conc. HF and conc. H_2SO_4 in a covered platinum crucible. Triplicate determinations of FeO were carried out on each sample; determinations differed by less than 0.1% FeO from each other. The values of total iron as Fe_2O_3 determined by X.R.F. were corrected for FeO and the difference was regarded as Fe_2O_3 .

The following FeO values were determined for the U.S.G.S. standard rocks (average values from Flanagan (1969) are given in parentheses):

G-2 1.52% (1.44%)
GSP-1 2.52% (2.30%)
BCR-1 8.92% (8.91%)
DTS-1 7.17% (6.79%)

A.2.3.5 Loss on Ignition

The loss on ignition values for the rocks were obtained by heating a previously weighed (half gram) sample in an electric furnace at 1000°C , to constant weight.

The loss for the minerals was obtained directly from the fused glass disc; the loss of weight of the flux being taken into account.

A.2.3.6 Trace Elements

Trace elements (except uranium*) were measured by X-ray fluorescence spectrography using finely powdered pressed mounts of the rock samples with a boracic acid backing (cf. Norrish and Chappell, 1967). Standard rocks were used for calibration and mass absorption corrections were applied.

Mass absorption values were calculated from the major element chemical analyses using the FORTRAN IV program given in Appendix 4.

The operating conditions of the X.R.F. for the different trace elements are given in Table A.2.3. The standards used are listed in Table A.2.4.

Background corrections were applied by calculating the slope factor between the peak and background positions.

ZrK_{α₁} values were corrected for interference from SrK_{β₁} by measuring the SrK_{α₁} counts, calculating the relationship between total counts SrK_{α₁} and SrK_{β₁} and subtracting the SrK_{β₁} counts from the ZrK_{α₁} counts.

A.2.4 X-Ray Diffraction

A.2.4.1 Alkali Feldspars

A Philips X-ray diffractometer was used to determine the structural state of the alkali feldspars. Samples were finely powdered, mixed with a silicon internal standard and smeared as an acetone-powder slurry onto an oriented quartz plate. Operating conditions of the machine were as follows:

Radiation	: CuKα
Generator	: 40 kv / 24 mA
Slit Width	: 1° - 1°
Counting rate	: 300 c.p.s.
M.P.E.	: 5%
Goniometer drive	: ½°/min.

* Determined by fluorimetric techniques at Australian Mineral Development Laboratories (AMDEL).

TABLE A.2.3
OPERATING CONDITIONS FOR X.R.F. TRACE ELEMENT ANALYSES

Element	Spectral Line	θ_{20}^*	Background $2\theta^*$	Primary Radiation	kv	mA	E.H.T.	Crystal	Collimator	Counter
Sr	$K\alpha_1$	35.85	34.79	Mo	60	40	354.5	LiF ₂₂₀	Coarse	Scint
Rb	$K\alpha_1$	37.97	39.03	Mo	60	40	354.5	LiF ₂₂₀	Coarse	Scint
Zr	$K\alpha_1$	31.95	32.65	Au	50	30	341	LiF ₂₂₀	Fine	Scint
Ba	$L\beta_1$	98.40	100.00	Cr	60	40	388	LiF ₂₂₀	Coarse	Scint
Th	$L\alpha_1$	39.15	38.65	Mo	60	40	358.5	LiF ₂₂₀	Fine	Scint
La	$L\alpha_1$	83.1	84.2	Au	50	30	379.0	LiF ₂₀₀	Fine	Flow Prop.
Ce	$L\beta_1$	111.7	110.2	Au	50	30	381.2	LiF ₂₂₀	Fine	Flow Prop.

* 2θ values taken from X.R.F. goniometer in December 1971. Realignment may cause slight fluctuations in the position of the peak and background.

TABLE A.2.4
STANDARDS USED IN TRACE ELEMENT ANALYSES

Element	Standard	Value	Source
Sr	AGV-1	653 p.p.m.	Dr. J.A. Cooper <u>pers.comm.</u> Dept. of Geology and Mineralogy, University of Adelaide.
Rb	NBS-70A	530 p.p.m.	"
Zr	G-2	320 p.p.m.	Carmichael (1967b)
Ba	G-2	2350 p.p.m.	"
Th	GSP-1	110 p.p.m.	"
La	GSP-1	155 p.p.m.	Dr. J.T. Hutton <u>pers.comm.</u> C.S.I.R.O. Division of Soils, Adelaide, S.A.
Ce	GSP-1	400 p.p.m.	"

The feldspar lines were indexed following the method of Wright and Stewart (1968). 2 θ values were calculated for the indexed peaks from the 2s measurements by a Diehl Combitron S Calculator program which corrected for chart drive variation. Cell dimensions were refined from the diffractometer powder data by use of a FORTRAN IV program adapted from a program written by Evans et al. (1963).

A.2.4.2 Powder Photographs

Powder photographs of the garnets, for cell edge determinations, were taken with a 114.6 mm diameter camera with Straumanis mounting. Spindles of the garnets were prepared by mixing powdered samples with tragacanth gum.

A.2.5 Electron Probe Analyses

The electron probe analyses were performed commercially by AMDEL (with the author in attendance) on a J.E.O.L. microprobe analyser. Analyses were carried out using a slightly defocussed beam (which varied in diameter from 2 to 10 μ), generated by an accelerating voltage of 15 kv. The specimen current was about 0.1 micro-amp. A chemically analysed pyroxene was used as a standard for the majority of the analyses. The results obtained were corrected by computer for mass absorption, atomic number and secondary fluorescence effects.

A.2.6 Petrographic Methods

A.2.6.1 Refractive Indices

Refractive indices for plagioclase and garnet were determined by plucking suitably oriented grains from thin sections and immersing them in oils of suitable refractive index. Oils were mixed until a match was obtained between the grain and the oil. The refractive index of the liquid was then measured using either an Abbé or a Leitz Jolley refractometer.

A.2.6.2 Modal Analyses

Modal analyses were carried out using a Swift Automatic Point Counter. 1500 to 2000 points were counted for each section examined.

CALCULATION OF THE MESONORM AND CATANORM

The mineralogical norm is a convenient way of listing the chemical analyses of rocks in terms of standard mineral molecules.

In this thesis the meso- and catanorms were calculated following a modified scheme proposed by Dr. A.W. Kleeman (pers.comm.) (Department of Geology and Mineralogy, University of Adelaide).

The methods of calculation proposed by Dr. Kleeman are given below.

A.3.1 Modified Calculation of the Mesonorm

All elements have been calculated as ionic percentages.

This version does not cope with elements F, Cl and S and takes no account of conditions where Na + K exceeds Al, nor of other unusual compositions.

1. The amount of Calcite (CaCO_3) is equal to 2 x amount CO.
Reduce Ca by the amount CO.
 2. The amount of Apatite ($\text{Ca}_5\text{P}_3\text{FO}_{12}$) is equal to 8/3 x amount P.
Reduce Ca by 5/3 x amount P.
 3. The amount of Orthoclase (KAlSi_3O_8) is equal to 5 x amount K.
Reduce Al by the amount K. Reduce Si by 3 x the amount K.
 4. The amount of Albite ($\text{NaAlSi}_3\text{O}_8$) is equal to 5 x amount Na.
Reduce Al by the amount Na. Reduce Si by 3 x amount Na.
 5. Test $\text{Ca} > 0.5\text{Al}$.
 - (a) $\text{Ca} > 0.5\text{Al}$ - all Al goes to form Anorthite ($\text{CaAl}_2\text{Si}_2\text{O}_8$).
The amount of anorthite is equal to 2.5 x amount Al.
Reduce Si by the amount Al. Reduce Ca by 0.5 x amount Al.
continue at Step 9
 - (b) $\text{Ca} < 0.5\text{Al}$ - all Ca goes to form Anorthite. The amount of anorthite is equal to 5 x amount Ca.
Reduce both Al and Si by 2 x amount Ca.
Remaining Al forms sillimanite. The amount of sillimanite is equal to 1.5 x amount Al.
Reduce Si by 0.5 x amount Al.
-

6. With no Ca remaining Ti forms Ilmenite (FeTiO_3).
The amount of Ilmenite is equal to 2 x amount Ti.
Reduce Fe2 by the amount Ti.
7. The amount of Magnetite (Fe_3O_4) is equal to 1.5 x amount Fe3.
Reduce Fe2 by 0.5 x amount Fe3.
8. To calculate biotite add Fe2 to Mg to form Fm.
Biotite ($\text{KMg}_3(\text{AlSi}_3\text{O}_{10})(\text{OH})_2$) is equal to $5\text{Or} + 3\text{Fm}$.
The amount of Biotite is equal to $8/3$ x amount Fm.
Reduce the amount Or calculated above (Step 3) by an amount equal to $5/3$ Fm.

(This concludes the norm calculation for rocks with normative sillimanite.)
9. Ca remains after Step 5a, hence Ti forms sphene CaTiSiO_5 .
The amount of Sphene is equal to 3 x amount Ti.
Reduce Ca and Si by amount Ti.
(In the unusual case where Ca is insufficient, make as much sphene as the Ca will allow, and then form Ilmenite as in Step 6 and continue through steps 7 and 8.)
10. The amount of Magnetite is calculated as in Step 8.
The amount of Magnetite is equal to 1.5 x amount Fe3.
Reduce Fe2 by amount equal to 0.5 x amount Fe3.
Add remaining Fe2 to Mg to form Fm.
11. If $\text{Ca} > \text{Fm}$ form Diopside ($\text{CaMgSi}_2\text{O}_6$) and Wollastonite (CaSiO_3) - all Fm goes into diopside.
The amount of Diopside is equal to 4 x amount Fm.
Reduce Si by 2 x the amount Fm. Reduce Ca by the amount Fm.
The amount of Wollastonite is equal to 2 x amount of Ca.
Reduce Si by the amount Qa.
12. If $\text{Ca} < \text{Fm}$ form Actinolite and either Biotite or Diopside.
(a) If $\text{Ca} > 0.4 \text{ Fm}$ form Actinolite and Diopside. CAH is equal to $2/3 (\text{Fm} - \text{Ca})$
The amount of Actinolite is equal to 7.5 x the amount CAH.

Reduce Si by 4 x amount CAH. Reduce Ca by the amount CAH.
 The amount of Diopside is equal to 4 x amount Ca.
 Reduce Si by 2 x amount Ca.

(b) If $Ca < 0.4 Fm$ form Actinolite and Biotite --

The amount of Actinolite is equal to 7.5 x amount Ca.

Reduce Si by 4 x amount Ca. Reduce Fm by 2.5 x amount Ca.

Remaining Fm forms biotite and if there is insufficient Or to
 convert all Fm to Biotite - Tschermackite $Ca_2(Mg_3Al_2)(Si_6Al_2)O_{22}$
 $(OH)_2$ is also formed.

If $Fm < 3/5 Or$ all biotite is formed as in Step 8.

If $Fm > 3/5 Or$ use up all Or.

Bi is equal to 8/5 x amount of Or.

Reduce Fm by amount equal to 3/5 x amount of Or.

Remaining Fm forms Tschermackite.

Amount Tsc is equal to 5 x amount Fm.

Reduce Si by amount equal to 2/3 x Fm.

Reduce An calculated in Step 5a - by amount equal to 10/3 x amount
 of Fm.

13. If Si is now reduced to a negative quantity there are two ways of
 saving silica.

$5Ab + 15Act$ is equal to $16Ed + 4Q$ and $5Ab$ is equal to $3Ne + 2Si$.

Ne is Nepheline ($NaAlSi_3O_8$).

Ed is Edenite ($NaCa_2Mg_5(AlSi_7O_{11})OH_2$)

if $Ab > 1/3 Act$ and deficiency of Si is $< 4/15 x Act$.

or $Ab < 1/3 Act$ and deficiency of Si is $< 4/5 x Ab$.

proceed as in 14 otherwise proceed as in 15.

14. The amount of Edenite is equal to 4 x deficiency of Si.

Reduce Albite calculated above by an amount equal to 5/4 x
 deficiency of Si.

Reduce Actinolite by amount equal to 15/4 x deficiency of Si.

15. If deficiency in Si is too great, make as much Edenite as possible - either:

(a) $Ab > 1/3 Act.$

The amount of Edenite is equal to $16/15$ x the amount of Actinolite.

Reduce the Si deficiency by amount equal to $4/15$ of amount of Actinolite.

Reduce Albite by an amount equal to $1/3$ of the amount of Actinolite.

Desilicate Albite to Nepheline as necessary $5Ab = 3Ne + 2Q.$

(b) $Ab < 1/3 Act.$

The amount of Edenite is equal to $16/5$ x amount of Albite.

Reduce the Silica deficiency by amount equal to $4/5$ x amount of Albite.

Reduce Actinolite by amount equal to 3 x amount of Albite.

NOTE: If there is still a deficiency of Silica after these two alternative steps (15(a) and (b)) the rock is too basic to apply this system of norm calculations. If the deficiency is trivial it can be ignored as possible analytical error.

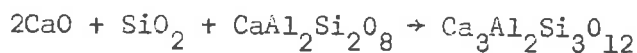
A.3.2 Modified Calculation of the Catanorm

Barth (1962) simply states that the catanorm should correspond in detail to the C.I.P.W. norm except that it is based on cation percentages and the minerals are calculated as molecular equivalents.

The present catanorm program follows the C.I.P.W. scheme in general, but inasmuch as it is designed for rocks metamorphosed in the granulite facies there are certain variations. Also it follows the modified mesonorm in calculating Titanium as sphene in subaluminous rocks.

With these qualifications the minerals formed in rocks similar in composition to igneous rocks would be those of the C.I.P.W. scheme. Peralkaline rocks form Acmite $NaFe^{3+}Si_2O_6$. Rocks with excess calcium

form Grossular $\text{Ca}_3\text{Al}_2\text{Si}_3\text{O}_8$ and Wollastonite, Grossular is formed from Anorthite according to the reaction:



Rocks richer in aluminium may form Pyralspite $(\text{Mg,Fe,Mn})_3\text{Al}_2\text{Si}_3\text{O}_{12}$, Cordierite $(\text{Mg,Fe})\text{Al}_4\text{Si}_5\text{O}_{18}$ and Sillimanite - or in rocks low in silica-spinel.

Calculation of the Catanorm from Cation Percentages

1. Apatite is formed from Ca and P in the proportions 5:3.
If Fluorine is reported in the analysis, an amount of F equal to $1/3 \times P$ should be deducted at this stage.
2. Calcite is formed from Ca and CO_3 in equal amounts.
In the rare case where CO_3 exceeds Ca the excess CO_3 will form Magnesite.
3. Fluorite is formed from an amount of Ca equal to half the amount of F remaining after Step 1.
4. Halite is formed from an amount of Na equal to the amount of Cl present.
5. Pyrite is formed from an amount of Fe^{2+} equal to half the amount of S present.
6. Anhydrite is formed from equal amounts of Ca and SO_4 .
7. Zircon is formed from equal amounts of Ca and SO_4 .
8. Orthoclase is formed from K, Al and Si in proportions 1:1:3.
9. Albite is formed from Na, Al, Si in the proportions 1:1:3.
In the general case where Al exceeds Na + K, Anorthite appears in the norm - Step 11.
If there is insufficient Al to use up all the Na, Acmite is formed - Step 10.
10. Acmite is formed from Na, Fe^{3+} , and Si in proportions 1:1:2.
If there is insufficient Fe^{3+} , the excess Na is combined with an equal amount of Si to form Sodium disilicate ($\text{Na}_2\text{Si}_2\text{O}_5$).
Proceed at Step 12 or 13.

11. Anorthite is formed from Ca, Al and Si in proportions 1:2:2.
12. If there is no Ca left at this stage, Ilmenite is formed from equal amounts of Ti and Fe^{2+} . In the rare case where Ti exceeds Fe^{2+} , Rutile is formed.
Magnetite is formed from Fe^{3+} and Fe^{2+} in proportions 2:1.
Excess Fe^{3+} is called Haematite.
Excess Fe^{2+} is combined with Mg, Mn and Ni to form Fm.
13. If there is still some Ca remaining after Step 11, Sphene is formed from Ca, Ti and Si in equal proportions. If there is excess Ti, Ilmenite is formed. Magnetite, Haematite and Fm are formed as in Step 12.
14. If Ca still remains after Step 13, there are two possibilities:
 - (a) Ca exceeds Fm; Diopside is formed with either Grossular or Wollastonite or both - Step 15.
 - (b) Ca is less than Fm; Diopside and Hypersthene are formed - Step 16.
15. Diopside is formed from Ca, Fm and Si in proportions 1:1:2.
Excess Ca is combined with any previously formed Anorthite and Si in the proportion 2:5:1 - to form Grossular.
Any excess Ca after this stage produces Wollastonite - by taking Ca and Si in equal proportions.
16. Diopside is formed from Ca, Fm and Si in proportions 1:1:2.
Excess Fm is added to an equal amount of Si to form Hypersthene.
17. Peraluminous rocks - have three possibilities:
If Fm/Al ratio exceeds 1.5, Pyralspite and Hypersthene are formed - Step 18.
If Fm/Al ratio lies between 1.5 and 0.5, Pyralspite and Cordierite are formed - Step 19.
If Fm/Al ratio is less than 0.5, Cordierite and Sillimanite are formed - Step 20.
18. Pyralspite is formed from Fm, Al and Si in proportions 3:2:3,
excess Fm is added to an equal amount of Si to form Hypersthene.

19. To calculate the amount of Al that goes to Pyralspite, rather than to Cordierite - use the formula $Al_{ga} = Fm - Al/2$.
Pyralspite is formed from Fm, Al_{ga} and Si in the proportions 3:2:3.
The remaining Al is added to Fm and Si in proportions 4:2:5 to form Cordierite.
20. All of the Fm is added to Al and Si in proportions 2:4:5 to form Cordierite.
The excess Al is added to Si in the proportions 2:1 to form Sillimanite.
21. At this stage all of the cations should have been used up and there should be either an excess or deficiency of Si.
Excess Si is called Quartz.
If there is a deficiency of Si, some minerals must be desilicated.
22. In rocks containing Diopside and Hypersthene, sufficient Hypersthene should be converted to Olivine to balance the Si budget.
 $4 \text{ Hyp} = 3 \text{ Ol} + \text{Si}$.
If this is insufficient Albite is reduced to Nepheline and Orthoclase to Kalsilite.
 $NaAlSi_3O_8 \rightarrow NaAlSiO_4 + 2SiO_2$ $5 \text{ Ab} = 3 \text{ Ne} + 2 \text{ Si}$
 $KAlSi_3O_8 \rightarrow KAlSiO_4 + 2SiO_2$ $5 \text{ Or} = 3 \text{ Kal} + 2 \text{ Si}$
23. In Peraluminous rocks the following reactions should be used in sequence:
- (a) $(Mg,Fe)_2Al_4Si_5O_{18} \rightarrow 2(Mg,Fe)Al_2O_4 + 5SiO_2$
 $11 \text{ Cord} = 6 \text{ Spin} + 5 \text{ Si}$
- (b) $(Mg,Fe)_3Al_2Si_3O_{12} \rightarrow (Mg,Fe)_2SiO_4 + (Mg,Fe)Al_2O_4 + 2SiO_2$
 $8 \text{ Pyral} = 3 \text{ Ol} + 3 \text{ Spin} + 2 \text{ Si}$
- (c) $Al_2SiO_5 \rightarrow Al_2O_3 + SiO_2$ $3 \text{ Sill} = 2 \text{ Cor} + \text{Si}$
- (d) $(Mg,Fe)_2Si_2O_6 \rightarrow (Mg,Fe)_2SiO_4 + SiO_2$ $4 \text{ Hyp} = 3 \text{ Ol} + \text{Si}$
- Beyond this feldspars may be desilicated as in Step 22.
24. These steps should reduce the silica deficiency in all normal rocks. If there is still a significant deficiency of Si the analysis should be calculated by a special procedure appropriate to the observed mineralogy.

LIST OF NORMATIVE MINERALS IN THE CATANORM

3.8

Symbol	Mineral	Ideal Composition	No. of Cations
Q	Quartz	SiO_2	1
OR	Orthoclase	KAlSi_3O_8	5
AB	Albite	$\text{NaAlSi}_3\text{O}_8$	5
AN	Anorthite	$\text{CaAl}_2\text{Si}_2\text{O}_8$	5
NEPH	Nepheline	NaAlSiO_4	3
KAL	Kalsilite	KAlSiO_4	3
NASIL	Sodium Disilicate	$\text{Na}_2\text{Si}_2\text{O}_5$ (= $\text{NaSiO}_{2.5}$)	2
SILL	Sillimanite	Al_2SiO_5	3
COR	Corundum	Al_2O_3	2
DIOP	Diopside	$\text{CaMgSi}_2\text{O}_6$	4
WO	Wollastonite	CaSiO_3	2
HYP	Hypersthene	MgSiO_3	2
AC	Acmite	$\text{NaFeSi}_2\text{O}_6$	4
OL	Olivine	Mg_2SiO_4	3
GROSS	Grossular	$\text{Ca}_3\text{Al}_2\text{Si}_3\text{O}_{12}$	8
PYRAL	Pyralspite	$(\text{Mg,Fe,Mn})_3\text{Al}_2\text{Si}_3\text{O}_{12}$	8
CORD	Cordierite	$\text{Mg}_2\text{Al}_4\text{Si}_5\text{O}_{18}$	11
APAT	Apatite	$\text{Ca}_5(\text{PO}_4)_3\text{F}$	8
CALC	Calcite	CaCO_3	2
MAS	Magnesite	MgCO_3	2
ANHY	Anhydrite	CaSO_4	2
FLU	Fluorite	CaF_2	1
HAL	Halite	NaCl	1
SPIN	Spinel	MgAl_2O_4	3
MAG	Magnetite	Fe_3O_4	3
ILM	Ilmenite	FeTiO_3	2
SPH	Sphene	CaTiSiO_5	3
RU	Rutile	TiO_2	1
HEM	Haematite	Fe_2O_3	2
PYR	Pyrite	FeS_2	1
ZIR	Zircon	ZrSiO_4	2

Note: In all formulae Mg denotes Mg + Fe²

CALCULATION OF MASS ABSORPTION COEFFICIENTS

The listing given below was written to calculate mass absorption values from oxide weight percentages, following the method described in Norrish and Chappell (1967, pp.168-169). Mass absorption coefficients for the absorbing elements at the wavelength corresponding to the spectral line of the trace element being determined were taken from Heinrich (1966). (See over page)

```

PROGRAM MASSAB (INPUT,OUTPUT,TAPE7=INPUT)
C PROGRAM TO CALCULATE MASS ABSORPTIONS FROM OXIDE PERCENTAGES
C WRITTEN BY A.W.KLEEMAN AND K.D.COLLERSON NOVEMBER 1971
REAL MG,MN,NA,K,LAL
10 PRINT 11
11 FORMAT(*1          MASS ABSORPTION CORRECTIONS *//
1*O  NO          RB-KA1      SR-KA1      ZR-KA1      BA-LB1      LA-LA1
2   CE-LB1      TH-LA1 *)
NL=0
20 READ 21,SPEC,SI,AL,FE3,FE2,MG,CA,NA,K,TI,MN
21 FORMAT(A6,8F4.2,2F3.2)
IF(EOF,7)99,22
22 CONTINUE
RBK=NA*.06216+MG*.06956+AL*.0781+SI*.08663+K*.29167+CA*.28972+      RB1
1TI*.31516+FE3*.55488+FE2*.61321+MN*.55298                          RB2
SRK=NA*.05345+MG*.05917+AL*.06675+SI*.07368+K*.24931+CA*.24827+      SR1
1TI*.27+FE3*.47504+FE2*.52504+MN*.47441                             SR2
ZRK=NA*.03903+MG*.04373+AL*.04917+SI*.05453+K*.18586+CA*.18481+      ZR1
1TI*.20125+FE3*.35473+FE2*.39211+MN*.35434                           ZR2
BAL=NA*1.07168+MG*1.20177+AL*1.3369+SI*1.46618+K*4.80647+          BA1
1CA*4.73367+TI*.76741+FE3*1.24074+FE2*1.31854+MN*1.18325           BA2
LAL=NA*1.42601+MG*1.69772+AL*1.91545+SI*2.11495+K*5.48445+        LA1
1CA*5.50742+TI*1.21765+FE3*1.37518+FE2*1.46445+MN*1.518           LA2
CEL=NA*.84366+MG*.94585+AL*1.0526+SI*1.15571+K*3.7964+CA*3.74146+      CE1
1TI*4.03379+FE3*.98065+FE2*1.0421+MN*.93559                         CE2
THL=NA*.06679+MG*.07582+AL*.08486+SI*.09377+K*.31774+CA*.3153+      TH1
1TI*.34234+FE3*.60304+FE2*.66651+MN*.60145                          TH2
50 PRINT 51,SPEC,RBK,SRK,ZRK,BAL,LAL,CEL,THL
51 FORMAT(1H0,A6,7(2X,F10.5))
NL=NL+1
IF(NL.GE.25)10,20
99 STOP
END

```

The codes RB1, RB2, SR1, SR2, etc. were punched in columns 73-80 as card identifications and do not form part of the program.

SUMMARY OF DATA FOR LINEAR REGRESSION ANALYSIS AND CALCULATION OF
REDUCED MAJOR AXES

Following the procedure described by Shaw (1968a) the variables used in the linear regression analysis of K and Rb data in Chapter 4.2 are:

$$x = 1 + \log_{10} (\%K)$$

$$y = \log_{10} (\text{p.p.m. Rb})$$

Both regression lines y on x and x on y were calculated. The regression lines are described by the equation $y = a + bx$, where a is the intercept and b is the regression coefficient. Data used in the calculation of the regression lines are presented in Table A.5.1.

The reduced major axis (R.M.A.) of the two regression lines (y/x and x/y) was calculated following the methods described by Miller and Kahn (1962). The R.M.A. is described by the equation $y = b + Kx$ where K is the slope of the line and b is the intercept. A summary of data used in the construction of the reduced major axes is presented in Table A.5.2.

TABLE A.5.1
SUMMARY OF DATA FOR LINEAR REGRESSION ANALYSES

	Granulite Facies Terrain			Transitional Terrain					Amphibolite Facies Terrain
	Quartzo-feldspathic	Mafic	Total*	Quartzo-feldspathic	Mafic	Micaceous Mafic	Total Mafic	Total	Total
n	6	12	19	6	4	4	10*	16*	6
\bar{x}	1.2571	0.5541	0.7911	1.4690	0.5908	1.3987	0.8602	1.0751	1.4634
\bar{y}	1.5278	0.6305	0.9585	1.9561	0.9896	2.1789	1.4001	1.5963	2.0245
r _{xy}	0.9895	0.2645	0.8280	0.9875	0.8934	0.6761	0.9370	0.9295	0.9841
Regression y/x									
a	-0.4920	0.4555	0.0785	-1.0038	0.6121	0.7686	0.3311	0.2793	0.2108
b	1.6068	0.3159	1.1124	2.0149	0.6390	1.0083	1.2427	1.2250	0.6187
S _b	0.1177	0.3642	0.1827	0.1615	0.2272	0.7770	0.1544	0.1255	0.0561
t	13.6478	0.8672	6.0879	12.4753	2.8127	1.2977	8.0488	9.7629	11.0285
d.f.	4	10	17	4	2	2	8	14	4
Regression x/y									
a	0.3261	0.4145	0.2004	0.5224	-0.6454	0.4109	-0.1289	-0.0508	-0.2659
b	0.6094	0.2215	0.6163	0.4839	1.2491	0.4534	0.7065	0.7053	1.5652
S _b	0.0445	0.2554	0.1012	0.0388	0.4441	0.3494	0.0878	0.0723	0.1414
t	13.7035	0.8672	6.0879	12.4739	2.8127	1.2977	8.0488	9.7629	11.0693
d.f.	4	10	17	4	2	2	8	14	4

* Including A325-2050C

n = number of samples
r_{xy} = coefficient of correlation
S_b = standard error of regression coefficient
d.f. = number of degrees of freedom (n-2)

TABLE A.5.1

DATA FOR ADIRONDACK HIGHLANDS TAKEN FROM WHITNEY (1969, p.1206)

	Granulite Facies	Amphibolite Facies	
	Paragneiss	Paragneiss	Granite Gneiss
n	22	20	9
\bar{x}	1.4562	1.4484	1.5303
\bar{y}	1.9687	2.0844	2.1153
rx _y	0.9191	0.3550	0.9613
Regression y/x			
a	0.6393	1.6238	0.6794
b	0.9130	0.3180	0.9383
S _b	0.0875	0.1974	0.1016
t	10.4338	1.6110	9.2341
d.f.	20	18	7
Regression x/y			
a	-0.3656	0.6225	-0.5530
b	0.9254	0.3962	0.9849
S _b	0.0887	0.2460	0.1067
t	10.4338	1.6110	9.2340
d.f.	20	18	7

TABLE A.5.2
SUMMARY OF DATA FOR REDUCED MAJOR AXES

Granulite Facies Terrain

	Quartzo- feldspathic	Mafic	Total
K	1.6240	1.1941	1.3435
S _k	0.0958	0.3324	0.1728
b	-0.5137	-0.0311	-0.1043

Transitional Terrain

	Quartzo- feldspathic	Mafic	Micaceous Mafic	Total Mafic	Total
K	2.0406	0.7159	1.4908	1.3261	1.3180
S _k	0.1313	0.1608	0.5492	0.1397	0.1179
b	-1.0415	0.5667	0.0938	0.2594	0.1794

Amphibolite Facies Terrain

	Total
K	0.5772
S _k	0.0420
b	1.1798

Data for Adirondack Highlands taken from Whitney (1969, p.1206)

	Granulite Facies	Amphibolite Facies	
	Paragneiss	Paragneiss	Granite Gneiss
K	0.9943	0.8987	0.9808
S _k	0.0835	0.1879	0.0901
b	0.5209	0.7827	0.6144

S_k = standard error of slope K

PETROLOGY OF THE MAFIC ROCKS ('PLAGIOCLASE ECLOGITES'(?)) FROM THE
DAVENPORT SHEAR

As mentioned in Chapters 1 and 2, the Davenport Shear is composed essentially of a central core of altered basic 'igneous' rocks, bounded on the north by a narrow mylonite zone giving way to granulite facies lithologies and on the south by a more extensive mylonite zone which is gradational to the gneisses and mafic lithologies of the transitional terrain.

A.6.1 Petrography

In hand specimen the mafic rocks of the shear zone are generally massive, although a weak banding may be discerned on weathered surfaces. They are medium to fine grained and dark green to grey black in colour.

Two microstructural varieties are present, viz. a very fine grained microporphyroblastic variety (e.g. A325-907q) and a fine to medium grained granoblastic variety (e.g. A325-912h). The former variety seldom exhibits a schistosity in thin section; in contrast, the latter type displays a prominent schistosity.

Both varieties consist predominantly of aggregates of clinopyroxene and garnet together with small amounts of quartz and plagioclase. Hornblende is present in some sections. Rutile, biotite, epidote, sphene(?), zircon and opaques occur sporadically as accessories.

The following assemblages of essential phases have been recognised (these were verified in some cases by X-ray diffractometer traces):

1. clinopyroxene - garnet - quartz - plagioclase - opaques
2. clinopyroxene - garnet - quartz - plagioclase - opaques - amphibole
3. clinopyroxene - garnet - quartz - plagioclase - opaques - rutile - amphibole

The clinopyroxene occurs as irregular xenoblastic, often poikiloblastic grains up to 0.6 x 0.6 mm in size, averaging 0.02 x 0.02 mm and 0.3 x 0.1 mm in the two microstructural varieties respectively.

Grain boundaries are straight, curved or embayed. Grains commonly exhibit a faint pleochroism:

α neutral
β pale green
γ pale green

and they have low birefringence colours (upper first order) $2V\gamma$'s range from 62° to 75° .

Fractured idioblastic to xenoblastic poikiloblastic grains of garnet, pale pink in colour are ubiquitous. In the fine grained microporphyroblastic rocks they seldom exceed 0.02×0.02 mm in size whereas in the granoblastic fine to medium grained lithologies garnets range up to 0.6×0.6 mm in size. Grain boundaries are straight or curved. Irregular to rounded inclusions of quartz and feldspar are common.

Hornblende occurs as nematoblastic to xenoblastic grains with straight to embayed boundaries, averaging 0.02×0.02 mm and 0.4×0.2 mm in the two microstructural varieties respectively. As well as forming discrete grains it also forms small alteration zones around xenoblasts of clinopyroxene. The following pleochroic schemes have been observed:

α neutral to pale green
β pale green
γ blue green
and
α neutral
β pale brown green
γ brown green

with intensity $\gamma > \beta > \alpha$

Plagioclase and quartz occur as small xenoblastic grains averaging either less than 0.01×0.01 mm or 0.04×0.04 mm respectively in the two microstructural varieties. Grain boundaries are straight, embayed or serrated. The plagioclase occasionally displays faint albite twin lamellae. Where the plagioclase is untwinned it is extremely difficult to distinguish from quartz as both species have crisp extinction.

Biotite occurs as rare (α neutral, $\beta=\gamma$ dark brown) flakes averaging 0.3 x 0.07 mm in size. Microstructural relationships suggest that it may be of secondary origin; possibly altering from the garnet or clinopyroxene.

Irregular xenoblastic grains of rutile and opaque oxides aligned in trains parallel to the schistosity (in the fine to medium grained variety) range in size from less than 0.007 x 0.007 mm to greater than 0.04 x 0.02 mm.

A.6.2 Mineral Chemistry

Probe analyses of garnets, clinopyroxenes and a plagioclase from two specimens of the Davenport Shear are listed in Table A.6.1.

A.6.2.1 Garnets

Garnets from the two types of Davenport Shear Zone rocks; A325-907q (very fine grained microporphyroblastic variety) and A325-912k (fine to medium grained granoblastic variety) are compositionally similar with respect to almandine, viz. 56.1% and 54.4%. However, pyrope and grossularite contents vary considerably, viz. pyrope 21.2% and 12.5%, grossularite 21.2% and 32.2%. In contrast, the analysed garnet from the mafic granulite A325-1105 (Table 4.23) contains a significantly higher content of pyrope, 32.05%, and lower grossularite + andradite, 17.07%, and almandine, 48.96%.

A.6.2.2 Clinopyroxenes

Clinopyroxenes from the two lithologies are likewise quite similar in composition. They are characterized by moderately high Na_2O , viz. 3.71% and 4.64%, and Al_2O_3 , viz. 4.59% and 4.31%. With the exception of A325-14 (from the transitional terrain) the analysed clinopyroxenes from mafic granulites and transitional lithologies are significantly lower in SiO_2 and Na_2O , although they do show high contents of Al_2O_3 .

As the oxidation states of iron are not distinguished in microprobe analyses it was not possible to calculate the proportions of acmite, jadeite and Tschermak's silicate following the schemes proposed

TABLE A.6.1

MICROPROBE ANALYSES OF MINERALS FROM THE
DAVENPORT SHEAR ZONE LITHOLOGIES

SPECIMEN NO. A325/-	GARNET		CLINOPYROXENE		PLAGIOCLASE
	912k	907q	912k	907q	912k
SiO ₂	36.91	37.49	51.62	51.61	64.51
Al ₂ O ₃	21.34	22.17	4.31	4.59	21.29
ΣFe as FeO	25.52	26.26	10.04	8.19	0.02
MgO	3.28	5.57	10.11	11.20	0.01
CaO	11.79	7.83	19.72	20.62	2.28
Na ₂ O	n.m.	n.m.	4.64	3.71	12.55
TiO ₂	0.56	0.08	0.16	0.19	0.01
MnO	0.35	0.58	0.05	0.04	0.00
Total	99.78	99.98	100.65	100.15	100.67
<u>Structural Formulae</u>					
Si	5.844 ¹	5.864 ¹	1.933 ²	1.925 ²	
Al ^{IV}	0.156	0.136	0.067	0.075	
Al ^{VI}	3.827	3.951	0.123	0.126	
Ti	0.067	0.009	0.005	0.005	
Mg	0.774	1.299	0.564	0.623	
Fe ²⁺	3.379	3.435	0.314	0.255	
Mn	0.051	0.077	0.002	0.001	
Ca	2.000	1.312	0.791	0.824	
Na	-	-	0.337	0.268	
Z	6.000	6.000	2.000	2.000	
Y	3.893	3.960	1.008	1.011	
X	6.205	6.123	1.128	1.092	
<u>Proportions of End Members (assuming all Fe as Fe²⁺)</u>					
Almandine	54.4	56.1			Ab84.6
Spessartine	0.8	1.3			An15.4
Pyrope	12.5	21.2			
Grossularite	32.2	21.2			

1. Based on 24 oxygen atoms

2. Based on 6 oxygen atoms

Analyst: A.R. Milnes

by Yoder and Tilley (1962, pp.366-367) and White (1964, p.884). Therefore, it has not been possible to classify them unequivocally as omphacites; nevertheless, their chemistry and optical properties suggest that they have affinities with that group of pyroxene.

A.6.2.3 Plagioclase

The analysed plagioclase from A325-912k has the composition of oligoclase, a composition which is noteworthy in view of the lime rich character of the associated ferromagnesian phases.

A.6.3 Metamorphic Affinities

The presence of minerals listed above, viz. garnet, clinopyroxene, quartz, plagioclase and hornblende indicates that the rocks have 'eclogite' affinities.

In the early literature Hally (1822) used the term eclogite to denote a rock that was essentially composed of diallage (omphacite) and garnet accompanied by kyanite, quartz and amphibole. Eskola (1921) in a detailed review of the Norwegian eclogites, regarded eclogites as consisting predominantly of omphacite and Ca-Mg garnet. Banno (1966) was more liberal in his interpretation of the composition of minerals occurring in eclogites and used the term eclogite 'to denote rocks consisting mainly of Ca-rich clinopyroxene and pyrope-almandine garnet'. Green and Ringwood (1967) classified eclogites more specifically as rocks with basaltic chemistry and consisting of garnet (almandine-pyrope solid solution), clinopyroxene (having a high jadeite/Tschermak's silicate ratio) with or without minor amounts of quartz, kyanite, hypersthene or olivine. In particular they considered that plagioclase was absent as a primary phase from eclogites sensu stricto. However, they regard the 'plagioclase eclogite' described by Kozłowski (1958), containing pyroxene with a high jadeite/Tschermak's silicate ratio, as 'eclogite' even though it contained oligoclase. Church (1964) and Velde et al. (1970) described similar rocks from Donegal and the Uzerche area of central France, respectively. Green and Ringwood (1967) however considered that Church's 'plagioclase eclogites' were more strictly granulite facies lithologies as the pyroxenes were low in

jadeite and rich in acmite and Tschermak's silicate. The plagioclase bearing amphibole eclogites described by Velde et al. (1970) on the other hand contain clinopyroxene with a high jadeite to Tschermak's silicate ratio of 19 and therefore they have clear eclogitic affinities.

The rocks of the Davenport Shear are similar to both the 'plagioclase eclogite' described by Kozłowski (1958) and the amphibole eclogites described by Velde et al. (1970). For example, Kozłowski (1958) reports garnets with the composition almandine 52.4%, pyrope 19.5%, grossularite 27.0% and spessartine 0.15%. Velde et al. (1970) similarly describe grossularite rich garnets but with slightly higher pyrope contents, viz. almandine 46%, pyrope 25%, grossularite 28% and spessartine 1%. A relatively low pyrope content as in A325-912k, is not unknown in garnets from eclogites, e.g. Eskola (1921, p.31) describes a garnet from Vanelvsdalen, Norway with almandine 60.2%, pyrope 13.8%, spessartine 1.3% and grossularite + andradite 24.3%. In Coleman et al.'s (1965) classification of eclogites based on pyrope contents, the garnet bearing rocks of the Davenport Shear zone can be equated with the Group C eclogites which contain garnets with less than 30% pyrope.

In the absence of jadeite/Tschermak's silicate ratios for the pyroxenes from the Davenport Shear it cannot be stated unequivocally that these rocks contain omphacitic pyroxene. However, the high $2V\gamma$'s and sodium rich character of the clinopyroxenes is in support of their having an omphacitic composition.

It is highly likely therefore that the Davenport Shear Zone mafic rocks have 'eclogitic' affinities. They are regarded as metamorphosed basic igneous rocks (probably dolerites) which were intruded into the shear zone.

MOLE FRACTIONS OF ELEMENTS USED IN THE
CALCULATION OF DISTRIBUTION COEFFICIENTS

SPECIMEN NO. A325/-	$X_{Fe^{2+}}^{opx}$	$X_{Fe^{2+}}^{cpx}$	$X_{Mg^{2+}}^{opx}$	$X_{Mg^{2+}}^{cpx}$	$X_{Fe^{2+}}^{Hb}$	X_{Mg}^{Hb}
339	0.4011	0.2956	0.5989	0.7044	0.2848	0.7152
295	0.2935	0.2349	0.7065	0.7651	-	-
523	0.3318	0.2676	0.6682	0.7324	0.2977	0.7023
517	0.3604	0.2930	0.6396	0.7070	-	-
81	0.3852	0.3367	0.6148	0.6633	-	-
138b	0.4495	0.3873	0.5505	0.6127	-	-
119	0.4342	0.3137	0.5658	0.6864	-	-
1105	0.3824	0.3433	0.6176	0.6567	0.3385	0.6615
121	0.4032	0.3048	0.5968	0.6952	-	-
60	0.3371	0.2756	0.6630	0.7247	-	-
949	0.2565	0.2100	0.7435	0.7900	0.2808	0.7192

REFERENCES

- ABDULLAH, M.I., 1965. The Fe-Ti oxide phases in metamorphism, in Controls of Metamorphism. Pitcher, W.S. & Flinn, G.W. (Eds.) Oliver and Boyd, Edinburgh, 368 pp.
- ABDULLAH, M.I. & ATHERTON, M.P., 1964. The thermometric significance of magnetite in low grade metamorphic rocks. Am. J. Sci., 262, 904-917.
- ADAMS, F.D. & BARLOW, A.E., 1910. Geology of the Haliburton and Bancroft areas, Province of Ontario. Geol. Surv. Canada Mem. 6, 419 pp.
- ALBEE, A.L., 1952. Comparison of the chemical analyses of sedimentary and metamorphic rocks. Bull. geol. Soc. Am., 63, 1229.
- ALTHAUS, E., 1968. Der einfluss des wassers auf metamorphe mineralreaktionen. Neues Jb. Miner. Mh., 9, 289-305.
- ALTHAUS, E., 1969. Das system $Al_2O_3 - SiO_2 - H_2O$. Experimentelle untersuchungen und folgerungen für die petrogenese der metamorphen gesteine. Neues Jb. Miner. Abh., 111, 74-161.
- ALTHAUS, E., KAROTKE, E., NITSCH, K.-H. & WINKLER, H.G.F., 1970. An experimental re-examination of the upper stability limit of muscovite plus quartz. Neues Jb. Miner. Mh., 1970, 325-336.
- ANNERSTEN, H., 1968. A mineral chemical study of a metamorphosed iron formation in Northern Sweden. Lithos, 1, 374-397.
- AOKI, K., 1971. Petrology of mafic inclusions from Itinome-gata, Japan. Contr. Miner. Petrology, 30, 314-331.
- AOKI, K. & KUSHIRO, I., 1968. Some clinopyroxenes from ultramafic inclusions in Dreiser Weiher, Eifel. Contr. Miner. Petrology, 18, 326-337.
- ARHENS, L.H., PINSON, W.H. & KEARNS, M.M., 1952. Association of rubidium and potassium and their abundance in igneous rocks and meteorites. Geochim. cosmochim. Acta, 2, 229-242.

- ARRIENS, P.A. & LAMBERT, J.B., 1969. On the age and strontium isotopic geochemistry of granulite-facies rocks from the Fraser Range, Western Australia and the Musgrave Range, Central Australia. *Spec. Publs. geol. Soc. Aust.*, 2, 377-388.
- ATHERTON, M.P., 1965. Composition of garnet in regionally metamorphosed rocks, in *Controls of Metamorphism*, Pitcher, W.S. & Flinn, G.W. (Eds.), Oliver and Boyd, Edinburgh, 368 pp.
- BALK, R., 1952. Fabrics of quartzite near thrust faults. *Bull. geol. Soc. Am.*, 60, 415-536.
- BANNO, S., 1964. Alumina content of orthopyroxene as a geologic barometer. *Jap. J. Geol. Geogr.*, 35, 117-121.
- BANNO, S., 1966. Eclogite and eclogite facies. *Jap. J. Geol. Geogr.*, 37, 105-122.
- BANNO, S. & MATSUI, Y., 1966. Intracrystalline exchange equilibrium in orthopyroxene. *Proc. Jap. Acad.*, 42, 629-633.
- BANNO, S., TATSUMI, T., OYURA, Y. & KATSURA, T., 1963. Petrographic studies on rocks from the area around Lützow-Holmbukta. In *Adie R.J. (Ed.), Antarctic Geology, Proc. 1st Int. Symp. Antarct. Geol.*, North Holland Publ. Co., Amsterdam, 405-414.
- BARD, J.P., 1970. Composition of hornblendes formed during the Hercynian progressive metamorphism of the Ararcena Metamorphic Belt, S.W. Spain. *Contr. Miner. Petrology*, 28, 117-134.
- BARNES, L., 1968. The petrography and geochemistry of some high grade metamorphic rocks from the Mt. Davies-Giles region, central Australia. Unpublished Honours thesis, Univ. Adelaide.
- BARTH, T.F.W., 1959. Principles of classification and norm calculations of metamorphic rocks. *J. Geol.*, 67, 135-152.
- BARTH, T.F.W., 1962. A final proposal for calculating the mesonorms of metamorphic rocks. *J. Geol.*, 70, 497-498.
- BARTH, T.F.W., 1966. Aspects of the crystallization of quartzofeldspathic plutonic rocks. *Tschermaks Min. Petr. Mitt.*, 11, 209-222.

- BARTH, T.F.W., 1969. Granulite facies rocks of the Precambrian of South Norway, particularly around Arendal. *Sciences de la Terre*, 14, 359-369.
- BARTHOLOME, P., 1961. Co-existing pyroxenes in igneous and metamorphic rocks. *Geol. Mag.*, 98, 346-348.
- BARTHOLOME, P., 1962. Iron-magnesium ratio in associated pyroxenes and olivines. *In* Engel, A.E.J., James, H.L. & Leonard, B.F. (Eds.), *Petrological Studies (Buddington Volume)*, Geol. Soc. Am., 660 pp.
- BASEDOW, H., 1905. Geological report on the country traversed by the S.A. Government Prospecting Expedition, 1903. *Trans. R. Soc. S. Aust.*, 29, 51-102.
- BASTA, E.Z., 1960. Natural and synthetic titanomagnetites (the system $\text{Fe}_3\text{O}_4 - \text{Fe}_2\text{TiO}_4 - \text{FeTiO}_3$). *Neues Jb. Miner. Abh.*, 94, 1017-1048.
- BEHR, H.J., DEN TEX, E., DE WAARD, D., MEHNERT, K.R., SCHARBERT, H.G., SOBOLEV, V.St., WATZNAUER, A., WINKLER, H.G.F., WYNNE-EDWARDS, H.R., ZOUBEK, V. & ZWART, H.J., 1971. Granulites, results of a discussion. *Neues Jb. Miner. Mh.*, 1971, 97-123.
- BERTHELSEN, A., 1960. Structural studies in the Precambrian of west Greenland, geology of Tovquassap nuna. *Meddr. Grønland*, 123, 223 pp.
- BHATTACHARYYA, C., 1970. Pyroxene and biotite from the charnockitic rocks of Garbham area, Srikakulam district, Andhra Pradesh, India. *Miner. Mag.*, 37, 682-692.
- BHATTACHARYYA, C., CHOUDHURY, S. & NANDI, K., 1970. Metamorphic status of charnockitic garnet with a note on the garnet from granulitic rocks of the Eastern Ghats, Srikakulam district, Andhra Pradesh, India. *Neues Jb. Miner. Mh.*, 2, 83-92.
- BINNS, R.A., 1962. Metamorphic pyroxenes from the Broken Hill district, New South Wales. *Miner. Mag.*, 33, 320-338.

- BINNS, R.A., 1964. Zones of progressive regional metamorphism in the Willyama Complex, Broken Hill, N.S.W. *J. geol. Soc. Aust.*, 11, 283-320.
- BINNS, R.A., 1965a. The mineralogy of metamorphosed basic rocks from the Willyama Complex, Broken Hill district, New South Wales. Part I: Hornblendes. *Miner. Mag.*, 35, 306-326.
- BINNS, R.A., 1965b. The mineralogy of metamorphosed basic rocks from the Willyama Complex, Broken Hill district, New South Wales. Part II: Pyroxenes, garnets, plagioclases and opaque oxides. *Miner. Mag.*, 35, 561-587.
- BINNS, R.A., 1969. Ferromagnesian minerals in high grade metamorphic rocks. *Spec. Publs. geol. Soc. Aust.*, 2, 323-332.
- BINNS, R.A., DUGGAN, M.B. & WILKINSON, J.F.G., 1970. High pressure megacrysts in alkaline lavas from north-eastern New South Wales. *Am. J. Sci.*, 269, 132-168.
- BOETTCHER, A.L. & WYLLIE, P.J., 1968. Melting of granite with excess water to 30 kilobars pressure. *J. Geol.*, 76, 235-244.
- BÖHM, A., 1883. Über die gesteine des uechsels. *Min. u. Petr. Mitt.*, 5.
- BOLFA, J., De La ROCHE, H., KERN, R. & CAPITANT, M., 1961. Sur la nature mineralogique exacte d'exsolutions dans les 'ilmenites' de Vohibarika (Madagascar) déterminée à la microsonde electronique. *Bull. Soc. franc. Miner. Crist.*, 84, 400-401.
- BOWES, D.R., WRIGHT, A.E. & PARK, R.G., 1961. Field relations of rocks containing co-existing pyroxenes. *Geol. Mag.*, 98, 530-531.
- BOYD, F.R. & ENGLAND, J.L., 1960. Minerals of the mantle. *Carnegie Inst. Wash. Yearb.*, 59, 47-52.
- BOYD, F.R. & ENGLAND, J.L., 1964. The system enstatite-pyrope. *Carnegie Inst. Wash. Yearb.*, 63, 157-161.
- BRACE, W.F., 1955. Quartzite pebble deformation in central Vermont. *Am. J. Sci.*, 253, 129-145.

- BRETT, R., 1964. Experimental data from the system Cu-Fe-S and their bearing on exsolution textures in ores. *Econ. Geol.*, 59, 1241-1269.
- BROOKS, C.K., 1969. On the distribution of zirconium and hafnium in the Skaergaard Intrusion, east Greenland. *Geochim. cosmochim. Acta.*, 33, 357-374.
- BROWN, H.Y.L., 1990. Report on journey from Warrina to Musgrave Ranges. *Parl. Paper S. Aust.*, paper 45.
- BUDDINGTON, A.F., 1939. Adirondack igneous rocks and their metamorphism. *Mem. geol. Soc. Am.*, 7, 354 pp.
- BUDDINGTON, A.F., 1963. Isograds and the role of H₂O in metamorphic faces of orthogneisses of the northwest Adirondack area, New York. *Bull. geol. Soc. Am.*, 74, 1155-1182.
- BUDDINGTON, A.F., FAHEY, J. & VLISIDIS, A., 1963. Degree of oxidation of Adirondack iron oxide and iron-titanium oxide minerals in relation to petrogeny. *J. Petrology*, 4, 138-169.
- BUDDINGTON, A.F. & LINDSLEY, D.H., 1964. Iron-titanium oxide minerals and their synthetic equivalents. *J. Petrology*, 5, 310-357.
- BUGGE, J.A.W., 1943. Geological and petrological investigations in the Kongsberg-Bamble formation. *Norges. geol. Unders.*, 160, 155 pp.
- BUMA, G., FREY, F.A. & WONES, D.R., 1971. New England granites: Trace element evidence regarding their origin and differentiation. *Contr. Miner. Petrology*, 31, 300-320.
- BURNHAM, W.C., 1967. Hydrothermal fluids at the magmatic stage. In Barnes, H.L. (Ed.), *Geochemistry of Hydrothermal Ore Deposits*. Holt, Rinehart and Winston, New York, 670 pp.
- BURNHAM, C.W. & SHADE, J.W., 1968. Hydrolysis equilibria in the system K₂O-Al₂O₃-SiO₂-H₂O. *Spec. Pap. Geol. Soc. Am.*, 101, 32-33.

- BURNS, R.G., 1966. Origin of optical pleochroism in orthopyroxenes. *Miner. Mag.*, 35, 715-719.
- BURNS, R.G., 1968. Crystal-field phenomena and iron enrichments in pyroxenes and amphiboles. *In* *Papers and Proc. 5th Gen. Meet. Int. Mineralog. Assoc. (1966)*, 170-183.
- BUTLER, P.Jr., 1969. Mineral compositions and equilibria in the metamorphosed iron formation of the Gagnon Region, Quebec, Canada. *J. Petrology*, 10, 56-101.
- CARMICHAEL, C.M., 1961. The magnetic properties of ilmenite-haematite crystals. *Proc. Roy. Soc. Lond.*, 263, 508-530.
- CARMICHAEL, I.S.E., 1963. The crystallization of feldspar in volcanic acid liquids. *Q. Jl. geol. Soc. Lond.*, 119, 95-131.
- CARMICHAEL, I.S.E., 1967a. The iron-titanium oxides of salic volcanic rocks and their associated ferromagnesian silicates. *Contr. Miner. Petrology*, 14, 36-64.
- CARMICHAEL, I.S.E., 1967b. Private communication to F.J. Flanagan in Flanagan, F.J., 1969. U.S. Geological Survey standards - 11 First compilation of data for the new U.S.G.S. rocks. *Geochim. cosmochim. Acta*, 33, 81-120.
- CARTER, N.L., CHRISTIE, J.M. & GRIGGS, D.T., 1964. Experimental deformation and recrystallization of quartz. *J. Geol.*, 72, 687-733.
- CHAKRAPANI NAIDU, M.G. & JAGANNATHA RAO, J., 1967. Co-existing pyroxenes from charnockitic rocks of Salur-Bobbili area, Srikakulam District, A.P. *Bull. Geochem. Soc. Ind.*, 2, 27-30.
- CHAYES, F., 1952. Notes on the staining of potash feldspar with sodium cobaltinitrate in thin sections. *Am. Miner.*, 37, 337-340.
- CHINNER, G.A., 1960. Pelitic gneisses with varying ferrous/ferric ratios from Glen Clova, Angus, Scotland. *J. Petrology*, 1, 178-217.

- CHRISTIE, J.M., 1963. The Moine thrust zone in the Assynt region of northwest Scotland. *California Univ. Pubs. Geol. Sci.*, 40, 345-440.
- CHURCH, W.R., 1964. Metamorphic eclogites from Co. Donegal, Eire. *Indian Mineral.*, *Internat. Mineral. Assoc. Special Paper No.* 22-23.
- CLARK, F.W., 1924. Data of geochemistry. *Bull. geol. Surv. U.S.*, 770, 841 pp.
- COIN, C.D.A., 1970. A study of the granulite facies terrain near Amata. Unpublished Honours thesis, Univ. Adelaide.
- COLEMAN, R.G., LEE, D.E., BEATTY, L.B. & BRANNOCK, W.W., 1965. Eclogites and eclogites; their differences and similarities. *Bull. geol. Soc. Am.*, 76, 483-508.
- COLLERSON, K.D. & ETHERIDGE, M.A., 1972. A contribution to the discussion of granulite terminology. *Neues Jb. Miner. Mh.* (in press).
- COLLERSON, K.D., OLIVER, R.L. & RUTLAND, R.W.R., 1972. An example of structural and metamorphic relationships in the Musgrave Orogenic Belt, central Australia. *J. geol. Soc. Aust.*, 18, 379-393.
- COOMBS, D.S., 1965. Sedimentary analcime rocks and sodium rich gneisses. *Miner. Mag.*, 34, 144-158.
- CONDIE, K.C. & LO, H.H., 1971. Trace element geochemistry of the Louis Lake batholith of early Precambrian age, Wyoming. *Geochim. cosmochim. Acta*, 35, 1099-1119.
- COORAY, P.G., 1969. Charnockites as metamorphic rocks. *Am. J. Sci.*, 267, 969-982.
- CROSBY, P., 1971. Composition and structural state of alkali feldspars from charnockitic rocks on Whiteface Mountain, New York. *Am. Miner.*, 56, 1788-1811.

- CURRIE, K.L., 1971. The reaction $3 \text{ Cordierite} = 2 \text{ Garnet} + 4 \text{ Sillimanite} + 5 \text{ Quartz}$ as a geological thermometer in the Opinicon Lake Region, Ontario. *Contr. Miner. Petrology*, 33, 215-226.
- DALZIEL, I.W.D. & BAILEY, S.W., 1968. Deformed garnets in a mylonitic rock from the Grenville front, Ontario, and their tectonic significance. *Am. J. Sci.*, 266, 542-562.
- DALZIEL, I.W.D., BROWN, J.M. & WARREN, T.E., 1969. The structural and metamorphic history of the rocks adjacent to the Grenville front near Sudbury, Ontario, and Mount Wright, Quebec. *Geol. Assoc. Can. Spec. Pap.*, 5, 207-224.
- DANIEL, V. & LIPSON, H., 1943. An X-ray study of the dissociation of an alloy of copper iron and nickel. *Proc. Roy. Soc. Lond.*, 181, 368-378.
- DANIEL, V. & LIPSON, H., 1944. The dissociation of an alloy of copper, iron and nickel: further X-ray work. *Proc. Roy. Soc. Lond.*, 182, 378-387.
- DAVIDSON, L.R., 1968. Variation in ferrous iron-magnesium distribution coefficients of metamorphic pyroxenes from Quairading, Western Australia. *Contr. Miner. Petrology*, 19, 239-259.
- DAVIDSON, L.R., 1969. Fe^{2+} - Mg^{2+} distribution in co-existing metamorphic pyroxenes. *Spec. Publs. geol. Soc. Aust.*, 2, 333-339.
- DAVIDSON, L.R., 1971. Metamorphic hornblendes from basic granulites of the Quairading district, Western Australia. *Neues Jb. Miner. Mh.*, 8, 337-384.
- DAWES, P.R., 1970. The plutonic history of the Tasiussaq area, south Greenland, with special reference to a high-grade gneiss complex. *Meddr. Grønland*, 189, 125 pp.
- DEER, W.A., 1938. The composition and paragenesis of the hornblendes of the Glen Tilt complex, Perthshire. *Miner. Mag.*, 25, 56-74.

- DEGENHARDT, H., 1957. Untersuchungen zur geochemischen verteilung des zirkonioms in der Lithosphäre. *Geochim. cosmochim. Acta*, 11, 279-309.
- DEMIN, A.M. & KHITAROV, D.N., 1958. Geochemistry of potassium, rubidium and thallium in application to problems in petrology. *Geokhimiya* (translation), 721-734.
- EADE, K.E., FAHRIG, W.F. & MAXWELL, J.A., 1966. Composition of crystalline shield rocks and fractionating effects of regional metamorphism. *Nature*, 211, 1245-1249.
- ECKELMANN, F.D. & POLDERVAART, A., 1957. Geological evolution of the Beartooth Mountains Montana and Wyoming, Pt. 1: Archean history of the Quad Creek area. *Bull. geol. Soc. Am.*, 68, 1225-1262.
- ENGEL, A.E.J. & ENGEL, C.G., 1951. Origin and evolution of hornblende andesine amphibolites and kindred facies. *Bull. geol. Soc. Am.*, 62, 1435-1436.
- ENGEL, A.E.J. & ENGEL, C.G., 1953. Grenville series in the north west Adirondack Mountains, New York. *Bull. geol. Soc. Am.*, 64, 1013-1097.
- ENGEL, A.E.J. & ENGEL, C.E., 1958. Progressive metamorphism and granitization of the major paragneiss, northwest Adirondack Mountains, New York. I: Total Rock. *Bull. geol. Soc. Am.*, 69, 1369-1414.
- ENGEL, A.E.J. & ENGEL, C.G., 1960. Progressive metamorphism and granitization of the major paragneiss, northwest Adirondack Mountains, New York. II: Mineralogy. *Bull. geol. Soc. Am.*, 71, 1-58.
- ENGEL, A.E.J. & ENGEL, C.G., 1962a. Progressive metamorphism of amphibolite, northwest Adirondack Mountains, New York. In Engel, A.E.J., James, H.L. & Leonard, B.F. (Eds.), *Petrological Studies* (Buddington volume). *Geol. Soc. Am.*, 660 pp.
- ENGEL, A.E.J. & ENGEL, C.G., 1962b. Hornblendes formed during progressive metamorphism of amphibolites, northwest Adirondack Mountains, New York. *Bull. geol. Soc. Am.*, 73, 1499-1514.

- ENGEL, A.E.J., ENGEL, C.G. & HAVENS, R.G., 1964. Mineralogy of amphibolite interlayers in the gneiss complex, northwest Adirondack Mountains, New York. *J. Geol.*, 72, 131-156.
- ERLANK, A.J., DANCHIN, R.V. & FULLARD, C.C., 1968. High K/Rb ratios in rocks from the Bushveld Igneous Complex, South Africa. *Earth Plan. Sci. Lett.*, 4, 22-29.
- ERNST., W.G., 1966. Synthesis and stability relations of ferro-tremolite. *Am. J. Sci.*, 267, 37-69.
- ESKOLA, P., 1921. On the eclogites of Norway. *Oslo Vidensk. Skr. Mat-Naturw. Kl.*, 8, 1-118.
- ESKOLA, P., 1939. Die metamorphen Geiteine, in Barth, T.F.W., Correns, C.W. & Eskola, P., Die entstehung der Geiteine. Julius Springer, Berlin.
- ESKOLA, P., 1952. On the granulites of Lapland. *Am. J. Sci.* (Bowen Volume), 133-171.
- ESKOLA, P., 1957. On the mineral facies of charnockites. *J. Madras Univ.*, 27, 101-119.
- EUGSTER, H.P., 1959. Reduction and oxidation in metamorphism. In Abelson, P.H. (Ed.), *Researches in Geochemistry*. Vol. I. John Wiley and Sons, New York. 511 pp.
- EUGSTER, H.P. & WONES, D.R., 1962. Stability relations of ferruginous biotite, annite. *J. Petrology*, 3, 82-125.
- EVANS, B.W., 1965. Application of a reaction rate method to the breakdown equilibria of muscovite and muscovite plus quartz. *Am. J. Sci.*, 263, 647-667.
- EVANS, B.W. & LEAKE, B.E., 1960. The composition and origin of the striped amphibolites of Connemara, Ireland. *J. Petrology*, 1, 337-363.
- EVANS, H.T. Jr., APPLEMAN, D.E. & HANDWERKER, D., 1963. The least squares refinement of crystal unit cells with powder diffraction data by an automatic computer indexing method (abstr.). *Amer. Crystallogr. Assoc., Ann. Meet. Prog.*, 42-43.

- FAHRIG, W.F., EADE, K.E. & ADAMS, J.A.S., 1967. Abundances of radioactive elements in crystalline shield rocks. *Nature*, 214, 1002-1003.
- FAURE, G. & HURLEY, P.M., 1963. The isotopic composition of strontium in oceanic and continental basalts: application to the origin of igneous rocks. *J. Petrology*, 4, 31-50.
- FLANAGAN, F.J., 1969. U.S. Geological Survey standards - II First compilation of data for the new U.S.G.S. rocks. *Geochim. cosmochim Acta*, 33, 81-120.
- FLEISCHER, M., 1965. Some aspects of the geochemistry of yttrium and the lanthanides. *Geochim. cosmochim. Acta*, 29, 755-772.
- FLEISCHER, M. & ALTSCHULER, Z.S., 1969. The relationship of the rare earth composition of minerals to geological environment. *Geochim. cosmochim. Acta*, 33, 725-732.
- FLETCHER, C.J.N., 1971. Local equilibrium in a two-pyroxene amphibolite. *Can. J. Earth Sci.*, 8, 1065-1080.
- FLEUTY, M.J., 1964. The description of folds. *Proc. Geol. Soc.*, 75, 461-492.
- FOSTER, M.D., 1960. Interpretation of the composition of trioctahedral micas. *Prof. Pap. U.S. geol. Surv.*, 354, 24-49.
- FRY, N. & FYFE, W.S., 1969. Eclogites and water pressure. *Contr. Miner. Petrology*, 24, 1-6.
- FYFE, W.S., 1970. Some thoughts on granitic magmas. In Newall, G. & Rast, N. (Eds.), *Mechanism of Igneous Intrusion*. Spec. Issue *J. Geol.*, 2, 201-216.
- FYFE, W.S., TURNER, F.J. & VERHOOGEN, J., 1958. Metamorphic reactions and metamorphic facies. *Geol. Soc. Am. Mem.* 73. 259 pp.
- GAST, P.W., 1965. Terrestrial ratio of potassium to rubidium and the composition of earth's mantle. *Science*, 147, 858-860.
- GAVRILOVA, L.K. & TURANSKAYA, R.V., 1958. Distribution of rare earths in rock forming minerals and accessory minerals of certain granites. *Geokhimiya*, (translation), 163-170.

- GHALY, T.S., 1969. Metamorphic differentiation in some Lewisian rocks of northwest Scotland. *Contr. Miner. Petrology*, 22, 276-289.
- GHOSE, S. & HAFNER, S., 1967. Mg^{2+} - Fe^{2+} distribution in metamorphic and volcanic orthopyroxenes. *Z. Kristallogr.*, 155, 157-162.
- GILBERT, M.C., 1966. Synthesis and stability relations of the hornblende ferropargasite. *Am. J. Sci.*, 264, 698-742.
- GILES, E., 1874. Parl. Paper S. Aust., Paper 215, 1-67 (with map). 'Mr. E. Giles's explorations, 1873'.
- GILL, J.B. & MURTHY, V.R., 1970. Distribution of K, Rb, Sr and Ba in Nain anorthosite plagioclase. *Geochim. cosmochim. Acta*, 34, 401-408.
- GJELSVIK, T., 1952. Metamorphosed dolerites in the gneiss area of Sunnmore on the west coast of southern Norway. *Norsk geol. Tidssk.*, 30, 33-134.
- GOLDSMITH, J.R. & LAVES, F., 1954. The microcline-sanidine stability relations. *Geochim. cosmochim Acta*, 5, 1-19.
- GOODE, A.D.T., 1970. The petrology and structure of the Kalka and Ewarara layered basic intrusions, Giles complex, central Australia. Unpublished Ph.D. thesis, Univ. Adelaide.
- GOODE, A.D.T. & KRIEG., G.W., 1965. The geology of Ewarara intrusion, Giles complex, central Australia. Unpublished Honours thesis, Univ. Adelaide.
- GOSSE, W.C., 1874. Parl. Paper S. Aust., Paper 48, 1-69. 'W.C. Gosse's explorations, 1873'.
- GREEN, D.H., 1964. The petrogenesis of the high-temperature peridotite intrusion in the Lizard area, Cornwall. *J. Petrology*, 5, 134-188.
- GREEN, D.H. & LAMBERT, I.B., 1965. Experimental crystallization of anhydrous granite at high pressures and temperatures. *J. geophys. Res.*, 70, 5259-5268.

- GREEN, D.H. & RINGWOOD, A.E., 1967. An experimental investigation of the gabbro to eclogite transformation and its petrological applications. *Geochim. cosmochim. Acta*, 31, 767-833.
- GREEN, T.H., 1967. An experimental investigation of sub-solidus assemblages formed at high pressure in high alumina basalt, kyanite eclogite and grosspydrite compositions. *Contr. Miner. Petrology*, 16, 84-114.
- GREEN, T.H., 1970. High pressure experimental studies on the mineralogical constitution of the lower crust. *Phys. Earth Planet Interiors*, 3, 441-450.
- GREEN, T.H., BRUNFELT, A.O. & HEIER, K.S., 1969. Rare earth element distribution in anorthosites and associated high grade metamorphic rocks, Lofoten-Vesteraalen, Norway. *Earth Plan. Sci. Lett.*, 7, 93-98.
- GREENWOOD, H.J., 1961. The system $\text{NaAlSi}_2\text{O}_6\text{-H}_2\text{O-Argon}$: Total pressure and water pressure in metamorphism. *J. geophys. Res.*, 66, 3923-3946.
- GRIFFIN, W.L., 1971. Genesis of coronas in anorthosites of the Upper Jotun Nappe, Indre Sogn, Norway. *J. Petrology*, 12, 219-243.
- GRIFFIN, W.L. & HEIER, K.S., 1969. Parageneses of garnet in granulite facies rocks, Lofoten Vesteraalen, Norway. *Contr. Miner. Petrology*, 23, 89-116.
- GRIFFIN, W.L., JENSEN, B.B. & MISRA, S.N., 1971. Anomalously elongated rutile in eclogite facies pyroxene and garnet. *Norsk geol. Tidssk.*, 51, 177-185.
- GRIFFIN, W.L. & MURTHY, V.R., 1968. Abundances of K, Rb, Sr and Ba in some ultramafic rocks and minerals. *Earth Plan. Sci. Lett.*, 4, 497-501.
- GRIFFIN, W.L. & MURTHY, V.R., 1969. Distribution of K, Rb, Sr and Ba in some minerals relevant to basalt genesis. *Geochim. cosmochim. Acta*, 33, 1389-1414.

- GRIFFIN, W.L., MURTHY, V.R. & PHINNEY, W.C., 1967. K/Rb in amphiboles and amphibolites from north eastern Minnesota. *Earth Plan. Sci. Lett.*, 3, 367-370.
- GROVER, J.E. & ORVILLE, P.M., 1969. The partitioning of cations between co-existing single- and multi-site phases with application to the assemblages: orthopyroxene-clinopyroxene and orthopyroxene-olivine. *Geochim. cosmochim. Acta*, 33, 205-226.
- GROVER, J.E. & ORVILLE, P.M., 1970. Partitioning of cations between co-existing single- and multi-site phases: A reply with incidental corrections. *Geochim. cosmochim. Acta*, 34, 1361-1364.
- HAMILTON, E.I., 1964. Isotopic composition of strontium in carbonatites. *Nature*, 201, 599.
- HARGREAVES, M.E., 1951. Modulated structures in some copper-nickel iron alloys. *Acta Cryst.*, 4, 301-309.
- HARRY, W.T., 1950. Aluminium replacing silicon in some silicate lattices. *Miner. Mag.*, 29, 142-149.
- HART, S.R., 1968. Discussion of 'K/Rb in amphiboles and amphibolites from north eastern Minnesota' by W.L. Griffin, V. Rama Murthy and W.C. Phinney. *Earth Plan. Sci. Lett.*, 4, 30-31.
- HART, S.R., 1969. K, Rb, Cs contents and K/Rb, K/Cs ratios of fresh and altered submarine basalts. *Earth Plan. Sci. Lett.*, 6, 295-303.
- HART, S.R. & ALDRICH, L.T., 1967. Fractionation of K/Rb by amphiboles: implications regarding mantle composition. *Science*, 155, 325-327.
- HASKIN, L.A., FREY, F.A., SCHMITT, R.A. & SMITH, R.H., 1966. Meteoritic, solar and terrestrial rare earth distributions. *Phys. Chem. Earth*, 7, 169-321.
- HASKIN, L.A. & HASKIN, M.A., 1968. Rare earth elements in the Skaergaard Intrusion. *Geochim. cosmochim. Acta*, 32, 433-447.
- HAUY, R.J., 1822. *Traité de minéralogie*, Bachelier, Paris.

- HEDGE, C.E. & WALTHALL, F.G., 1963. Radiogenic strontium-87 as an index of geologic processes. *Science*, 140, 1214-1217.
- HEIER, K.S., 1957. Phase relations of potash feldspars in metamorphism. *J. Geol.*, 65, 468-479.
- HEIER, K.S., 1960. Petrology and geochemistry of high grade metamorphic and igneous rocks on Langby, northern Norway. *Norges geol. Undersøkelse*, 207, 246 pp.
- HEIER, K.S., 1961. The amphibolite-granulite facies transition reflected in the mineralogy of potassium feldspars. *Cursillos Conf. Inst. Lucas Mallada*, 8, 131-137.
- HEIER, K.S., 1962. The possible origin of amphibolites in an area of high metamorphic grade. *Norsk geol. Tidssk.*, 42, 157-165.
- HEIER, K.S., 1964. Rb/Sr and Sr^{87}/Sr^{86} ratios in deep crustal material. *Nature*, 202, 477-478.
- HEIER, K.S., 1965a. Metamorphism and the chemical differentiation of the crust. *Geol. Fören. Stockh. Förh.*, 87, 249-256.
- HEIER, K.S., 1965b. Radioactive elements in the continental crust. *Nature*, 208, 479-480.
- HEIER, K.S., 1966. Some crystallochemical relations of nephelines and feldspars on Stjernoy, north Norway. *J. Petrology*, 7, 95-113.
- HEIER, K.S. & ADAMS, J.A.S., 1964. Geochemistry of the alkali metals. *Phys. Chem. Earth*, 5, 253-381.
- HEIER, K.S. & ADAMS, J.A.S., 1965. Concentration of radioactive elements in deep crustal material. *Geochim. cosmochim. Acta*, 29, 53-61.
- HEIER, K.S. & TAYLOR, S.R., 1959. Distribution of Li, Na, K, Rb, Cs, Pb and Tl in southern Norwegian pre-Cambrian alkali feldspars. *Geochim. cosmochim. Acta*, 15, 284-304.
- HEIER, K.S. & THORESEN, K., 1971. Geochemistry of high grade metamorphic rocks, Lofoten-Vesterålen, north Norway. *Geochim. cosmochim. Acta*, 35, 89-99.

- HEINRICH, E.W., 1948. Pegmatites of Eight Mile Park, Freemont County, Colorado. *Am. Miner.*, 33, 420-448, 550-588.
- HEINRICH, K.F.J., 1966. X-ray absorption uncertainty, *in* McKinley, T.D., Heinrich, K.F.J. & Wittry, D.B. (Eds.), *The Electron Microprobe*, 296-377. J. Wiley, New York, 1035 pp.
- HENSEN, B.J. & GREEN, D.H., 1969. Experimental data on the stability of garnet and cordierite in high-grade metamorphic rocks. *Spec. Publs. geol. Soc. Aust.*, 2, 345-347.
- HENSEN, B.J. & GREEN, D.H., 1970. Experimental data on co-existing cordierite and garnet under high grade metamorphic conditions. *Phys. Earth Planet. Interiors*, 3, 431-440.
- HENSEN, B.J. & GREEN, D.H., 1971. Experimental study of the stability of cordierite and garnet in pelitic compositions at high pressures and temperatures: I. Compositions with excess alumino-silicate. *Contr. Miner. Petrology*, 33, 309-330.
- HERRMANN, A.G., 1969. Yttrium and lanthanides, *in* Wedepohl, K.H. (Ed.), *Handbook of Geochemistry*. Springer Verlag, Berlin.
- HEVESY, G. von & WÜRSTLIN, K., 1934. Die Häufigkeit des zirkoniums. *Z. Anorg. Allgem. Chem.*, 216, 305-311.
- HIMMELBERG, G.R. & PHINNEY, W.C., 1967. Granulite facies metamorphism, Granite Falls - Montivideo area, Minnesota. *J. Petrology*, 8, 325-348.
- HIRSCHBERG, A. & WINKLER, H.G.F., 1968. Stabilitätsbeziehungen zwischen chlorit, cordierit und almandin bei der metamorphose. *Contr. Miner. Petrology*, 18, 17-42.
- HOBBS, B.E., 1968. Recrystallization of single crystals of quartz. *Tectonophysics*, 6, 353-401.
- HOEFS, J., 1965. Ein Beitrag zur Geochemie des Kohlenstoffs in magnetischen und metamorphen gesteinen. *Geochim. cosmochim. Acta*, 29, 399-428.
- HOLDHUS, S., 1971. Para-amphibolite from Gurskøy and Sandsøy, Sunnmøre, West Norway. *Norsk geol. Tidssk.*, 51, 231-246.

- HOLLAND, J.G. & LAMBERT, R.St.J., 1969. Structural regimes and metamorphic facies. *Tectonophysics*, 7, 197-217.
- HOOPER, P.R., 1968. The 'a' lineation and the trend of the Caledonides of north Norway. *Norg. geol. Unders.*, 48, 261-268.
- HOSSFELD, P.S., 1954. Stratigraphy and structure of the Northern Territory of Australia. *Trans. R. Soc. S. Aust.*, 77, 103-161.
- HOUNSLOW, A.W. & MOORE, J.M., 1967. Chemical petrology of Grenville schists near Fernleigh, Ontario. *J. Petrology*, 8, 1-28.
- HOWIE, R.A., 1955. The geochemistry of the charnockite series of Madras, India. *Trans. roy. Soc. Edinburgh*, 62, 725-768.
- HOWIE, R.A., 1958. African charnockites and related rocks. *Congo Belge Serv. Géol. Bull.*, 8, 1-14.
- HOWIE, R.A., 1963. Cell parameters of orthopyroxenes. *Spec. Pap. Miner. Soc. Am.*, 1, 213-222.
- HOWIE, R.A., 1964. Some orthopyroxenes from Scottish metamorphic rocks. *Miner. Mag.*, 33, 903-911.
- HOWIE, R.A., 1965. The pyroxenes of metamorphic rocks, *in* Pitcher, W.S. & Flinn, G.W. (Eds.), *Controls of Metamorphism*. Oliver and Boyd, Edinburgh, 368 pp.
- HOWIE, R.A. & SMITH, J.V., 1966. X-ray emission microanalysis of rock forming minerals. V. Orthopyroxenes. *J. Geol.*, 74, 443-462.
- HOWIE, R.A. & SUBRAMANIAM, A.P., 1956. The paragenesis of garnet in charnockite, enderbite and related granulites. *Miner. Mag.*, 31, 565-586.
- HSU, L.C., 1968. Selected phase relationships in the system Al-Mn-Fe-Si-O-H.: A model for garnet equilibria. *J. Petrology*, 9, 40-83.
- HUBAUX, A., 1956. Different types de minerais noirs de la region d'Egersund (Norvege). *Ann. de la Soc. Géol. de Belg.*, 79, 203-215.

- HUDSON, D.R., WILSON, A.F. & THREADGOLD, I.M., 1967. A new polytype of taffeite - a rare beryllium mineral from the granulites of central Australia. *Miner. Mag.*, 36, 305-310.
- HUCKENHOLZ, H.G. & YODER, H.S.Jr., 1971. Andradite stability relations in the CaSiO_3 - Fe_2O_3 join up to 30 Kb. *Neues Jb. Miner. Abh.*, 114, 246-280.
- HURLEY, P.M., 1968a. Absolute abundance and distribution of Rb, K and Sr in the earth. *Geochim. cosmochim. Acta*, 32, 273-283.
- HURLEY, P.M., 1968b. Correction to: Absolute abundance and distribution of Rb, K and Sr in the earth. *Geochim. cosmochim. Acta*, 32, 1025-1030.
- ITO, K. & KENNEDY, G.C., 1971. An experimental study of the basalt-garnet granulite-eclogite transition, in Heacock, J.G. (Ed.), *The structure and physical properties of the earth's crust*. *Am. Geophys. Union Geophys. Mon.*, 14, 303-314.
- JACK, R.L., 1915. The geology and prospects of the region to the south of the Musgrave Ranges, and the geology of the western portion of the Great Australian Artesian Basin. *Bull. geol. Surv. S. Aust.*, 5.
- JAMES, H.L., 1955. Zones of regional metamorphism in the Precambrian of northern Michigan. *Bull. geol. Soc. Am.*, 66, 1455-1488.
- JOHNSON, M.R.W., 1957. The structural geology of the Moine thrust zone in Coulin Forest, Wester Ross. *Q. Jl. geol. Soc. Lond.*, 113, 241-264.
- JOHNSON, M.R.W., 1967. Belemnite deformation at Fernigen, Switzerland. *Geol. Mag.*, 104, 268-273.
- JONES, J.B., 1966. Order in alkali feldspars. *Nature*, 210, 1352-1353.
- JOPLIN, G.A., 1968. A petrography of Australian metamorphic rocks. Angus and Robertson, Sydney, 262 pp.
- KALSBECK, F. & LEAKE, B.E., 1970. The chemistry and origin of some basement amphibolites between Ivigtut and Frederikshab, southwest Greenland. *Meddr Grønland*, 190, 36 pp.

- Van De KAMP, P.C., 1968. Geochemistry and origin of metasediments in the Haliburton-Madoc area, S.E. Ontario. *Can. J. Earth Sci.*, 5, 1337-1372.
- Van De KAMP, P.C., 1969. Origin of amphibolites in the Beartooth Mountains, Montana, and Wyoming; new data and interpretation. *Bull. geol. Soc. Am.*, 80, 1127-1136.
- Van De KAMP, P.C., 1970. Origin of the Green Bed Series of Scotland. *J. Geol.*, 70, 281-303.
- KANISAWA, S., 1969. Garnet-amphibolites at Yokokawa in the Abukuma Metamorphic Belt, Japan. *Contr. Miner. Petrology*, 20, 164-176.
- KATZ, M.B., 1968. The fabric of the granulites of Mont Tremblant Park, Quebec. *Can. J. Earth Sci.*, 5, 801-812.
- KATZ, M.B., 1969. The nature and origin of the granulites of Mont Tremblant Park, Quebec. *Bull. geol. Soc. Am.*, 8, 2019-2038.
- KATZ, M.B., 1970. Notes on the mineralogy and co-existing pyroxenes from the granulites of Mont Tremblant Park, Quebec. *Can. Mineralogist*, 10, 247-251.
- KEESMANN, I., MATTHES, S., SCHREYER, W. & SEIFERT, F., 1971. Stability of almandine in the system $\text{FeO}-(\text{Fe}_2\text{O}_3)-\text{Al}_2\text{O}_3-\text{SiO}_2-(\text{H}_2\text{O})$ at elevated pressures. *Contr. Miner. Petrology*, 31, 132-144.
- KHOURY, S.G., 1968. The structural geometry and geological history of the Lewisian rocks between Kylesku and Geisgeil, Sutherland, Scotland. *Krystalinikum*, 6, 41-78.
- KLEEMAN, A.W., 1965. The origin of granitic magmas. *J. geol. Soc. Aust.*, 12, 35-52.
- KLEEMAN, A.W., 1967. Sampling error in chemical analysis. *J. geol. Soc. Aust.*, 14, 43-48.
- Von KNORRING, O. & KENNEDY, W.Q., 1958. The mineral paragenesis and metamorphic status of garnet-hornblende-pyroxene-scapolite gneiss from Ghana (Gold Coast). *Miner. Mag.*, 31, 846-859.

- KOARK, H.J., 1961. Zur deformation des Venna-Konglomerates im Trondheim Gebiete, Norwegen. Uppsala Univ. Geol. Inst. Bull., 40, 139-163.
- KORNPROBST, J., 1969. Le massif ultrabasique des Beni Bouchera (Rif Interne, Maroc): Etude des péridotites de haute temperature et de haute pression, et des pyroxenolites, à grenat ou sans grenat, qui leur sont associées. Contr. Miner. Petrology, 23, 283-322.
- KORZHINSKII, D.S., 1959. Physiochemical basis of the analysis of the paragenesis of minerals. Consultants Bureau, New York, 142 pp.
- KOZŁOWSKI, K., 1958. On the eclogite-like rocks of Stary Gieraltów (East Sudeten). Bull. Acad. Polon. Sci. Ser. Chem. Geol. Geogr., 6, 723-728.
- KRAUSE, H., 1965. Mineralien und ihre verteilung auf der ilmenitlagerstaette von Abu Ghalaya Aegypten. Neues Jb. Miner. Abh., 104, 29-52.
- KRETSCHMAR, V.H. & McNUTT, R.H., 1971. A study of the Fe-Ti oxides in the Whitestone anorthosite, Dunchurch, Ontario. Can. J. Earth Sci., 8, 947-960.
- KRETZ, R., 1959. Chemical study of garnet, biotite and hornblende from gneisses of south western Quebec with emphasis on distribution of elements in co-existing minerals. J. Geol., 67, 371-402.
- KRETZ, R., 1960. The distribution of certain elements among co-existing calcic pyroxenes, calcic amphiboles and biotites in skarns. Geochim. cosmochim. Acta, 20, 161-191.
- KRETZ, R., 1961. Some applications of thermodynamics to co-existing minerals of varying composition. Examples: orthopyroxene-clinopyroxene and orthopyroxene-garnet. J. Geol., 69, 361-386.
- KRETZ, R., 1963. Distribution of magnesium and iron between orthopyroxene and calcic pyroxene in natural mineral assemblages. J. Geol., 71, 773-785.

- KRETZ, R., 1964. Analysis of equilibrium in garnet-biotite-sillimanite gneisses from Quebec. *J. Petrology*, 5, 1-20.
- KRETZ, R., 1966. Interpretation of the shape of mineral grains in metamorphic rocks. *J. Petrology*, 7, 68-94.
- KUNO, H., 1954. Study of orthopyroxenes from volcanic rocks. *Am. Miner.*, 39, 30-46.
- KUNO, H., 1960. High alumina basalt. *J. Petrology*, 1, 121-145.
- KVALÉ, A., 1948. Petrologic and structural studies in the Bergsdalen quadrangle, western Norway, Part II. Structural Geology. Bergens Mus. Arbok, 1946-1947, Naturv. rekke, 1.
- KVALÉ, A., 1953. Linear structures and their relation to movement in the Caledonides of Scandinavia and Scotland. *Q. Jl. geol. Soc. Lond.*, 109, 51-73.
- LAMBERT, I.B., 1971. The composition and evolution of the deep continental crust. *Spec. Publs geol. Soc. Aust.*, 3, 419-428.
- LAMBERT, I.B. & HEIER, K.S., 1967. The vertical distribution of uranium, thorium and potassium in the Continental Crust. *Geochim. cosmochim. Acta*, 31, 377-390.
- LAMBERT, I.B. & HEIER, K.S., 1968. Geochemical investigations of deep seated rocks in the Australian Shield. *Lithos*, 1, 30-53.
- LANGE, I.M., REYNOLDS, R.C.Jr. & LYONS, J.B., 1966. K/Rb ratios in co-existing K feldspars and biotites from some New England granites and metasediments. *Chem. Geol.*, 1, 317-322.
- LANIZ, R.V., STEVENS, R.E. & NORMAN, M.B., 1964. Staining of plagioclase feldspars and other minerals with F.D. and C.Red No.2. *Prof. Pap. U.S. geol. Surv.*, 501-B, 152-153.
- LAPADU-HARGUES, P., 1953. Sur la composition chimique moyenne des amphibolites. *Bull. Soc. Géol. France*, 3, 153-173.
- LARSEN, E.S., 1942. In F. Birch, J.F. Schairer & H.C. Spicer (Eds.), *Handbook of Physical Constants*. Geol. Soc. Am., Spec. Papers, 36, 3.

- LAVES, F. & GOLDSMITH, J.R., 1961. Polymorphism, order, disorder, diffusion and confusion in the feldspars. *Cursillos Conf. Inst. Lucas Mallada*, 8, 71-80.
- LEAKE, B.E., 1963. Origin of amphibolites from north west Adirondacks, New York. *Bull. geol. Soc. Am.*, 74, 1193-1202.
- LEAKE, B.E., 1964. The chemical distinction between ortho- and para-amphibolites. *J. Petrology*, 5, 238-254.
- LEAKE, B.E., 1965. The relationship between composition of calciferous amphibole and grade of metamorphism, *in* Pitcher, W.S. & Flinn, G.W. (Eds.), *Controls of Metamorphism*. Oliver and Boyd, Edinburgh, 368 pp.
- LEAKE, B.E., 1968. A catalogue of analysed calciferous and sub-calciferous amphiboles together with their nomenclature and associated minerals. *Spec. Pap. geol. Soc. Am.*, 98, 210 pp.
- LEAKE, B.E., 1971. On aluminous and edenitic hornblendes. *Miner. Mag.*, 38, 389-407.
- LEELANANDAM, C., 1967a. Chemical study of pyroxenes from the charnockitic rocks of Kondapalli (Andhra Pradesh), India, with emphasis on the distribution of elements in co-existing pyroxenes. *Miner. Mag.*, 36, 153-179.
- LEELANANDAM, C., 1967b. Scapolite from Kondapalli. *Curr. Sci.*, 36, 635-636.
- LEELANANDAM, C., 1967c. On the significance of occurrence of orthoclase in the Kondapalli charnockites. *Bull. geol. Soc. India*, 4, 105-107.
- LEELANANDAM, C., 1968. Paired pyroxenes from Kondapalli. *J. Indian Geosci. Assoc.*, 8, 89-92.
- LEELANANDAM, C., 1970a. Chemical mineralogy of hornblendes and biotites from the charnockitic rocks of Kondapalli, India. *J. Petrology*, 11, 475-505.
- LEELANANDAM, C., 1970b. Cell dimensions of garnets from Kondapalli, India. *Neues Jb. Miner. Mh.*, 2, 92-95.

- LINDSLEY, D.H., 1962. Investigations in the system $\text{FeO-Fe}_2\text{O}_3\text{-TiO}_2$.
Carnegie Inst. Wash. Yearb., 61, 100-106.
- LINDSLEY, D.H., 1963. Equilibrium relations of co-existing pairs of
Fe-Ti oxides. Carnegie Inst. Wash. Yearb., 62, 60-66.
- LOVERING, J.F. & WHITE, A.J.R., 1964. The significance of primary
scapolite in granulite inclusions from deep seated pipes. J.
Petrology, 5, 195-218.
- LOVERING, J.F. & WHITE, A.J.R., 1969. Granulitic and eclogitic
inclusions from basic pipes at Delegate, Australia. Contr. Miner.
Petrology, 21, 9-52.
- LOVERING, J.F. & WIDDOWSON, J.R., 1968. The petrological environment
of magnesian ilmenites. Earth Plan. Sci. Lett., 4, 310-314.
- LUTH, W.C., JAHNS, R.H. & TUTTLE, O.F., 1964. The granite system at
pressures of 4 to 10 kilobars. J. geophys. Res., 69, 759-773.
- MacDONALD, G.A. & KATSURA, T., 1964. Chemical composition of
Hawaiian lavas. J. Petrology, 5, 82-133.
- MacGREGOR, I.D. & RINGWOOD, A.E., 1964. The natural system enstatite-
pyrope. A. Rep. Dir. geophys. Lab., Yb. Carnegie Inst.
Washington, 63, 161-163.
- MackENZIE, W.S. & SMITH, J.V., 1961. Experimental and geological
evidence for the stability of alkali feldspars. Cursos Conf.
Inst. Lucas Mallada, 8, 53-69.
- MAJOR, R.B., 1970. Woodroffe Thrust Zone in the Musgrave Ranges.
Quart. Notes Geol. Surv. S. Aust., 35, 9-11.
- MAJOR, R.B., JOHNSON, J.E., LEESON, B. & MIRAMS, R.C., 1967.
Geological Atlas of South Australia, Sheet Woodroffe 1:250,000
series.
- MARMO, V., 1959. On the TiO_2 content of magnetites as a petrogenetic
hint. Am. J. Sci., 257, 144-149.
- MARTIN, H., 1935. Ueber striemung, transport und gefuege. Geol.
Rundsch., 26, 103-108.

- MASON, V., 1967. Geochemistry of basaltic rocks: Major elements. In Hess, H.H. & Poldervaart, A. (Eds.) Basalts: the Poldervaart treatise on rocks of basaltic composition. Interscience, New York. 862 pp.
- MATEJOVSKÁ, D., 1970. Composition of co-existing garnet and biotite from some granulites of Moldanubicum, Czechoslovakia. Neues Jb. Miner. Mh., 6, 249-263.
- MATSUI, Y. & BANNO, S., 1965. Intracrystalline exchange equilibrium in silicate solid solutions. Proc. Jap. Acad., 41, 461-466.
- MAUCHER, A. & REHWALD, G., 1961. Bildkartei den erzmikroskopie. Umschau Vlg., Frankfurt am Main. 1000 pp.
- McINTYRE, D.B., 1951. The tectonics of the area between Grantown and Tomintoul (mid-Strathspey). Q. Jl. geol. Soc. Lond., 107, 1-22.
- MEHNERT, K.R. (in press). Granulites, results of a discussion II. Neues Jb. Miner. Mh.
- MILLER, R.L. & KAHN, J.S., 1962. Statistical Analysis in the Geological Sciences. John Wiley and Sons, New York. 483 pp.
- MISRA, S.N., 1971. Chemical distinction of high-grade ortho- and para-metabasites. Norsk geol. Tidssk, 51, 311-316.
- MIYASHIRO, A., 1958. Regional metamorphism of the Gosaisyo-Takanuki district in the Central Abukuma Plateau. J. Fac. Sci. Univ. Tokyo, 11, 219-272.
- MIYASHIRO, A., 1964. Oxidation and reduction in the earth's crust with special reference to the role of graphite. Geochim. cosmochim. Acta, 28, 717-729.
- MIYASHIRO, A., 1968. Metamorphism of mafic rocks. In Hess, H.H. & Poldervaart, A. (Eds.), Basalts: the Poldervaart treatise on rocks of basaltic composition. Interscience, New York. 862 pp.
- MOORE, A.C., 1968. Rutile exsolution in orthopyroxene. Contr. Miner. Petrology, 17, 233-236.

- MOORE, A.C., 1970a. Descriptive terminology for the textures of rocks in granulite facies terrains. *Lithos*, 3, 123-127.
- MOORE, A.C., 1970b. The geology of the Gosse Pile ultramafic intrusion and of the surrounding granulites, Tomkinson Ranges, central Australia. Unpublished Ph.D. thesis, Univ. Adelaide.
- MOORE, A.C., 1971. The mineralogy of the Gosse Pile ultramafic intrusion, central Australia. II Pyroxenes. *J. geol. Soc. Aust.*, 18, 243-258.
- MORSE, S.A., 1968. Feldspars. *Carnegie Inst. Wash. Yearb.*, 67, 120-126.
- MORSE, S.A., 1970. Alkali feldspars with water at 5 Kb pressure. *J. Petrology*, 11, 221-251.
- MOTTANA, A., 1970. Distribution of elements among co-existing phases in amphibole bearing eclogites. *Neues Jb. Miner. Abh.*, 112, 161-187.
- MOTTANA, A. & EDGAR, A.D., 1970. The significance of amphibole compositions in the genesis of eclogites. *Lithos*, 3, 37-49.
- MUELLER, R.F., 1960. Compositional characteristics and equilibrium relations in mineral assemblages of a metamorphosed iron formation. *Am. J. Sci.*, 258, 449-497.
- MUELLER, R.F., 1961a. Oxidation in high temperature petrogenesis. *Am. J. Sci.*, 259, 460-480.
- MUELLER, R.F., 1961b. Analysis of relations among Mg, Fe and Mn in certain metamorphic minerals. *Geochim. cosmochim Acta*, 25, 267-296.
- MUELLER, R.F., 1962. Energetics of certain silicate solid solutions. *Geochim. cosmochim. Acta*, 26, 581-598.
- MUELLER, R.F., GHOSE, S. & SAXENA, S.K., 1970. Partitioning of cations between co-existing single- and multi-site phases: A discussion. *Geochim. cosmochim. Acta*, 34, 1356-1360.

- MÜLLER, G. & SCHEIDER, A., 1971. Chemistry and genesis of garnets in metamorphic rocks. *Contr. Miner. Petrology*, 31, 178-200.
- MURTY, M.S., 1964a. Role of titanium in orthopyroxene of the charnockite series. *Nature*, 202, 283-284.
- MURTY, M.S., 1964b. Pleochroism of orthopyroxenes. *Nature*, 204, 279-280.
- MURTHY, V.R. & GRIFFIN, W.L., 1970. K/Rb fractionation by plagioclase feldspars. *Chem. Geol.*, 6, 265-271.
- NARAYANASWAMY, R. & VENKATASUBRAMANIAN, V.S., 1969. Uranium and thorium contents of co-existing gneisses, granites and pegmatites. *Geochim. cosmochim. Acta*, 33, 1007-1009.
- NAZIFIGER, R.H. & MUAN, A., 1967. Equilibrium phase compositions and thermodynamic properties of olivines and pyroxenes in the system MgO-'FeO'-SiO₂. *Am. Miner.*, 52, 1364-1385.
- NESBITT, R.W., GOODE, A.D.T., MOORE, A.C. & HOPWOOD, T.P., 1970. The Giles Complex, central Australia: a stratified sequence of mafic and ultramafic intrusions. *Spec. Publs geol. Soc. S. Afr.*, 1, 547-564.
- NESBITT, R.W. & KLEEMAN, A.W., 1964. Layered intrusions of the Giles Complex, central Australia. *Nature*, 203, 391-393.
- NESBITT, R.W. & TALBOT, J.L., 1966. The layered basic and ultrabasic intrusives of the Giles Complex, central Australia. *Contr. Miner. Petrology*, 13, 1-11.
- NICHOLSON, R. & RUTLAND, R.W.R., 1969. A section across the Norwegian Caledonides Budø to Sulitjelma. *Norg. geol. Unders.*, 260, 86 pp.
- NIKITINA, L.P., ZEVELEVA, E.E. & MARCHAK, V.P., 1967. Iron-magnesium isomorphism in co-existing iron-magnesium minerals from basic granulites in the east Sayan (in Russian). *Geokhimiya*, 8, 947-953.

- NISHIKAWA, M., KUSHIRO, I. & UYEDA, S., 1971. Stability of natural hornblende at high water pressures: preliminary experiments. *Jap. J. Geol. Geogr.*, 41, 41-50.
- NOCKOLDS, S.R., 1954. Average chemical compositions of some igneous rocks. *Bull. geol. Soc. Am.*, 65, 1007-1052.
- NOCKOLDS, S.R. & ALLEN, R., 1953. The geochemistry of some igneous rock series. *Geochim. cosmochim. Acta*, 4, 105-142.
- NORRISH, K. & CHAPPELL, B.W., 1967. X-ray fluorescence spectrography, *in* Zussman, J. (Ed.) *Physical Methods in Determinative Mineralogy*. Academic Press, London. 514 pp.
- NORRISH, K. & HUTTON, J.T., 1969. An accurate X-ray spectrographic method for the analysis of a wide range of geological samples. *Geochim. cosmochim. Acta*, 33, 431-453.
- O'HARA, M.J., 1960. A garnet-hornblende-pyroxene rock from Glenelg, Inverness-shire. *Geol. Mag.*, 97, 145-156.
- O'HARA, M.J., 1961. Zoned ultrabasic and basic gneiss masses in the Early Lewisian metamorphic complex at Scourie, Sutherland. *J. Petrology*, 2, 248-276.
- O'HARA, M.J. & MERCY, E.L.P., 1963. Petrology and petrogenesis of some garnetiferous peridotites. *Trans. roy. Soc. Edinburgh*, 65, 251-314.
- OHTA, Y. & KIZAKI, K., 1966. Petrographic studies of potash feldspar from Yamato Sanmyaku, East Antarctica. *J.A.R.E. Sci. Rept.*, 5, 40 pp.
- ORVILLE, P.M., 1963. Alkali ion exchange between vapour and feldspar phases. *Am. J. Sci.*, 261, 201-237.
- ORVILLE, P.M., 1969. A model for metamorphic differentiation origin of thin layered amphibolites. *Am. J. Sci.*, 267, 64-86.
- OSBORN, E.F., 1959. Role of oxygen pressure in the crystallization and differentiation of basaltic magma. *Am. J. Sci.*, 257, 609-647.

- OSBORN, E.F. & ROEDER, P.L., 1960. Effect of oxygen pressure on crystallization in simplified basalt systems. 21st Int. geol. Congr., Pt.13, 147-155.
- PARK, R.G., 1969. Structural correlation in metamorphic belts. Tectonophysics, 7, 323-338.
- PARRAS, K., 1958. On the charnockites in the light of a highly metamorphic rock complex in southwestern Finland. Bull. Comm. géol. Finl., 181, 1-37.
- PARSLOW, G.R., 1969. Mesonorms of granitic rock analyses. Miner. Mag., 37, 262-269.
- PETTIJOHN, F.J., 1957. Sedimentary Rocks. 2nd edition. Harper and Brothers, New York. 718 pp.
- PETTIJOHN, F.J., 1963. Chemical composition of sandstones - excluding carbonate and volcanic sands. Prof. Pap. U.S. geol. Surv., 440-S, Fleischer, M. (Ed.).
- PHILLIPS, F.C., 1937. A fabric study of some Moine schists and associated rocks. Q. Jl. geol. Soc. Lond., 93, 581-607.
- PHILPOTTS, J.A. & SCHNETZLER, C.C., 1970. Phenocryst-matrix partition coefficients for K, Rb, Sr and Ba, with applications to anorthosite and basalt gneisses. Geochim. cosmochim. Acta, 34, 307-322.
- POLDERVAART, A., 1953. Metamorphism of basaltic rocks, a review. Bull. geol. Soc. Am., 64, 259-274.
- POLDERVAART, A., 1955. Chemistry of the earth's crust. Spec. Pap. geol. Soc. Am., 62, 119-144.
- PRIDER, R.T., 1945. Charnockitic and related cordierite-bearing rocks from Dangin, Western Australia. Geol. Mag., 82, 145-172.
- QUENSEL, P., 1951. The charnockite series of the Varberg district on the south-western coast of Sweden. Arkiv Min. Geol., 1, 229-332.
- RAMBERG, H., 1944. Petrologic significance of subsolidus phase transitions in mixed crystals. Norsk geol. Tidssk., 24, 42-74.

- RAMBERG, H., 1951. Remarks on the average chemical composition of granulite facies and amphibolite facies gneisses in West Greenland. *Medd. Dansk. Geol. Foren.*, 12, 27-34.
- RAMBERG, H., 1952. Chemical bonds and the distribution of cations in silicates. *J. Geol.*, 60, 331-355.
- RAMBERG, H., 1954. Relative stabilities of some simple silicates as related to the polarization of the oxygen ions. *Amer. Miner.*, 39, 256-271.
- RAMBERG, H. & De VORE, G.W., 1951. The distribution of Fe^{2+} and Mg^{2+} in co-existing olivines and pyroxenes. *J. Geol.*, 59, 193-210.
- RAMSAY, J.G., 1967. *Folding and Fracturing of Rocks*. McGraw Hill, New York. 568 pp.
- RANKAMA, K. & SAHAMA, Th.G., 1950. *Geochemistry*. University of Chicago Press, Chicago, 910 pp.
- RAY, S., 1970. Significance of hornblende compositions from basic granulites of the type charnockite area near Madras. *Neues Jb. Miner. Mh.*, 10, 456-466.
- RAY, S. & SEN, S.K., 1970. Partitioning of major exchangeable cations among orthopyroxene, calcic pyroxene and hornblende in basic granulites from Madras. *Neues Jb. Miner. Abh.*, 114, 61-88.
- REINHARDT, E.W., 1968. Phase relations in cordierite bearing gneisses from the Gananoque area, Ontario. *Can. J. Earth Sci.*, 5, 455-482.
- RHODES, J.M., 1969. On the chemistry of potassium feldspars in granitic rocks. *Chem. Geol.*, 4, 373-392.
- RICHARDSON, S.W., 1968. Staurolite stability in part of the system Fe-Al-Si-O-H. *J. Petrology*, 9, 467-488.
- RICHARDSON, S.W., BELL, P.M. & GILBERT, M.C., 1968. Kyanite-sillimanite equilibrium between 700° and 1500°C. *Am. J. Sci.*, 266, 513-541.
- RICHARDSON, S.W., GILBERT, M.C. & BELL, P.M., 1969. Experimental determination of kyanite-andalusite and andalusite-sillimanite equilibria; the aluminium silicate triple point. *Am. J. Sci.*, 267, 259-272.

- RICKWOOD, P.C., 1968. On recasting analyses of garnet into end-member molecules. *Contr. Miner. Petrology*, 18, 175-198.
- RILEY, J.P. & WILLIAMS, H.P., 1959. The microanalysis of silicate and carbonate minerals, III. *Microchim. Acta*, 6, 804-824.
- RINGWOOD, A.E. & GREEN, D.H., 1966. An experimental investigation of the gabbro-eclogite transformation and some geophysical implications. *Tectonophysics*, 3, 383-427.
- ROBINSON, E.G., 1949. The petrological nature of some rocks from the Mann, Tompkinson and Ayres Ranges. *Trans. R. Soc. S. Aust.*, 73, 29-39.
- RUTLAND, R.W.R. & SUTHERLAND, D.S., 1967. The chemical composition of granitic gneisses and spragmitic meta-sediments in the Glomfjord Region, Northern Norway. *Norsk geol. Tidssk.*, 47, 359-374.
- SADASHIVAIAN, M.S. & SUBBARAYUDU, G.V., 1970. Orthopyroxenes from the Kondavidu charnockites, Guntur District, Andhra Pradesh. *Proc. Indian Acad. Sci.*, 72, 139-148.
- SANDER, B., 1930. *Gefuegekunde der Gesteine*. Springer Verlag, Berlin. 352 pp.
- SAXENA, S.K., 1968a. Chemical study of phase equilibria in charnockites, Varberg, Sweden. *Am. Miner.*, 53, 1674-1695.
- SAXENA, S.K., 1968b. Distribution of iron and magnesium between co-existing garnet and clinopyroxene in rocks of varying metamorphic grade. *Am. Miner.*, 53, 2018-2024.
- SAXENA, S.K., 1968c. Distribution of elements between co-existing minerals and the nature of solid solution in garnet. *Am. Miner.*, 53, 994-1014.
- SAXENA, S.K., 1968d. Crystal-chemical aspects of distribution of elements among certain co-existing rock-forming silicates. *Neues. Jb. Miner. Abh.*, 108, 292-323.

- SAXENA, S.K., 1968e. Nature of mixing in ferromagnesian silicates and the significance of the distribution coefficient. *Neues Jb. Miner. Mh.*, 8, 275-286.
- SAXENA, S.K., 1969. Distribution of elements in co-existing minerals and the problem of chemical disequilibrium in metamorphosed basic rocks. *Contr. Miner. Petrology*, 20, 177-197.
- SAXENA, S.K. & GHOSE, S., 1971. Mg^{2+} - Fe^{2+} order-disorder and the thermodynamics of the orthopyroxene crystalline solution. *Am. Miner.*, 56, 532-559.
- SCHMIDT, W., 1926. Gefuegesymmetrie und Tektonik. *Jahrb. Geol. Reichsanstalt Wien*, 76, 407-430.
- SCHREYER, W. & YODER, H.S.Jr., 1964. The system Mg-cordierite- H_2O and related rocks. *Neues Jb. Miner. Abh.*, 101, 271-342.
- SCHWERDTNER, W.M., 1970. Hornblende lineations in Trout Lake area, Lac la Rouge map sheet, Saskatchewan. *Can. J. Earth Sci.*, 7, 884-899.
- SEKI, Y., 1958. Glauconitic regional metamorphism in the Kanto Mountains, central Japan. *Jap. J. Geol. Geogr.*, 29, 233-258.
- SEN, N., NOCKOLDS, S.R. & ALLEN, R., 1959. Trace elements in minerals from rocks of the southern Californian batholith. *Geochim. cosmochim. Acta*, 16, 58-78.
- SEN, S.K., 1959. Potassium content of natural plagioclases and the origin of antiperthites. *J. Geol.*, 67, 479-495.
- SEN, S.K., 1970. Magnesium-iron compositional variance in hornblende pyroxene granulites. *Contr. Miner. Petrology*, 29, 76-88.
- SEN, S.K. & RAY, S., 1971. Hornblende-pyroxene granulites versus pyroxene granulites: A study from the type charnockite area. *Neues Jb. Miner. Abh.*, 115, 291-314.
- SEN, S.K. & REGE, S.M., 1966. Distribution of magnesium and iron between metamorphic pyroxenes from Saltora, West Bengal, India. *Miner. Mag.*, 35, 759-762.

- SEN, S.K. & SAHU, J.R., 1970. Phase relations in three charnockites from Pallavaram-Tambaram. *Contr. Miner. Petrology*, 27, 239-243.
- SHAW, D.M., 1956. Geochemistry of pelitic rocks, part III. *Bull. geol. Soc. Am.*, 67, 919-934.
- SHAW, D.M., 1960. The geochemistry of scapolite: II Trace elements, petrology and general geochemistry. *J. Petrology*, 1, 261-285.
- SHAW, D.M., 1968a. A review of K-Rb fractionation trends by covariance analysis. *Geochim. cosmochim. Acta*, 32, 573-601.
- SHAW, D.M., 1968b. Radioactive elements in the Canadian Precambrian Shield and the interior of the Earth. In Ahrens, L.H. (Ed.), *Origin and Distribution of the Elements*, Pergamon, Oxford, 1178 pp.
- SHAW, D.M. & KUDO, A.M., 1965. A test of the discriminant function in the amphibolite problem. *Miner. Mag.*, 34, (Tilley Vol.), 423-435.
- SHAW, D.M., REILLY, G.A., MUYSSON, J.R., PATTENDEN, G.E. & CAMPBELL, F.E., 1967. An estimate of the chemical composition of the Canadian Precambrian Shield. *Can. J. Earth Sci.*, 4, 829-853.
- SHERATON, J.W., 1970. The origin of the Lewisian gneisses of north-west Scotland, with particular reference to the Drumbeg area, Sutherland. *Earth Plan. Sci. Lett.*, 8, 301-310.
- SHIDO, F. & MIYASHIRO, A., 1959. Hornblendes of basic metamorphic rocks. *J. Fac. Sci. Univ. Tokyo*, 12, 85-102.
- SIGHINOLFI, G.P., 1969. K-Rb ratio in high grade metamorphism: a confirmation of the hypothesis of continual crustal evolution. *Contr. Miner. Petrology*, 21, 346-356.
- SIGHINOLFI, G.P., 1971. Investigations into deep crustal levels: fractionating effects and geochemical trends related to high-grade metamorphism. *Geochim cosmochim. Acta*, 35, 1005-1021.
- SKINNER, B.J. & BOYD, F.R., 1964. Aluminous enstatites. *Carnegie Inst. Wash. Yearb.*, 63, 163-165.

- SMITH, C.S., 1948. Grains, phases and interfaces: an interpretation of microstructure. *Trans. Am. Inst. Min. Engrs.*, 175, 15-51.
- SMITH, C.S., 1953. Microstructure. *Trans. Am. Soc. Metals.*, 45, 533-575.
- SMITH, C.S., 1964. Some elementary principles of polycrystalline microstructure. *Metallurgical Rev.*, 9, 1-48.
- SMITHSON, S.B., FIKKAN, P.R. & HOWTON, R.S., 1971. Amphibolitization of calc silicate metasedimentary rocks. *Contr. Miner. Petrology*, 31, 228-237.
- SMITHSON, S.B. & HEIER, K.S., 1971. K, U and Th distribution between normal and charnockitic facies of a deep granitic intrusion. *Earth Plan. Sci. Lett.*, 12, 325-326.
- SPRIGG, R.C. & WILSON, B., 1958. The Musgrave Mountain belt in South Australia. *Geol. Rdsch.*, 47, 531-542.
- SPRY, A., 1969. *Metamorphic Textures*. Pergamon, Oxford. 350 pp.
- STANTON, R.L., 1964. Mineral interfaces in stratiform ores. *Bull. Instn. Min. Metall. Lond.*, 74, 45-79.
- STAUFFER, M.R., 1967. Tectonic strain in some volcanic, sedimentary and intrusive rocks near Canberra, Australia: a comparative study of deformation fabrics. *New Zealand J. Geol. Geophys.*, 10, 1079-1108.
- STAUFFER, M.R., 1970. Deformation textures in tectonites. *Can. J. Earth. Sci.*, 7, 498-511.
- STEIGER, R.H. & HART, S.R., 1967. Microcline orthoclase transition within a contact aureole. *Am. Miner.*, 52, 87-116.
- STEWART, D.B. & RIBBE, P.H., 1969. Structural explanation for variations in cell parameters of alkali feldspar with Al/Si ordering. *Am. J. Sci.*, 267, 444-462.
- STORRE, B. & KAROTKE, E., 1971. An experimental determination of the upper stability limit of muscovite + quartz in the range 7-20 Kb water pressure. *Neues Jb. Miner. Mh.*, 1971, 237-240.

- STREICH, V., 1893. Scientific reports of Elder Exploration Expedition 1891-2, Geology. Trans. R. Soc. S. Aust., 16, 74-115.
- STUEBER, A.M. & MURTHY, V.R., 1966. Strontium isotope and alkali element abundances in ultramafic rocks. Geochim. cosmochim. Acta, 30, 1243-1259.
- SUBRAMANIAM, A.P., 1956. Mineralogy and petrology of the Sittampundi complex, Salem District, Madras State, India. Bull. geol. Soc. Am., 67, 317-390.
- SUWA, K., 1968. Petrological studies on the metamorphic rocks from the Lützow-Holmbukta area, East Antarctica. 23rd Int. geol. Congr. Sect. 4, 171-187.
- TALBOT, H.W.B. & CLARKE, E.deC., 1917. A geological reconnaissance of the country between Laverton and the South Australian Border (near Latitude 26°) including part of the Mt. Margaret Gold field. Bull. geol. Survey. West. Aust., 75.
- TALBOT, H.W.B. & CLARKE, E.deC., 1918. The geological results of an expedition to the South Australian Border, and some comparisons between central and Western Australian geology suggested thereby. J. Proc. R. Soc. West. Aust., 3, 70-98.
- TALBOT, J.L. & HOBBS, B.E., 1968. Relationship of metamorphic differentiation to other structural features at three localities. J. Geol., 76, 581-587.
- TALIAFERRO, N.L., 1943. Franciscan-Knoxville problem. Bull. Amer. Ass. Petrol. Geol., 27, 109-219.
- TATSUMOTO, M., HEDGE, C.E. & ENGEL, A.E.J., 1965. Potassium, rubidium, strontium, thorium, uranium and the ratio of Sr⁸⁷ to Sr⁸⁶ in oceanic tholeiitic basalt. Science, 150, 886-888.
- TAYLOR, H.P. & EPSTEIN, S., 1962. Relationship between O^{18}/O^{16} ratios in co-existing minerals of igneous and metamorphic rocks. Bull. geol. Soc. Am., 73, 675-694.
- TAYLOR, S.R., 1960. Occurrence of alkali metals in some Gulf of Mexico sediments: amended Rb values and K/Rb ratios. J. Sediment. Petrol., 30, 317-321.

- TAYLOR, S.R., 1962. Meteoritic and terrestrial rare earth abundance patterns. *Geochim. cosmochim. Acta*, 26, 81-88.
- TAYLOR, S.R., 1965. The application of trace element data to problems in petrology. *Phys. Chem. Earth.*, 6, 133-213.
- TAYLOR, S.R., EMELEUS, C.H. & EXLEY, C.S., 1956. Some anomalous K/Rb ratios in igneous rocks and their petrological significance. *Geochim. cosmochim. Acta*, 10, 224-229.
- THOMPSON, J.B., 1947. Role of aluminium in rock forming silicates. *Bull. geol. Soc. Am.*, 58, 1232.
- THOMPSON, J.B.Jr., 1957. The graphical analysis of mineral assemblages in pelitic schists. *Am. Miner.*, 42, 842-858.
- THOMPSON, J.B.Jr. & WALDBAUM, D.R., 1969. Mixing properties of sanidine crystalline solutions: III Calculations based on two phase data. *Am. Miner.*, 54, 811-838.
- THOMSON, B.P., 1969. Precambrian crystalline basement. *In* Parkin, L.W. (Ed.), *Handbook of South Australian geology*. Geol. Surv. S. Aust., Adelaide. 268 pp.
- THOMSON, B.P., 1970. A review of the Precambrian and Lower Palaeozoic tectonics of South Australia. *Trans. R. Soc. S. Aust.*, 71, 193-221.
- THOMSON, B.E., MIRAMS, R.C. & JOHNSON, J.E., 1962. *Geological Atlas of South Australia*, Sheet Mann, 1:250,000 series.
- THOMSON, J.A., 1911. On rock specimens from central and Western Australia. *J. Proc. R. Soc. N.S.W.*, 45, 292-317.
- TILLEY, C.E., 1921. The granite-gneisses of southern Eyre Peninsula (South Australia) and their associated amphibolites. *Q. Jl. geol. Soc. Lond.*, 77, 75-134.
- TOURET, J., 1971. Le facies granulite en Norvege meridionale. 1. Les associations mineralogiques. *Lithos*, 4, 239-249.
- TURNER, F.J., 1968. *Metamorphic Petrology*. McGraw Hill, New York. 403 pp.

- TURNER, F.J. & WEISS, L.E., 1963. Structural analysis of Metamorphic Tectonites. McGraw Hill, New York. 545 pp.
- TUTTLE, O.F. & BOWEN, N.L., 1958. Origin of granite in the light of experimental studies in the system $\text{NaAlSi}_3\text{O}_8 - \text{KAlSi}_3\text{O}_8 - \text{SiO}_2 - \text{H}_2\text{O}$. Mem. geol. Soc. Am., 74, 5-98.
- VAASJOKI, O. & HEIKKINEN, A., 1963. On the significance of some textural and compositional properties of the magnetites of titaniferous iron ores. Bull. Comm. géol. Finl., 204, 141-153.
- VELDE, B., HERVÉ, F. & KORNPORST, J., 1970. The eclogite-amphibolite transition at 650°C and 6.5 Kbar pressure, as exemplified by basic rocks of the Uzerche area, central France. Am. Miner., 55, 953-974.
- VERNON, R.H., 1968. Microstructures of high-grade metamorphic rocks at Broken Hill, Australia. J. Petrology, 9, 1-22.
- VERNON, R.H., 1970. Comparative grain-boundary studies of some basic and ultrabasic granulites nodules and cumulates. Scott. J. Geol., 6, 337-351.
- VIRGO, D., 1966. Some elemental distributions between co-existing feldspars in metamorphic rocks. Unpublished Ph.D. thesis, Univ. Adelaide.
- VIRGO, D., 1968. Partitioning of strontium between co-existing K-feldspar and plagioclase in some metamorphic rocks. J. Geol., 76, 331-346.
- VIRGO, D., 1969. Partitioning of sodium between co-existing K-feldspar and plagioclase from some metamorphic rocks. J. Geol., 77, 173-182.
- VIRGO, D. & HAFNER, S., 1969. Fe^{2+} , Mg order-disorder in heated orthopyroxenes. Spec. Pap. Miner. Soc. Am., 2, 67-81.
- de WAARD, D., 1966. On water vapour pressure in zones of regional metamorphism and the nature of the hornblende-granulite facies. Proc. K. ned. Akad. Wet., 69, 453-458.

- de WAARD, D., 1967a. Absolute P-T conditions of granulite facies metamorphism in the Adirondacks. *Proc. K. ned. Akad. Wet.*, 70, 400-410.
- de WAARD, D., 1967b. The occurrence of garnet in the granulite facies terrain of the Adirondack highlands and elsewhere: an amplification and reply. *J. Petrology*, 8, 210-232.
- de WAARD, D., 1969. Facies series and P-T conditions of metamorphism in the Adirondack Mountains. *Proc. K. ned. Akad. Wet.*, 72, 124-131.
- WAGER, L.R. & MITCHELL, R.L., 1951. The distribution of trace elements during strong fractionation of basic magmas: a further study of the Skaergaard Intrusion, east Greenland. *Geochim. cosmochim. Acta*, 1, 129-209.
- WALDBAUM, D.R. & THOMPSON, J.B.Jr., 1969. Mixing properties of sanidine crystalline solutions: IV Phase diagrams from equations of state. *Am. Miner.*, 54, 1274-1298.
- WALKER, K.R., JOPLIN, G.A., LOVERING, J.F. & GREEN, R., 1960. Metamorphic and metasomatic convergence of basic igneous and lime-magnesia sediments of the Precambrian of north-western Queensland. *J. geol. Soc. Aust.*, 6, 149-178.
- WARD, R.F., 1959. Petrology and metamorphism of the Wilmington Complex, Delaware, Pennsylvania and Maryland. *Bull. geol. Soc. Am.*, 70, 1425-1458.
- WATTERSON, J., 1960. Homogeneous deformation of the gneisses of Vesterland, south west Greenland. *Meddr Grønland*, 175, 72 pp.
- WEDEPOHL, K.H., 1969. Composition and Abundance of Common Igneous Rocks. *In* Wedepohl, K.H. (Ed.), *Handbook of Geochemistry*. Springer-Verlag, Berlin.
- WEDEPOHL, K.H., 1969. Composition and Abundance of Common Sedimentary Rocks. *In* Wedepohl, K.H. (Ed.), *Handbook of Geochemistry*. Springer Verlag, Berlin.

- WHITE, A.J.R., 1959. Scapolite bearing marbles and calc-silicate rocks from Tungkillo and Milendella, South Australia. *Geol. Mag.*, 96, 285-306.
- WHITE, A.J.R., 1964. Clinopyroxenes from eclogites and basic granulites. *Am. Miner.*, 49, 883-888.
- WHITE, A.J.R., 1966. Genesis of migmatites from the Palmer Region of South Australia. *Chem. Geol.*, 1, 165-200.
- WHITE, A.J.R., 1969. Some mineral characteristics of high temperature-high pressure 'granulite facies' assemblages. *Spec. Publs. geol. Soc. Aust.*, 2, 353-359.
- WHITNEY, P.R., 1969. Variations of the K/Rb ratio in migmatitic paragneisses of the northwest Adirondacks. *Geochim. cosmochim. Acta*, 33, 1203-1211.
- WHITTLE, A.P., 1968. The Pretty Hill Sandstone of the Otway Basin, Australia - A study of provenience. Unpublished Honours thesis, Univ. Adelaide.
- WILCOX, R.E. & POLDERVAART, A., 1958. Metadolerite dike swarm in Bakersville Roan Mt. area, North Carolina. *Bull. geol. Soc. Am.*, 69, 1323-1368.
- WILSON, A.F., 1947. The charnockitic and associated rocks of north-western South Australia. I. The Musgrave Ranges - an introductory account. *Trans. R. Soc. S. Aust.*, 71, 195-211.
- WILSON, A.F., 1948. The charnockitic and associated rocks of north-western South Australia. II. Dolerites from the Musgrave and Everard Ranges. *Trans. R. Soc. S. Aust.*, 72, 178-200.
- WILSON, A.F., 1950. Some unusual alkali-feldspars in the central Australian charnockitic rocks. *Miner. Mag.*, 29, 215-224.
- WILSON, A.F., 1952a. The charnockite problem in Australia. *Sir. D. Mawson Anniv. Vol.*, University of Adelaide, 203-224.
- WILSON, A.F., 1952b. Metamorphism of granite rocks by olivine dolerite in central Australia. *Geol. Mag.*, 89, 73-86.

- WILSON, A.F., 1953. Significance of lineation in central Australia. Aust. J. Sci., 16, 47-50.
- WILSON, A.F., 1954a. Significance of lineation in central Australia - a reply. Aust. J. Sci., 16, 242-243.
- WILSON, A.F., 1954b. Studies on Australian charnockitic rocks and related problems. Unpublished D.Sc. thesis, Univ. Western Australia.
- WILSON, A.F., 1958. The charnockitic rocks of Australia. Geol. Rdsch., 47, 491-510.
- WILSON, A.F., 1959. Notes on the fabric of some charnockitic rocks from central Australia. J. Proc. R. Soc. West. Aust., 42, 56-64.
- WILSON, A.F., 1960. The charnockitic granites and associated granites of central Australia. Trans. R. Soc. S. Aust., 83, 37-76.
- WILSON, A.F., 1969a. Granulite terrains and their tectonic setting and relationship to associated metamorphic rocks in Australia. Spec. Publs geol. Soc. Aust., 2, 243-258.
- WILSON, A.F., 1969b. Problems of exploration for metals in granulite terrains with particular reference to Australian localities. Spec. Publs geol. Soc. Aust., 2, 375-376.
- WILSON, A.F., COMPSTON, W., JEFFERY, P.M. & RILEY, G.H., 1960. Radioactive ages from the Precambrian rocks in Australia. J. geol. Soc. Aust., 6, 179-195.
- WILSON, A.F., GREEN, D.C. & DAVIDSON, L.R., 1970. The use of oxygen isotope geothermometry on the granulites and related intrusives, Musgrave Ranges, central Australia. Contr. Miner. Petrology, 27, 166-178.
- WILSON, A.F. & HUDSON, D.B., 1967. The discovery of beryllium-bearing sapphirine in the granulites of the Musgrave Ranges, (central Australia). Chem. Geol., 2, 209-215.
- WINKLER, H.G.F., 1965. Petrogenesis of Metamorphic Rocks. Springer-Verlag, Berlin. 220 pp.

- WONES, D.R. & EUGSTER, H.P., 1965. Stability of biotite: Experiment, theory and application. *Am. Miner.*, 50, 1228-1272.
- WRIGHT, T.L., 1967. The microcline-orthocline transformation in the contact aureole of the Eldore Stock, Colorado. *Am. Miner.*, 52, 117-136.
- WRIGHT, T.L. & STEWART, D.B., 1968. X-ray and optical study of alkali feldspar: I. Determination of composition and structural state from refined unit-cell parameters and 2V. *Am. Miner.*, 53, 38-87.
- WYNNE-EDWARDS, H.R., 1967. Westport map area, Ontario, with special emphasis on the Precambrian rocks. *Geol. Surv. Can., Mem.* 346.
- YODER, H.S.Jr., 1952. The $MgO-Al_2O_3-SiO_2-H_2O$ system and the related metamorphic facies. *Am. J. Sci. (Bowen Volume)*, 569-627.
- YODER, H.S.Jr., 1955. Role of water in metamorphism. *In* Poldervaart, A. (Ed.), *Spec. Pap. Geol. Soc. Am.*, 62, 505-524.
- YODER, H.S.Jr., STEWART, D.B. & SMITH, J.R., 1956. Ternary Feldspars. *Carnegie Inst. Wash. Yearb.*, 55, 190-194.
- YODER, H.S.Jr., STEWART, D.B. & SMITH, J.R., 1957. Ternary Feldspars. *Carnegie Inst. Wash. Yearb.*, 56, 206-214.
- YODER, H.S.Jr. & TILLEY, C.E., 1962. Origin of basalt magmas: An experimental study of natural and synthetic rock systems. *J. Petrology*, 3, 342-532.
- ZARTMAN, R.E., 1964. A geochronologic study of the Lone Grove pluton from the Llano uplift, Texas. *J. Petrology*, 5, 359-408.
- ZEN, E.-An., 1969. The stability relations of the polymorphs of aluminium silicate: A survey and some comments. *Am. J. Sci.*, 67, 297-309.